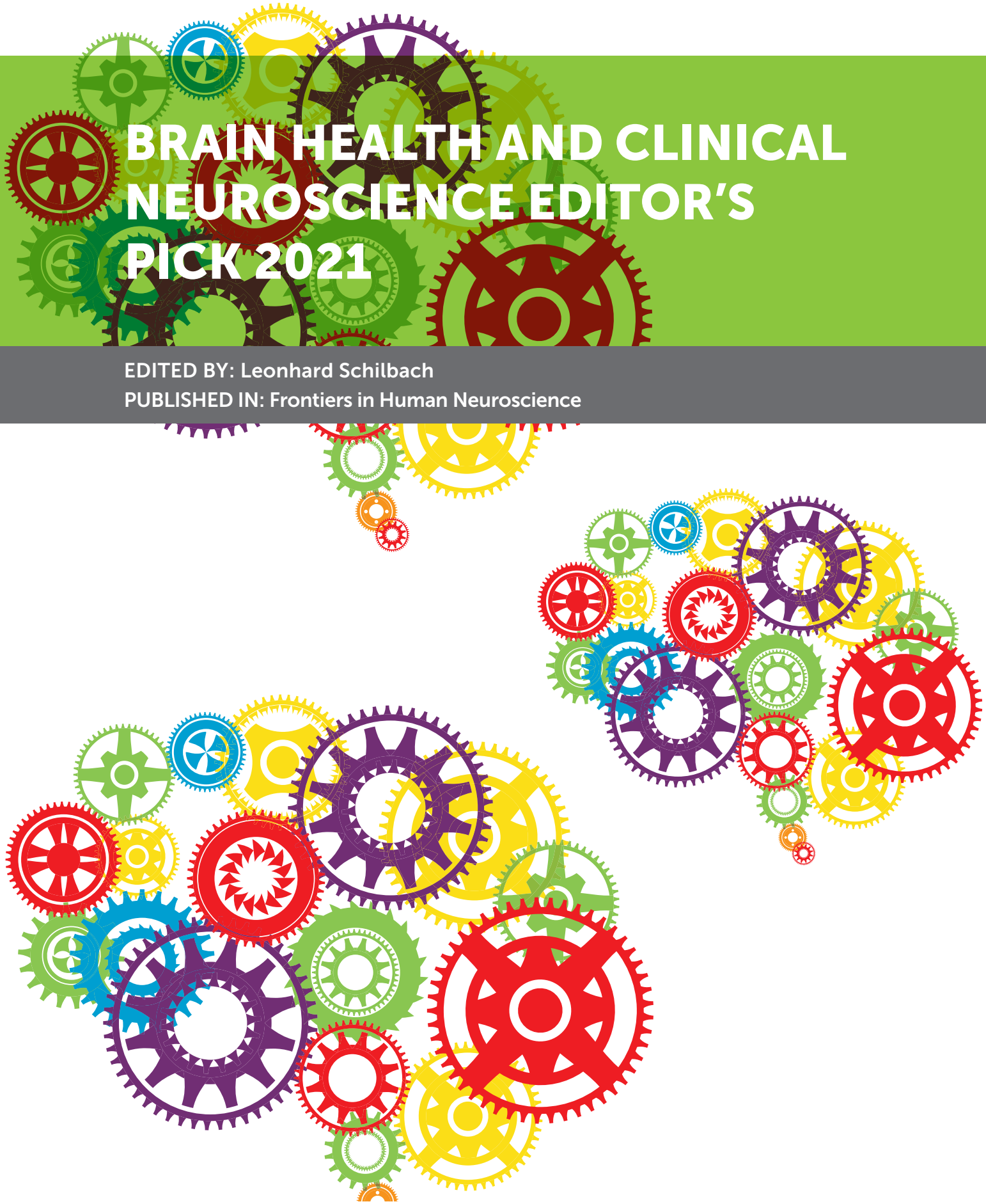

BRAIN HEALTH AND CLINICAL NEUROSCIENCE EDITOR'S PICK 2021

EDITED BY: Leonhard Schilbach

PUBLISHED IN: Frontiers in Human Neuroscience

frontiers Research Topics

frontiers

ISSN 1664-8714
ISBN 978-2-88971-162-8
DOI 10.3389/978-2-88971-162-8

About Frontiers

Frontiers is more than just an open-access publisher of scholarly articles: it is a pioneering approach to the world of academia, radically improving the way scholarly research is managed. The grand vision of Frontiers is a world where all people have an equal opportunity to seek, share and generate knowledge. Frontiers provides immediate and permanent online open access to all its publications, but this alone is not enough to realize our grand goals.

Frontiers Journal Series

The Frontiers Journal Series is a multi-tier and interdisciplinary set of open-access, online journals, promising a paradigm shift from the current review, selection and dissemination processes in academic publishing. All Frontiers journals are driven by researchers for researchers; therefore, they constitute a service to the scholarly community. At the same time, the Frontiers Journal Series operates on a revolutionary invention, the tiered publishing system, initially addressing specific communities of scholars, and gradually climbing up to broader public understanding, thus serving the interests of the lay society, too.

Dedication to Quality

Each Frontiers article is a landmark of the highest quality, thanks to genuinely collaborative interactions between authors and review editors, who include some of the world's best academicians. Research must be certified by peers before entering a stream of knowledge that may eventually reach the public - and shape society; therefore, Frontiers only applies the most rigorous and unbiased reviews.
Frontiers revolutionizes research publishing by freely delivering the most outstanding research, evaluated with no bias from both the academic and social point of view. By applying the most advanced information technologies, Frontiers is catapulting scholarly publishing into a new generation.

What are Frontiers Research Topics?

Frontiers Research Topics are very popular trademarks of the Frontiers Journals Series: they are collections of at least ten articles, all centered on a particular subject. With their unique mix of varied contributions from Original Research to Review Articles, Frontiers Research Topics unify the most influential researchers, the latest key findings and historical advances in a hot research area! Find out more on how to host your own Frontiers Research Topic or contribute to one as an author by contacting the Frontiers Editorial Office: frontiersin.org/about/contact

BRAIN HEALTH AND CLINICAL NEUROSCIENCE EDITOR'S PICK 2021

Topic Editor:
Leonhard Schilbach, Ludwig Maximilian University of Munich, Germany

Citation: Schilbach, L., ed. (2021). Brain Health and Clinical Neuroscience Editor's Pick 2021. Lausanne: Frontiers Media SA. doi: 10.3389/978-2-88971-162-8

Table of Contents

frontiers in Human Neuroscience

ORIGINAL RESEARCH
published: 29 January 2019
doi: 10.3389/fnhum.2019.00012

Anatomical and Neurochemical Correlates of Parental Verbal Abuse: A Combined MRS—Diffusion MRI Study

*Dohyun Kim[1], Jae Hyun Yoo[1], Young Woo Park[2], Minchul Kim[1], Dong Woo Shin[1] and Bumseok Jeong[1]**

[1]*Graduate School of Medical Science and Engineering, Korea Advanced Institute for Science and Technology (KAIST), Daejeon, South Korea,* [2]*School of Electrical Engineering, Korea Advanced Institute of Science and Technology (KAIST), Daejeon, South Korea*

Despite the critical impact of parental dialog on children who remain physically and psychologically dependent, most studies have focused on brain alterations in people exposed to moderate-to-high levels of emotional maltreatment with/without psychopathology. We measured metabolites in the pregenual anterior cingulate cortex (pgACC) acquired with single-voxel proton magnetic resonance spectroscopy and anatomical connectivity assessed with probabilistic tractography in 46 healthy young adults who experienced no-to-low level parental verbal abuse (paVA) during their childhood and adolescence. The partial least square regression (PLSR) model showed that individual variance of perceived paVA was associated with chemical properties and structural connectivity of pregenual anterior cingulate cortex (pgACC; prediction R^2 = 0.23). The jackknife test was used to identify features that significantly contributed to the partial least square regression (PLSR) model; a negative association of paVA was found with myo-inositol concentration, anatomical connectivities with the right caudate and with the right transverse temporal gyrus. Of note, positive associations were also found with the left pars triangularis, left cuneus, right inferior temporal cortex, right entorhinal cortex and right amygdala. Our results showing both a negative association of frontal glial function and positive associations of anatomical connectivities in several networks associated with threat detection or visual information processing suggest both anatomical and neurochemical adaptive changes in medial frontolimbic networks to low-level paVA experiences.

Keywords: verbal abuse, frontolimbic circuit, magnetic resonance spectroscopy, diffusion tensor imaging, probabilistic tractography, pregenual anterior cingulate cortex, maltreatment

OPEN ACCESS

Edited by:
Guido van Wingen, University of Amsterdam, Netherlands

Reviewed by:
Layla Banihashemi, University of Pittsburgh, United States
Anouk Marsman, Danish Research Centre for Magnetic Resonance (DRCMR), Denmark

****Correspondence:***
Bumseok Jeong
bs.jeong@kaist.ac.kr

Received: *02 October 2018*
Accepted: *10 January 2019*
Published: *29 January 2019*

Citation:
Kim D, Yoo JH, Park YW, Kim M, Shin DW and Jeong B (2019) Anatomical and Neurochemical Correlates of Parental Verbal Abuse: A Combined MRS—Diffusion MRI Study. Front. Hum. Neurosci. 13:12. doi: 10.3389/fnhum.2019.00012

INTRODUCTION

As children and adolescents remain physically and psychologically dependent, maltreatment by caregivers can have considerable consequences in both psychosocial development and brain development. A survey of 4,141 participants reported that exhibiting a greater number of lifetime anxiety disorders is associated with a higher likelihood of childhood physical and sexual abuse history (Cougle et al., 2010). In a 32-year prospective longitudinal study, exposure to adverse

psychosocial experiences such as maltreatment elevated the risk of depression in adulthood (Danese et al., 2009). In a prior study (Danese et al., 2009), incidence rate ratios indexing the association between depression risk in adulthood and childhood maltreatment were 1.81 in the definite group (having experienced two and more among five maltreatment indicators) and 1.37 in the probable group (having experienced one indicator of maltreatment). Furthermore, depression (Hovens et al., 2012; Nanni et al., 2012) and bipolar disorder (Post et al., 2015) emerge earlier in maltreated individuals, and these individuals have a more sustained or difficult treatment course. As childhood maltreatment precedes clinical states and occurs in developmental periods, one possible hypothesis is that such maltreatment experiences can modulate the structure of a person's model regarding the external world and one's self. This modulation could be reflected in the structure and function of the brain, as reported in previous studies with healthy subjects (Choi et al., 2009; Lee et al., 2015). Thus, the difficult progression of mood disorders in maltreated individuals may be more likely associated with aberrancy of a person's inner model for perception of the world rather than simply with the comorbidity of two conditions (e.g., The world around me is not safe and requires high surveillance. Life is hard on me.).

Previous neuroimaging studies in clinical patients having experienced physical or emotional maltreatment have reported anatomical, functional, and neurochemical changes in the brain. A multimodal study of bipolar disorder showed the association of severity of childhood trauma with altered prefrontolimbic functional connectivity and uncinate fasciculus fractional anisotropy (Souza-Queiroz et al., 2016). A magnetic resonance spectroscopy (MRS) study in maltreated children and adolescents with posttraumatic stress disorder (PTSD) reported a decreased N-acetyl aspartate (NAA) to creatine (Cr) ratio of the anterior cingulate cortex, indicative of neuronal loss or neuronal dysfunction (De Bellis et al., 2000). In a functional magnetic resonance imaging (fMRI) study, emotionally neglected adolescents showed blunted ventral striatum development, which predicted the emergence of depressive symptoms (Hanson et al., 2015). Regardless of comorbid psychopathology, subjects with moderate-to-high maltreatment have decreased intermodular connections in terms of network architecture (Ohashi et al., 2017). These anatomical and functional changes were also reported in healthy subjects with a history of childhood maltreatment. Young adults with parental verbal abuse (paVA) history but without significant psychopathology showed decreased fractional anisotropy in the arcuate fasciculus, the fornix, and the cingulum bundle (Choi et al., 2009) and larger gray matter (GM) volume of the left primary auditory cortex (Tomoda et al., 2011). The degree of peer verbal abuse was negatively correlated with the white matter (WM) integrity of the corpus callosum and the corona radiata (Teicher et al., 2010). Functional connectivity between the right amygdala and the rostral anterior cingulate during processing of negative emotion was associated with previous verbal abuse experience (Lee et al., 2015). This alteration of the frontolimbic circuit during emotional processing was also reported in a longitudinal sample of adults (aged from 23 to 37 years) having experienced one or more forms of maltreatment from among emotional maltreatment, physical neglect, physical abuse and sexual abuse (Jedd et al., 2015).

Neuroimaging results from previous studies in subjects with or without comorbid psychiatric disorders indicate that childhood maltreatment experiences are associated with anatomical, functional, and neurochemical alterations in the brain, including ventromedial and orbitofrontal-limbic networks, and have deleterious effects on psychopathology (Teicher and Samson, 2016). However, unless comorbid psychiatric disorders are controlled, it is difficult to disentangle which of the changes in the brain are due to maltreatment, the associated psychiatric conditions or a combination or interaction of both (Hart and Rubia, 2012).

Not all persons with a history of maltreatment experience problematic outcomes. Although there is controversy over the interpretation of maltreatment-related brain alterations, experience-dependent plastic adaptation to a threatening environment can be a plausible interpretation as well as diathesis-stress mechanism (Teicher et al., 2016). Teicher et al. (2016) suggested that alterations of frontolimbic regions in healthy subjects with maltreatment experiences may be associated with altered models of perception of the external world, such as threat detection, sensory filtering, and reward processing. Regarding previous results showing anatomical, functional, and neurochemical alterations in frontolimbic regions, evaluating the whole-brain connectivity with core brain regions and chemical properties might be beneficial to elucidate the impact of maltreatment experiences on the brain. In particular, the pregenual anterior cingulate cortex (pgACC) is highly connected with the limbic system and is thought to be one of the key regulatory regions of the frontolimbic circuit, which is implicated in emotional processing and reward processing (Etkin et al., 2011; Marusak et al., 2016). The connectivity-based segmentation of the cingulate cortex allows the identification of structural connectivity between the cingulate and the rest of the brain (Beckmann et al., 2009). Measuring the chemical concentration in a predefined volume of interest (VOI), such as the pgACC, using single-voxel proton magnetic resonance spectroscopy (^{1}H-MRS), can provide additional information that differs from that derived from diffusion tensor image (DTI). Thus, an integrated multimodal approach with ^{1}H-MRS metabolites and anatomical connectivity of the pgACC might be useful to investigate brain changes in healthy young adults with a history of emotional maltreatment, such as verbal abuse.

In the current study, we investigated whether variance in the perceived intensity of paVA during childhood and adolescence in healthy young adults with a low level of paVA is associated with both anatomical connectivity of the pgACC to the whole brain and the chemical properties of the pgACC, which is a crucial region of the frontolimbic circuit (Etkin et al., 2011). We assumed that significant predictors would show both a positive association and a negative association if neural alterations to a low level of paVA resulted from maltreatment-related adaptation. In line with the adaptation hypothesis, clinical symptoms such as

alexithymia or depression scores may not be able to be predicted with neural features.

Considering the maltreatment-related adaptation hypothesis, it is more likely that depending on the function of the tract, WM integrity may increase for some tracts, while WM integrity may decrease for other tracts. In functional studies, for example, a study on reward processing reported decreased striatum activity in maltreated subjects (Dillon et al., 2009), while another study reported a maltreatment-related amygdala hyperresponse during negative emotional processing (Dannlowski et al., 2012). However, most previous studies on WM alterations in maltreated subjects have reported a reduction in the number of fiber streams (Ohashi et al., 2017) or decreased WM integrity assessed by decreased fractional anisotropy or increased radial diffusivity (Eluvathingal et al., 2006; Choi et al., 2009; Rodrigo et al., 2016). Greening and Mitchell (2015) reported a positive association between structural connectivity and trait anxiety using seed-based probabilistic tractography. Compared with the whole-brain approach, the seed-based connectivity approach can provide specific information of tracts (Greening and Mitchell, 2015). To achieve our goals, we exploited partial least square regression (PLSR) with data acquired from probabilistic tractography and ^{1}H-MRS of the pgACC. Because recent studies described a reliable prediction model for various dimensions of psychiatric symptoms or cognitive performance using anatomical or functional connectivity (Greening and Mitchell, 2015; Meskaldji et al., 2016; Rosenberg et al., 2016; Yoo et al., 2018), we focused on the effect of paVA rather than on effects of confounding factors such as current psychopathology on the medial frontolimbic circuit.

MATERIALS AND METHODS

Participants

We recruited 51 young adults from Korea Advanced Institute of Science and Technology (KAIST). The subjects were interviewed by skilled psychiatrists (DK and JY) using the Korean version of the Diagnostic Interview for Genetic Studies (DIGS-K version 2.0; Joo et al., 2004). Two subjects were excluded because of incomplete self-report questionnaires and structured interviews. The remaining subjects had no history of psychiatric or neurological illness or of other types of abuse, such as physical abuse or sexual abuse. Subjects also underwent MRI scans consisting of T1-weighted (T1w) imaging, ^{1}H-MRS, DTI, and resting and task-related fMRI (fMRI data are not reported here). After the quality control process, an additional three subjects were excluded because of excessive motion on DTI (N = 2) and poor spectrum fitting of ^{1}H-MRS (N = 1; see section "Quality Control" in the "Materials and Method" section). Finally, 46 subjects (mean age = 24.1 ± 4.2 years, male:female = 29:17, total intelligence quotient = 120.5 ± 9.6) were included in the further analysis. All procedures performed in this study involving human participants were in accordance with the ethical standards of the Institutional Review Board of KAIST and with the 1964 Helsinki declaration and its later amendments or comparable ethical standards. All participants signed informed consent. The Korean version of the verbal abuse questionnaire (VAQ; Teicher et al., 2006; Jeong et al., 2015) was used to measure the perceived severity of paVA experiences during the subjects' childhood and adolescence. The VAQ is composed of 15 items covering scolding, yelling, swearing, blaming, insulting, threatening, demeaning, ridiculing, criticizing, and belittling. Perceived severity was reported using an 8-point Likert scale from 0 (not at all) to 7 (everyday). The Korean version of the VAQ was successfully used in our previous studies for adolescents and young adults (Jeong et al., 2015). A VAQ score above 40 delineates a level of verbal abuse that is unusually high in both North American and Korean populations. The group averaged VAQ score was 7.0 (SD = 6.7, range = 0–29). Accompanying psychiatric disorders could make difficult to disentangle which of the changes of the brain are due to maltreatment or associated psychiatric conditions. The recruitment of subjects with high VAQ scores but without an accompanying psychiatric disorder could possibility introduce a type of selection bias considering the aspect of resilience. Thus, here, we enrolled subjects with VAQ scores below 40. There was no gender difference in the VAQ score ($Mean_{male}$ = 6.6, $Mean_{female}$ = 7.7, t = −0.56, p-value = 0.57). Because self-report questionnaires including the VAQ rely on recall and subjectivity, such questionnaires may reflect a person's inner model for perception of their maltreatment-related experience rather than accurate intensity of maltreatment. Thus, we assumed that the VAQ score represents the perceived intensity of paVA experiences in their childhood and adolescence. In addition to the VAQ, subjects were also asked to fill out self-report questionnaires such as the Center for Epidemiological Studies–Depression (CES-D, mean ± SD = 9.33 ± 6.8) questionnaire and the Toronto alexithymia scale (TAS, mean ± SD = 43.7 ± 10.4) questionnaire.

MRI and MRS: Data Acquisition

Data acquisition was performed using a Siemens 3T Verio scanner (Erlangen, Germany) at KAIST. High resolution T1w structural images (MPRAGE, TR/TE/TI: 2,400 ms/2.02 ms/1,000 ms, flip angle: 8°, FOV: 224 × 224 mm, voxel size: 0.7 × 0.7 × 0.7 mm^3) were acquired from the participants. After structural image acquisition, shimming was performed using FASTESTMAP, and water suppression pulses were calibrated for ^{1}H-MRS. Single-voxel ^{1}H-MRS using semilocalization by adiabatic selective refocusing (sLASER, TR/TE = 5,000 ms/28 ms, 64 scans, 2,048 complex points were acquired from VOI (size = 20 × 15 × 20 mm^3) within pgACC (**Figure 1**), which was manually positioned by a psychiatrist or a neurologist (DK, JY, and DS). The sLASER sequence has advantages in terms of maintaining a relatively uniform B1 field and a desired flip angle within voxels (Zhu and Barker, 2011). In the sagittal view, the VOI was placed at the front of the genu of the corpus callosum. In coronal and axial views, the VOI was positioned at the midline of the pgACC to cover the maximum volume of GM in the region (**Figure 1**). Unsuppressed water signals were also

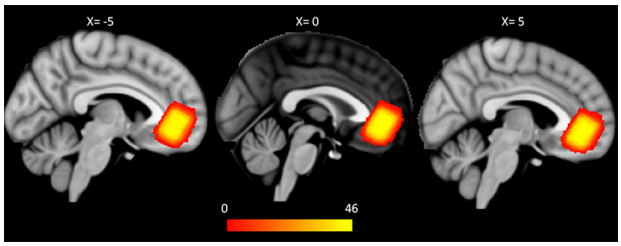

FIGURE 1 | Group-wise pgACC VOI for magnetic resonance spectroscopy (MRS). Each binary mask for the pgACC VOI was transformed from native T1 space to the MNI 1 mm space. The VOIs partly overlap the mOFC and the rACC on the DKT atlas in all of the subjects. The color bar represents the number of overlapped VOIs of the subjects (pgACC, pregenual anterior cingulate cortex; VOI, volume of interest; mOFC, medial orbitofrontal cortex; rACC, rostral anterior cingulate cortex; DKT, Desikan-Killiany-Tourville).

collected to preprocess the data, such as eddy current and phase correction.

Participants additionally underwent DTI scanning. The diffusion images were acquired with a multiband protocol (TR/TE: 5,520 ms/94.2 ms, voxel size: $2 \times 2 \times 2$ mm^3, multiband factor = 4). The acquired multi *b*-value diffusion-weighted images consisted of two B0 images (b factor = 0 s/m^2) with opposite phase encoding directions (from right to left and from left to right) and 30 diffusion-weighted images for each *b*-value (1,000, 1,500, 2,000 s/m^2).

MRI and MRS Data Preprocessing

Quality Control

The diffusion data were corrected for motion artifacts and eddy current-induced distortion by using the *topup* (Andersson et al., 2003) and *eddy* (Andersson and Sotiropoulos, 2016) functions of the FMRIB Software Library (FSL[1]). To estimate the susceptibility off-resonance field, two B0 images with right-to-left and left-to-right phase encoding directions were used.

The preprocessing pipeline for ^{1}H-MRS data consisted of eddy current correction, frequency correction using a cross-correlation algorithm and phase correction using the least square algorithm, part of MRspa software (version 1.5e[2]). Taking into account the CSF fraction within the VOI, the metabolite concentrations were estimated using LCModel software version 6.3-1J (Provencher, 1993) and a basis set (Deelchand et al., 2015). The estimates with Cramèr-Rao lower bounds (CRLB) of less than 20% were considered reliable (Ip et al., 2017). Five of the metabolites—NAA + NAA-gluatamate (total NAA), myo-inositol, glutamate + glutamine (Glx), total choline (Glycerylphosphorylcholine + Phosphorylcholine), and total Cr (Cr + phosphocreatine)—met the CRLB criterion (**Supplementary Table S1** in Supplementary Material).

Visual inspection and preprocessing step described above, we conducted a further investigation for quality control. We investigated the LCModel fitting signal-to-noise ratio (SNR) and motion parameters for the MRS and diffusion data, respectively. In the diffusion data, motion parameters were defined as root mean squares (RMS) of displacements across intracerebral voxels (Andersson and Sotiropoulos, 2016). Among the RMS of motion of 90 diffusion-weighted images (30 directions for each *b*-value), we took the maximum value as the motion parameter of each subject. One subject was excluded due to an LCModel signal-to-noise ratio (SNR) <10, and two subjects were excluded due to a maximum RMS of motion >3 (**Supplementary Figure S1** in Supplementary Material).

Anatomical Consistency Among Individuals' VOIs

In this study, VOIs of ^{1}H-MRS were used not only as positions for metabolite quantification but also as seeds for probabilistic tractography. Thus, the anatomical consistency of VOIs across subjects must be assessed. Transformation matrices for each subject were acquired for transformation of B0 to T1w images to the standard 1 mm^3 Montreal Neurological Institute (MNI) space using Advanced Normalization Tools (ANTs[3]). Then, each subject's VOI was transformed from the subject's T1w space to the standard space using the transformation matrix. Finally, the generalized dice similarity coefficient as a measure of overlap was computed from the intersection and union of VOIs (Crum et al., 2006; Park et al., 2018). The generalized dice coefficient of VOIs of 46 subjects was 0.71 (**Figure 1**). Because a dice similarity coefficient of 0.7 or greater is regarded as excellent agreement for similarities between pairs (Zou et al., 2004; Crum et al., 2006), our data can be considered reliable for anatomical consistency.

Network Construction With Probabilistic Tractography From pgACC VOI to Whole Brain

Individual cortical Desikan-Killiany-Tourville (DKT) and subcortical parcellation images, which consist of 76 regions (**Supplementary Table S2** in Supplementary material), were obtained from T1w images using the pipeline of the Freesurfer software[4]. Then, the parcellated image in each subject was transformed to the DTI space using the transformation matrix acquired from the ANTs algorithm. Using the GM-WM boundary shell (Bonilha et al., 2015), target masks were defined as the boundary shell within the cortical DKT atlas and the subcortical atlas. Seed masks were defined as voxels in the VOI that overlapped with the boundary shell. Among the 76 DKT target regions, the medial orbitofrontal cortex (mOFC) and the rostral cingulate cortex of the bilateral hemisphere were excluded because the seed regions (i.e., VOI for MRS) occupied the two regions bilaterally in 46 subjects. After Bayesian estimation of diffusion parameters at each voxel of the diffusion image exploiting FSL bedpostX, probabilistic tractography (Behrens et al., 2007) was performed in the diffusion space. To determine the connectivity map from the pgACC VOI with the rest of the brain, we adapted the method introduced by Greening and Mitchell (2015). Connectivity frequency maps to the target regions were generated while avoiding the ventricle mask of each subject. To generate the frequency map, 25,000 samples were initiated within the seed voxels (step length = 0.5, step size = 1,000, curvature threshold = 0.2). Finally,

[1]https://fsl.fmrib.ox.ac.uk/fsl
[2]https://www.cmrr.umn.edu/downloads/mrspa/
[3]http://stnava.github.io/ANTs/
[4]https://surfer.nmr.mgh.harvard.edu/

we generated 72 likelihood maps of seed-target connectivity for each subject and then took the average value within the connectivity likelihood map of each target region of interest (ROI) in the subject diffusion space for the connectivity feature of the prediction model. The processing step of diffusion data is summarized in **Supplementary Figure S2** in Supplementary Material.

Statistical Analysis

The analysis was performed using 72 connectivity and five chemical features. For problems with high dimension (p) and small sample size (n) for which $p > n$, PLSR is useful for predicting behavior from neuroimaging data (Krishnan et al., 2011). We used the PLSR algorithm (for more details, see supplementary methods in Supplementary Material) implemented in the *pls* package (Mevik and Wehrens, 2007) of R 3.4.3 software[5]. PLSR benefits from dimension reduction by using few components (Meskaldji et al., 2016). Compared with principal component analysis, PLSR finds components from a predictor, which can predict dependent variables (Abdi, 2010). All features were scaled across subjects (features were converted to value between 0 and 1) within the training set using the "scale" option in the *plsr* function in the *pls* package. To find the optimal number of components, bootstrap resampling was performed 100,000 times. For each iteration, PLSR was performed using a bootstrapped sample, and then the root mean squared error of prediction (RMSEP) of each number of components from 0 to 20 was obtained. RMSEP corresponding to each number of components was defined as the median value of RMSEP values acquired from 100,000-time resampling.

The PLSR model with the optimal number of components was built on data from 45 subjects and tested with the remaining one subject [i.e., leave-one-out cross validation (LOOCV)], and this process was repeated for all 46 subjects (**Figure 2**). To evaluate the significance of the model, a correlation analysis between the reported VAQ value and the predicted VAQ value was performed. We repeated the evaluation process for 100,000 permutations, shuffling the VAQ scores across the subjects to estimate the significance of the PLSR model. For each permutation, Pearson's correlation coefficient (r) between the predicted and shuffled VAQ score was obtained to generate a nonparametric distribution. The significance was evaluated by: (1) ranking the coefficient value of the PLSR model using the original data among the generated distribution; and (2) estimating the cross-validated prediction R^2, which is given by

$$R^2 = 1 - \frac{\text{Residual estimated sum of square for prediction (PRESS)}}{\text{Total sum of square (SST)}}$$

We compared the predictive ability of two PLSR models each incorporating a single modality (MRS alone and tractography alone) with the predictive ability of the multimodality PLSR model. Then, we use the jackknife test to approximate the t-test of the regression coefficient for the identification of significant features. The significance of features was determined at a p-value < 0.05. We performed additional PLSR using CES-D or TAS as a dependent variable to explore whether brain alteration is associated with psychopathology, such as depression or alexithymia. In the PLSR, CES-D score and TAS score were used as dependent variables, and both the connectivity features of 72 variables and the chemical features of five variables were used as independent variables, similar to the PLSR model for the VAQ score described above.

Furthermore, the prediction results were validated using different cross-validation schemes (i.e., five-fold, and 10-fold cross validation). Because the number of total subjects ($N = 46$) is not a multiple of 5 or 10, the subjects were divided into six groups of five subjects and four groups of four subjects for 10-fold cross validation and divided into one group of 10 subjects and four groups of nine subjects for five-fold cross validation. There are a number of ways to divide subjects into training sets and test sets; therefore, we repeated the process 10,000 times. The accuracy of the prediction was assessed using the mean of the cross-validated prediction R^2 for each process.

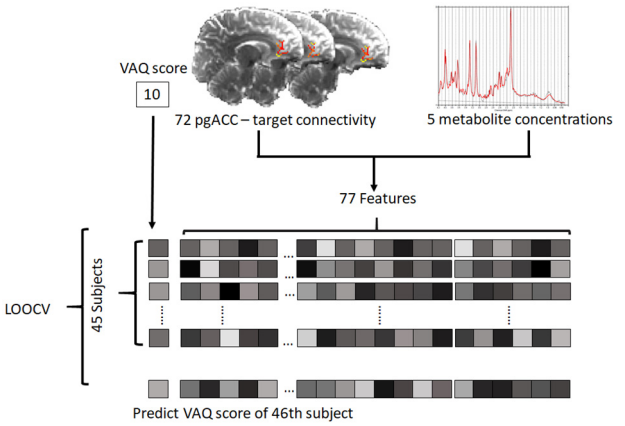

FIGURE 2 | Schematic of the prediction model. For each subject, 72 connectivity features and five metabolite features were defined as predictors. The predictive model was trained on data from 45 subjects and tested with the remaining subject. The test was performed iteratively for all subjects (pgACC, pregenual anterior cingulate cortex; LOOCV, leave-one-out cross validation; VAQ, verbal abuse questionnaire).

RESULTS

Prediction Performance of the Model

The RMSEP plot represents the optimal number of components of the three PLSR models that include chemical properties, anatomical connectivity, and both anatomical connectivity and chemical properties, respectively (**Figure 3**). According to the plots, the optimal number of model components, corresponding to the lowest RMSEP value, was 2 in all three models. The model with two components of anatomical connectivity and the MRS chemical property of pgACC VOIs significantly outperformed the models trained on shuffled data (permutation $p = 8.9 \times 10^{-4}$, **Figure 4**). Pearson's correlation between the predicted VAQ and the self-reported VAQ was significant ($r = 0.53$, $p = 1.2 \times 10^{-4}$, **Figure 4**), and the estimated prediction R^2 was 0.23 (for

[5]https://www.r-project.org/

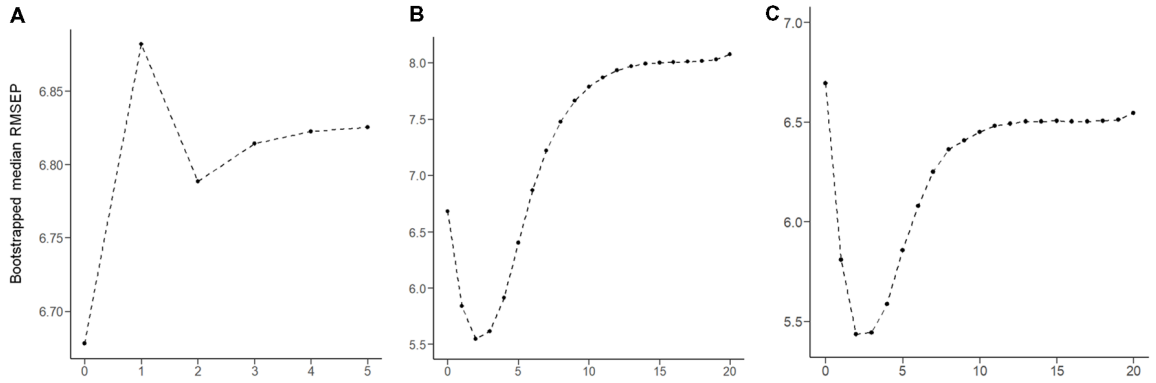

FIGURE 3 | Root mean squared error of prediction (RMSEP) plot produced for 100,000 bootstrap resampling iterations. For each iteration, RMSEP values of the partial least square regression (PLSR) model were obtained. The median RMSEP corresponding to each component is depicted. **(A)** PLSR model trained on the chemical properties of five features. **(B)** PLSR model trained on the connectivity of 72 features. **(C)** PLSR model trained on 77 features of both connectivity and chemical properties.

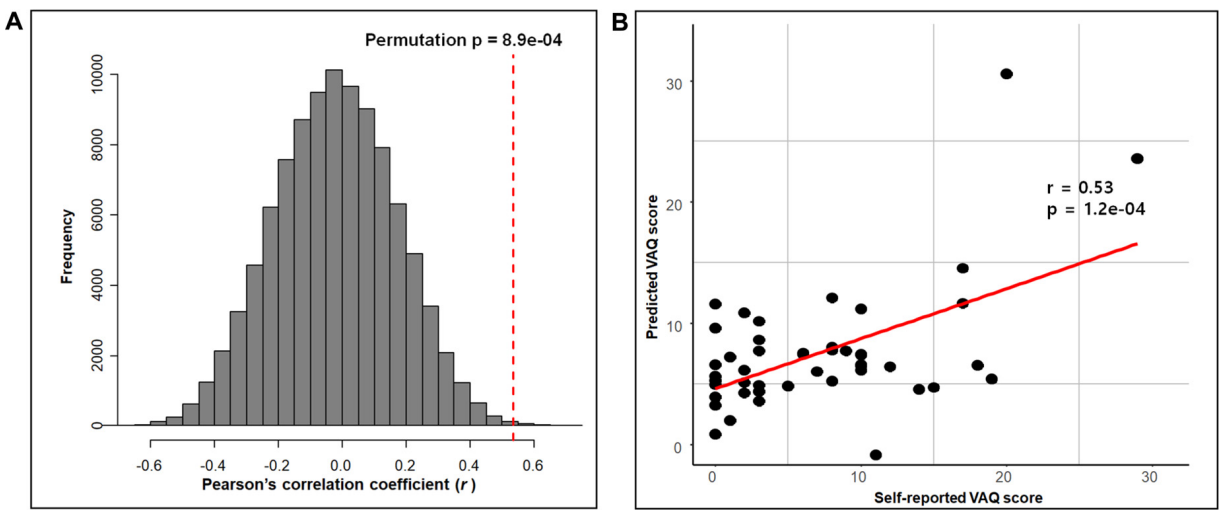

FIGURE 4 | Prediction performance of the PLSR model with both connectivity and chemical properties of the pgACC. **(A)** The performance of the PLSR model tested by comparing the models trained on the shuffled data with 100,000 iterations. The red-dashed line represents the correlation coefficient between the self-reported VAQ score and the predicted VAQ score. For each iteration, the correlation coefficient between the shuffled VAQ score and the predicted VAQ score trained on the shuffled data was calculated. **(B)** Scatter plot of the self-reported VAQ score and the predicted VAQ score using the model. Predicted values were obtained using leave-one-out testing. We perform a correlation analysis between the predicted value and the self-reported value. The correlation coefficient was 0.53 (p = 1.2e-04).

validation test of the relationship, see Supplementary Material). The R^2 of the PLSR model trained on anatomical connectivity alone was 0.20, while the PLSR model trained on chemical properties did not have predictive ability (R^2 = −0.18). TAS and CES-D scores could not be predicted using the PLSR models trained on pgACC connectivity or chemical properties (R^2 = −0.35 and −0.56, respectively, **Supplementary Figure S3** in Supplementary Material).

Significant Features

Given that the model could predict paVA experience from the connectivity and chemical properties of the pgACC VOI, we sought to determine which features make a reliable contribution to the PLSR model. To identify these features, we used the jackknife test (for more details, see Supplementary Material) to estimate t-scores and p-values corresponding to the coefficients of features (**Figure 5**, **Table 1**, **Supplementary Table S3** and **Supplementary Figure S4** in Supplementary Material). The jackknife test showed that a high paVA score was negatively associated with pgACC connectivity with the right caudate, pgACC connectivity with the right transverse temporal cortex and myo-inositol concentration. Additionally, we found that pgACC connectivity with the left pars triangularis, with the left cuneus, with the right inferior temporal cortex, with the right entorhinal cortex and with the right amygdala were positively associated with VAQ score.

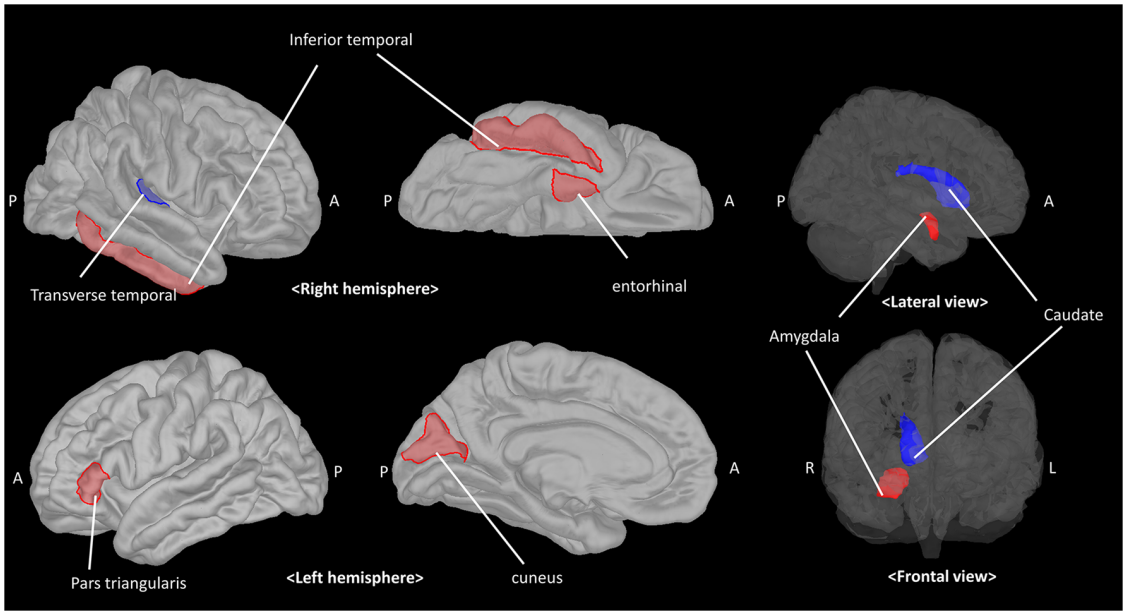

FIGURE 5 | The pgACC connectivity features contributing to predicting the parental verbal abuse (paVA) score in the PLSR model. Red and blue patches represent target brain regions with significantly positive and negative coefficients, respectively. The estimated coefficient for each target is described in **Table 1** (pgACC, pregenual anterior cingulate cortex; PLSR, partial least square regression; A, anterior; P, posterior; R, right; L, left).

Validation of the Prediction Model Using Different Cross-Validations

The mean cross-validated prediction R^2 was 0.05 [range: −3.74 to 0.41] and 0.16 [range: −1.92 to 0.39] for five-fold cross-validation and 10-fold cross-validation, respectively. Five-fold cross-validation had 7,818 predictable cases ($R^2 > 0$) and 10-fold cross validation had 9,636 predictable cases ($R^2 > 0$) among the 10,000 iterations. A histogram of prediction R^2 values in each validation procedure (**Supplementary Figure S5** in Supplementary Material) showed that prediction accuracy was also maintained when different cross-validation schemes were used.

DISCUSSION

Using multimodal neuroimaging data consisting of the structural connectivity and chemical properties of the pgACC, we found significant association between perceived paVA and frontolimbic properties (cross-validated prediction R^2 = 0.23). On the other hand, psychopathology scores, such as depressive symptoms (CES-D) or alexithymia (TAS), were not associated with the frontolimbic alterations. In other words, these structural and chemical alterations of the brain may reflect perceived paVA rather than psychopathology. These findings suggest that the significant neurobiological features found in our study may be attributed to individual experiences, such as perceived intensity to paVA experience.

TABLE 1 | Features significantly contributing to the model for predicting perceived parental verbal abuse.

Features	Coefficient	Standard error	*t*-value	*p*-value
Right caudate	−0.780	0.366	−2.166	0.045
Right transverse temporal cortex	−0.719	0.345	−2.118	0.042
Myo-inositol	−0.768	0.335	−2.13	0.026
Right entorhinal	0.620	0.236	2.591	0.014
Left pars triangularis	0.703	0.212	3.258	0.003
Right inferior temporal cortex	0.781	0.323	2.377	0.024
Left cuneus	0.764	0.37	2.086	0.044
Right amygdala	0.808	0.322	2.478	0.018

The significantly contributing predictors in our study were consistent with the findings of previous neuroimaging studies of mentally healthy subjects (Choi et al., 2009; Dannlowski et al., 2012; Lee et al., 2015). Specifically, our results showing negative associations with perceived paVA suggest that more verbal abuse experience is associated with altered glial function indicated by lower myo-inositol concentration (Chang et al., 2013) and reduced pgACC connectivity with regions associated with auditory processing, the transverse temporal gyrus, and regions associated with reward processing, such as the caudate. Although most prior studies on maltreatment have reported a negative relationship between WM connectivity and the severity of maltreatment (Eluvathingal et al., 2006; Choi et al., 2009, 2012; Rodrigo et al., 2016), few studies reported positive association between maltreatment and WM tract (Hanson et al., 2013; Ugwu et al., 2015). We also found predictors showing a positive association with perceived paVA. Interestingly these predictors indicate connectivity of the pgACC with regions involved in threat detection, such as the amygdala, and with alertness, such as the cingulate-inferior frontal gyrus pathway (Sadaghiani and D'Esposito, 2015; Coste and Kleinschmidt,

2016). These findings revealing alterations of the frontolimbic region even in subjects with a mild intensity of perceived paVA below 40 suggest that the effect of maltreatment on the frontolimbic circuit is an adaptation to the external environment.

Many recent studies have attempted to predict cognitive performance or psychopathology using connectivity features (Greening and Mitchell, 2015; Rosenberg et al., 2016; Yoo et al., 2018). The significant prediction features not only contribute to accurate prediction but also demonstrate neurobiological background. Greening and Mitchell (2015) reported a prediction model for trait anxiety using the structural connectivity value from the amygdala to the rest of the brain based on the neurobiological background of anxiety. Because structural connectivity can be indicative of functional connectivity and can be affected by experience (May, 2011; Hermundstad et al., 2013), the perceived intensity of paVA can be reliably predicted using the pgACC connectivity value alone. However, the PLSR model trained on both connectivity and metabolite concentration offered a slight numerical advantage over the PLSR model trained with a single modality. Chemical properties can also be affected by psychiatric disorders and experiences and are associated with brain structure (Coupland et al., 2005; Zheng et al., 2010; Forde et al., 2018). Chemical properties also provide additional information, such as information on glial function and cytoarchitecture (Chang et al., 2013; Forde et al., 2018), compared with DTI tractography. Therefore, chemical properties may provide more neurobiological information and contribute to the accuracy of the prediction model.

We demonstrate that pgACC myo-inositol is negatively associated with perceived paVA experience. It is well-known that stress-induced neural alterations likely depends on specific characteristics of the brain regions such as hippocampus (Heim et al., 2008). In a MRS study with major depressive disorder patients, blood cortisol showed significant negative correlation with myo-inositol levels and dehydroepiandrosterone-sulfate (DHEAS) displayed a significant negative relation with glutamate levels in right hippocampus, but not mPFC (Shirayama et al., 2017). Unlike the cortisol response, which decreased after repeated exposure to the stressor, the DHEAS response concentrations increase in response to both acute and chronic (repeated) stress in a primate study (Maninger et al., 2010). Thus, it is controversial the direct linkage between stress-induced excitotoxicity and the reduced myo-inositol in pgACC of subjects having PaVA exposure experience. Rather, this finding supports previous studies implicating myo-inositol in maltreatment or other biological or mechanistic alteration. In a mouse study, myo-inositol was decreased in the prefrontal cortex of mice that experienced social isolation (Corcoba et al., 2017). Few studies have investigated the effect of maltreatment *per se* on the chemical properties of the human brain, but several studies have investigated the relationship between the chemical properties of the brain and psychopathology. The myo-inositol to Cr ratio was reduced in adult depression patients with and without childhood trauma history (Coupland et al., 2005), while the NAA to Cr ratio was lower in maltreated subjects with posttraumatic stress disorder (PTSD; De Bellis et al., 2000). Decreased myo-inositol can be found in the prefrontal and cingulate regions of subjects with depressive disorder (Frey et al., 1998; Gruber et al., 2003; Coupland et al., 2005; Zheng et al., 2010), whereas other studies reported unchanged myo-inositol concentrations in depression patients (Auer et al., 2000; Farchione et al., 2002). Depression-related myo-inositol decrease was found in young adult subjects; thus, inconsistent results may be attributed to the confounding effect of age (Coupland et al., 2005; Zheng et al., 2010). Because myo-inositol measured by ^{1}H-MRS is considered a biomarker for glia in many studies (Chang et al., 2013; Harris et al., 2015; Plitman et al., 2015), the decrease suggests altered glial function. Myo-inositol concentration is associated with maintenance of osmotic concentration (Rango et al., 2008) or cerebral metabolism (Weissenborn et al., 2007). Further, the hypo-osmolarity or its induced brain edema is a possible mechanism of the reduced myo-inositol in minimal hepatic encephalopathy which has no overt cognitive impairment (Kooka et al., 2016). Thus, biological changes in osmotic homeostasis, or brain metabolism may be also a possible explanation of our finding, the negative association of myo-inositol concentration in the pgACC with paVA.

We observed that several structural connectivities of the pgACC were negatively associated with perceived paVA experience. These connectivities include the connectivity of the pgACC with the right caudate and with the transverse temporal gyrus. Structural connectivity between the pgACC and the caudate can be considered part of the reward system. A task fMRI study on adults with childhood maltreatment history reported a blunted response to reward cues, decreased activity of the pallidum, and an association between childhood adversity and symptoms of anhedonia (Dillon et al., 2009). Other task fMRI studies have consistently reported decreased striatal responses to anticipated reward in maltreated individuals. Adolescent who experienced deprivation and adoption also showed reduced recruitment of the striatal reward system in an fMRI study (Mehta et al., 2010). A recent longitudinal fMRI study revealed that changes in ventral striatum activity were negatively correlated with the severity of emotional neglect (Hanson et al., 2015). These results are consistent with our findings. Blunted reward sensitivity makes people choose avoidance in approach-avoidance conflict to remain in a safe environment (Guyer et al., 2006; Teicher et al., 2016). The reduced connectivity in this study may be considered a potential protective adaptation to threatening environments, but further studies are needed to confirm this hypothesis.

Another novel observation that we observed was that weaker pgACC connectivity with the auditory cortex was related to paVA experience. Studies have reported changes in the cortical sensory region and tract associated with exposure to various types of maltreatment. The WM integrity of the left arcuate fasciculus associated with language processing was decreased in subjects with paVA (Choi et al., 2009). A similar voxel-based morphometry study revealed that young adults with repeated paVA have altered GM density in the primary auditory cortex within the superior temporal gyrus (Tomoda et al., 2011).

Another study reported that decreased cortical thickness of the somatosensory cortex was associated with tactile sensation of the genital area in women with a childhood sexual abuse history (Heim et al., 2013). Another study of young adults who had suffered from witnessing interparental violence during their childhood revealed that these subjects had decreased WM integrity in the inferior longitudinal fasciculus, which connects visual association regions to temporal regions (Choi et al., 2012). Alterations of brain regions associated with primary sensory processing may reduce the specific type of distressing stimulus (i.e., maltreatment) and may be a potentially protective effect. However, further studies are needed to confirm this hypothesis.

We found that some patterns of connectivity of the pgACC with other regions are positively associated with VAQ score. From the perspective of the adaptation hypothesis (Belsky and Pluess, 2009; Teicher et al., 2016), this finding regarding pgACC connectivity has significant implications. This positive association of maltreatment-related brain changes with paVA suggests the experience-related plastic adaptation rather than diathesis-stress mechanism. Furthermore, as maltreatment-related experiences can be accepted as threats to survival, the strengthening of structure or functions of the brain may provide advantages in survival in aspect of the experience-related plastic adaptation. We found that structural connectivity between the pgACC and limbic regions was positively related to perceived paVA experience. The target regions of the connectivity included the amygdala and the entorhinal cortex. A recent study reported an inverse relationship between activities in the prefrontal region and the amygdala during the processing of a negative emotional stimulus (Amting et al., 2010). Increased functional connectivity between the rostral ACC and the amygdala is associated with emotional resilience (Kaiser et al., 2018). An association between WM connectivity and functional connectivity of these regions was reported (Lapate et al., 2016). Strong structural connectivity between the PFC region and the amygdala facilitates the easy processing of emotional stimuli and may protect against deleterious outcomes such as anxiety (Greening and Mitchell, 2015; Lapate et al., 2016). Therefore, our results suggest that stronger connection between the pgACC and the amygdala may be a consequence of developmental adaptation to maltreatment.

We also observed that paVA experience is associated with stronger connectivity between the pgACC and the inferior frontal region, such as the pars triangularis. This result is consistent with the framework of the plastic adaptation hypothesis. High cognitive performance, especially attention and alertness, is helpful for survival and adaptation. Several fMRI studies revealed a role of the cingulo-opercular network in the maintenance of attention-related cognitive processing (Dosenbach et al., 2008; Sadaghiani and D'Esposito, 2015; Coste and Kleinschmidt, 2016). Alertness can be defined as requiring cognitive resources, maintaining attention, and preparing to respond with less prior information. Those who experienced paVA have attempted to maintain their attention and prepare appropriate responses under repetitive negative stimuli. In this alert state, cingulo-opercular networks may be frequently induced. One possible interpretation is that in individuals who have experienced verbal abuse experience, an induced functional network, which is associated with negative emotional processing and maintenance of alertness, may enhance the structural network in the cingulate-limbic region and the cingulo-opercular region through plastic alterations, such as through a Hebbian process.

The connectivity of the pgACC with the right inferior temporal cortex and the left cuneus was positively associated with paVA experience. Although the significance of the association remains elusive, recent research can provide some clues. White matter integrity (assessed by fractional anisotropy) of the inferior fronto-longitudinal fasciculus (IFOF) in patients with trauma is correlated with emotional prosody and facial affect recognition (Schmidt et al., 2013; Genova et al., 2015), and the microstructure of the IFOF predicted emotional recognition performance (Unger et al., 2016). The pgACC connectivity may be part of the IFOF, which begins in occipital region and terminates in the frontal region via the temporal lobe. The IFOF plays roles in facial recognition, semantic memory, and emotional recognition. One possibility is that stronger IFOF connectivity is associated with more severe paVA experience to detect the caregiver's emotion. Furthermore, considering the function of the cuneus and the inferior temporal cortex in visual recognition (Kravitz et al., 2013), strengthening this connectivity may be helpful for detecting emotional expressions, such as facial expressions.

The retrospective evaluation of paVA in a cross-sectional analysis of a cohort of subjects is a key limitation that risks the inclusion of recall bias in the results, although this bias could be related to the effect of emotional maltreatment on one's inner model of perception of the world during his or her development. In addition, as we did not perform behavioral experiments associated with brain alterations, such as threat detection or reward processing, our neuroimaging results should not be interpreted as direct evidence of behavioral alterations. Subsequent work involving behavioral experiments may further elucidate the maltreatment-related adaptation hypothesis. Brain structures other than the pgACC, such as the corpus callosum and the hippocampus, are also associated with maltreatment (Teicher et al., 2010; Lee et al., 2018). Because we focused on pgACC-related regions as significant features for perceived paVA, the other structures were not considered. Although we cannot use interhemispheric connections as features of the model because of the limitations of our methodology, focusing on the medial frontolimbic circuit may be meaningful when considering the neurobiological background of maltreatment. However, it is necessary to investigate other prediction models using other seed regions, such as the hippocampus or the amygdala, in future studies. In addition, both low intensity of paVA and the modest sample size leads low variability and can reduce statistical power. Thus, further validation studies with independent larger samples including subjects with high intensity of paVA are also needed.

CONCLUSION

Despite several limitations, this combined MRS and diffusion MRI study demonstrating the association of medial frontolimbic networks with a low level of paVA in healthy young adults indicates that exposure to emotional maltreatment, even at mild intensity, by key caregivers during childhood

and adolescence can impact the development of brain circuits associated with reward, auditory, and emotional information processing.

AUTHOR CONTRIBUTIONS

BJ, DK and JY designed research; YP, DK and DS acquired diffusion image and MRS data; YP and DK preprocessed MRS data; DK and MK preprocessed diffusion image; DK and JY interviewed the participants for past history; DK performed statistical analysis; BJ and DK wrote the manuscript.

FUNDING

This research was supported by the Brain Research Program through the National Research Foundation of Korea (NRF) funded by the Ministry of Science & ICT (NRF-2016M3C7A1914448 and NRF-2017M3C7A1031331) and by BK21 Plus Fund (22A20151313464). Institute of Information & Communications Technology Planning & Evaluation (IITP) grant funded by the Korea government (MSIT-2017-0-00780 to BJ).

ACKNOWLEDGMENTS

The authors wish to acknowledge H. W. Park for helping data acquisition.

SUPPLEMENTARY MATERIAL

The Supplementary Material for this article can be found online at: https://www.frontiersin.org/articles/10.3389/fnhum.2019.00012/full#supplementary-material

REFERENCES

Abdi, H. (2010). Partial least squares regression and projection on latent structure regression (PLS Regression). *Wiley Interdiscip. Rev. Comput. Stat.* 2, 97–106. doi: 10.1002/wics.51

Amting, J. M., Greening, S. G., and Mitchell, D. G. (2010). Multiple mechanisms of consciousness: the neural correlates of emotional awareness. *J. Neurosci.* 30, 10039–10047. doi: 10.1523/JNEUROSCI.6434-09.2010

Andersson, J. L. R., Skare, S., and Ashburner, J. (2003). How to correct susceptibility distortions in spin-echo echo-planar images: application to diffusion tensor imaging. *Neuroimage* 20, 870–888. doi: 10.1016/s1053-8119(03)00336-7

Andersson, J. L. R., and Sotiropoulos, S. N. (2016). An integrated approach to correction for off-resonance effects and subject movement in diffusion MR imaging. *Neuroimage* 125, 1063–1078. doi: 10.1016/j.neuroimage.2015.10.019

Auer, D. P., Putz, B., Kraft, E., Lipinski, B., Schill, J., and Holsboer, F. (2000). Reduced glutamate in the anterior cingulate cortex in depression: an *in vivo* proton magnetic resonance spectroscopy study. *Biol. Psychiatry* 47, 305–313. doi: 10.1016/s0006-3223(99)00159-6

Beckmann, M., Johansen-Berg, H., and Rushworth, M. F. (2009). Connectivity-based parcellation of human cingulate cortex and its relation to functional specialization. *J. Neurosci.* 29, 1175–1190. doi: 10.1523/JNEUROSCI.3328-08.2009

Behrens, T. E., Berg, H. J., Jbabdi, S., Rushworth, M. F., and Woolrich, M. W. (2007). Probabilistic diffusion tractography with multiple fibre orientations: what can we gain? *Neuroimage* 34, 144–155. doi: 10.1016/j.neuroimage.2006.09.018

Belsky, J., and Pluess, M. (2009). Beyond diathesis stress: differential susceptibility to environmental influences. *Psychol. Bull.* 135, 885–908. doi: 10.1037/a0017376

Bonilha, L., Gleichgerrcht, E., Nesland, T., Rorden, C., and Fridriksson, J. (2015). Gray matter axonal connectivity maps. *Front. Psychiatry* 6:35. doi: 10.3389/fpsyt.2015.00035

Chang, L., Munsaka, S. M., Kraft-Terry, S., and Ernst, T. (2013). Magnetic resonance spectroscopy to assess neuroinflammation and neuropathic pain. *J. Neuroimmune Pharmacol.* 8, 576–593. doi: 10.1007/s11481-013-9460-x

Choi, J., Jeong, B., Polcari, A., Rohan, M. L., and Teicher, M. H. (2012). Reduced fractional anisotropy in the visual limbic pathway of young adults witnessing domestic violence in childhood. *Neuroimage* 59, 1071–1079. doi: 10.1016/j.neuroimage.2011.09.033

Choi, J., Jeong, B., Rohan, M. L., Polcari, A. M., and Teicher, M. H. (2009). Preliminary evidence for white matter tract abnormalities in young adults exposed to parental verbal abuse. *Biol. Psychiatry* 65, 227–234. doi: 10.1016/j.biopsych.2008.06.022

Corcoba, A., Gruetter, R., Do, K. Q., and Duarte, J. M. N. (2017). Social isolation stress and chronic glutathione deficiency have a common effect on the glutamine-to-glutamate ratio and myo-inositol concentration in the mouse frontal cortex. *J. Neurochem.* 142, 767–775. doi: 10.1111/jnc.14116

Coste, C. P., and Kleinschmidt, A. (2016). Cingulo-opercular network activity maintains alertness. *Neuroimage* 128, 264–272. doi: 10.1016/j.neuroimage.2016.01.026

Cougle, J. R., Timpano, K. R., Sachs-Ericsson, N., Keough, M. E., and Riccardi, C. J. (2010). Examining the unique relationships between anxiety disorders and childhood physical and sexual abuse in the National Comorbidity Survey-Replication. *Psychiatry Res.* 177, 150–155. doi: 10.1016/j.psychres.2009.03.008

Coupland, N. J., Ogilvie, C. J., Hegadoren, K. M., Seres, P., Hanstock, C. C., and Allen, P. S. (2005). Decreased prefrontal Myo-inositol in major depressive disorder. *Biol. Psychiatry* 57, 1526–1534. doi: 10.1016/j.biopsych.2005.02.027

Crum, W. R., Camara, O., and Hill, D. L. (2006). Generalized overlap measures for evaluation and validation in medical image analysis. *IEEE Trans. Med. Imaging* 25, 1451–1461. doi: 10.1109/tmi.2006.880587

Danese, A., Moffitt, T. E., Harrington, H., Milne, B. J., Polanczyk, G., Pariante, C. M., et al. (2009). Adverse childhood experiences and adult risk factors for age-related disease: depression, inflammation, and clustering of metabolic risk markers. *Arch. Pediatr. Adolesc. Med.* 163, 1135–1143. doi: 10.1001/archpediatrics.2009.214

Dannlowski, U., Stuhrmann, A., Beutelmann, V., Zwanzger, P., Lenzen, T., Grotegerd, D., et al. (2012). Limbic scars: long-term consequences of childhood maltreatment revealed by functional and structural magnetic resonance imaging. *Biol. Psychiatry* 71, 286–293. doi: 10.1016/j.biopsych.2011.10.021

De Bellis, M. D., Keshavan, M. S., Spencer, S., and Hall, J. (2000). N-Acetylaspartate concentration in the anterior cingulate of maltreated children and adolescents with PTSD. *Am. J. Psychiatry* 157, 1175–1177. doi: 10.1176/appi.ajp.157.7.1175

Deelchand, D. K., Adanyeguh, I. M., Emir, U. E., Nguyen, T. M., Valabregue, R., Henry, P. G., et al. (2015). Two-site reproducibility of cerebellar and brainstem neurochemical profiles with short-echo, single-voxel MRS at 3T. *Magn. Reson. Med.* 73, 1718–1725. doi: 10.1002/mrm.25295

Dillon, D. G., Holmes, A. J., Birk, J. L., Brooks, N., Lyons-Ruth, K., and Pizzagalli, D. A. (2009). Childhood adversity is associated with left basal ganglia dysfunction during reward anticipation in adulthood. *Biol. Psychiatry* 66, 206–213. doi: 10.1016/j.biopsych.2009.02.019

Dosenbach, N. U., Fair, D. A., Cohen, A. L., Schlaggar, B. L., and Petersen, S. E. (2008). A dual-networks architecture of top-down control. *Trends Cogn. Sci.* 12, 99–105. doi: 10.1016/j.tics.2008.01.001

Eluvathingal, T. J., Chugani, H. T., Behen, M. E., Juhász, C., Muzik, O., Maqbool, M., et al. (2006). Abnormal brain connectivity in children after early severe socioemotional deprivation: a diffusion tensor imaging study. *Pediatrics* 117, 2093–2100. doi: 10.1542/peds.2005-1727

Etkin, A., Egner, T., and Kalisch, R. (2011). Emotional processing in anterior cingulate and medial prefrontal cortex. *Trends Cogn. Sci.* 15, 85–93. doi: 10.1016/j.tics.2010.11.004

Farchione, T. R., Moore, G. J., and Rosenberg, D. R. (2002). Proton magnetic resonance spectroscopic imaging in pediatric major depression. *Biol. Psychiatry* 52, 86–92. doi: 10.1016/s0006-3223(02)01340-9

Forde, N. J., Naaijen, J., Lythgoe, D. J., Akkermans, S. E. A., Openneer, T. J. C., Dietrich, A., et al. (2018). Multi-modal imaging investigation of anterior cingulate cortex cytoarchitecture in neurodevelopment. *Eur. Neuropsychopharmacol.* 28, 13–23. doi: 10.1016/j.euroneuro.2017.11.021

Frey, R., Metzler, D., Fischer, P., Heiden, A., Scharfetter, J., Moser, E., et al. (1998). Myo-inositol in depressive and healthy subjects determined by frontal 1H-magnetic resonance spectroscopy at 1.5 tesla. *J. Psychiatr. Res.* 32, 411–420. doi: 10.1016/s0022-3956(98)00033-8

Genova, H. M., Rajagopalan, V., Chiaravalloti, N., Binder, A., Deluca, J., and Lengenfelder, J. (2015). Facial affect recognition linked to damage in specific white matter tracts in traumatic brain injury. *Soc. Neurosci.* 10, 27–34. doi: 10.1080/17470919.2014.959618

Greening, S. G., and Mitchell, D. G. (2015). A network of amygdala connections predict individual differences in trait anxiety. *Hum. Brain Mapp.* 36, 4819–4830. doi: 10.1002/hbm.22952

Gruber, S., Frey, R., Mlynárik, V., Stadlbauer, A., Heiden, A., Kasper, S., et al. (2003). Quantification of metabolic differences in the frontal brain of depressive patients and controls obtained by 1H-MRS at 3 Tesla. *Invest. Radiol.* 38, 403–408. doi: 10.1097/01.rli.0000073446.43445.20

Guyer, A. E., Kaufman, J., Hodgdon, H. B., Masten, C. L., Jazbec, S., Pine, D. S., et al. (2006). Behavioral alterations in reward system function: the role of childhood maltreatment and psychopathology. *J. Am. Acad. Child Adolesc. Psychiatry* 45, 1059–1067. doi: 10.1097/01.chi.0000227882.50404.11

Hanson, J. L., Adluru, N., Chung, M. K., Alexander, A. L., Davidson, R. J., and Pollak, S. D. (2013). Early neglect is associated with alterations in white matter integrity and cognitive functioning. *Child Dev.* 84, 1566–1578. doi: 10.1111/cdev.12069

Hanson, J. L., Hariri, A. R., and Williamson, D. E. (2015). Blunted ventral striatum development in adolescence reflects emotional neglect and predicts depressive symptoms. *Biol. Psychiatry* 78, 598–605. doi: 10.1016/j.biopsych.2015.05.010

Harris, J. L., Choi, I.-Y., and Brooks, W. M. (2015). Probing astrocyte metabolism *in vivo*: proton magnetic resonance spectroscopy in the injured and aging brain. *Front. Aging Neurosci.* 7:202. doi: 10.3389/fnagi.2015.00202

Hart, H., and Rubia, K. (2012). Neuroimaging of child abuse: a critical review. *Front. Hum. Neurosci.* 6:52. doi: 10.3389/fnhum.2012.00052

Heim, C. M., Mayberg, H. S., Mletzko, T., Nemeroff, C. B., and Pruessner, J. C. (2013). Decreased cortical representation of genital somatosensory field after childhood sexual abuse. *Am. J. Psychiatry* 170, 616–623. doi: 10.1176/appi.ajp.2013.12070950

Heim, C., Newport, D. J., Mletzko, T., Miller, A. H., and Nemeroff, C. B. (2008). The link between childhood trauma and depression: insights from HPA axis studies in humans. *Psychoneuroendocrinology* 33, 693–710. doi: 10.1016/j.psyneuen.2008.03.008

Hermundstad, A. M., Bassett, D. S., Brown, K. S., Aminoff, E. M., Clewett, D., Freeman, S., et al. (2013). Structural foundations of resting-state and task-based functional connectivity in the human brain. *Proc. Natl. Acad. Sci. U S A* 110, 6169–6174. doi: 10.1073/pnas.1219562110

Hovens, J. G., Giltay, E. J., Wiersma, J. E., Spinhoven, P., Penninx, B. W., and Zitman, F. G. (2012). Impact of childhood life events and trauma on the course of depressive and anxiety disorders. *Acta Psychiatr. Scand.* 126, 198–207. doi: 10.1111/j.1600-0447.2011.01828.x

Ip, I. B., Berrington, A., Hess, A. T., Parker, A. J., Emir, U. E., and Bridge, H. (2017). Combined fMRI-MRS acquires simultaneous glutamate and BOLD-fMRI signals in the human brain. *Neuroimage* 155, 113–119. doi: 10.1016/j.neuroimage.2017.04.030

Jedd, K., Hunt, R. H., Cicchetti, D., Hunt, E., Cowell, R. A., Rogosch, F. A., et al. (2015). Long-term consequences of childhood maltreatment: altered amygdala functional connectivity. *Dev. Psychopathol.* 27, 1577–1589. doi: 10.1017/s0954579415000954

Jeong, B., Lee, S. W., Lee, J. S., Yoo, J. H., Kim, K. W., Cho, S., et al. (2015). The psychometric properties of the korean version of the verbal abuse questionnaire in university students. *Psychiatry Investig.* 12, 190–196. doi: 10.4306/pi.2015.12.2.190

Joo, E. J., Joo, Y. H., Hong, J. P., Hwang, S., Maeng, S. J., Han, J. H., et al. (2004). Korean version of the diagnostic interview for genetic studies: validity and reliability. *Compr. Psychiatry* 45, 225–229. doi: 10.1016/j.comppsych.2004.02.007

Kaiser, R. H., Clegg, R., Goer, F., Pechtel, P., Beltzer, M., Vitaliano, G., et al. (2018). Childhood stress, grown-up brain networks: corticolimbic correlates of threat-related early life stress and adult stress response. *Psychol. Med.* 48, 1157–1166. doi: 10.1017/s0033291717002628

Kooka, Y., Sawara, K., Endo, R., Kato, A., Suzuki, K., and Takikawa, Y. (2016). Brain metabolism in minimal hepatic encephalopathy assessed by 3.0-Tesla magnetic resonance spectroscopy. *Hepatol. Res.* 46, 269–276. doi: 10.1111/hepr.12519

Kravitz, D. J., Saleem, K. S., Baker, C. I., Ungerleider, L. G., and Mishkin, M. (2013). The ventral visual pathway: an expanded neural framework for the processing of object quality. *Trends Cogn. Sci.* 17, 26–49. doi: 10.1016/j.tics.2012.10.011

Krishnan, A., Williams, L. J., McIntosh, A. R., and Abdi, H. (2011). Partial Least Squares (PLS) methods for neuroimaging: a tutorial and review. *Neuroimage* 56, 455–475. doi: 10.1016/j.neuroimage.2010.07.034

Lapate, R. C., Rokers, B., Tromp, D. P., Orfali, N. S., Oler, J. A., Doran, S. T., et al. (2016). Awareness of emotional stimuli determines the behavioral consequences of amygdala activation and amygdala-prefrontal connectivity. *Sci. Rep.* 6:25826. doi: 10.1038/srep25826

Lee, S. W., Yoo, J. H., Kim, K. W., Kim, D., Park, H., Choi, J., et al. (2018). Hippocampal subfields volume reduction in high schoolers with previous verbal abuse experiences. *Clin. Psychopharmacol. Neurosci.* 16, 46–56. doi: 10.9758/cpn.2018.16.1.46

Lee, S. W., Yoo, J. H., Kim, K. W., Lee, J. S., Kim, D., Park, H., et al. (2015). Aberrant function of frontoamygdala circuits in adolescents with previous verbal abuse experiences. *Neuropsychologia* 79, 76–85. doi: 10.1016/j.neuropsychologia.2015.10.029

Maninger, N., Capitanio, J. P., Mason, W. A., Ruys, J. D., and Mendoza, S. P. (2010). Acute and chronic stress increase DHEAS concentrations in rhesus monkeys. *Psychoneuroendocrinology* 35, 1055–1062. doi: 10.1016/j.psyneuen.2010.01.006

Marusak, H., Thomason, M., Peters, C., Zundel, C., Elrahal, F., and Rabinak, C. (2016). You say 'prefrontal cortex' and I say 'anterior cingulate': meta-analysis of spatial overlap in amygdala-to-prefrontal connectivity and internalizing symptomology. *Transl. Psychiatry* 6:e944. doi: 10.1038/tp.2016.218

May, A. (2011). Experience-dependent structural plasticity in the adult human brain. *Trends Cogn. Sci.* 15, 475–482. doi: 10.1016/j.tics.2011.08.002

Mehta, M. A., Gore-Langton, E., Golembo, N., Colvert, E., Williams, S. C., and Sonuga-Barke, E. (2010). Hyporesponsive reward anticipation in the basal ganglia following severe institutional deprivation early in life. *J. Cogn. Neurosci.* 22, 2316–2325. doi: 10.1162/jocn.2009.21394

Meskaldji, D. E., Preti, M. G., Bolton, T. A., Montandon, M. L., Rodriguez, C., Morgenthaler, S., et al. (2016). Prediction of long-term memory scores in MCI based on resting-state fMRI. *Neuroimage Clin.* 12, 785–795. doi: 10.1016/j.nicl.2016.10.004

Mevik, B. H., and Wehrens, R. (2007). The pls package: principal component and partial least squares regression in R. *J. Stat. Softw.* 18, 1–23. doi: 10.18637/jss.v018.i02

Nanni, V., Uher, R., and Danese, A. (2012). Childhood maltreatment predicts unfavorable course of illness and treatment outcome in depression: a meta-analysis. *Am. J. Psychiatry* 169, 141–151. doi: 10.1176/appi.ajp.2011.11020335

Ohashi, K., Anderson, C. M., Bolger, E. A., Khan, A., McGreenery, C. E., and Teicher, M. H. (2017). Childhood maltreatment is associated with alteration in global network fiber-tract architecture independent of history of depression and anxiety. *Neuroimage* 150, 50–59. doi: 10.1016/j.neuroimage.2017.02.037

Park, Y. W., Deelchand, D. K., Joers, J. M., Hanna, B., Berrington, A., Gillen, J. S., et al. (2018). AutoVOI: real-time automatic prescription of volume-of-interest for single voxel spectroscopy. *Magn. Reson. Med.* 80, 1787–1798. doi: 10.1002/mrm.27203

Plitman, E., de la Fuente-Sandoval, C., Reyes-Madrigal, F., Chavez, S., Gómez-Cruz, G., León-Ortiz, P., et al. (2015). Elevated myo-inositol, choline, and

glutamate levels in the associative striatum of antipsychotic-naive patients with first-episode psychosis: a proton magnetic resonance spectroscopy study with implications for glial dysfunction. *Schizophr. Bull.* 42, 415–424. doi: 10.1093/schbul/sbv118

Post, R. M., Altshuler, L. L., Kupka, R., McElroy, S. L., Frye, M. A., Rowe, M., et al. (2015). Verbal abuse, like physical and sexual abuse, in childhood is associated with an earlier onset and more difficult course of bipolar disorder. *Bipolar Disord.* 17, 323–330. doi: 10.1111/bdi.12268

Provencher, S. W. (1993). Estimation of metabolite concentrations from localized *in vivo* proton NMR spectra. *Magn. Reson. Med.* 30, 672–679. doi: 10.1002/mrm.1910300604

Rango, M., Cogiamanian, F., Marceglia, S., Barberis, B., Arighi, A., Biondetti, P., et al. (2008). Myoinositol content in the human brain is modified by transcranial direct current stimulation in a matter of minutes: a 1H-MRS study. *Magn. Reson. Med.* 60, 782–789. doi: 10.1002/mrm.21709

Rodrigo, M. J., León, I., Góngora, D., Hernández-Cabrera, J. A., Byrne, S., and Bobes, M. A. (2016). Inferior fronto-temporo-occipital connectivity: a missing link between maltreated girls and neglectful mothers. *Soc. Cogn. Affect. Neurosci.* 11, 1658–1665. doi: 10.1093/scan/nsw080

Rosenberg, M. D., Finn, E. S., Scheinost, D., Papademetris, X., Shen, X., Constable, R. T., et al. (2016). A neuromarker of sustained attention from whole-brain functional connectivity. *Nat. Neurosci.* 19, 165–171. doi: 10.1038/nn.4179

Sadaghiani, S., and D'Esposito, M. (2015). Functional characterization of the cingulo-opercular network in the maintenance of tonic alertness. *Cereb. Cortex* 25, 2763–2773. doi: 10.1093/cercor/bhu072

Schmidt, A. T., Hanten, G., Li, X., Wilde, E. A., Ibarra, A. P., Chu, Z. D., et al. (2013). Emotional prosody and diffusion tensor imaging in children after traumatic brain injury. *Brain Inj.* 27, 1528–1535. doi: 10.3109/02699052.2013.828851

Shirayama, Y., Takahashi, M., Osone, F., Hara, A., and Okubo, T. (2017). Myo-inositol, glutamate, and glutamine in the prefrontal cortex, hippocampus, and amygdala in major depression. *Biol. Psychiatry Cogn. Neurosci. Neuroimaging* 2, 196–204. doi: 10.1016/j.bpsc.2016.11.006

Souza-Queiroz, J., Boisgontier, J., Etain, B., Poupon, C., Duclap, D., d'Albis, M. A., et al. (2016). Childhood trauma and the limbic network: a multimodal MRI study in patients with bipolar disorder and controls. *J. Affect. Disord.* 200, 159–164. doi: 10.1016/j.jad.2016.04.038

Teicher, M. H., and Samson, J. A. (2016). Annual research review: enduring neurobiological effects of childhood abuse and neglect. *J. Child Psychol. Psychiatry* 57, 241–266. doi: 10.1111/jcpp.12507

Teicher, M. H., Samson, J. A., Anderson, C. M., and Ohashi, K. (2016). The effects of childhood maltreatment on brain structure, function and connectivity. *Nat. Rev. Neurosci.* 17, 652–666. doi: 10.1038/nrn.2016.111

Teicher, M. H., Samson, J. A., Polcari, A., and McGreenery, C. E. (2006). Sticks, stones, and hurtful words: relative effects of various forms of childhood maltreatment. *Am. J. Psychiatry* 163, 993–1000. doi: 10.1176/appi.ajp.163.6.993

Teicher, M. H., Samson, J. A., Sheu, Y. S., Polcari, A., and McGreenery, C. E. (2010). Hurtful words: association of exposure to peer verbal abuse with elevated psychiatric symptom scores and corpus callosum abnormalities. *Am. J. Psychiatry* 167, 1464–1471. doi: 10.1176/appi.ajp.2010.10010030

Tomoda, A., Sheu, Y. S., Rabi, K., Suzuki, H., Navalta, C. P., Polcari, A., et al. (2011). Exposure to parental verbal abuse is associated with increased gray matter volume in superior temporal gyrus. *Neuroimage* 54, S280–S286. doi: 10.1016/j.neuroimage.2010.05.027

Ugwu, I. D., Amico, F., Carballedo, A., Fagan, A. J., and Frodl, T. (2015). Childhood adversity, depression, age and gender effects on white matter microstructure: a DTI study. *Brain Struct. Funct.* 220, 1997–2009. doi: 10.1007/s00429-014-0769-x

Unger, A., Alm, K. H., Collins, J. A., O'Leary, J. M., and Olson, I. R. (2016). Variation in white matter connectivity predicts the ability to remember faces and discriminate their emotions. *J. Int. Neuropsychol. Soc.* 22, 180–190. doi: 10.1017/s1355617715001009

Weissenborn, K., Ahl, B., Fischer-Wasels, D., van den Hoff, J., Hecker, H., Burchert, W., et al. (2007). Correlations between magnetic resonance spectroscopy alterations and cerebral ammonia and glucose metabolism in cirrhotic patients with and without hepatic encephalopathy. *Gut* 56, 1736–1742. doi: 10.1136/gut.2006.110569

Yoo, K., Rosenberg, M. D., Hsu, W. T., Zhang, S., Li, C. R., Scheinost, D., et al. (2018). Connectome-based predictive modeling of attention: comparing different functional connectivity features and prediction methods across datasets. *Neuroimage* 167, 11–22. doi: 10.1016/j.neuroimage.2017.11.010

Zheng, H., Zhang, L., Li, L., Liu, P., Gao, J., Liu, X., et al. (2010). High-frequency rTMS treatment increases left prefrontal myo-inositol in young patients with treatment-resistant depression. *Prog. Neuropsychopharmacol. Biol. Psychiatry* 34, 1189–1195. doi: 10.1016/j.pnpbp.2010.06.009

Zhu, H., and Barker, P. B. (2011). "MR spectroscopy and spectroscopic imaging of the brain," in *Magnetic Resonance Neuroimaging*, eds. M. Modo and J. W. M. Bulte (Totowa, NJ: Springer), 203–226.

Zou, K. H., Warfield, S. K., Bharatha, A., Tempany, C. M., Kaus, M. R., Haker, S. J., et al. (2004). Statistical validation of image segmentation quality based on a spatial overlap index1: scientific reports. *Acad. Radiol.* 11, 178–189. doi: 10.1016/s1076-6332(03)00671-8

Conflict of Interest Statement: The authors declare that the research was conducted in the absence of any commercial or financial relationships that could be construed as a potential conflict of interest.

frontiers in Human Neuroscience

ORIGINAL RESEARCH
published: 01 February 2019
doi: 10.3389/fnhum.2019.00006

Atypical Flexibility in Dynamic Functional Connectivity Quantifies the Severity in Autism Spectrum Disorder

Vatika Harlalka[1], *Raju S. Bapi*[2,3], *P. K. Vinod*[1]* *and Dipanjan Roy*[4]*

[1] Center for Computational Natural Sciences and Bioinformatics, IIIT Hyderabad, Hyderabad, India, [2] Cognitive Science Lab, IIIT Hyderabad, Hyderabad, India, [3] School of Computer and Information Sciences, University of Hyderabad, Hyderabad, India, [4] Cognitive Brain Dynamics Lab, National Brain Research Centre, Manesar, India

Resting-state functional connectivity (FC) analyses have shown atypical connectivity in autism spectrum disorder (ASD) as compared to typically developing (TD). However, this view emerges from investigating static FC overlooking the whole brain transient connectivity patterns. In our study, we investigated how age and disease influence the dynamic changes in functional connectivity of TD and ASD. We used resting-state functional magnetic resonance imaging (rs-fMRI) data stratified into three cohorts: children (7–11 years), adolescents (12–17 years), and adults (18+ years) for the analysis. The dynamic variability in the connection strength and the modular organization in terms of measures such as flexiblity, cohesion strength, and disjointness were explored for each subject to characterize the differences between ASD and TD. In ASD, we observed significantly higher inter-subject dynamic variability in connection strength as compared to TD. This hyper-variability relates to the symptom severity in ASD. We also found that whole-brain flexibility correlates with static modularity only in TD. Further, we observed a core-periphery organization in the resting-state, with Sensorimotor and Visual regions in the rigid core; and DMN and attention areas in the flexible periphery. TD also develops a more cohesive organization of sensorimotor areas. However, in ASD we found a strong positive correlation of symptom severity with flexibility of rigid areas and with disjointness of sensorimotor areas. The regions of the brain showing high predictive power of symptom severity were distributed across the cortex, with stronger bearings in the frontal, motor, and occipital cortices. Our study demonstrates that the dynamic framework best characterizes the variability in ASD.

Keywords: resting-state functional MRI, autism, flexibility, dynamic connectivity, ABIDE

OPEN ACCESS

Edited by:
Juan Helen Zhou,
Duke-NUS Medical School, Singapore

Reviewed by:
Xing Qian,
Duke-NUS Medical School, Singapore
Alessandro Tonacci,
Istituto di Fisiologia Clinica (IFC), Italy

***Correspondence:**
P. K. Vinod
vinod.pk@iiit.ac.in
Dipanjan Roy
dipanjan.nbrc@gov.in

Received: *14 August 2018*
Accepted: *08 January 2019*
Published: *01 February 2019*

Citation:
Harlalka V, Bapi RS, Vinod PK and Roy D (2019) Atypical Flexibility in Dynamic Functional Connectivity Quantifies the Severity in Autism Spectrum Disorder. Front. Hum. Neurosci. 13:6. doi: 10.3389/fnhum.2019.00006

INTRODUCTION

Autism spectrum disorder (ASD) is a neuro-developmental disorder encompassing a range of disorders including Asperger's syndrome and pervasive developmental disorder. Resting state functional MRI, which measures blood oxygen level-dependant signals (BOLD) (Deco et al., 2013; Lee et al., 2013) has been used to study both physiology and pathology. The statistical analysis of the matrix obtained by using Pearson cross-correlation of the regional BOLD time series across

pairs of regions of interest (ROIs) has been found to reveal several properties that are of clinical relevance. Recently, a number of studies have explored brain networks as graphs (van den Heuvel and Hulshoff Pol, 2010; Sporns, 2013). Graph-theoretic analyses have shown that the functional connectivity in the human brain is divided into well-organized modules or subnetworks which are densely connected within themselves and sparsely connected to each other. Disease and age affect this modular organization (Chen et al., 2013; Song et al., 2014; Ye et al., 2015). Song et al. (2014) reported that modularity decreases with aging, suggesting less distinct functional divisions and specialization across whole brain networks. They reported a decline in cognitive functioning and intact primary information processing with age in typical development (TD).

Several studies on neurocognitive diseases have reported atypical fluctuation in modularity. Recently, in ASD, alterations in the network properties (global and local efficiency, assortativity, clustering coefficients, characteristic path length, small world properties, etc.) with maturation and disease were found in our and other studies (Rudie et al., 2013; Harlalka et al., 2018b; Henry et al., 2018). Using static networks, a significant decrease in modularity has been observed. Both the functional connectivity *between* major networks (i.e., functional segregation) and connectivity *within* different networks (i.e., functional integration) are altered in ASD (Rudie et al., 2012, 2013). Studies have shown under-connectivity in various functional networks, especially in the Default Mode Network (DMN) (Hahamy et al., 2015; Yerys et al., 2015).

However, in recent times, it has been found that analyses based on static functional connectivity have several shortcomings. Static functional connectivity (FC) does not sufficiently incorporate time-varying (or dynamic) changes that occur through the brain scan (Chang and Glover, 2010). Dynamic functional connectivity (dFC) analyses have shown to reveal patterns of brain states that occur commonly as well as transitions among them (Damaraju et al., 2014; Preti et al., 2017). They also give an idea about the dynamic reconfiguration that occurs during tasks (Bassett et al., 2011; Braun et al., 2016; Gerraty et al., 2018). To analyze dynamic or instantaneous connectivity, the BOLD timeseries is divided into overlapping intervals, and a functional correlation matrix is derived for each of these intervals. The sliding window or tapered sliding window approach has been widely used to study dynamic connectivity of functional brain networks estimated from fMRI BOLD data (Xu and Lindquist, 2015; Park et al., 2017). With recent studies reporting that modularity of dynamic functional networks varies on very short timescales (Betzel et al., 2016, 2017), there is a possibility of tracking instantaneous changes in functional connectivity between brain regions. Particularly, while static communities represent sub-networks densely connected among themselves and sparsely connected to the rest of the brain, community structures in dynamic networks would project the ongoing changes in communities over time (Bassett et al., 2011; Cole et al., 2013).

Recent studies have explored the dynamic nature of atypical information processing in ASD (Falahpour et al., 2016; Chen et al., 2017; de Lacy et al., 2017; Watanabe and Rees, 2017; Rashid et al., 2018). Watanabe and Rees (2017) reported that the autistic brain shows fewer state transitions compared to those of typically developing, and such atypically stable brain dynamics relates to symptom severity in ASD. Some studies reported altered dynamic functional connectivity between specific areas (Falahpour et al., 2016). Several whole-brain studies found dominant brain states as well as their dwell times. Resting state fMRI analysis of ASD cohort reveals that the dynamics spends more time in globally disconnected states with fewer state transitions as compared to TD (de Lacy et al., 2017; Rashid et al., 2018). Flexibility of brain also provides an alternate way of quantifying the dynamic changes in fMRI studies (Garcia et al., 2018). Intuitively, it can be thought of as a measure to quantify the dynamic reconfiguration that occurs in the brain over time. It has been applied to obtain insights into altered dynamic pattern in various disease states such as schizophrenia (Braun et al., 2016) and epilepsy (Tailby et al., 2018). The influence of resting-state flexibility on disease and age has not been studied, particularly in ASD.

Therefore, we adopt this framework to investigate the dynamic changes in functional activity of TD and ASD. We stratified the data (ASD and TD) into groups of children, adolescents, and adults. We attempted to quantify the variability in dynamic FC in two plausible ways. Firstly, we quantified the variability in the connection strength. Secondly, dynamic metrics, flexibility, cohesion, and disjointness were used to study the differences between ASD and TD. The pipeline is summarized in **Figure 1**.

MATERIALS AND METHODS

Data Acquisition and Preprocessing

We used single-site data (NYU) from the ABIDE Preprocessed Initiative (Cameron et al., 2013). Institutional review board approval was provided by each data contributor in the ABIDE database. Detailed recruitment and assessment protocols and inclusion criteria are all available on the ABIDE website.

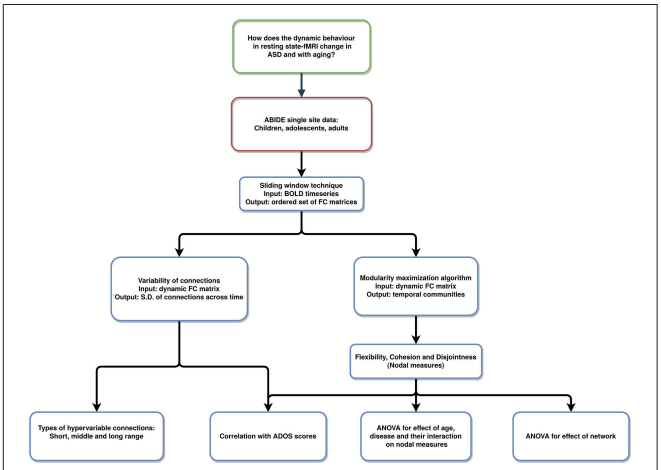

FIGURE 1 | Pipeline of the analysis: resting-state fMRI data used to analyze varying temporal dynamics in ASD and TD.

The data was preprocessed using the DPARSF pipeline (Data Preprocessing Assistant for Resting State fMRI) (Chao-Gan and Yu-Feng, 2010). Briefly, acquisition time correction and head motion correction (Friston 24-parameter model) were done for each subject. The functional images were re-aligned using a 6 degrees-of-freedom transformation. The structural image was co-registered with the mean functional image. The following nuisance signals were removed as part of the ABIDE preprocessing initiative: head motion effects (using Friston 24-parameter model), signals from white matter and cerebrospinal fluid, linear, and quadratic trends. The images were warped into MNI space. Temporal filtering (0.01–0.1 Hz) was performed on the regressed time series (Liu and Duyn, 2013). Global signal regression (GSR) has been shown to cause anti-correlation in resting state brain networks and to distort group differences in intrinsic functional connectivity (Murphy et al., 2009; Weissenbacher et al., 2009; Saad et al., 2012). Therefore, we did not use GSR. Details of the preprocessing steps can be found here: http://preprocessed-connectomes-project.org/abide/dparsf.html. We used the Automated Anatomical Labeling template (AAL) for parcellating the brain into 90 regions of interest (ROIs). We have provided the mapping between names of the ROIs and their abbreviations in **Supplementary Table 1**.

ABIDE Preprocessed Initiative (Cameron et al., 2013) provides visual assessment of the functional data from 3 manual functional raters. Subjects were excluded if (1) Any of the 3 raters gave it a "Maybe" or a "Fail" rating. (2) failed visual inspection of anatomical images and surfaces; (3) mean framewise displacement > 0.1 mm. Further, the data was age-stratified into three cohorts: young children under 11 years of age, adolescents from 11 to 18 years of age, and adults above 18 years of age (**Table 1**). Overall, we did not find significant differences in within-group properties for age and IQ between ASD and TD subjects. Non-parametric *t*-tests were used to calculate differences in mean relative motion and IQ scores. While motion was slightly higher in children compared to adolescents and adults, we found that there were no significant differences in these measures between ASD and TD.

TABLE 1 | Demographic details of the samples included in this study.

	ASD	TD	*p*
CHILDREN			
Age: mean (SD)	9.51 (1.12)	9.10 (1.32)	0.241
range	7.15–10.06	6.47–10.86	
Gender	24M/2F	19M/7F	
FIQ	76–142	80–136	0.103
ADOS total score (SD)	10.89 (4.2)	–	
mean FD (SD)	0.08 (0.04)	0.05 (0.02)	0.091
ADOLESCENT			
Age: mean (SD)	13.71 (1.79)	14.01 (1.74)	0.362
range	11.01–17.88	11.32–16.93	
Gender	23M/5F	23M/5F	
FIQ	78–132	80–121	0.526
ADOS total score (SD)	11.45 (4.46)	–	
mean FD (SD)	0.07 (0.03)	0.06 (0.03)	0.303
ADULT			
Age: mean (SD)	24.13 (3.92)	25.41 (5.87)	0.325
range	18.58–39.1	18.59–31.78	
Gender	14M/4F	14M/4F	
FIQ	80–137	81–139	0.607
ADOS total score (SD)	10.82 (3.9)	–	
mean FD (SD)	0.05 (0.03)	0.05 (0.02)	0.202

Dynamic FC

We used the DynamicBC toolbox (Liao et al., 2014) for Dynamic FC creation. We used a tapered sliding window length of 30 s in accordance with previous studies (Allen et al., 2014; Betzel et al., 2016) and the window was moved with a stride of 1. A set of sliding window correlation matrices was calculated for each subject. A Fisher Z-Transformation (to transform the Pearson's *r*, i.e., the correlation coefficient) was then applied to improve the normality of the distribution of the correlation matrices. Finally, the dynamic FC variability matrix, dFCvar was calculated for each subject where $D(i,j)$ is the standard deviation of the connection strength between ROIs i and j across the temporal windows. This matrix has also been referred to as the *connection flexibility matrix* in previous studies (Bassett et al., 2011; Betzel et al., 2016). Therefore, a higher $D(i,j)$ would imply a hyper-variable connection between areas i and j. Then the Network Based Statistics (NBS) method (Zalesky et al., 2010) was used to find a significantly different component (p_connection < 0.01, p-cluster < 0.05, 10,000 iterations), both hyper-or-hypo-variant in the dFCvar matrix between ASD and TD in each age group. The significant variable connections are classified into short, middle, and long range connections. All the connections i.e., distances between the centers of every two ROIs in the AAL atlas were listed and sorted. The shortest 33% connections are *short-range*, highest 33% connections are *long-range* and the other connections are defined as *intermediate-range*.

We also estimated the correlation between dFCvar matrix and severity score of ASD. We used the permutation method for calculating significance of correlation with null hypothesis of no correlation between each edge and the ADOS scores (FDR corrected). More details about the methods used for network correlation with ADOS score as well as supplementary analysis to check for robustness of our results with different window parameters are provided in the **Supplementary Information**.

Modularity Maximization

We used the modularity maximization algorithm to determine the temporal communities in the multilayer dynamic functional connectivity matrix. For visualization, one can imagine a super adjacency matrix consisting of multiple adjacency matrices. Multilayer modularity algorithm finds communities within this super adjacency matrix. Similar to static networks, regions in the same temporal communities are also expected to have higher intra-community connectivity compared to regions in different communities. This algorithm identifies communities across time by maximizing a Louvain-like

modularity function (Q):

$$Q = \frac{1}{2\mu} \sum_{ijlr} \left(\left(A_{ijl} - \gamma_l . P_{ijl} \right) \delta_{lr} + \delta_{ij} . \omega_{jlr} \right) \delta \left(g_{il}, g_{jr} \right)$$

In the above expression, A_{ijl} is the correlation of regions i and j in layer l. P_{ijl} is the expected correlation in an appropriate null model. Two free parameters γ and ω, are used to scale the number of communities and the strength of the inter-layer edges that link each node to itself, respectively. In our study, we used the Newman-Girvan null model and the default values of 1 for the two free parameters. We used the Genlouvain Matlab toolbox (Jutla et al., 2011–2012) to calculate the community assignments. Since the output could vary in each run due to the stochastic nature of optimizing the partition function, we repeated the algorithm 50 times and calculated the three dynamic metrics—flexibility, cohesion, and disjointness for each run. The final value of each metric for each subject is the average of the 50 runs.

Flexibility

The multilayer modularity maximization algorithm detected the community affiliations of each ROI at each window i.e., the output is $G = N \times T$ matrix where each element (n,t) is the community that ROI n belongs to at window t. Regional flexibility (f) of an ROI i, is defined as the ratio of the number of times it changed its community affiliation through the temporal windows to the possible number of community changes (as shown in the expression below). It is a number between 0 and 1 where zero implies most rigidity and one implies the most flexibility in terms of community changes through time.

$$f_i = 1 - \frac{1}{T-1} \sum_{s=1}^{T-1} \delta \left(G_{i,s}, G_{i,s+1} \right)$$

Nodes with low flexibility form the rigid temporal core while nodes with high flexibility form the temporal periphery. Global flexibility (F) for a subject is calculated as the mean flexibility score across all ROIs ($F = \frac{1}{N} \sum_{i=1}^{N} f_i$). For our analysis, we calculated both the regional and global flexibility scores for 50 runs of the modularity algorithm and averaged the values across runs for statistical analysis. We also correlated the regional and global flexibility scores with the subject-wise ADOS scores and the modularity of each subject. Further, we repeated the analysis with different values for parameters γ and ω of the multilayer modularity algorithm.

Relationship Between Modularity and Flexibility

Static modularity is a metric that quantifies the subdivision of a network into communities. Higher modularity implies higher within-module connectivity and lower between-module connectivity. We first calculated the static FC using the pearson cross-correlation of the BOLD timeseries. We binarized the matrix using 10% proportional thresholding. We used the Louvain algorithm (Blondel et al., 2008) to calculate the modularity for each subject. Non-parametric correlation method was used to calculate the correlation between global/regional flexibility scores of the ROIs and modularity.

Cohesion and Disjointness

Although flexibility characterizes the modular changes in each brain area through the scan time, it does not capture changes in community affiliation. For this, we use two network measures: Cohesion strength and node disjointness. These are complementary measures of dynamic networks. Node disjointness quantifies the fraction of times a node changes its community independently, without other nodes from its module. Node cohesion strength is calculated as a cohesion matrix, where the edge weight denotes the number of times a pair of nodes changes to the same community together. Cohesion strength of an ROI i is the sum of its row values in the cohesion matrix. We analyzed the correlations between ADOS scores and cohesion/disjointness.

RESULT

Hyper-Variance of Connections in ASD

We calculated the dFCvar matrix, for every subject where each connection (i,j) of dFCvar is the standard deviation of the connection strength between ROIs i and j across the temporal windows. We found significantly hypervariant cluster of connections in the ASD group in all age groups—children, adolescents and adults. In the children group, the cluster had 37 connections. Most of these were intra-modular DMN-DMN connections, and most were long-range connections (43%). In the adolescents group, the cluster had 42 connections, around one third of which were intramodular and most were short-range connections (45%). Interestingly, in adults, similar to children, we observed high number of long-range (37%) and medium-range (37%) connections **(Figure 2)**.

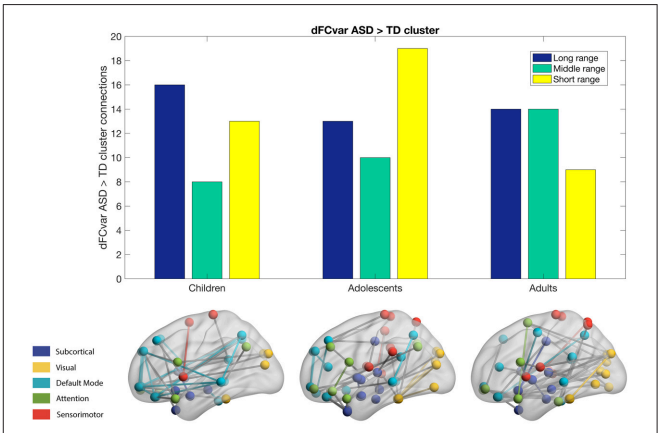

FIGURE 2 | Hypervariant ASD connections in the dFCvar matrix. Majority of connections in children and adults are long-range while adolescents are seen to have majority short-range connections.

Relationship Between dFCvar and ADOS Scores

We found that there were 8 hypervariant connections that showed very significant correlation ($r > 0.4$, $p < 10^{-5}$, survived FDR correction) with ADOS score **(Table 2)**. These connections did not show effect of age (one-way ANOVA, $p > 0.05$) indicating that this correlation was present in all age groups. These mostly included connections between inferior parietal areas and temporal regions. At the network level, we found that the mean DMN dFCvar connections showed significant correlation ($r = 0.34$, $p < 0.05$) with ADOS score as well as the mean DMN-Attention dFCvar connections ($r = 0.39$, $p < 0.05$). These too, did not show age effect with one-way ANOVA indicating that this effect is present for all age groups. However, the average functional connectivity did not show significant correlation with ADOS total scores (p-values did not survive permutation testing). All within-network and between-network correlations are reported in **Supplementary Table 2**. Overall, this shows that the inter-subject connection variability relates to symptom severity.

Negative Correlation of Flexibility and Modularity

In the next analysis, we calculated the multilayer dynamic FC using a multilayer modularity algorithm to partition the brain regions into communities across layers. We found that each subject had between 8 and 26 distinct communities (mean: 18.1). The flexibility of each region is calculated as the fraction of times the region changed its community assignment (**Figure 3**).

Further, we calculated the modularity of static functional connectivity for each subject using Louvain algorithm and correlated it with the local and global flexibility values. In dynamic systems, different brain connectivity configurations can be interpreted as different attractor states. While modularity measures the depth of the attractor states, flexibility measures the frequency of the brain transitioning between states. Deeper states are more stable and will be more resistant to change, and so the regions in these states will have lower flexibility and vice versa (Ramos-Nuñez et al., 2017). We found that in the TD group, the mean whole-brain flexibility shows a significant ($p = 0.001$) correlation ($r = -0.35$) with modularity (**Figure 4A**).

TABLE 2 | Connections showing significant correlation ($p < 10^{-5}$) to ADOS total score.

ROI_1	ROI_2	Correlation
Frontal_Inf_Orb_R	Parietal_Inf_L	0.47
Parietal_Inf_L	Temporal_Mid_L	0.42
Parietal_Inf_L	Temporal_Inf_L	0.45
Precentral_L	Insula_R	0.43
Precentral_L	Putamen_L	0.48
Supp_Motor_Area_R	Insula_R	0.44
Insula_L	Precuneus_L	0.47
Caudate_R	Temporal_Pole_Mid_R	0.43

However, ASD did not show a correlation between flexibility and modularity. On stratifying the data based on age group and then calculating the correlation, we found that in the children's age group, TD did not show any significant correlation of whole brain mean flexibility with modularity score (TD: $r = -0.06$, $p > 0.1$, ASD: $r = -0.08$, $p > 0.1$). In adolescents and adults, we found that TD showed a significant correlation ($r > -0.39$, $p < 0.01$).

Further, we found that there were several areas that showed a significant correlation between local flexibility score and modularity in TD while only two of these areas (rectus gyrus and paracentral lobule) showed this correlation in the ASD group (**Figure 4B**). The areas showing significant correlation in TD group include DMN areas: middle temporal gyrus (MTG), gyrus rectus (REC), superior frontal medial, and dorsal gyrus (SFGdor, SFGmed); attention areas: inferior and middle frontal orbital areas (ORBinf, ORBmid) and inferior parietal areas (IPL); subcortical areas: putamen (PUT), pallidum (PAL), thalamus (THA); visual areas: calcarine fissure (CAL), occipital inferior gyrus (IOG), and fusiform gyrus (FFG); sensorimotor/auditory areas: rolandic operculum(ROL), heschl gyrus (HES), superior temporal yrus (STG), supplementary motor area (SMA).

Significant Network Level Differences in Dynamic Network Measures

To examine if changes in whole-brain flexibility are driven by a biologically relevant organization of brain regions or instead driven by randomness/noise in the whole brain, we tested the average flexibility of functional networks (DMN, Attention, Subcortical, Sensorimotor, and Visual networks). We conducted a repeated-measures ANOVA with functional network as a within-subject factor and with age and disease as between-subject factors. We found a significant main effect of functional network [$F_{(4, 142)} = 3.8$, $p < 0.0001$], while there was no significant effect of interaction of network and disease [$F_{(4, 142)} = 0.84$, $p = 0.13$], or interaction of network, disease and age [$F_{(8, 142)} = 1.61$, $p = 0.16$]. The significant differences are listed in **Supplementary Table 3**. Overall, the results primarily indicate that the visual and sensorimotor areas show the least flexibility and the highest standard deviation indicating that they form the rigid temporal core. This is in contrast to DMN, Subcortical and Attention areas which have higher flexibility and lower standard deviation that form the flexible temporal periphery (See **Supplementary Tables 3**, **4**). Although there is no disease effect observed at the network-level, it is possible that variation in ASD is not captured when it is considered as one group in the ANOVA analysis. Interestingly, we found that at the network level, mean visual, and auditory flexibility scores show a positive correlation with the ADOS scores. However, static modularity scores did not correlate with the ADOS scores **(Figures 5A,B)**.

To further explore the differences in the dynamics at the network level, we also analyzed other dynamic measures: cohesion strength and disjointness. We observed that cohesion strength shows a significant network level effect [$F_{(4, 142)} = 3.9$, $p < 0.01$] with sensorimotor network showing high cohesion strength. There is a significant effect of network [$F_{(4, 142)} = 43.05$, $p < 0.0001$] on node disjointness with DMN network

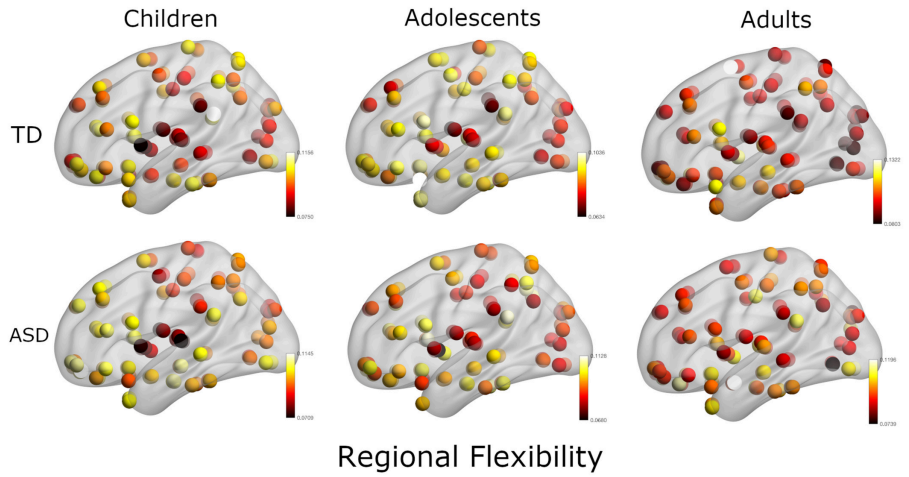

FIGURE 3 | Plot of regional flexibility values for TD and ASD groups where the data is stratified into three groups: Children, adolescents, and adults.

having highest disjointness and sensorimotor, visual networks having lowest disjointness. This analysis provides insights into the organization of the dynamic resting state functional brain.

Effect of Age and Disease on Dynamic Metrics

We used 2-factor ANOVA with factors as disease (2 levels: TD, ASD) and age (3 levels: children, adolescents and adults) to analyze their effects on regional flexibility, cohesion, and disjointness. We found a main effect of disease and of age on flexibility. The superior temporal gyrus (TPOsup) shows significantly [$F_{(1,\ 144)} = 4.66$, $p = 0.03$, partial eta-squared = 0.06 - medium effect size] reduced flexibility in ASD. To confirm that this difference was not driven by the difference in overall variance of the node but purely by the dynamic reconfiguration caused by the reduced flexibility, we also controlled for the mean dFCvar connections of this particular node. We still found a significant difference ($p < 0.01$) between ASD and TD groups. We also found several regions that show effect of age including: superior frontal orbital [ORBsup, $F_{(1,\ 144)} = 3.92$, $p = 0.02$], PAL [$F_{(1,\ 144)} = 6.93$, $p = 0.001$], amygdala (AMYG), cuneous (CUN), inferior occipital gyrus (IOG), left inferior parietal (IPL), angular gyrus (ANG), caudate nucleus (CAU), putamen (PUT), thalamus (THAL), SFGdor, and left superior temporal (STG). Comparisons on group statistics of pallidus gyrus (periphery region) showed a significant increase in flexibility in adults as compared to both adolescents ($p = 0.01$) and children ($p = 0.0002$) while the superior frontal orbital (periphery region) shows a significant ($p = 0.005$) increase of flexibility in adults as compared to adolescents (**Table 3**, **Figure 6A**).

On analyzing the effects of aging and disease on cohesion strength as well as disjointness for each individual node, we found certain nodes that show significant effect ($p < 0.05$) of disease, age, and their interaction. Specifically, we found that attention areas like middle frontal, inferior frontal orbital and the parietal node as well as the caudate nucleus show significant decrease in cohesion in ASD ($p < 0.05$, partial $\eta^2 \sim 0.05$). While STG showed an increase in cohesion with age, areas like caudate nucleus, superior and inferior frontal areas show a general trend of decrease with age (**Figure 6B**, **Table 4**).

We found areas showing significant main effect of disease and age on node disjointness, but not of their interaction. The rolandic operculum gyrus, lingual and occipital gyrus as well as the medial frontal orbital show a significant increase in disjointness in ASD ($p < 0.05$, partial $\eta^2 \sim 0.06$). Further, several nodes in DMN and Sensorimotor network show significant decrease in node disjointness with aging ($p < 0.05$, partial $\eta^2 \sim 0.07$) (**Figure 6C**, **Table 5**). Overall, ASD shows an increase in disjointness and a decrease in node cohesion strength.

Correlation of Dynamic Metrics (Local Dynamics) With ADOS Scores

To analyze the relation between symptom severity and dynamic measures—flexibility, cohesion strength, and disjointness, we found their correlations with the ADOS scores. We did not find a significant correlation between mean whole brain flexibility scores with ADOS scores. At the functional network level, we found the mean flexibility score by averaging the individual scores of each node in a functional network. We found that an increase in flexibility score of visual system areas positively correlated with the ADOS total symptom severity score ($r = 0.37$, $p < 0.01$); ADOS Social score ($r = 0.38$, $p < 0.01$, uncorrected). We did not find any significant correlation with the other functional networks. At the level of individual ROIs, we found that the flexibility of several visual and auditory areas showed positive correlation with ADOS total and communication scores (**Supplementary Table 5** and **Supplementary Figure 1**). Further, on dividing the subjects into 3 age groups - children, adolescents and adults, we found that adolescents and adults show a very strong positive correlation of ADOS social score and flexibility in rigid regions. Children show a strong negative correlation of

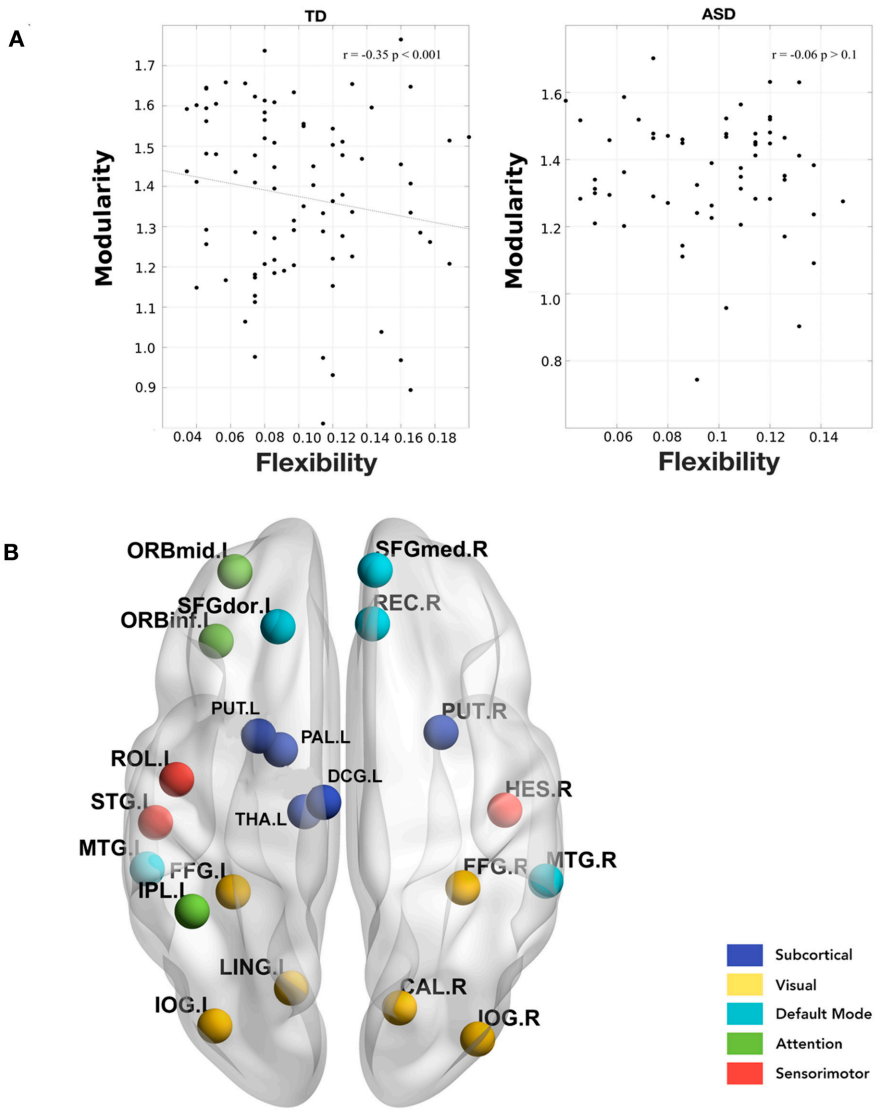

FIGURE 4 | (A) Correlation between whole-brain mean flexibility score and modularity. A significant weak negative correlation is observed only in TD group. **(B)** Areas showing a significant negative correlation between local flexibility score and modularity in TD adults. None of these are significant in the ASD group.

ADOS score and flexibility of DMN region—which is a flexible periphery region **(Table 6)**.

On analyzing correlation between the dynamic properties of node disjointness as well as node cohesion strength with ADOS scores, we find that for adults, the mean node disjointness i.e., the average over the whole brain; shows a significant positive correlation ($r = 0.45$, $p < 0.01$) with the symptom severity ADOS scores. We also find several nodes that show significant correlation of cohesion strength with the ADOS scores. We have listed the details of the correlations with ADOS scores in **Tables 7**, **8**.

Overall, the cohesion strength of sensorimotor regions shows a negative correlation with ADOS scores for ASD adults while cohesion strength of visual, attention and DMN areas show positive correlation. DMN areas show negative correlation of disjointness with ADOS scores and vice versa for sensorimotor areas.

DISCUSSION

Autism is a neurodevelopmental disorder characterized by altered neural network dynamics. The presence of alterations in the dynamic configuration of the resting-state functional connectome and their association with ASD symptom severity are yet to be studied. To address this gap in knowledge, we applied temporal modularity metrics to analyze dynamics in resting-state fMRI data.

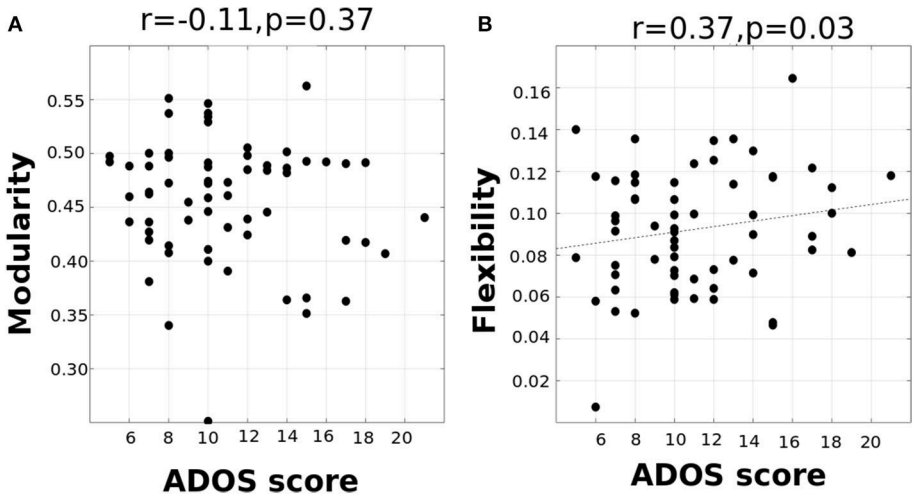

FIGURE 5 | (A) correlation between ADOS total score and modularity **(B)** correlation between ADOS score and visual/auditory system flexibility ($p < 0.05$).

TABLE 3 | Areas showing significant effect ($p < 0.05$, FDR corrected) of age and disease on flexibility.

		Disease			Flexibility (SD)		
ROI	**Name**	**Abbreviation**	**Network**	***p***	**ASD**	**TD**	
83	Temporal_Pole_Sup_L	TPOsup.L	Attention	0.036	0.092 (0.043)	0.107 (0.035)	
		Age			**Children**	**Adolescents**	**Adults**
6	Frontal_Sup_Orb_R	ORBsup.R	DMN	0.021	0.100 (0.034)	0.095 (0.037)	0.118 (0.034)
41	Amygdala_L	AMYG.L	Subcortical	0.011	0.095 (0.040)	0.094 (0.036)	0.116 (0.037)
48	Lingual_R	LING.R	Visual	0.043	0.090 (0.029)	0.074 (0.034)	0.084 (0.036)
53	Occipital_Inf_L	IOG.L	Visual	0.008	0.104 (0.033)	0.084 (0.035)	0.103 (0.044)
54	Occipital_Inf_R	IOG.R	Visual	0.013	0.108 (0.034)	0.087 (0.037)	0.105 (0.031)
61	Parietal_Inf_L	IPL.L	Attention	0.039	0.102 (0.039)	0.091 (0.032)	0.108 (0.038)
74	Putamen_R	PUT.R	Subcortical	0.021	0.089 (0.043)	0.082 (0.037)	0.105 (0.038)
75	Pallidum_L	PAL.L	Subcortical	0.001	0.089 (0.038)	0.089 (0.038)	0.119 (0.044)
77	Thalamus_L	THA.L	Subcortical	0.030	0.085 (0.038)	0.091 (0.046)	0.110 (0.038)
81	Temporal_Sup_L	STG.L	Sensorimotor	0.011	0.078 (0.046)	0.075 (0.036)	0.102 (0.048)

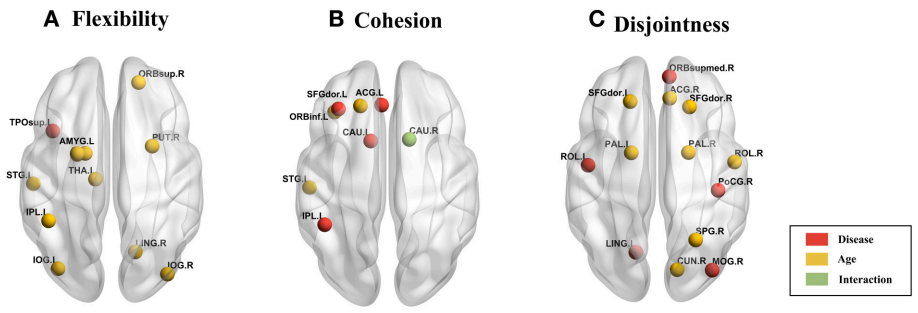

FIGURE 6 | Brain plot of areas showing significant effect of age and disease on **(A)** flexibility, **(B)** cohesion strength, and **(C)** disjointness.

In our first analysis, we found that mean dFCvar between the Attention and DMN networks is positively correlated with the ADOS scores (**Table 2**). This indicates that the inter-subject variability is related to the symptom severity. It has been reported that higher dFCvar is associated with better performance in task and poor performance in resting-state (Douw et al., 2016).

TABLE 4 | Nodes showing significant effect ($p < 0.05$, FDR corrected) of age, disease, and interaction on cohesion strength.

		Effect of disease			Node cohesion strength (SD)		
ROI	**Name**	**Abbreviation**	**Network**	***p***	**ASD**	**TD**	
7	Frontal_Mid_L	MFG.L	Attention	0.021	65.8 (10.4)	77.9 (22.6)	
15	Frontal_Inf_Orb_L	ORBinf.L	Attention	0.029	65.2 (9.91)	77.9 (22.8)	
31	Cingulum_Ant_L	ACG.L	DMN	0.014	55.3 (9.72)	69.4 (20.1)	
61	Parietal_Inf_L	IPL.L	Attention	0.017	75.4 (13.1)	64.8 (10.8)	
71	Caudate_L	CAU.L	Subcortical	0.016	62.9 (10.3)	72.9 (13.5)	
72	Caudate_R	CAU.R	Subcortical	0.012	62.2 (7.51)	74.3 (20.7)	
		Effect of age			**Children**	**Adolescents**	**Adults**
3	Frontal_Sup_L	SFGdor.L	DMN	0.035	80.4 (19.4)	66.2 (13.4)	61.9 (12.6)
15	Frontal_Inf_Orb_L	ORBinf.L	Attention	0.023	74.5 (21.7)	79.2 (19.2)	58.1 (6.2)
72	Caudate_R	CAU.R	Subcortical	0.024	83.9 (27.5)	65.9 (14.7)	67.3 (10.5)
81	Temporal_Sup_L	STG.L	Sensorimotor	0.019	50.6 (13.9)	61.4 (16.6)	71.2 (16.5)
		Effect of Interaction					
72	Caudate_R	CAU.R	Subcortical	0.004			

TABLE 5 | Nodes showing significant effect ($p < 0.05$, FDR corrected) of age, disease, and interaction on node disjointness.

		Effect of disease			Node disjointness (SD)		
ROI	**Name**	**Abbreviation**	**Network**	***p***	**ASD**	**TD**	
17	Rolandic_Oper_L	ROL.L	Sensorimotor	0.012	0.0039 (0.005)	0.0022 (0.004)	
26	Frontal_Med_Orb_R	ORBsupmed.R	DMN	0.039	0.0048 (0.007)	0.0034 (0.004)	
47	Lingual_L	LING.L	Visual	0.037	0.0047 (0.007)	0.0029 (0.006)	
53	Occipital_Inf_L	IOG.L	Visual	0.009	0.0074 (0.006)	0.0045 (0.001)	
58	Postcentral_R	PoCG.R	Sensorimotor	0.009	0.0067 (0.006)	0.0041 (0.006)	
		Effect of age			**Children**	**Adolescents**	**Adults**
3	Frontal_Sup_L	SFGdor.L	DMN	0.014	0.0075 (0.006)	0.0040 (0.005)	0.0055 (0.006)
4	Frontal_Sup_R	SFGdor.R	DMN	0.037	0.0051 (0.003)	0.0061 (0.004)	0.0030 (0.006)
18	Rolandic_Oper_R	ROL.R	Sensorimotor	0.001	0.0019 (0.006)	0.0020 (0.007)	0.0052 (0.005)
32	Cingulum_Ant_R	ACG.R	DMN	0.028	0.0067 (0.005)	0.0063 (0.004)	0.0033 (0.006)
46	Cuneus_R	CUN.R	Visual	0.005	0.0032 (0.005)	0.0029 (0.006)	0.0060 (0.007)
60	Parietal_Sup_R	SPG.R	Sensorimotor	0.029	0.0063 (0.007)	0.0056 (0.006)	0.0027 (0.004)
75	Pallidum_L	PAL.L	Subcortical	0.031	0.0036 (0.005)	0.0054 (0.004)	0.0074 (0.006)
76	Pallidum_R	PAL.R	Subcortical	0.033	0.0066 (0.005)	0.0090 (0.006)	0.0060 (0.008)

Similarly, Lin et al. (2016) reported that higher variability in the connection strength of posterior cingulate cortex (PCC) to other DMN areas in the resting-state is related to slower reaction times on a subsequent attention task. The hypervariance in ASD could lead to a globally disconnected state in its dynamics as reported in a previous study (Rashid et al., 2018). These results taken together indicate that there could be a relation between the atypical hypervariance in ASD which leads to increase in ADOS score and decrease in cognitive performance. We also found significant number of hyper-variable small, medium and long-range connections in three groups (**Figure 2**). The long-range connections define the backbone of the functional network and often connect the hubs regions to minimize wiring and energy costs (Chen et al., 2017). In ASD, the hypervariance in the long-range connections could cause instability in information transmission between hubs. Interestingly, for adolescents, we found higher number of hyper-variable short-range connections. The hypervariance in short-range connections could indicate instability of local-module connectivity (Chen et al., 2017). Further, several nodes including Frontal_Inf_Orb and Caudate

TABLE 6 | Areas showing significant correlation between region flexibility and ADOS social scores in each age group.

Node flexibility					
ROI	**Abbreviation**	**Network**	**Name**	***r***	***p***
CHILDREN					
50	SOG.R	Visual	Occipital_Sup_R	0.50	0.012
86	MTG.R	DMN	Temporal_Mid_R	−0.41	0.037
ADOLESCENTS					
17	ROL.L	Sensorimotor	Rolandic_Oper_L	0.46	0.023
43	CAL.L	Visual	Calcarine_L	0.52	0.008
45	CUN.L	Visual	Cuneus_L	0.41	0.036
46	CUN.R	Visual	Cuneus_R	0.47	0.019
48	LING.R	Visual	Lingual_R	0.53	0.007
50	SOG.R	Visual	Occipital_Sup_R	0.49	0.010
72	CAU.R	Subcortical	Caudate_R	0.47	0.022
ADULTS					
21	OLF.L	Sensorimotor	Olfactory_L	0.69	0.004
43	CAL.L	Visual	Calcarine_L	0.61	0.012
45	CUN.L	Visual	Cuneus_L	0.56	0.027

TABLE 7 | Nodes showing significant correlation of node cohesion strength with ADOS social score.

ROI	Abbreviation	ROI name	Network	*r*	*p*
CHILDREN					
7	MFG.L	Frontal_Mid_L	Attention	0.44	0.021
13	IFGtriang.L	Frontal_Inf_Tri_L	Attention	0.40	0.044
23	SFGmed.L	Frontal_Sup_Medial_L	DMN	0.47	0.009
ADOLESCENT					
45	CUN.L	Cuneus_L	Visual	0.41	0.035
ADULT					
18	ROL.R	Rolandic_Oper_R	Sensorimotor	−0.60	0.011
43	CAL.L	Calcarine_L	Visual	0.67	0.006
51	MOG.L	Occipital_Mid_L	Visual	0.56	0.033
57	PoCG.L	Postcentral_L	Sensorimotor	−0.52	0.038

showed both hyper-variability in connection strength and altered modular organization (flexibility) in ASD (**Figures 2**, **3**).

In the next analysis, we explored dynamic network measures such as network flexibility, cohesion and disjointness to understand changes in functional connectivity that occur over time. Recent work in the field of network flexibility has centered around the relationship between task-performance or task-sentiment analysis with dynamic reconfiguration of the brain (Park et al., 2017; Telesford et al., 2017) especially in the memory areas (Douw et al., 2015). Changes in flexibility have been associated with mood (Betzel et al., 2017), inter-subject differences have been linked to learning (Bassett et al., 2011), working memory performance (Braun et al., 2015), and reinforcement learning (Gerraty et al., 2018). The metric has also been found to correlate with schizophrenia risk, and is altered by an NMDA-receptor antagonist (Braun et al., 2016). Flexibility also has age-based variation (Schlesinger et al., 2017).

TABLE 8 | Nodes showing significant correlation of node disjointness with ADOS social score.

ROI	Abbreviation	ROI name	Network	*r*	*p*
CHILDREN					
14	IFGtriang.R	Frontal_Inf_Tri_R	Attention	0.46	0.022
34	DCG.R	Cingulum_Mid_R	Subcortical	0.57	0.003
84	TPOsup.R	Temporal_Pole_Sup_R	Sensorimotor	0.51	0.009
ADOLESCENT					
24	SFGmed.R	Frontal_Sup_Medial_R	DMN	−0.57	0.003
46	CUN.R	Cuneus_R	Visual	0.52	0.008
48	LING.R	Lingual_R	Visual	0.55	0.005
82	STG.R	Temporal_Sup_R	Sensorimotor	0.47	0.012
86	MTG.R	Temporal_Mid_R	DMN	−0.56	0.004
ADULT					
42	AMYG.R	Amygdala_R	Subcortical	0.52	0.039
50	SOG.R	Occipital_Sup_R	Visual	0.57	0.021

Recent work has established that there is a significant negative correlation between flexibility and modularity using task-based fMRI studies (Ramos-Nuñez et al., 2017).

In our study, we found that such a correlation exists even in the resting-state functional brain as well. We found that while dynamic flexibility correlates negatively with the static metric of modularity in TD, such a correlation does not exist in ASD (**Figure 4**). However, both TD and ASD showed a range of flexibilities, indicating that the whole-brain flexibility remains intact. This indicates that the modular re-organization with variations in flexibility is not observed in ASD. It is possible that there are network/nodal changes that compensate for the change in flexibility. We also found that modularity scores did not correlate with the symptom severity ADOS score while network-based flexibility scores showed a significant positive/negative correlation (**Figure 5**). This further indicates that static network measures are unable to capture the underlying variability in ASD with respect to the ADOS scores. In contrast, dynamic network measures have significant predictive power of ADOS scores.

We found that in the resting-state functional brain, regions with lower flexibility are those involved in visual, hearing and motor processes while those with higher flexibility are those typically associated with the default mode network, cognitive control and executive function. This organization has been previously reported in task-based fMRI studies (Cole et al., 2013; Braun et al., 2015; Mattar et al., 2015; Schlesinger et al., 2017). Cole et al. (2013) reported that higher flexibility in fronto-pareital network was associated with better task performance. de Lacy et al. (2017) reported that the number of state transitions were reduced in ASD as compared to TD, due to disruptions in the fronto-pareital network and impaired state transitions in the cingulo-opercular systems. In our study, we found that there is reduced flexibility of periphery regions (DMN, subcortical and attention areas) in ASD which could impair the state transitions.

Although network flexibility did not show disease or age effect, we found regions (nodes) that show their independent effect. Significant effect of disease is observed in TPOsup, which is an important area linked to verbal and non-verbal communication

identified to show abnormal behavior in autism. It is a key periphery region which shows increased flexibility in the TD group. The decrease of flexibility of TPOsup could contribute to the nature of atypical verbal behavior observed in ASD. Only one region shows the effect of disease while several regions show correlation of ADOS score and flexibility. We hypothesize that in the ANOVA analysis, the underlying variability in ASD with respect to symptom severity is lost as they are considered as a single group. We also observed that ASD showed an atypical decrease in node cohesion strength and an increase in disjointness. Telesford et al. (2017) found that node cohesion strength showed positive correlation with performance in a task. Our results suggest that for resting-state dynamics, sensorimotor and visual regions show high cohesion strength while DMN shows relatively high disjointness.

Further, cohesion strength of sensorimotor regions correlates negatively ($r = -0.6$) with ADOS symptom severity score (**Table 6**), while regions of other networks show positive correlation ($r \sim 0.5$). The findings suggest that while sensorimotor areas are the least flexible, they are required to be less cohesive as well.

Our study differs in several aspects from previously reported dynamic whole-brain network-level investigations in ASD (Chen et al., 2017; de Lacy et al., 2017; Rashid et al., 2018). Most of the previous studies on dynamic functional connectivity in ASD combined sliding window analysis with *k*-means clustering to identify common brain states among all subjects (both ASD and TD). On the other hand, Watanabe and Rees (2017) concatenated the timeseries of ASD subjects to characterize the energy landscape of ASD. However, in our study, we have captured the variability among subjects by performing dynamic analysis on each individual subject. We uncovered the effect of development, disease, and their interactions on the dynamic metrics.

CONCLUSION

To the best of our knowledge, this is one of the first studies to use dynamic modularity metrics like flexibility and cohesion to study altered dynamics in ASD and TD.

We found very high correlation of ADOS score with the flexibility and disjointness of Sensorimotor regions. This is indicative of the importance of maintaining the cohesion and rigidity of motor cortex regions in TD. It can be noted that in our study, static modularity does not show a correlation with ADOS scores. Using temporal modularity metrics for dynamic analysis is a recent approach and lacks standardization across clinical studies. Whole brain connectivity anomaly and differences are highly sensitive to the parameters used while partitioning the BOLD timeseries into instantaneous dynamic FC matrices. To study the robustness of our results, we also repeated the dFCvar analysis using different window parameters and found consistent results (**Supplementary Information**).

We also re-run the multi-layer modularity algorithm with different sets of parameter values for γ and ω. We found consistently a positive correlation between ADOS scores and visual network connections (**Supplementary Information**). Further, it is also extremely important to correct for head motion as it is an important confounding factor. Several studies have shown that not correcting for it can lead to spurious instantaneous connections, either increased or decreased. In our study, we have exercised scrutiny by using samples from a single site which are corrected for motion artifacts and considered samples with low framewise displacement scores that were approved by manual functional QA raters. This resulted in fewer samples in each age group affecting the statistics.

We observed very high correlation between dynamic connectivity metrics (flexibility, cohesion, and disjointness) and ADOS scores (**Tables 6–8**), however the *p*-values did not survive multiple comparisons. Increasing the number of participants in each group will help to validate our findings. Overall, this study provides insights into the patterns observed in the functional brain systems of TD and ASD from a dynamic perspective, which can be further extended using a longitudinal design, including a larger subject pool across sites and combining structural data as well.

ETHICS STATEMENT

We used data from the ABIDE Preprocessed Initiative repository. Each site participating in ABIDE is required to confirm that the local Institutional Review Board (IRB) have allowed the collection as well as sharing of the data.

AUTHOR CONTRIBUTIONS

VH, DR, and PV have designed the research problem. VH, PV, RB, and DR carried out the original research. VH analyzed data. VH, PV, RB, and DR have all contributed in writing this original research article.

FUNDING

DR is supported by the Ramalingaswami fellowship (BT/RLF/Re-entry/07/2014) and DST extramural grant (SR/CSRI/21/2016). PV acknowledges financial support from the Early Career Research Award Scheme (ECR/2016/000488), Science and Engineering Research Board, DST, India.

ACKNOWLEDGMENTS

The pre-print of this article is released on BiorXiv (Harlalka et al., 2018a).

SUPPLEMENTARY MATERIAL

The Supplementary Material for this article can be found online at: https://www.frontiersin.org/articles/10.3389/fnhum.2019.00006/full#supplementary-material

REFERENCES

Allen, E. A., Damaraju, E., Plis, S. M., Erhardt, E. B., Eichele, T., and Calhoun, V. D. (2014). Tracking whole-brain connectivity dynamics in the resting state. *Cereb. Cortex* 24, 663–676. doi: 10.1093/cercor/bhs352

Bassett, D. S., Wymbs, N. F., Porter, M. A., Mucha, P. J., Carlson, J. M., and Grafton, S. T. (2011). Dynamic reconfiguration of human brain networks during learning. *Proc. Natl. Acad. Sci. U.S.A.* 108, 7641–7646. doi: 10.1073/pnas.1018985108

Betzel, R. F., Fukushima, M., He, Y., Zuo, X.-N., and Sporns, O. (2016). Dynamic fluctuations coincide with periods of high and low modularity in resting-state functional brain networks. *NeuroImage* 127, 287–297. doi: 10.1016/j.neuroimage.2015.12.001

Betzel, R. F., Satterthwaite, T. D., Gold, J. I., and Bassett, D. S. (2017). Positive affect, surprise, and fatigue are correlates of network flexibility. *Sci. Rep.* 7:520. doi: 10.1038/s41598-017-00425-z

Blondel, V. D., Guillaume, J.-L., Lambiotte, R., and Lefebvre, E. (2008). Fast unfolding of communities in large networks. *J. Stat. Mech.* 2008:P10008. doi: 10.1088/1742-5468/2008/10/P10008

Braun, U., Schäfer, A., Bassett, D. S., Rausch, F., Schweiger, J. I., Bilek, E., et al. (2016). Dynamic brain network reconfiguration as a potential schizophrenia genetic risk mechanism modulated by NMDA receptor function. *Proc. Natl. Acad. Sci. U.S.A.* 113, 12568–12573. doi: 10.1073/pnas.1608819113

Braun, U., Schäfer, A., Walter, H., Erk, S., Romanczuk-Seiferth, N., Haddad, L., et al. (2015). Dynamic reconfiguration of frontal brain networks during executive cognition in humans. *Proc. Natl. Acad. Sci. U.S.A.* 112, 11678–11683. doi: 10.1073/pnas.1422487112

Cameron, C., Yassine, B., Carlton, C., Francois, C., Alan, E., András, J., et al. (2013). The neuro bureau preprocessing initiative: open sharing of preprocessed neuroimaging data and derivatives. *Front. Neuroinformat.* 2013:00041. doi: 10.3389/conf.fninf.2013.09.00041

Chang, C., and Glover, G. H. (2010). Time–frequency dynamics of resting-state brain connectivity measured with fMRI. *NeuroImage* 50, 81–98. doi: 10.1016/j.neuroimage.2009.12.011

Chao-Gan, Y., and Yu-Feng, Z. (2010). DPARSF: a MATLAB toolbox for "pipeline" data analysis of resting-state fMRI. *Front. Syst. Neurosci.* 4:13. doi: 10.3389/fnsys.2010.00013

Chen, G., Zhang, H.-Y., Xie, C., Chen, G., Zhang, Z.-J., Teng, G.-J., et al. (2013). Modular reorganization of brain resting state networks and its independent validation in Alzheimer's disease patients. *Front. Hum. Neurosci.* 7:00456. doi: 10.3389/fnhum.2013.00456

Chen, H., Nomi, J. S., Uddin, L. Q., Duan, X., and Chen, H., (2017). intrinsic functional connectivity variance and state-specific under-connectivity in autism: state-related functional connectivity in autism. *Hum. Brain Mapp.* 38, 5740–5755. doi: 10.1002/hbm.23764

Cole, M. W., Reynolds, J. R., Power, J. D., Repovs, G., Anticevic, A., and Braver, T. S. (2013). Multi-task connectivity reveals flexible hubs for adaptive task control. *Nat. Neurosci.* 16, 1348–1355. doi: 10.1038/nn.3470

Damaraju, E., Allen, E. A., Belger, A., Ford, J. M., McEwen, S., Mathalon, D. H., et al. (2014). Dynamic functional connectivity analysis reveals transient states of dysconnectivity in schizophrenia. *NeuroImage* 5, 298–308. doi: 10.1016/j.nicl.2014.07.003

de Lacy, N., Doherty, D., King, B. H., Rachakonda, S., and Calhoun, V. D. (2017). Disruption to control network function correlates with altered dynamic connectivity in the wider autism spectrum. *NeuroImage* 15, 513–524. doi: 10.1016/j.nicl.2017.05.024

Deco, G., Ponce-Alvarez, A., Mantini, D., Romani, G. L., Hagmann, P., and Corbetta, M. (2013). Resting-state functional connectivity emerges from structurally and dynamically shaped slow linear fluctuations. *J Neurosci.* 33, 11239–11252. doi: 10.1523/JNEUROSCI.1091-13.2013

Douw, L., Leveroni, C. L., Tanaka, N., Emerton, B. C., Cole, A. C., Reinsberger, C., et al. (2015). Loss of resting-state posterior cingulate flexibility is associated with memory disturbance in left temporal lobe epilepsy. *PLoS ONE* 10:e0131209. doi: 10.1371/journal.pone.0131209

Douw, L., Wakeman, D. G., Tanaka, N., Liu, H., and Stufflebeam, S. M. (2016). State-dependent variability of dynamic functional connectivity between frontoparietal and default networks relates to cognitive flexibility. *Neuroscience* 339, 12–21. doi: 10.1016/j.neuroscience.2016.09.034

Falahpour, M., Thompson, W. K., Abbott, A. E., Jahedi, A., Mulvey, M. E., Datko, M., et al. (2016). Underconnected, but not broken? dynamic functional connectivity mri shows underconnectivity in autism is linked to increased intra-individual variability across time. *Brain Connect.* 6, 403–414. doi: 10.1089/brain.2015.0389

Garcia, J. O., Ashourvan, A., Muldoon, S., Vettel, J. M., and Bassett, D. S. (2018). Applications of community detection techniques to brain graphs: algorithmic considerations and implications for neural function. *Proc. IEEE* 106, 846–867. doi: 10.1109/JPROC.2017.2786710

Gerraty, R. T., Davidow, J. Y., Foerde, K., Galvan, A., Bassett, D. S., and Shohamy, D. (2018). Dynamic flexibility in striatal-cortical circuits supports reinforcement learning. *J. Neurosci.* 38, 2442–2453. doi: 10.1523/JNEUROSCI.2084-17.2018

Hahamy, A., Behrmann, M., and Malach, R. (2015). The idiosyncratic brain: distortion of spontaneous connectivity patterns in autism spectrum disorder. *Nat. Neurosci.* 18, 302–309. doi: 10.1038/nn.3919

Harlalka, V., Bapi Raju, S., Vinod, P. K., and Roy, D. (2018a). Atypical flexibility in dynamic functional connectivity quantifies the severity in autism spectrum disorder. *bioXriv* doi: 10.1101/387886

Harlalka, V., Bapi Raju, S., Vinod, P. K., and Roy, D. (2018b). Age, disease and their interaction effects on intrinsic connectivity of children and adolescents in autism spectrum disorder using functional connectomics. *Brain Connect.* doi: 10.1089/brain.2018.0616. [Epub ahead of print].

Henry, T. R., Dichter, G. S., and Gates, K. (2018). Age and gender effects on intrinsic connectivity in autism using functional integration and segregation. *Biol. Psychiatry Cogn. Neurosci. Neuroimaging* 3, 414–422. doi: 10.1016/j.bpsc.2017.10.006

Jutla, I. S., Jeub, L. G. S., and Mucha, P. J. (2011–2012). *A Generalized Louvain Method for Community Detection Implemented in Matlab*. Available online at: http://netwiki.amath.unc.edu/GenLouvain

Lee, M. H., Smyser, C. D., and Shimony, J. S. (2013). Resting-State fMRI: a review of methods and clinical applications. *Am. J. Neuroradiol.* 34, 1866–1872. doi: 10.3174/ajnr.A3263

Liao, W., Wu, G.-R., Xu, Q., Ji, G.-J., Zhang, Z., Zang, Y.-F., and Lu, G. (2014). DynamicBC : a matlab toolbox for dynamic brain connectome analysis. *Brain Connect.* 4, 780–790. doi: 10.1089/brain.2014.0253

Lin, P., Yang, Y., Jovicich, J., De Pisapia, N., Wang, X., Zuo, C. S., and Levitt, J. J. (2016). Static and dynamic posterior cingulate cortex nodal topology of default mode network predicts attention task performance. *Brain Imaging Behav.* 10, 212–225. doi: 10.1007/s11682-015-9384-6

Liu, X., and Duyn, J. H. (2013). Time-varying functional network information extracted from brief instances of spontaneous brain activity. *Proc. Natl. Acad. Sci. U.S.A.* 110, 4392–4397. doi: 10.1073/pnas.1216856110

Mattar, M. G., Cole, M. W., Thompson-Schill, S. L., and Bassett, D. S. (2015). A functional cartography of cognitive systems. *PLoS Computat. Biol.* 11:e1004533. doi: 10.1371/journal.pcbi.1004533

Murphy, K., Birn, R. M., Handwerker, D. A., Jones, T. B., and Bandettini, P. A. (2009). The impact of global signal regression on resting state correlations: are anti-correlated networks introduced? *Neuroimage* 44, 893–905. doi: 10.1016/j.neuroimage.2008.09.036.

Park, J. E., Jung, S. C., Ryu, K. H., Oh, J. Y., Kim, H. S., Choi, C.-G., et al. (2017). Differences in dynamic and static functional connectivity between young and elderly healthy adults. *Neuroradiology* 59, 781–789. doi: 10.1007/s00234-017-1875-2

Preti, M. G., Bolton, T. A., and Van De Ville, D. (2017). The dynamic functional connectome: State-of-the-art and perspectives. *NeuroImage* 160, 41–54. doi: 10.1016/j.neuroimage.2016.12.061

Ramos-Nuñez, A. I., Fischer-Baum, S., Martin, R. C., Yue, Q., Ye, F., and Deem, M. W. (2017). Static and dynamic measures of human brain connectivity predict complementary aspects of human cognitive performance. *Front. Hum. Neurosci.* 11:420. doi: 10.3389/fnhum.2017.00420

Rashid, B., Blanken, L. M. E., Muetzel, R. L., Miller, R., Damaraju, E., Arbabshirani, M. R., et al. (2018). Connectivity dynamics in typical development and its relationship to autistic traits and autism spectrum disorder. *Hum. Brain Mapp.* 39, 3127–3142. doi: 10.1002/hbm.24064

Rudie, J. D., Brown, J. A., Beck-Pancer, D., Hernandez, L. M., Dennis, E. L., Thompson, P. M., et al. (2013). Altered functional and structural brain

network organization in autism. *NeuroImage* 2, 79–94. doi: 10.1016/j.nicl.2012.11.006

Rudie, J. D., Shehzad, Z., Hernandez, L. M., Colich, N. L., Bookheimer, S. Y., Iacoboni, M., et al. (2012). Reduced functional integration and segregation of distributed neural systems underlying social and emotional information processing in autism spectrum disorders. *Cereb. Cortex* 22, 1025–1037. doi: 10.1093/cercor/bhr171

Saad, Z. S., Gotts, S. J., Murphy, K., Chen, G., Jo, H. J., Martin, A., et al. (2012). Trouble at rest: how correlation patterns and group differences become distorted after global signal regression. *Brain Connect.* 2, 25–32. doi: 10.1089/brain.2012.0080

Schlesinger, K. J., Turner, B. O., Lopez, B. A., Miller, M. B., and Carlson, J. M. (2017). Age-dependent changes in task-based modular organization of the human brain. *NeuroImage* 146, 741–762. doi: 10.1016/j.neuroimage.2016.09.001

Song, J., Birn, R. M., Boly, M., Meier, T. B., Nair, V. A., Meyerand, M. E., et al. (2014). Age-related reorganizational changes in modularity and functional connectivity of human brain networks. *Brain Connect.* 4, 662–676. doi: 10.1089/brain.2014.0286

Sporns, O. (2013). Structure and function of complex brain networks. *Dialog. Clin. Neurosci.* 15, 247–262.

Tailby, C., Kowalczyk, M. A., and Jackson, G. D. (2018). Cognitive impairment in epilepsy: the role of reduced network flexibility. *Ann. Clin. Transl. Neurol.* 5, 29–40. doi: 10.1002/acn3.503

Telesford, Q. K., Ashourvan, A., Wymbs, N. F., Grafton, S. T., Vettel, J. M., and Bassett, D. S. (2017). Cohesive network reconfiguration accompanies extended training: cohesive network reconfiguration. *Hum. Brain Mapp.* 38, 4744–4759. doi: 10.1002/hbm.23699

van den Heuvel, M. P., and Hulshoff Pol, H. E. (2010). Exploring the brain network: a review on resting-state fMRI functional connectivity. *Eur. Neuropsychopharmacol.* 20, 519–534. doi: 10.1016/j.euroneuro.2010.03.008

Watanabe, T., and Rees, G. (2017). Brain network dynamics in high-functioning individuals with autism. *Nat. Commun.* 8:16048. doi: 10.1038/ncomms16048

Weissenbacher, A., Kasess, C., Gerstl, F., Lanzenberger, R., Moser, E., and Windischberger, C. (2009). Correlations and anticorrelations in resting-state functional connectivity MRI: a quantitative comparison of preprocessing strategies. *Neuroimage* 47, 1408–1416. doi: 10.1016/j.neuroimage.2009.05.005

Xu, Y., and Lindquist, M. A. (2015). Dynamic connectivity detection: an algorithm for determining functional connectivity change points in fMRI data. *Front. Neurosci.* 9:00285. doi: 10.3389/fnins.2015.00285

Ye, M., Yang, T., Qing, P., Lei, X., Qiu, J., and Liu, G. (2015). Changes of functional brain networks in major depressive disorder: a graph theoretical analysis of resting-State fMRI. *PLoS ONE* 10:e0133775. doi: 10.1371/journal.pone.0133775

Yerys, B. E., Gordon, E. M., Abrams, D. N., Satterthwaite, T. D., Weinblatt, R., Jankowski, K. F., et al. (2015). Default mode network segregation and social deficits in autism spectrum disorder: Evidence from non-medicated children. *NeuroImage* 9, 223–232. doi: 10.1016/j.nicl.2015.07.018

Zalesky, A., Fornito, A., and Bullmore, E. T. (2010). Network-based statistic: identifying differences in brain networks. *NeuroImage* 53, 1197–1207. doi: 10.1016/j.neuroimage.2010.06.041

Conflict of Interest Statement: The authors declare that the research was conducted in the absence of any commercial or financial relationships that could be construed as a potential conflict of interest.

frontiers in Human Neuroscience

ORIGINAL RESEARCH
published: 14 March 2019
doi: 10.3389/fnhum.2019.00075

Structural Magnetic Resonance Imaging Demonstrates Abnormal Regionally-Differential Cortical Thickness Variability in Autism: From Newborns to Adults

Jacob Levman[1,2,3]*, *Patrick MacDonald*[1], *Sean Rowley*[3], *Natalie Stewart*[1], *Ashley Lim*[1], *Bryan Ewenson*[3], *Albert Galaburda*[4] *and Emi Takahashi*[1,2]

[1] *Division of Newborn Medicine, Department of Medicine, Boston Children's Hospital, Harvard Medical School, Boston, MA, United States,* [2] *Athinoula A. Martinos Center for Biomedical Imaging, Massachusetts General Hospital, Harvard Medical School, Charlestown, MA, United States,* [3] *Department of Mathematics, Statistics and Computer Science, St. Francis Xavier University, Antigonish, NS, Canada,* [4] *Department of Neurology, Beth Israel Deaconess Medical Center, Harvard Medical School, Boston, MA, United States*

Autism is a group of complex neurodevelopmental disorders characterized by impaired social interaction and restricted/repetitive behavior. We performed a large-scale retrospective analysis of 1,996 clinical neurological structural magnetic resonance imaging (MRI) examinations of 781 autistic and 988 control subjects (aged 0–32 years), and extracted regionally distributed cortical thickness measurements, including average measurements as well as standard deviations which supports the assessment of intra-regional cortical thickness variability. The youngest autistic participants (<2.5 years) were diagnosed after imaging and were identified retrospectively. The largest effect sizes and the most common findings not previously published in the scientific literature involve abnormal intra-regional variability in cortical thickness affecting many (but not all) regions of the autistic brain, suggesting irregular gray matter development in autism that can be detected with MRI. Atypical developmental patterns have been detected as early as 0 years old in individuals who would later be diagnosed with autism.

Keywords: autistic, cortical thickness, development, neuroanatomy, variability

OPEN ACCESS

Edited by:
Srikantan S. Nagarajan, University of California, San Francisco, United States

Reviewed by:
Madhura A. Ingalhalikar, Symbiosis International University, India
Carly Demopoulos, University of California, San Francisco, United States

***Correspondence:**
Jacob Levman
jacob.levman@childrens.harvard.edu

Received: *21 September 2017*
Accepted: *13 February 2019*
Published: *14 March 2019*

Citation:
Levman J, MacDonald P, Rowley S, Stewart N, Lim A, Ewenson B, Galaburda A and Takahashi E (2019) Structural Magnetic Resonance Imaging Demonstrates Abnormal Regionally-Differential Cortical Thickness Variability in Autism: From Newborns to Adults. Front. Hum. Neurosci. 13:75. doi: 10.3389/fnhum.2019.00075

INTRODUCTION

Autism is characterized by impaired social communication, deficits in social reciprocity and repetitive/stereotyped behaviors (Gillberg, 1993; Wing, 1997). Evidence for the existence of neuroanatomical differences between participants with autism and control subjects comes from a variety of postmortem and neuroimaging research (Toal et al., 2005; Amaral et al., 2008). Magnetic resonance imaging (MRI) provides a wide variety of physiological/anatomical measurements of a participant's brain, information that may assist in both clinical applications and basic research. The most commonly used MRI method produces structural information related to the concentration of hydrogen protons, providing clinically useful soft tissue contrast. In the brain, structural MRI provides for the ability to differentiate between gray matter, white matter and cerebrospinal fluid, which forms the basis for the extraction of a variety of measurements distributed across brain

regions, such as white matter volume measurements, cortical thickness measurements, cortical folding/gyration-based measurements, cortical surface area measurements, and more (Fischl, 2012).

The analysis of autistic participants who have undergone structural MRI examinations has been the subject of many studies in the literature that have incorporated distributed quantification of volumes, cortical thicknesses, surface areas etc. with automated biomarker extraction technologies, such as FreeSurfer (Fischl, 2012). However, existing studies have been limited in the populations assessed, providing incomplete data regarding the developmental stages of autistic participants, particularly in terms of the ages of participants included in the analysis and the number of participants included in the age range being evaluated (Dziobek et al., 2010; Ecker et al., 2010, 2013, 2014; Groen et al., 2010; Jiao et al., 2010; Schumann et al., 2010; Schaer et al., 2013, 2015; Wallace et al., 2013; Zielinski et al., 2014; Lefebvre et al., 2015; Richter et al., 2015; Haar et al., 2016; Yang et al., 2016). Furthermore, although investigating average cortical thickness is common in the literature (Jiao et al., 2010; Ecker et al., 2013, 2014; Zielinski et al., 2014; Yang et al., 2016), none of the studies appears to have considered intra-regional cortical thickness variability as a measurement of potential interest in autism. Intra-regional cortical thickness variability measurements are readily available in FreeSurfer (Fischl, 2012) in the form of the standard deviation of within-region cortical thickness measurements. Examples of two examinations exhibiting differing cortical thickness standard deviation measurements are provided in **Figure 1** to illustrate intra-regional cortical thickness variability to the reader.

It is particularly challenging to assess imaging features of autism in a pediatric population, because of the structural changes between children and adults (Reiss et al., 1996; Casey et al., 1997; Thomas et al., 2001; Bunge et al., 2002; Gogtay et al., 2004; Fair et al., 2009; Supekar et al., 2009). Important information regarding brain function is encoded in distributed patterns of brain activity and structure (Mesulam, 1981; Vaadia et al., 1995; McIntosh et al., 1996; Fox et al., 2005), and identifying these patterns is particularly challenging in a pre-adult population, because of a rapidly changing anatomy and physiology, a high degree of brain plasticity, small brain sizes, participant motion, and an incomplete understanding of brain development.

In the present study, we hypothesize that the assessment of cortical thickness from clinical structural MRI examinations has the potential to assist in the diagnosis of autism and to improve our understanding of brain physiology associated with the condition. This study attempts to provide a thorough assessment of the clinical potential for structural MRI in assessing cortical thickness by including all available autistic participants who received MRI examinations at Boston Children's Hospital (BCH) at 3 Tesla producing volumetric T1 examinations compatible with the automated extraction of distributed measurements (Fischl, 2012). We hypothesize that regional differences in average cortical thickness and cortical thickness variability measurements are associated with the clinical presentation of the autistic brain and can be identified by structural MRI. These differences were assessed individually in each identified brain region in order to see whether our analysis is sensitive to region-specific neurodevelopmental abnormalities associated with autism.

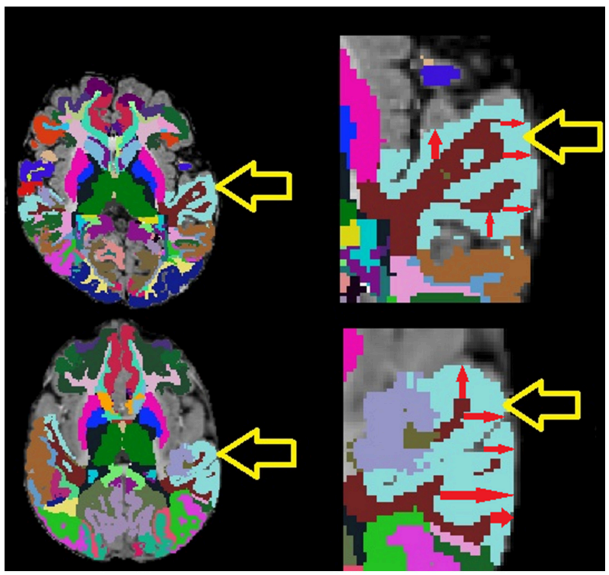

FIGURE 1 | Example MRI examinations with FreeSurfer ROIs (colored regions) with magnifications. Yellow arrows point to the light blue superior temporal cortex, red arrows provide demonstrative examples of some of the many within-region cortical thickness measurements computed by FreeSurfer. Note that the exam on top exhibits lower cortical thickness variability than the exam on the bottom which exhibits highly varying cortical thickness measurements.

MATERIALS AND METHODS

Participants

Following approval by BCH's Institutional Review Board (informed consent was waived due to the lack of risk to participants included in this retrospective analysis), the clinical imaging electronic database at BCH was reviewed for the present analysis from 01/01/2008 until 02/24/2016, and all brain MRI examinations of participants aged 0 to 32 years at the time of imaging were included for further analysis if autism was indicated in the participant's electronic medical records. More detailed diagnostic information (such as Autism Diagnostic Interview, Revised–ADI-R and Autism Diagnostic Observation Schedule–ADOS gold standard diagnoses) were not available in this dataset and this issue is addressed in more detail in the limitations section of the discussion. Examinations deemed to be of low quality (because of excessive participant motion, large metal artifact from a participant's dental hardware, lack of a T1 structural imaging volume providing diagnostically useful axial, sagittal and coronal oriented images etc.) were excluded from the study. Examinations that were inaccessible for technical reasons were also excluded. This yielded 1,003 examinations from 781 autistic participants. Control subjects were assembled retrospectively in a previous analysis (Levman et al., 2017) by selecting participants on the basis of a normal MRI examination, as assessed by a BCH neuroradiologist,

and whose medical records provided no indication of any neurological problems (participants with any known disorder were excluded such as autism, cerebral palsy, traumatic brain injury, brain cancer, developmental delay, multiple sclerosis, tuberous sclerosis complex, stroke, neurofibromatosis, cortical dysplasia, epilepsy, attention deficit hyperactivity disorder, etc.). Participants with any form of non-neurological cancer were also excluded to avoid data exhibiting growth trajectories negatively affected by treatments such as chemotherapy. The same exclusion criteria applied to the autistic population were also applied to the control subjects. This yielded 993 examinations from 988 control subjects. Histograms demonstrating the age distributions for both the control subjects and autistic groups are provided in **Figure 2**. **Table 1** provides a breakdown of the autistic and healthy populations divided by age groups used in the statistical analysis section of this manuscript's Methods.

MRI Data Acquisition and Preprocessing

Participants were imaged with clinical 3 Tesla MRI scanners (Skyra, Siemens Medical Systems, Erlangen, Germany) at BCH yielding T1 structural volumetric images accessed through the Children's Research and Integration System (Pienaar et al., 2014). Because of the clinical and retrospective nature of this study, there is variability in the pulse sequences employed to acquire these volumetric T1 examinations. Spatial resolution varied in the x and y directions from 0.219 to 1.354 mm (mean: 0.917 mm, standard deviation: 0.124 mm). Through-plane slice thickness varied from 0.500 to 2.000 mm (mean: 0.996 mm, standard deviation: 0.197 mm). Strengths and limitations of the large-scale varying MR protocol approach taken in this study are addressed in the Discussion. Motion correction was not performed, but examinations with substantial motion artifacts were carefully excluded based on visual assessment. These motion corruption exclusions were performed to compensate for the additional difficulties autistic patients have remaining still during image acquisition relative to the control subjects. T1 structural examinations were processed with FreeSurfer (Fischl, 2012) using the recon_all command which aligns the input examination to all available atlases. Those atlases that include cortical thickness measurements were included for further analysis (aparc, aparc.a2009, aparc.DKTatlas40, BA, BA.thresh, entorhinal_*exvivo*). These combined atlases include definitions of 331 cortical regions. Each FreeSurfer output T1 structural examination was displayed with label map overlays and visually inspected for quality of regional segmentation results. If FreeSurfer results were observed to substantially fail, they were excluded from this analysis (i.e. FreeSurfer regions-of-interest (ROIs) that do not align to the MRI and examinations where major problems were observed with an ROI such as a cerebellar segmentation extending far beyond the extent of the cerebellum).

Statistical Analysis

This study included the acquisition of 662 regionally distributed cortical thickness measurements per imaging examination, as extracted by FreeSurfer's recon-all command which processes the input examination with all available atlases (Fischl, 2012). This included extracting measurements of both average and the standard deviation of within-region cortical thicknesses for each supported gray matter region. This includes all sub-regions of the brain supporting cortical thickness measurements across all FreeSurfer supported atlases. Study participants were divided into four groups based on age: early childhood (0–5 years old), late childhood (5–10 years old), early adolescence (10–15 years old), and late adolescence (15–20 years old). We had very few participants older than 20 years and so did not include them in a separate group, however, all scatter plots included all participants regardless of age to facilitate visual comparison. Trend lines in all scatter plots were established with a rolling average ($K = 150$) implemented in MATLAB. We are interested in the diagnostic potential of these clinically acquired measurements and so each measurement (as extracted by FreeSurfer) within each age range was compared in a group-wise manner (autism compared with control subjects) with receiver operating characteristic (ROC) curve analysis which is summarized with the area under the ROC curve (AUC) (Youngstrom, 2014), Cohen's d statistic (positive/negative values indicate a higher/lower average value in the autistic population relative to the control subjects) and a *p*-value based on the standard *t*-test (Student, 1908) for two groups of samples. The *p*-value was selected as an established method to demonstrate that it is unlikely that our findings were the result of random chance, Cohen's d was selected as it is the most established method to assess effect sizes and the AUC was selected to extend our analysis to the assessment of diagnostic potential. This yielded a total of $m = 2{,}648$ group-wise comparisons, yielding a Bonferroni corrected threshold for achieving statistical significance of $p < 0.05/m = 1.89e^{-5}$.

In order to confirm that the findings reported are the result of group-wise differences between the autistic and control subjects, a statistical model was constructed based on multivariate regression using MATLAB's (Natick, MA) mvregress function, adjusting each measurement within each age range in order to control for group-wise differences in age, gender, estimated total intracranial volume and the leading comorbid status of the most common secondary conditions from our two groups: headaches (7% in the autistic group, 19% in the control subjects), attention deficit hyperactivity disorder / ADHD (16% in the autistic group, 0% in the control subjects), epilepsy (13% in the autistic group, 0% in the control subjects), global developmental delay (26% in the autistic group, 0% in the control subjects), migraines (3% in the autistic group, 23% in the control subjects), and abdominal pain (14% in the autistic group, 11% in the control subjects). This model was used to adjust each cortical thickness (mean and standard deviation) measurement, in order to evaluate whether group-wise differences between our autistic and control subjects are the result of age, gender, intracranial volume or comorbid effects.

A preliminary statistical validation was performed on the independently acquired Autism Brain Imaging Data Exchange (ABIDE) dataset (Di Martino et al., 2014). The ABIDE dataset is a multi-center study with variability in data acquisition between centers. We have elected to perform a preliminary validation analysis assessing the leading five feature measurements identified in our findings (first five rows of **Table 2**) against the single ABIDE imaging center with the most

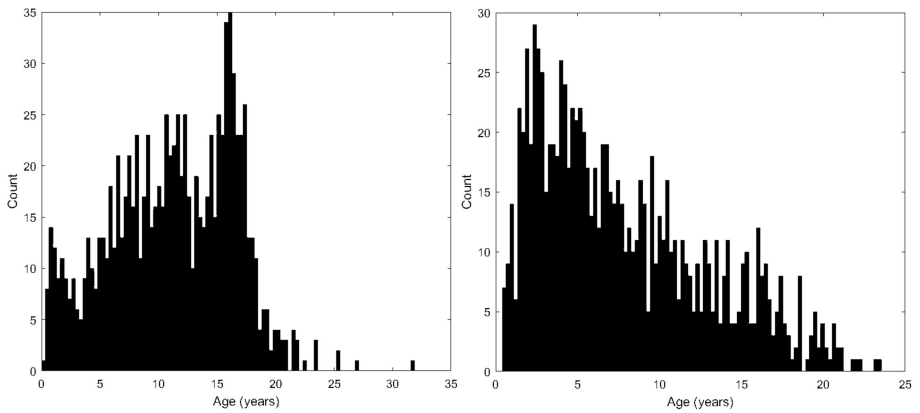

FIGURE 2 | Histograms demonstrating the population age distributions in this study's neurotypical participants **(left)** and autistic participants **(right)**.

TABLE 1 | Demographic breakdown of our two populations.

Group	0 to 5 years	5 to 10 years	10 to 15 years	15 to 20 years	20+ years
Neurotypical	M = 71, F = 68	M = 124, F = 137	M = 115, F = 177	M = 80, F = 194	M = 4, F = 23
	2.59 ± 1.43 yrs	7.63 ± 1.41 yrs	12.41 ± 1.41 yrs	16.70 ± 1.11 yrs	22.21 ± 2.63 yrs
Autistic	M = 278, F = 101	M = 242, F = 74	M = 144, F = 37	M = 97, F = 14	M = 12, F = 4
	2.89 ± 1.19 yrs	7.23 ± 1.47 yrs	12.17 ± 1.43 yrs	16.97 ± 1.42 yrs	21.27 ± 1.01 yrs

M, count of males; F, count of females; each are followed by the average and standard deviation of this group's ages in years (yrs).

participants aged 15–20 at imaging (the USM-ABIDE data) as this age range exhibited the largest group-wise differences in our study. Raw (unadjusted) measurements extracted by FreeSurfer from the ABIDE dataset are directly compared with raw (unadjusted) measurements extracted by FreeSurfer from our large clinical BCH dataset.

RESULTS

Many brain regions showed Bonferroni-corrected, statistically significant differences in cortical thickness measurements between participants with autism and control subjects (**Table 2**). Namely, there were a large number of regions of the brain exhibiting abnormal intra-regional variability in cortical thickness as measured with the standard deviation. Average cortical thickness differences between our control subjects and autistic participants were also observed across several regions of the brain (**Table 2**). Of the 2,648 group-wise comparisons performed, 21.9% exceeded the Bonferroni correction for statistical significance, indicating that many brain regions did not exhibit abnormal presentation of cortical thicknesses. Each measurement in **Table 2** exceeds the Bonferroni correction in at least one age group, however, all age groupings are provided for ease of comparison.

The age-dependent, d statistic and ROC curve analyses yielded a variety of measurements that offer diagnostic potential and may help elucidate the underlying anatomical and physiological conditions associated with autism. **Table 2** presents the leading measurements organized by AUC (highest AUC values are found at the top of the table), along with the associated d statistic as computed from the unadjusted measurement data produced by FreeSurfer. Thus, the superior temporal gyrus exhibits the most separation between groups (ages 15–20), the second most separation is found in the middle occipital gyrus (ages 15–20), etc. Our statistically adjusted data using multivariate-regression exhibits decreased p-values and increased separation between our autistic and control subjects relative to the raw data extracted with FreeSurfer. This was performed to confirm that the findings reported are not the result of age, gender, intracranial volume, or comorbid effects. We elected to present the raw results rather than the adjusted results because of the potential role of raw data in future diagnostic technologies and for ease of comparison with future studies.

Histograms demonstrating the age distributions for both the control subjects and autistic groups are provided in **Figure 2**. Examples of distributed gray and white matter ROIs of longitudinal relaxation (T1) structural MRI examinations of 11-months-old and 18-years-old autistic and control subjects are shown in **Figure 3** (left panel). The variability (standard deviation) of the thickness of the inferior and superior temporal cortices (yellow arrows in **Figure 3**) demonstrate group-wise differences between our autistic and control groups. Magnified ROIs are provided to assist in visualization of differences in cortical thickness variability. Note the reduced cortical thickness variability in the young autistic participant (bottom) as compared with the control subject (top) and the inversion of this effect among older participants. Scatter plots of the standard deviation (*SD*) of the cortical thickness in both our autistic and

TABLE 2 | Age-dependent ROC Analysis Results – Leading Measurements by AUC with Cohen's d statistic.

Cortical measurement of interest	Measurement type (CT)	Ages 0–5 years L&R: AUC/d	Ages 5–10 years L&R: AUC/d	Ages 10–15 years L&R: AUC/d	Ages 15–20 years L&R: AUC/d
Superior temporal cortex	Variability	L (0.58/−0.29) R (0.59/−0.34)	L (0.59/0.33) R (0.64/0.45)	L (0.64/0.54) R (0.63/0.49)	L (0.73/0.83) R (0.75/0.91)
Middle occipital gyrus	Variability	L (0.62/−0.40) R (0.60/−0.35)	L (0.65/0.54) R (0.62/0.44)	L (0.63/0.50) R (0.62/0.42)	L (0.74/0.90) R (0.71/0.72)
Superior parietal cortex	Variability	L (0.67/−0.57) R (0.67/−0.51)	L (0.53/0.12) R (0.54/0.16)	L (0.60/0.42) R (0.59/0.39)	L (0.71/0.74) R (0.74/0.90)
Brodmann's area 6	Variability	L (0.62/−0.37) R (0.64/−0.40)	L (0.56/0.19) R (0.54/0.12)	L (0.63/0.44) R (0.61/0.38)	L (0.73/0.78) R (0.71/0.70)
Superior temporal sulcus	Variability	L (0.66/−0.52) R (0.65/−0.49)	L (0.63/0.47) R (0.62/0.43)	L (0.67/0.63) R (0.62/0.43)	L (0.73/0.85) R (0.68/0.76)
Brodmann's area 18 (V2)	Variability	L (0.67/−0.61) R (0.62/−0.37)	L (0.60/0.45) R (0.55/0.26)	L (0.70/0.73) R (0.60/0.45)	L (0.73/0.91) R (0.67/0.71)
middle temporal visual area	Variability	L (0.63/−0.43) R (0.62/−0.50)	L (0.64/0.53) R (0.67/0.55)	L (0.67/0.60) R (0.66/0.57)	L (0.72/0.83) R (0.72/0.73)
Inferior temporal cortex	Variability	L (0.63/−0.41) R (0.61/−0.37)	L (0.60/0.42) R (0.60/0.35)	L (0.62/0.49) R (0.59/0.31)	L (0.72/0.85) R (0.70/0.72)
Brodmann's area 1	Variability	L (0.61/−0.35) R (0.61/−0.35)	L (0.52/0.00) R (0.50/−0.01)	L (0.55/0.20) R (0.55/0.14)	L (0.66/0.57) R (0.72/0.76)
Triangular part of inferior frontal gyrus	Variability	L (0.60/−0.35) R (0.59/−0.31)	L (0.57/0.17) R (0.57/0.17)	L (0.56/0.19) R (0.57/0.19)	L (0.69/0.68) R (0.72/0.78)
Supramarginal gyrus	Variability	L (0.62/−0.41) R (0.65/−0.53)	L (0.51/−0.06) R (0.53/0.07)	L (0.61/0.32) R (0.59/0.24)	L (0.72/0.73) R (0.67/0.53)
Superior parietal lobule	Variability	L (0.66/−0.53) R (0.66/−0.49)	L (0.52/0.06) R (0.52/0.09)	L (0.58/0.28) R (0.57/0.27)	L (0.67/0.59) R (0.71/0.79)
Banks of the superior temporal sulcus	Variability	L (0.60/−0.34) R (0.60/−0.26)	L (0.58/0.28) R (0.59/0.30)	L (0.61/0.48) R (0.59/0.36)	L (0.71/0.78) R (0.71/0.73)
Intraparietal sulcus	Variability	L (0.65/−0.54) R (0.67/−0.51)	L (0.50/0.03) R (0.54/0.15)	L (0.63/0.44) R (0.61/0.39)	L (0.70/0.64) R (0.71/0.77)
Brodmann's area 18 (V2)	Average	L (0.59/−0.25) R (0.59/−0.24)	L (0.59/0.33) R (0.58/0.32)	L (0.71/0.77) R (0.67/0.67)	L (0.67/0.71) R (0.71/0.82)
Inferior parietal cortex	Variability	L (0.66/−0.47) R (0.65/−0.50)	L (0.59/0.37) R (0.60/0.34)	L (0.64/0.51) R (0.61/0.43)	L (0.71/0.78) R (0.70/0.71)
Pars triangularis	Variability	L (0.61/−0.36) R (0.61/−0.33)	L (0.53/0.09) R (0.53/0.11)	L (0.52/0.08) R (0.58/0.26)	L (0.67/0.58) R (0.71/0.76)
Precuneus cortex	Variability	L (0.67/−0.57) R (0.67/−0.56)	L (0.54/0.11) R (0.56/0.17)	L (0.58/0.29) R (0.63/0.47)	L (0.69/0.69) R (0.71/0.72)
Medial orbitofrontal cortex	Average	L (0.63/−0.31) R (0.63/−0.30)	L (0.64/0.51) R (0.61/0.48)	L (0.71/0.78) R (0.67/0.69)	L (0.67/0.68) R (0.61/0.53)
Brodmann's area 2	Variability	L (0.64/−0.48) R (0.63/−0.42)	L (0.53/0.13) R (0.53/0.10)	L (0.54/0.21) R (0.58/0.29)	L (0.64/0.51) R (0.71/0.67)
Middle temporal gyrus	Variability	L (0.55/−0.20) R (0.61/−0.32)	L (0.56/−0.26) R (0.58/0.33)	L (0.59/0.35) R (0.65/0.56)	L (0.70/0.69) R (0.70/0.74)
Brodmann's area 45	Variability	L (0.61/−0.36) R (0.57/−0.26)	L (0.56/0.18) R (0.57/0.21)	L (0.54/0.14) R (0.59/0.23)	L (0.66/0.55) R (0.70/0.71)
Superior frontal cortex	Variability	L (0.63/−0.43) R (0.63/−0.44)	L (0.52/0.03) R (0.50/0.01)	L (0.59/0.32) R (0.60/0.33)	L (0.70/0.69) R (0.67/0.65)
Gyrus rectus	Average	L (0.61/−0.28) R (0.59/−0.21)	L (0.64/0.50) R (0.61/0.44)	L (0.70/0.75) R (0.61/0.48)	L (0.64/0.57) R (0.53/0.18)
Lateral orbitofrontal cortex	Average	L (0.62/−0.23) R (0.58/−0.01)	L (0.60/0.33) R (0.57/0.29)	L (0.67/0.60) R (0.70/0.71)	L (0.65/0.56) R (0.63/0.52)
Lateral aspect of superior temporal gyrus	Variability	L (0.59-0.26) R (0.59/−0.29)	L (0.50/0.05) R (0.57/0.23)	L (0.58/0.33) R (0.58/0.37)	L (0.70/0.74) R (0.70/0.69)
Middle frontal gyrus	Variability	L (0.66/−0.53) R (0.63/−0.48)	L (0.52/−0.04) R (0.51/−0.06)	L (0.54/0.17) R (0.55/0.18)	L (0.69/0.64) R (0.70/0.69)
Precentral cortex	Variability	L (0.60/−0.34) R (0.60/−0.30)	L (0.55/0.19) R (0.54/0.17)	L (0.57/0.27) R (0.53/0.11)	L (0.70/0.73) R (0.66/0.57)
Medial orbital sulcus	Average	L (0.60/−0.28) R (0.56/−0.16)	L (056/0.32) R (0.58/0.35)	L (0.63/0.53) R (0.68/0.65)	L (0.64/0.56) R (0.70/0.75)
Fusiform cortex	Variability	L (0.60/−0.35) R (0.59/−0.25)	L (0.69/0.69) R (0.65/0.52)	L (0.66/0.63) R (0.63/0.49)	L (0.65/0.62) R (0.66/0.64)
Occipital pole	Average	L (0.51/0.09) R (0.51/0.04)	L (0.59/0.33) R (0.62/0.44)	L (0.69/0.68) R (0.67/0.65)	L (0.67/0.61) R (0.69/0.74)
Lateral occipital Cortex	Variability	L (0.65/−0.48) R (0.63-0.42)	L (0.60/0.42) R (0.55/0.27)	L (0.59/0.38) R (0.61/0.38)	L (0.69/0.78) R (0.66/0.55)
Caudal middle frontal cortex	Variability	L (0.64/−0.44) R (0.62/−0.39)	L (0.52/−0.03) R (0.50/−0.02)	L (0.55/0.18) R (0.56/0.22)	L (0.69/0.67) R (0.69/0.63)
Paracentral sulcus and lobule	Variability	L (0.64/−0.44) R (0.60/−0.30)	L (0.51/0.05) R (0.52/0.10)	L (0.55/0.17) R (0.53/0.18)	L (0.63/0.41) R (0.69/0.66)
Brodmann's area 17 (V1)	Average	L (0.62/−0.37) R (0.61/−0.29)	L (0.64/0.50) R (0.57/0.30)	L (0.69/0.71) R (0.65/0.61)	L (0.65/0.60) R (0.62/0.48)
Lingual cortex	Variability	L (0.64/−0.53) R (0.64/−0.40)	L (0.53/0.19) R (0.51/0.12)	L (0.55/0.26) R (0.52/0.13)	L (0.69/0.71) R (0.58/0.32)
Lateral occipital cortex	Average	L (0.51/0.12) R (0.49/0.01)	L (0.50/0.01) R (0.54/0.17)	L (0.63/0.44) R (0.65/0.56)	L (0.69/0.69) R (0.69/0.70)
H-shaped orbital sulcus	Variability	L (0.51/−0.08) R (0.55/−0.11)	L (0.51/0.04) R (0.51/0.02)	L (0.53/0.04) R (0.57/0.27)	L (0.59/0.31) R (0.69/0.67)
Isthmus cingulate cortex	Variability	L (0.54/−0.12) R (0.54/−0.11)	L (0.56/0.23) R (0.58/0.35)	L (0.65/0.52) R (0.69/0.63)	L (0.63/0.52) R (0.61/0.40)
Cuneus gyrus	Average	L (0.56/−0.21) R (0.58/−0.24)	L (0.63/0.49) R (0.59/0.36)	L (0.69/0.75) R (0.65/0.60)	L (0.64/0.62) R (0.61/0.54)
Inferior part of the precentral sulcus	Variability	L (0.62/−0.43) R (0.64/−0.51)	L (0.53/0.10) R (0.50/−0.01)	L (0.57/0.21) R (0.59/0.28)	L (0.69/0.62) R (0.68/0.55)

R, right; L, left; CT, cortical thickness; Variability, standard deviation of cortical thickness; AUC, area under the ROC curve; d, Cohen's d statistic.

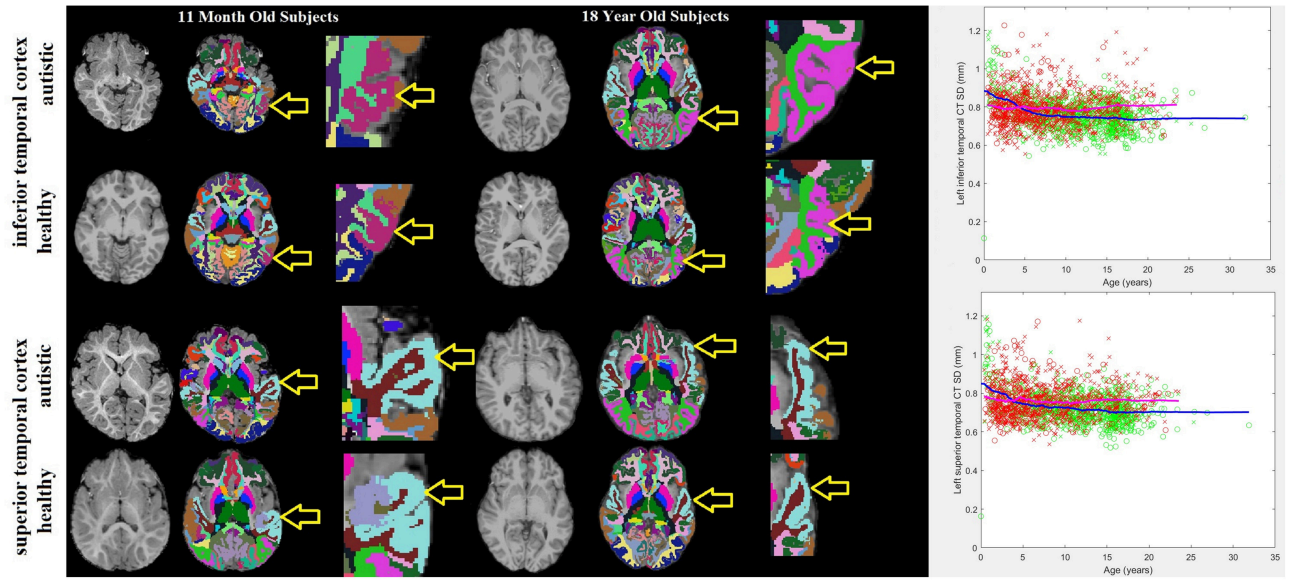

FIGURE 3 | 11-months-old and 18-years-old participants with autism and typically developing controls. Three images are provided for each participant: the MRI examination **(left)**, the automatically generated ROI with colors representing sub-regions of the brain identified **(center)** and a magnified image of the tissue-of-interest's ROI **(right)**. Yellow arrows point to the purple shaded inferior temporal cortex ROI and the light blue shaded superior temporal cortex ROI. To the far right are scatter plots of age variations with the standard deviation of the thickness of the left inferior and superior temporal cortices in autistic participants (red) and neurotypical controls (green). Male participants are represented by an "x," females with an "o." Trend lines are plotted (magenta = autistic, blue = neurotypical).

control subjects (**Figure 3**, right side) demonstrate age variability and gender.

Table 2 demonstrates that the leading cortical thickness measurements illustrating group-wise differences between our autistic and control subjects are mostly intra-regional variability with very few average thickness measurements. **Table 3** summarizes our leading measurements-of-interest while providing bilateral effect size statistics across all age groups to help elucidate potential physiological characteristics of autism. In order to support a thorough analysis, all available FreeSurfer brain atlases were included in this study, resulting in **Tables 2**,**3** reporting overlapping regions of interest including measurements across a region's cortex as well as localized gyral, sulcal, and lobular measurements when available.

We have performed a preliminary validation with the ABIDE dataset (Di Martino et al., 2014). We have elected to perform a preliminary validation analysis assessing the leading five feature measurements identified in our findings (first five rows of **Table 2**) against the ABIDE imaging center with the most participants aged 15–20 at imaging (the USM-ABIDE data) as this age range exhibited the largest group-wise differences in our study. Results confirm four out of our leading five cortical thickness variability measurements with reduced diagnostic potential relative to our BCH data: left superior temporal (BCH: AUC = 0.73, ABIDE: AUC = 0.64), right superior parietal (BCH: AUC = 0.74, ABIDE: AUC = 0.62), right Brodmann's area 6 (BCH: AUC = 0.71, ABIDE: AUC = 0.58), right superior temporal sulcus (BCH: AUC = 0.68, ABIDE: AUC = 0.61), and the left middle occipital gyrus (BCH: 0.74, ABIDE: 0.50). This confirmed our findings in four of our five leading measurements (all but the middle occipital gyrus), albeit with reduced separation between the control subjects and autistic groups in the ABIDE dataset. Reduced separation in the ABIDE dataset relative to BCH data may be caused by differences in distributions of autistic severity in each group with the routine clinical BCH data likely to exhibit increased proportions of unhealthy autistic children (those with comorbidities) which may also be correlated with more severe manifestations of autism. In contrast, the ABIDE dataset's autistic population's intelligence quotients (IQ) are similar to their control subject counterparts (Di Martino et al., 2014), implying that the dataset might disproportionately represent children with high functioning autism. While we were unable to confirm abnormal cortical thickness variability in the middle occipital gyrus in the ABIDE dataset, we did observe abnormal average cortical thickness in the left middle occipital gyrus (AUC = 0.64) and abnormal cortical thickness variability in the inferior occipital gyrus (AUC = 0.61) in this preliminary ABIDE validation.

DISCUSSION

We performed a large-scale cortical thickness analysis of structural MRI examinations of the brain in autistic and neurotypical individuals and demonstrated group-wise differences in cortical thickness variability as well as average values localized to select regions across the brain. Many brain regions showed differences in intra-regional variability of the cortical thickness, which was reported for the first time in this study. Atypical developmental patterns have been detected as early as 0 years old in individuals who would later be diagnosed

TABLE 3 | Summary of measurements with effect sizes potentially associated with known autistic characteristics.

Autistic characteristics	Potentially associated measurements	Brain regions affected	Ages 0–5 L&R: d	Ages 5–10 L&R: d	Ages 10–15 L&R: d	Ages 15–20 L&R: d
Facial & Visual processing	Inferior parietal cortex *SD*	Parietal	L ($d = -0.47$) R ($d = -0.50$)	L ($d = 0.37$) R ($d = 0.34$)	L ($d = 0.51$) R ($d = 0.43$)	L ($d = 0.78$) R ($d = 0.71$)
	Brodmann's area 1 *SD*	Parietal	L ($d = -0.35$) R ($d = -0.35$)	L ($d = 0.00$) R ($d = -0.01$)	L ($d = 0.20$) R ($d = 0.14$)	L ($d = 0.57$) R ($d = 0.76$)
	Intraparietal sulcus *SD*	Parietal	L ($d = -0.54$) R ($d = -0.51$)	L ($d = 0.03$) R ($d = 0.15$)	L ($d = 0.44$) R ($d = 0.39$)	L ($d = 0.64$) R ($d = 0.77$)
	Precuneus *SD*	Parietal	L ($d = -0.57$) R ($d = -0.56$)	L ($d = 0.11$) R ($d = 0.17$)	L ($d = 0.29$) R ($d = 0.47$)	L ($d = 0.69$) R ($d = 0.72$)
	Brodmann's area 2 *SD*	Parietal	L ($d = -0.48$) R ($d = -0.42$)	L ($d = 0.13$) R ($d = 0.10$)	L ($d = 0.21$) R ($d = 0.29$)	L ($d = 0.51$) R ($d = 0.67$)
	Inferior temporal cortex *SD*	Temporal	L ($d = -0.41$) R ($d = -0.37$)	L ($d = 0.42$) R ($d = 0.35$)	L ($d = 0.49$) R ($d = 0.31$)	L ($d = 0.85$) R ($d = 0.72$)
	Fusiform cortex *SD*	Temporal	L ($d = -0.35$) R ($d = -0.25$)	L ($d = 0.69$) R ($d = 0.52$)	L ($d = 0.63$) R ($d = 0.49$)	L ($d = 0.62$) R ($d = 0.64$)
	Superior temporal sulcus *SD*	Temporal	L ($d = -0.52$) R ($d = -0.49$)	L ($d = 0.47$) R ($d = 0.43$)	L ($d = 0.63$) R ($d = 0.43$)	L ($d = 0.85$) R ($d = 0.76$)
	Middle temporal visual area *SD*	Temporal	L ($d = -0.43$) R ($d = -0.50$)	L ($d = 0.53$) R ($d = 0.55$)	L ($d = 0.60$) R ($d = 0.57$)	L ($d = 0.83$) R ($d = 0.73$)
	Middle occipital gyrus *SD*	Occipital	L ($d = -0.40$) R ($d = -0.35$)	L ($d = 0.54$) R ($d = 0.44$)	L ($d = 0.50$) R ($d = 0.42$)	L ($d = 0.90$) R ($d = 0.72$)
	Brodmann's Area 18 mean	Occipital	L ($d = -0.25$) R ($d = -0.24$)	L ($d = 0.33$) R ($d = 0.32$)	L ($d = 0.77$) R ($d = 0.67$)	L ($d = 0.71$) R ($d = 0.82$)
	Brodmann's Area 17 mean	Occipital	L ($d = -0.37$) R ($d = -0.29$)	L ($d = 0.50$) R ($d = 0.30$)	L ($d = 0.71$) R ($d = 0.61$)	L ($d = 0.60$) R ($d = 0.48$)
	Lingual cortex *SD*	Occipital	L ($d = -0.53$) R ($d = -0.40$)	L ($d = 0.19$) R ($d = 0.12$)	L ($d = 0.26$) R ($d = 0.13$)	L ($d = 0.71$) R ($d = 0.32$)
	Cuneus gyrus mean	Occipital	L ($d = -0.21$) R ($d = -0.24$)	L ($d = 0.49$) R ($d = 0.36$)	L ($d = 0.75$) R ($d = 0.60$)	L ($d = 0.62$) R ($d = 0.54$)
Speech & Language processing	Triangular part of the inferior frontal gyrus *SD*	Frontal	L ($d = -0.35$) R ($d = -0.31$)	L ($d = 0.17$) R ($d = 0.17$)	L ($d = 0.19$) R ($d = 0.19$)	L ($d = 0.68$) R ($d = 0.78$)
	Pars triangularis *SD*	Frontal	L ($d = -0.36$) R ($d = -0.33$)	L ($d = 0.09$) R ($d = 0.11$)	L ($d = 0.08$) R ($d = 0.26$)	L ($d = 0.58$) R ($d = 0.76$)
	Brodmann's Area 45 *SD*	Frontal	L ($d = -0.36$) R ($d = -0.26$)	L ($d = 0.18$) R ($d = 0.21$)	L ($d = 0.14$) R ($d = 0.23$)	L ($d = 0.55$) R ($d = 0.71$)
	Supramarginal cortex *SD*	Parietal	L ($d = -0.41$) R ($d = -0.53$)	L ($d = -0.06$) R ($d = 0.07$)	L ($d = 0.32$) R ($d = 0.24$)	L ($d = 0.73$) R ($d = 0.53$)
	Superior temporal gyrus *SD*	Temporal	L ($d = -0.29$) R ($d = -0.34$)	L ($d = 0.33$) R ($d = 0.45$)	L ($d = 0.54$) R ($d = 0.49$)	L ($d = 0.83$) R ($d = 0.91$)
	Middle temporal gyrus *SD*	Temporal	L ($d = -0.20$) R ($d = -0.32$)	L ($d = -0.26$) R ($d = 0.33$)	L ($d = 0.35$) R ($d = 0.56$)	L ($d = 0.69$) R ($d = 0.74$)
	Lingual cortex *SD*	Occipital	L ($d = -0.53$) R ($d = -0.40$)	L ($d = 0.19$) R ($d = 0.12$)	L ($d = 0.26$) R ($d = 0.13$)	L ($d = 0.71$) R ($d = 0.32$)
Movement and Motor control	Precentral cortex *SD*	Frontal	L ($d = -0.34$) R ($d = -0.30$)	L ($d = 0.19$) R ($d = 0.17$)	L ($d = 0.57$) R ($d = 0.11$)	L ($d = 0.70$) R ($d = 0.57$)
	Brodmann's Area 6	Frontal	L ($d = -0.37$) R ($d = -0.40$)	L ($d = 0.19$) R ($d = 0.12$)	L ($d = 0.44$) R ($d = 0.38$)	L ($d = 0.78$) R ($d = 0.70$)
	Paracentral lobule and sulcus *SD*	Frontal	L ($d = -0.44$) R ($d = -0.30$)	L ($d = 0.05$) R ($d = 0.10$)	L ($d = 0.17$) R ($d = 0.18$)	L ($d = 0.41$) R ($d = 0.66$)
	Supramarginal cortex *SD*	Parietal	L ($d = -0.41$) R ($d = -0.53$)	L ($d = -0.06$) R ($d = 0.07$)	L ($d = 0.32$) R ($d = 0.24$)	L ($d = 0.73$) R ($d = 0.53$)
	Superior parietal *SD*	Parietal	L ($d = -0.57$) R ($d = -0.51$)	L ($d = 0.12$) R ($d = 0.16$)	L ($d = 0.42$) R ($d = 0.39$)	L ($d = 0.74$) R ($d = 0.90$)
	Intraparietal sulcus *SD*	Parietal	L ($d = -0.54$) R ($d = -0.51$)	L ($d = 0.03$) R ($d = 0.15$)	L ($d = 0.44$) R ($d = 0.39$)	L ($d = 0.64$) R ($d = 0.77$)
	Precuneus *SD*	Parietal	L ($d = -0.57$) R ($d = -0.56$)	L ($d = 0.11$) R ($d = 0.17$)	L ($d = 0.29$) R ($d = 0.47$)	L ($d = 0.69$) R ($d = 0.72$)
	Superior temporal gyrus *SD*	Temporal	L ($d = -0.29$) R ($d = -0.34$)	L ($d = 0.33$) R ($d = 0.45$)	L ($d = 0.54$) R ($d = 0.49$)	L ($d = 0.83$) R ($d = 0.91$)
	Lateral occipital cortex *SD*	Occipital	L ($d = -0.48$) R ($d = -0.42$)	L ($d = 0.42$) R ($d = 0.27$)	L ($d = 0.38$) R ($d = 0.38$)	L ($d = 0.78$) R ($d = 0.55$)
	Lateral occipital cortex mean	Occipital	L ($d = 0.12$) R ($d = 0.01$)	L ($d = 0.01$) R ($d = 0.17$)	L ($d = 0.44$) R ($d = 0.56$)	L ($d = 0.69$) R ($d = 0.70$)
	Brodmann's Area 18 mean	Occipital	L ($d = -0.25$) R ($d = -0.24$)	L ($d = 0.33$) R ($d = 0.32$)	L ($d = 0.77$) R ($d = 0.67$)	L ($d = 0.71$) R ($d = 0.82$)
Empathy deficits & Emotional processing	Lateral orbitofrontal cortex mean	Frontal	L ($d = -0.23$) R ($d = -0.01$)	L ($d = 0.33$) R ($d = 0.29$)	L ($d = 0.60$) R ($d = 0.71$)	L ($d = 0.56$) R ($d = 0.52$)
	Supramarginal cortex *SD*	Parietal	L ($d = -0.41$) R ($d = -0.53$)	L ($d = -0.06$) R ($d = 0.07$)	L ($d = 0.32$) R ($d = 0.24$)	L ($d = 0.73$) R ($d = 0.53$)
	Inferior parietal cortex *SD*	Parietal	L ($d = -0.47$) R ($d = -0.50$)	L ($d = 0.37$) R ($d = 0.34$)	L ($d = 0.51$) R ($d = 0.43$)	L ($d = 0.78$) R ($d = 0.71$)
	Precuneus *SD*	Parietal	L ($d = -0.57$) R ($d = -0.56$)	L ($d = 0.11$) R ($d = 0.17$)	L ($d = 0.29$) R ($d = 0.47$)	L ($d = 0.69$) R ($d = 0.72$)
	Superior temporal sulcus *SD*	Temporal	L ($d = -0.52$) R ($d = -0.49$)	L ($d = 0.47$) R ($d = 0.43$)	L ($d = 0.63$) R ($d = 0.43$)	L ($d = 0.85$) R ($d = 0.76$)

R, right; L, left; SD, standard deviation; d, Cohen's d statistic.

with autism. We have confirmed our results using a publicly open database. Reduced cortical thickness variability was observed in the early years followed by abnormally increased variability in later years in autism.

Potential Association Between Our Findings and Known Symptoms of Autism

The majority of the leading measurements of interest identified in this study have potential to be associated with known outward symptoms and characteristics (endophenotypes) of autism (**Table 3**), including disorders of visual and facial processing (Behrmann et al., 2006), empathy and emotional processing (Jones et al., 2010), speech and language processing (Kellerman et al., 2005; Wan and Schlaug, 2010), as well as movement and motor control (Dziuk et al., 2007).

We found brain regions potentially associated with disorders of visual facial processing including the left inferior temporal region (Haxby et al., 2000) (**Figure 3**), the bilateral inferior parietal region, which is involved in the perception of emotions in facial stimuli (Radua et al., 2010), the left superior temporal sulcus, which has been claimed to be involved in the perception of where others are directing their gaze, and is thought to be important in determining where others' emotions are being directed (Campbell et al., 1990), the right fusiform region, which has been observed to influence the amygdala's response to emotional faces (Stephanou et al., 2016) and activation therein has been observed in autistic participants viewing faces (Hadjikhani et al., 2004), the middle occipital gyrus, which is involved in visual processing, Brodmann's areas 1 (image texture processing), 2 (object size and shape processing), and areas 17 and 18, which are involved in primary visual processing and for which abnormal activation has been observed among the autistic (Soulieres et al., 2009; Clery et al., 2013), the intraparietal sulcus, which is involved in visual attention, the precuneus which is involved in visuo-spatial imagery (Cavanna and Trimble, 2006), and finally, the lingual region, which appears to provide input to the ventral face area (McCarthy et al., 1999).

Identified brain regions potentially associated with disorders of speech and language include the bilateral superior temporal region (**Figure 3**) and Heschl's gyrus, which contain Brodmann's areas 41, 42, 22, representing the primary and part of the association auditory cortex (Bigler et al., 2007), pars triangularis (bilaterally) (Brodmann's area 45, triangular part of the inferior frontal gyrus), corresponding to Broca's language area in the left frontal lobe, the supramarginal gyrus, which may be associated with language function as lesions therein may cause receptive aphasia (Gazzaniga et al., 2009), the middle temporal gyrus, which has been identified as a critical node in the brain's language network (Acheson and Hagoort, 2013) and finally, the lingual and fusiform regions, which have been shown to be involved in language tasks (Mechelli et al., 2000).

Measurements demonstrating group-wise differences were also found in brain regions potentially associated with movement and motor control disorders including: the bilateral supramarginal gyrus, which is involved in the perception of space and limb locations, the left lateral occipital region and the bilateral inferior temporal gyrus (Brodmann areas 18, 19, 37), which are involved in visual object recognition (Logothetis and Sheinberg, 1996), the precentral gyrus, which is the site of the primary motor cortex (Brodmann's area 4), the superior parietal region, which is thought to be involved with spatial orientation, Brodmann's area 6, which contains the premotor cortex and in which abnormal activation has been observed among autistic participants relative to control subjects (Mostofsky et al., 2009; Barbeau et al., 2015), the intraparietal sulcus, which incorporates visual control with motor movements, the precuneus, which is involved in attention to motor targets (Cavanna and Trimble, 2006), the paracentral sulcus and lobule, which corresponds to the supplementary motor area, and finally, the superior temporal cortex (**Figure 3**), whose right hemisphere mediates spatial awareness and exploration (Karnath, 2001).

Regions potentially linked to empathy deficits and disorders of emotional processing include the bilateral orbitofrontal region, which forms the basis for an existing test for autism (Stone et al., 1998), the superior temporal gyrus (**Figure 3**) and the bilateral inferior parietal region, which is involved in the perception of emotions in facial stimuli (Radua et al., 2010), the bilateral supramarginal region, which is thought to be associated with empathy (Silani, 2013), and finally, the precuneus, which has been shown to activate when a participant decides whether to act out of empathy or forgiveness (Farrow et al., 2001).

Additionally, the bilateral middle frontal region, which is thought to be involved in episodic memory retrieval (Rajah et al., 2011), also exhibits abnormalities among autistic participants, which may have a pervasive impact on the development of other brain regions if such development is reliant on recalling past stimuli.

Variability in cortical thickness may be indicative of underlying structural abnormalities prevalent among individuals with autism. These findings potentially implicate abnormal gray matter development among autistic participants. Given that group-wise comparisons demonstrate abnormally reduced cortical thickness variability in the early years followed by abnormally increased variability in later years in autism, it is possible that autism or autism-susceptible individuals tend to have late-onset cortical development followed by a rapid, "excessive maturation" potentially caused by genetic and/or environmental effects in a participant's teenaged years. It is also possible that genes linked to pubertal development are associated with the inversion of this effect in a participant's teenaged years.

Strengths of This Study

The main strength of this research is that it is the largest single center study of its type in terms of the number of exams and includes a wide range of developmental ages among the study's participants. This retrospective analysis included a cohort of very young participants who received imaging prior to their diagnosis of autism, a population difficult to include in a traditional prospective study design, which typically requires recruitment of participants based on a pre-existing diagnosis. This work also involved incorporating intra-regional variability of cortical thickness measurements (Fischl, 2012), making this study more thorough than typical approaches that focus only on average

cortical thickness measurements (Jiao et al., 2010; Zielinski et al., 2014). Results of our study indicated that for many sub-regions of the brain, the most discriminating measurements at multiple age groups was the variability (standard deviation) of the cortical thickness, a measurement that does not appear to have been considered in studies published in the literature.

Our dataset includes many examinations of participants aged 0–2.5 years, providing data on early stages of autism's development that is minimal in the scientific literature. Many of our youngest patients were imaged with MRI prior to their autism diagnosis. By including all samples available, we provide a thorough analysis of a clinical population, which is ideal for the assessment and development of diagnostic tests that ultimately would be applied to autistic participants who receive routine clinical imaging. Future generations of diagnostic technologies will be responsible for the correct identification of a variety of pathological conditions (autism included) from large pools of participants assessed with routine clinical imaging, making clinically imaged autistic participants an interesting population for further research despite this group not having been studied in-depth to date.

Relationship With Existing Literature Findings

MRI data acquisition involves measurement noise. Additional noise can be introduced by FreeSurfer technology. Furthermore, there is a natural amount of variability in both the control subjects investigated, as well as in our autistic participants. These factors result in substantial measurement variability when employing MRI and FreeSurfer to assess autistic and control subjects. This variability may explain the inconsistencies reported in the many MRI-based autism FreeSurfer studies that have been published in the literature, which are based on relatively small sample sizes, from widely ranging age groups, none of which cover the entire age range from newborn to adult (Groen et al., 2010; Jiao et al., 2010; Schumann et al., 2010; Schaer et al., 2013, 2015; Wallace et al., 2013; Ecker et al., 2014; Zielinski et al., 2014; Richter et al., 2015; Yang et al., 2016). With few samples available, differences between autistic and control subjects may appear to exist when the observed effect could merely be a by-product of high levels of measurement variability. With high measurement variability, few samples and many measurements evaluated, some measurements will exhibit substantial group-wise differences by chance. Insufficient sample sizes in the presence of high levels of measurement variability can lead to erroneous findings. Measurement variability can also obscure real effects as non-statistically significant when sample sizes are very low. Despite these shortcomings, our study was able to confirm literature findings of lowered average cortical thickness in the left parahippocampal region (6–15 years, AUC = 0.57, $p = 3.69e^{-5}$) and in the left frontal pole (6–15 years, AUC = 0.61, $p = 7.84e^{-8}$) as well as increased average cortical thickness in the left caudal anterior cingulate (6–15 years, AUC=0.58, $p = 5.48e^{-6}$) and increased thickness in the left precuneus (6–15 years, AUC = 0.58, $p = 4.10e^{-5}$) in agreement with literature findings (Jiao et al., 2010). We were also able to confirm increased average cortical thickness in the left pars opercularis (12–32 years, AUC = 0.62, $p = 4.33e^{-5}$), left rostral middle frontal (12–32 years, AUC = 0.60, $p = 3.93e^{-6}$), left frontal pole (12–32 years, AUC = 0.61, $p = 5.01e^{-7}$), right paracentral (12–32 years, AUC = 0.55, $p = 0.016$), and the right lateral occipital region (12–32 years, AUC = 0.68, $p = 3.11e^{-18}$) in agreement with literature findings (Zielinski et al., 2014). Our primary findings pertain to abnormal variability in regionally assessed cortical thickness in the developing autistic brain. When measurement variability is high, the number of samples required to have confidence in reported findings increases and provides motivation for conducting traditional average cortical thickness studies with large numbers of participants, in order to assist in producing literature findings that are consistent with one another.

Limitations

A major limitation of this study is a lack of gold standard diagnoses for autism (ADI-R and ADOS evaluations were unavailable). This problem is caused by the retrospective nature of this study, for which it was not feasible to interview each participant and thus electronic patient medical records were relied upon. While indications of autism are typically entered into the electronic patient medical records by a Boston Children's Hospital physician, this does not guarantee that our dataset does not include participants whose autistic status was established by a community physician who is not an expert in diagnosing autism. Additionally, intelligence quotient (IQ) information was unavailable for the participants in this study. The retrospective nature of this study makes it impossible to account for all variables tracked and controlled for in prospective studies, which include detailed participant interviews, but it is hoped that this work will identify physiological effects of interest that will be thoroughly validated in carefully controlled prospective studies as part of future work. It is also hoped that this work can help bridge the gap between prospective studies and what can be achieved clinically. An additional limitation of our study was the need to procure control subjects that were inferred to be typically developing from a routine clinical population. This was accomplished by excluding participants with indications of a long list of neurological issues while requiring each participant's MRI examination to have been assessed as normal by a BCH neuroradiologist (Levman et al., 2017). This process yielded 993 examinations from participants deemed most likely to represent control subjects from a large pool of MRI examinations, in order to best approximate a control population from large-scale routine clinical imaging. It is expected that the rate of false negatives (seemingly normal participants who in fact have a neurological issue) might be higher than the rate exhibited in typical well-controlled prospective studies and so may add variability to our control measurements and may represent an additional source of error in our study.

An additional limitation of this study is that it was performed retrospectively on participants that received imaging for a wide variety of reasons. Among the control subjects, the leading reasons for the MRI examinations were headaches (60%), to rule out intracranial pathologies (13%), vomiting (11%), and night awakenings (10%). Among our autistic participants, the

leading reasons for the MRI examinations were seizures (19%), to rule out intracranial pathologies (14%), and an abnormal EEG (9%). Since the population was drawn from routine clinical imaging, there is also a wide variety of comorbidities indicated in many of our participant's electronic medical records. The most common comorbidities in our control subjects are migraines (23%), headaches (19%), and abdominal pain (11%). The most common comorbidities in our autistic group are global developmental delay (26%), attention deficit hyperactivity disorder (16%), abdominal pain (14%), and epilepsy (13%). This study design was intended to provide a thorough analysis of a complete clinical population, providing a baseline of what to expect from other clinical populations and facilitating research into the next generation of diagnostic tests, which would be applied to populations akin to the one investigated in this study. Traditional MRI studies often involve imaging participants who are much healthier than is clinically realistic. The study design presented here allows for the assessment of what can be accomplished in a large-scale clinical context.

There is some variability in imaging parameters (spatial resolution, signal-to-noise ratio etc.) caused by variations in the pulse sequences employed; however, imaging was performed with a consistent set of 3 Tesla Siemens MRI scanners all installed at BCH in 2007. Ideally, this study would be performed on scans using a single MRI protocol; however, doing so would greatly reduce the number of samples available for inclusion in this analysis. Large sample sizes help to overcome potential bias associated with measurements that exhibit considerable variability. While limiting the analysis to a single imaging protocol would reduce potential bias caused by scan parameter variability, it would increase bias caused by sample size effects. Many measurements produced by FreeSurfer on our BCH dataset demonstrate that the discriminating power (between autistic and control subjects) of volumetric measurements (in mm^3) is approximately identical to the discriminating power of the voxel counts in those same regions (this includes ventricular volumes/voxel counts and corpus callosum volumes/voxel counts). Since voxel counts vary greatly based on spatial resolution variations, we believe the effect on our results caused by varying spatial resolutions in our MR protocols to be modest. In addition, we compared our large sample size findings with findings from an independent analysis performed at a single center with a single pulse sequence (USM-ABIDE). Thus, our primary findings have been confirmed independently with data that does not suffer from the issues.

An additional limitation of this study is that the age distributions of available participants for the two groups in this experiment vary considerably (**Figure 2**), because of the availability of appropriate participants that met our inclusion criteria from a large clinical population. This inevitably resulted in imbalanced pools of participants for further analysis. Our experiment did not involve age- or gender-based participant matching between our autistic and control subjects. Instead, we have opted to perform our statistical analyses in a group-wise manner, varying the age range under consideration, and to plot our main findings on an age-dependent basis while differentiating between male and female participants in our scatter plots. This methodology was selected to avoid the reduced sample size that would arise from only including those autistic participants who have a control subject counterpart with the same gender and identical age. Additionally, this methodology was selected in order to avoid having our analysis be influenced by the extent of difference between matched pairs of individuals, for which a variety of factors beyond age and gender might influence how appropriate it was for the participants to have been paired (brain volume, sub-structure volume, co-morbidities, etc.). We also performed a multivariate regression analysis that controls for the effects of age, gender, intracranial volume and several comorbidities in order to confirm that these factors aren't the cause of our reported findings. Comparative assessment of males and females from our control subjects revealed no major gender differences in terms of either mean or the standard deviation of the cortical thickness measurements. A large gender-segregated analysis of 442 control subjects has also been performed (Koolschijn and Crone, 2013) which did not identify our primary findings as exhibiting gender differences.

A variety of alternatives to the stringent Bonferroni correction were considered as alternative statistical analyses to be relied upon in this study. As a large-scale review of real-world clinical data, we are presenting an analysis of a considerably different type than is common in the literature. Our dataset, while having standardization advantages over many clinical centers (Boston Children's Hospital installed a suite of 3T Skyra Siemens MRI scanners in 2007, while most clinical centers have a variety of different MRI scanners), we have standardization disadvantages relative to typical prospective studies (in which all T1 volumetric examinations are normally acquired with an identical MRI pulse sequence). This inevitably introduces additional variability/error in our measurements and when designing our analytic strategies for assessing our data, we felt it important to be particularly cautious when presenting an effect that appears to be associated with the presentation of autism clinically. This is why the most stringent accepted method was used, to reduce the false discovery error rate and thus limit the likelihood that our analysis reports findings that will not be confirmed in future studies. Type II errors were of far less concern to us, as this is akin to accidentally declaring no effect associated with autism when a real effect was present. Our analysis is most concerned with assessing the largest effects and we recognize that a heterogeneous clinical population is not likely to be the best method available for assessing the existence of small effect sizes, thus our reduced concern for type II errors, which in turn lead to our decision to employ the extra-stringent Bonferroni correction in this analysis. Additionally, it should be noted that this was not a paired analysis, but instead a group-wise analysis performed on a large-scale real-world clinical population. In order to analyze a complete set of clinical data, there are inevitably differences between the two populations in terms of gender and age distributions (note that there are about 4 males with autism for every female, whereas there is about 1 control subject male for every female). The issues associated with these imbalances were addressed by comparing our results with an independent dataset (i.e., through external validation) and by employing multivariate linear regression to perform secondary analyses that demonstrate that our findings are still

statistically significant after controlling for the effects of gender and age.

An additional limitation of this study is that FreeSurfer is not optimized for the youngest participants in our analysis. As such, the rate at which FreeSurfer fails to extract measurements from clinical MRI examinations increases substantially for participants aged 0–8 months and the reliability of the results successfully produced by FreeSurfer on participants from this age range is uncertain. FreeSurfer's reliability was assessed as reasonable for participants 8-months-old and later (considering this is beyond the age range for which the technology was validated), at which point myelination contrast patterns have inverted so as to match the general pattern exhibited through the rest of life (with gray contrast located on the brain's periphery and white contrast occupying central regions). Research aimed at overcoming the problem of FreeSurfer's applicability and reliability in very young populations is ongoing (de Macedo Rodrigues et al., 2015; Zollei et al., 2017) and any developments in this venue will be incorporated into future work.

Future Work

In addition to incorporating infant FreeSurfer atlases, we will also extend this analysis to tractography, functional MRI (fMRI) and multivariate machine learning as well as to perform a detailed and thorough validation with the ABIDE dataset. Additional future work will involve correlating our dataset with detailed clinical information not available in the electronic patient medical records. This large-scale task may allow us to assess the potential association between MRI measurements and symptom severity, participant outcomes etc. Future work will also look at comparing the autistic group with groups at high risk for autism and groups that are clinically similar to autism in presentation in order to extend this work's diagnostic assessments to differential diagnosis.

Our results indicate that automatically extracted measurements can be used to predict the pathological status of a participant whose brain has been imaged with MRI; however, future work is needed to optimize the performance of such a diagnostic test. We hope that these research avenues will assist toward better understanding autism as well as improved characterization, diagnosis and classification of the disorder into subtypes.

AUTHOR CONTRIBUTIONS

PM, NS, and AL were responsible for data acquisition and analysis. BE and SR were responsible for the ABIDE validation. AG provided detailed feedback on study findings and their possible relation to brain function as well as manuscript editing. JL and ET designed the study and supervised PM, NS, and AL jointly. JL supervised BE and SR.

FUNDING

The authors would like to thank Dr. Henry Feldman, Principal Biostatistician at Boston Children's Hospital for advice on conducting statistical analyses. This work was supported by the National Institutes of Health (grant numbers R01HD078561, R21MH118739, R03NS091587, R21HD098606) to ET; Natural Science and Engineering Research Council of Canada's Canada Research Chair grant (grant number 231266) to JL, a Canada Foundation for Innovation and Nova Scotia Research and Innovation Trust infrastructure grant (R0176004) to JL and a St. Francis Xavier University research startup grant to JL (grant number R0168020).

REFERENCES

Acheson, D. J., and Hagoort, P. (2013). Stimulating the brain's language network: syntactic ambiguity resolution after TMS to the inferior frontal gyrus and middle temporal gyrus. *J. Cogn. Neurosci.* 25, 1664–1677. doi: 10.1162/jocn_a_00430

Amaral, D. G., Schumann, C. M., and Nordahl, C. W. (2008). Neuroanatomy of autism. *Trends Neurosci.* 31, 137–145. doi: 10.1016/j.tins.2007.12.005

Barbeau, E. B., Lewis, J. D., Doyon, J., Benali, H., Zeffiro, T. A., and Mottron, L. (2015). A greater involvement of posterior brain areas in interhemispheric transfer in autism: fMRI, DWI and behavioral evidences. *NeuroImage Clin.* 8, 267–280. doi: 10.1016/j.nicl.2015.04.019

Behrmann, M., Thomas, C., and Humphreys, K. (2006). Seeing it differently: visual processing in autism. *Trends Cogn. Sci.* 10, 258–264. doi: 10.1016/j.tics.2006.05.001

Bigler, E. D., Mortensen, S., Neeley, E. S., Ozonoff, S., Krasny, L., Johnson, M., et al. (2007). Superior temporal gyrus, language function, and autism. *Dev. Neuropsychol.* 31, 217–238. doi: 10.1080/87565640701190841

Bunge, S. A., Dudukovic, N. M., Thomason, M. E., Vaidya, C. J., and Gabrieli, J. D. (2002). Immature frontal lobe contributions to cognitive control in children: evidence from fMRI. *Neuron* 33, 301–311. doi: 10.1016/S0896-6273(01)00583-9

Campbell, R., Heywood, C. A., Cowey, A., Regard, M., and Landis, T. (1990). Sensitivity to eye gaze in prosopagnosic patients and monkeys with superior temporal sulcus ablation. *Neuropsychologia* 28, 1123–1142. doi: 10.1016/0028-3932(90)90050-X

Casey, B. J., Trainor, R. J., Orendi, J. L., Schubert, A. B., Nystrom, L. E., Giedd, J. N., et al. (1997). A developmental functional MRI study of prefrontal activation during performance of a go-no-go task. *J. Cogn. Neurosci.* 9, 835–847. doi: 10.1162/jocn.1997.9.6.835

Cavanna, A. E., and Trimble, M. R. (2006). The precuneus: a review of its functional anatomy and behavioral correlates. *Brain* 129, 564–583. doi: 10.1093/brain/awl004

Clery, H., Andersson, F., Bonnet-Brilhault, F., Phillipe, A., Wicker, B., and Gomot, M. (2013). fMRI investigation of visual change detection in adults with autism. *NeuroImage Clin.* 2, 303–312. doi: 10.1016/j.nicl.2013.01.010

de Macedo Rodrigues, K., Ben-Avi, E., Sliva, D. D., Choe, M., Drottar, M., Wang, R., et al. (2015). A freesurfer-compliant consistent manual segmentation of infant brains spanning the 0-2 year age range. *Front. Hum. Neurosci.* 9:21. doi: 10.3389/fnhum.2015.00021

Di Martino, A., Yan, C.-G., Li, Q., Denio, E., Castellanos, F. X., Alaerts, K., Anderson, J. S., et al. (2014). The autism brain imaging data exchange: towards large-scale evaluation of the intrinsic brain architecture in autism. *Mol. Psychiatry* 19, 659–667. doi: 10.1038/mp.2013.78

Dziobek, I., Bahnemann, M., Convit, A., and Heekeren, H. R. (2010). The role of the fusiform-amydala system in the pathophysiology of autism. *Arch. Gen. Psychiatry* 67, 397–405. doi: 10.1001/archgenpsychiatry.2010.31

Dziuk, M. A., Gidley Larson, J. C., Apostu, A., Mahone, E. M., Denckla, M. B., and Mostofsky, S. H. (2007). Dyspraxia in autism: association with motor, social, and communicative deficits. *Dev. Med. Child Neurol.* 49, 734–739. doi: 10.1111/j.1469-8749.2007.00734.x

Ecker, C., Ginestet, C., Feng, Y., Johnston, P., Lombardo, M. V., Lai, M. C., et al. Consortium (2013). Brain surface anatomy in adults with autism the relationship between surface area, cortical thickness, and autistic symptoms. *JAMA Psychiatry* 70, 59–70. doi: 10.1001/jamapsychiatry.2013.265

Ecker, C., Marquand, A., Mourao-Miranda, J., Johnston, P., Daly, E. M., Brammer, M. J., et al. (2010). Describing the brain in autism in five dimensions–magnetic resonance imaging-assisted diagnosis of autism spectrum disorders using a multiparameter classification approach. *J. Neurosci.* 30, 10612–10623. doi: 10.1523/JNEUROSCI.5413-09.2010

Ecker, C., Shahidiani, A., Feng, Y., Daly, E., Murphy, C., D'Almeida, V., et al. (2014). The effect of age, diagnosis, and their interaction on vertex-based measures of cortical thickness and surface area in autism spectrum disorder. *J Neural Transm.* 121, 1157–1170. doi: 10.1007/s00702-014-1207-1

Fair, D. A., Cohen, A. L., Power, J. D., Dosenbach, N. U., Church, J. A., Miezin, F. M., et al. (2009). Functional brain networks develop from a "local to distributed" organization. *PLoS Comput. Biol.* 5:e1000381. doi: 10.1371/journal.pcbi.1000381

Farrow, T. F., Zheng, Y., Wilkinson, I. D., Spence, S. A., Deakin, J. F., Tarrier, N., et al. (2001). Investigating the functional anatomy of empathy and forgiveness. *Neuroreport* 12, 2433–2438. doi: 10.1097/00001756-200108080-00029

Fischl, B. (2012). FreeSurfer. *Neuroimage* 62, 774–781. doi: 10.1016/j.neuroimage.2012.01.021

Fox, M. D., Snyder, A. Z., Vincent, J. L., Corbetta, M., Van Essen, D. C., and Raichle, M. E. (2005). The human brain is intrinsically organized into dynamic, anticorrelated functional networks. *Proc. Natl. Acad. Sci.U.S.A.* 102, 9673–9678. doi: 10.1073/pnas.0504136102

Gazzaniga, M. S., Ivry, R. B., and Mangun, G. R. (2009). *Cognitive Neuroscience, the Biology of the Mind.* New York, NY: W. W. Norton.

Gillberg, C. (1993). Autism and related behaviours. *J. Intellect. Disabil. Res.* 37(Pt. 4), 343–372. doi: 10.1111/j.1365-2788.1993.tb00879.x

Gogtay, N., Giedd, J. N., Lusk, L., Hayashi, K. M., Greenstein, D., Vaituzis, A. C., et al. (2004). Dynamic mapping of human cortical development during childhood through early adulthood. *Proc. Natl. Acad. Sci.U.S.A.* 101, 8174–8179. doi: 10.1073/pnas.0402680101

Groen, W., Teluij, M., Buitelaar, J., and Tendolkar, I. (2010). Amygdala and hippocampus enlargement during adolescence in autism. *J. Am. Acad. Child Adolesc. Psychiatry* 49, 552–560. doi: 10.1016/j.jaac.2009.12.023

Haar, S., Berman, S., Behrmann, M., and Dinstein, I. (2016). Anatomical abnormalities in autism? *Cerebr. Cortex* 26, 1440–1452. doi: 10.1093/cercor/bhu242

Hadjikhani, N., Joseph, R. M., Snyder, J., Chabris, C. F., Clark, J., Steele, S., et al. (2004). Activation of the fusiform gyrus when individuals with autism spectrum disorder view faces. *Neuroimage* 22, 1140–1150. doi: 10.1016/j.neuroimage.2004.03.025

Haxby, J. V., Hoffman, E. A., and Gobbini, M. I. (2000). The distributed human neural system for face perception. *Trends Cogn. Sci.* 4, 223–233. doi: 10.1016/S1364-6613(00)01482-0

Jiao, Y., Chen, R., Ke, X., Chu, K., Lu, Z., and Herskovits, E. H. (2010). Predictive models of autism spectrum disorder based on brain regional cortical thickness. *Neuroimage* 50, 589–599. doi: 10.1016/j.neuroimage.2009.12.047

Jones, A. P., Happe, F. G., Gilbert, F., Burnett, S., and Viding, E. (2010). Feeling, caring, knowing: different types of empathy deficit in boys with psychopathic tendencies and autism spectrum disorder. *J. Child Psychol. Psychiatry* 51, 1188–1197. doi: 10.1111/j.1469-7610.2010.02280.x

Karnath, H.-O. (2001). New insights into the functions of the superior temporal cortex. *Nat. Rev. Neurosci.* 2, 568–576. doi: 10.1038/35086057

Kellerman, G., Fan, J., and Gorman, J. M. (2005). Auditory abnormalities in autism: toward functional distinctions among findings. *CNS Spectr.* 10, 748–756. doi: 10.1017/S1092852900019738

Koolschijn, P. C., and Crone, E. A. (2013). Sex differences and structural brain maturation from childhood to early adulthood. *Dev. Cogn. Neurosci.* 5, 106–118. doi: 10.1016/j.dcn.2013.02.003

Lefebvre, A., Beggiato, A., Bourgeron, T., and Toro, R. (2015). Neuroanatomical diversity of corpus callosum and brain volume in autism: meta-analysis, analysis of the autism brain imaging data exchange project, and simulation. *Biol. Psychiatry* 78, 126–134. doi: 10.1016/j.biopsych.2015.02.010

Levman, J., MacDonald, P., Lim, A. R., Forgeron, C., and Takahashi, E. (2017). A pediatric structural MRI analysis of healthy brain development from newborns to young adults. *Hum. Brain Mapp.* 28, 5931–5942. doi: 10.1002/hbm.23799

Logothetis, N. K., and Sheinberg, D. L. (1996). Visual object recognition. *Annu. Rev. Neurosci.* 19, 577–621. doi: 10.1146/annurev.ne.19.030196.003045

McCarthy, G., Puce, A., Belger, A., and Allison, T. (1999). Electrophysiological studies of human face perception II: response properties of face-specific potentials generated in occipitotemporal cortex. *Cerebr. Cortex* 9, 431–444. doi: 10.1093/cercor/9.5.431

McIntosh, A. R., Bookstein, F. L., Haxby, J. V., and Grady, C. L. (1996). Spatial pattern analysis of functional brain images using partial least squares. *Neuroimage* 3, 143–157. doi: 10.1006/nimg.1996.0016

Mechelli, A., Humphreys, G. W., Mayall, K., Olson, A., and Price, C. J. (2000). Differential effects of word length and visual contrast in the fusiform and lingual gyri during reading. *Proc. Biol. Soc.* 267, 1909–1913. doi: 10.1098/rspb.2000.1229

Mesulam, M. M. (1981). A cortical network for directed attention and unilateral neglect. *Ann. Neurol.* 10, 309–325. doi: 10.1002/ana.410100402

Mostofsky, S. H., Powell, S. K., Simmonds, D. J., Goldberg, M. C., Caffo, B., and Pekar, J. J. (2009). Decreased connectivity and cerebellar activity in autism during motor task performance. *Brain* 132, 2413–2425. doi: 10.1093/brain/awp088

Pienaar, R., Rannou, N., Haehn, D., and Grant, P. E. (2014). "ChRIS: real-time web-based MRI data collection analysis, and sharing," in *20th Annual Meeting of the Organization for Human Brain Mapping* (Hamburg).

Radua, J., Phillips, M. L., Russel, T., Lawrence, N., Marshall, N., Kalidindi, S., et al. (2010). Neural response to specific components of fearful faces in healthy and schizophrenic adults. *NeuroImage* 49, 939–946. doi: 10.1016/j.neuroimage.2009.08.030

Rajah, M. N., Languay, R., and Grady, C. L. (2011). Age-related changes in right middle frontal gyrus volume correlate with altered episodic retrieval activity. *J. Neurosci.* 31, 17941–17954. doi: 10.1523/JNEUROSCI.1690-11.2011

Reiss, A. L., Abrams, M. T., Singer, H. S., Ross, J. L., and Denckla, M. B. (1996). Brain development, gender and IQ in children. A volumetric imaging study. *Brain* 119(Pt. 5), 1763–1774. doi: 10.1093/brain/119.5.1763

Richter, J., Poustka, L., Vomstein, K., Haffner, J., Parzer, P., Stieltjes, B., et al. (2015). Volumetric alterations in the heteromodal association cortex in children with autism spectrum disorder. *Eur. Psychiatry* 30, 214–220. doi: 10.1016/j.eurpsy.2014.11.005

Schaer, M., Kochalka, J., Padmanabhan, A., Supekar, K., and Menon, V. (2015). Sex differences in cortical volume and gyrification in autism. *Mol. Autism.* 6:42. doi: 10.1186/s13229-015-0035-y

Schaer, M., Ottet, M. C., Scariati, E., Dukes, D., Franchini, M., Eliez, S., et al. (2013). Decreased frontal gyrification correlates with altered connectivity in children with autism. *Front. Hum. Neurosci.* 7:750. doi: 10.3389/fnhum.2013.00750

Schumann, C. M., Bloss, C. S., Carter Barnes, C., Wideman, G. M., Carper, R. A., Akshoomoff, N., et al. (2010). Longitudinal magnetic resonance imaging study of cortical development through early childhood in autism. *J. Neurosci.* 30, 4419–4427. doi: 10.1523/JNEUROSCI.5714-09.2010

Silani, C. (2013). *I'm OK, You're Not OK: Right Supramarginal Gyrus Plays an Important Role in Empathy.* Rockville, MD: ScienceDaily.

Soulieres, I., Dawson, M., Samson, F., Barbeau, E. B., Sahyoun, C., Strangman, G. E., et al. (2009). Enhanced visual processing contributes to matrix reasoning in autism. *Hum. Brain Mapp.* 30, 4082–4107. doi: 10.1002/hbm.20831

Stephanou, K., Davey, C. G., Kerestes, R., Whittle, S., Pujol, J., Yucel, M., et al. (2016). Brain functional correlates of emotion regulation across adolescence and young adulthood. *Hum. Brain Mapp.* 37, 7–19. doi: 10.1002/hbm.22905

Stone, V. E., Baron-Cohen, S., and Knight, R. T. (1998). Frontal lobe contributions to theory of mind. *J. Med. Invest.* 10, 640–656.

Student, S. (1908). The probable error of a mean. *Biometrika* 6, 1–25. doi: 10.1093/biomet/6.1.1

Supekar, K., Musen, M., and Menon, V. (2009). Development of large-scale functional brain networks in children. *PLoS Biol.* 7:e1000157. doi: 10.1371/journal.pbio.1000157

Thomas, K. M., Drevets, W. C., Whalen, P. J., Eccard, C. H., Dahl, R. E., Ryan, N. D., et al. (2001). Amygdala response to facial expressions in children

and adults. *Biol. Psychiatry* 49, 309–316. doi: 10.1016/S0006-3223(00)01066-0

Toal, F., Murphy, D. G., and Murphy, K. C. (2005). Autistic-spectrum disorders: lessons from neuroimaging. *Br. J. Psychiatry* 187, 395–397. doi: 10.1192/bjp.187.5.395

Vaadia, E., Haalman, I., Abeles, M., Bergman, H., Prut, Y., Slovin, H., et al. (1995). Dynamics of neuronal interactions in monkey cortex in relation to behavioural events. *Nature* 373, 515–518. doi: 10.1038/373515a0

Wallace, G. L., Robustelli, B., Dankner, N., Kenworthy, L., Giedd, J. N., and Martin, A. (2013). Increased gyrification, but comparable surface area in adolescents with autism spectrum disorders. *Brain* 136(Pt. 6), 1956–1967. doi: 10.1093/brain/awt106

Wan, C. Y., and Schlaug, G. (2010). Neural pathways for language in autism: the potential for music-based treatments. *Future Neurol.* 5, 797–805. doi: 10.2217/fnl.10.55

Wing, L. (1997). The autistic spectrum. *Lancet* 350, 1761–1766. doi: 10.1016/S0140-6736(97)09218-0

Yang, D., Beam, D., Pelphrey, K. A., Abdullahi, S., and Jou, R. J. (2016). Cortical morphological markers in children with autism: a structural magnetic resonance imaging study of thickness, area, volume, and gyrification. *Mol. Autism*. 7:11. doi: 10.1186/s13229-016-0076-x

Youngstrom, E. A. (2014). A primer on receiver operating characteristic analysis and diagnostic efficiency statistics for pediatric psychology: we are ready to ROC. *J. Pediatr. Psychol.* 39, 204–221. doi: 10.1093/jpepsy/jst062

Zielinski, B. A., Prigge, M. B., Nielsen, J. A., Froelich, A. L., Abildskov, T. J., Anderson, J. S., et al. (2014). Longitudinal changes in cortical thickness in autism and typical development. *Brain* 137(Pt. 6), 1799–1812. doi: 10.1093/brain/awu083

Zollei, L., Ou, Y., Iglesias, J., Grant, P. E., and Fischl, B. (2017). "FreeSurfer image processing pipeline for infant clinical MRI images," in *Proceedings of the Organization for Human Brain Mapping Conference* (Vancouver, BC).

Conflict of Interest Statement: The authors declare that the research was conducted in the absence of any commercial or financial relationships that could be construed as a potential conflict of interest.

frontiers in Human Neuroscience

ORIGINAL RESEARCH
published: 14 May 2019
doi: 10.3389/fnhum.2019.00145

Mental Fatigue and Functional Near-Infrared Spectroscopy (fNIRS) – Based Assessment of Cognitive Performance After Mild Traumatic Brain Injury

Simon Skau[1], Lina Bunketorp-Käll[1,2], Hans Georg Kuhn[1,3] and Birgitta Johansson[1]*

[1] Institute of Neuroscience and Physiology, Sahlgrenska Academy, University of Gothenburg, Gothenburg, Sweden, [2] Centre for Advanced Reconstruction of Extremities, Sahlgrenska University Hospital, Mölndal, Sweden, [3] Department of Neurology, Center for Stroke Research, Charité – Universitätsmedizin, Berlin, Germany

Pathological mental fatigue after mild traumatic brain injury (TBI-MF) is characterized by pronounced mental fatigue after cognitive activity. The neurological origin is unknown, and we aimed in the present study to investigate how prolonged mental activity affects cognitive performance and its neural correlates in individuals with TBI-MF. We recruited individuals with TBI-MF (n = 20) at least 5 months after injury, and age-matched healthy controls (n = 20). We used functional near-infrared spectroscopy (fNIRS) to assess hemodynamic changes in the frontal cortex. The self-assessed mental energy level was measured with a visual analog scale (VAS) before and after the experimental procedure. A battery of six neuropsychological tests including Stroop–Simon, Symbol Search, Digit Span, Parallel Serial Mental Operation (PaSMO), Sustained Attention and Working Memory test, and Digit Symbol Coding (DSC) were used. The sequence was repeated once after an 8 min sustained-attention test. The test procedure lasted 2½ h. The experimental procedure resulted in a decrease in mental energy in the TBI-MF group, compared to controls (interaction, $p < 0.001$, $\eta_p^2 = 0.331$). The TBI-MF group performed at a similar level on both DSC tests, whereas the controls improved their performance in the second session (interaction, $p < 0.01$, $\eta_p^2 = 0.268$). During the Stroop–Simon test, the fNIRS event-related response showed no time effect. However, the TBI-MF group exhibited lower oxygenated hemoglobin (oxy-Hb) concentrations in the frontal polar area (FPA), ventrolateral motor cortex, and dorsolateral prefrontal cortex (DLPFC) from the beginning of the test session. A Stroop and Group interaction was found in the left ventrolateral prefrontal cortex showing that the TBI-MF group did have the same oxy-Hb concentration for both congruent and incongruent trials, whereas the controls had more oxy-Hb in the incongruent trial compared to the congruent trial (interaction, $p < 0.01$, $\eta_p^2 = 0.227$). In sum these results indicate that individuals with TBI-MF have a reduced ability to recruit the frontal cortex, which is correlated with self-reported mental fatigue. This may result both in deterioration of cognitive function and the experience of a mental fatigue after extended mental activity.

Keywords: mild TBI, fNIRS, mental fatigue, frontal cortex, conflict processing, processing speed

OPEN ACCESS

Edited by:
Yusuf Ozgur Cakmak, University of Otago, New Zealand

Reviewed by:
Makii Muthalib, Université de Montpellier, France
Vrinda Kalia, Miami University, United States
Didem Gokcay, Middle East Technical University, Turkey

****Correspondence:***
Hans Georg Kuhn
georg.kuhn@neuro.gu.se

Received: *01 November 2018*
Accepted: *16 April 2019*
Published: *14 May 2019*

Citation:
Skau S, Bunketorp-Käll L, Kuhn HG and Johansson B (2019) Mental Fatigue and Functional Near-Infrared Spectroscopy (fNIRS) – Based Assessment of Cognitive Performance After Mild Traumatic Brain Injury. Front. Hum. Neurosci. 13:145. doi: 10.3389/fnhum.2019.00145

INTRODUCTION

Traumatic brain injury (TBI) is a common neurological condition affecting people of all ages. Globally, approximately 295/100,000 people are treated in hospitals each year for TBI (Nguyen et al., 2016). This is mild for most patients who recover within 1–3 months (Carroll et al., 2004). For those who show insufficient recovery within this period, fatigue is common (King et al., 1995; Kraus et al., 2014; McInnes et al., 2017), irrespective of injury severity (Johansson et al., 2009). Long-lasting mental fatigue interferes considerably with daily living, the ability to work and has a negative impact on well-being and mental health (Cantor et al., 2008; Hawthorne et al., 2009; Johansson et al., 2009; Lannsjo et al., 2009; Ahman et al., 2013). Fatigue is also suggested to be a direct consequence of TBI and not a result of depression, pain or sleep disturbances (Cantor et al., 2008). Due to the current limitations in measuring fatigue and the complexities involved in objectively measuring fatigue, researchers frequently rely on subjective questionnaire-based reporting scales, both for the physical and the mental components.

Pathological mental fatigue (MF) is characterized by mental exhaustion during sensory stimulation or extended cognitive activity, and with a disproportionately long recovery. MF is a typical symptom in many neurological diseases (Lindqvist and Malmgren, 1993; Johansson et al., 2010). The underlying origin of MF is unknown, but it is suggested to be related to circuits that connect basal ganglia, amygdala, the thalamus and frontal cortex (Chaudhuri and Behan, 2004). These circuits mediate motivation, learning, planning, goal-directed behavior and emotion regulation. The integration of networks is important for appropriate behavior and cognitive functioning (Haber and Calzavara, 2009). Studies of MF after moderate and severe TBI using functional magnetic resonance imaging (fMRI) indicate a dysfunction within the cortico-striatal-thalamic circuits (Kohl et al., 2009; Nordin et al., 2016; Berginstrom et al., 2017; Moller et al., 2017; Wylie et al., 2017).

Cognitive impairment associated with MF after TBI has been related to reduced processing speed and attention (Park et al., 1999; Azouvi et al., 2004; Ziino and Ponsford, 2006a,b; Ashman et al., 2008; Belmont et al., 2009; Johansson et al., 2009, 2010; Ponsford et al., 2011), these being the cognitive functions most susceptible to brain injury (Frencham et al., 2005; Lannsjo et al., 2009). In our previous study, investigating individuals suffering from MF after acquired brain injuries, impaired cognitive performance in processing speed (Digit Symbol Coding) (Wechsler, 2010), attention (SAWM) (Johansson and Ronnback, 2015), attentional blink (Dux and Marois, 2009), and working memory (Digit Span) (Wechsler, 2010) over a 2 h test period was found, with no improvement for those suffering from MF whereas the controls improved (Jonasson et al., 2018). Similar results have been reported in additional studies (Ashman et al., 2008). These studies indicate that people suffering from MF after an acquired brain injury find it challenging to repeat cognitive tasks, whereas improvement can be achieved for healthy controls.

In this study, we aimed to explore how prolonged mental activity affects cognitive performance as well as exploring the neural correlates of conflict processing in individuals with MF after TBI (TBI-MF). This was done with a block of six neuropsychological tests including Stroop–Simon (Egner et al., 2007), Symbol Search (Wechsler, 2010), Digit Span (Wechsler, 2010), Parallel Serial Mental Operation (PaSMO) (Reitan and Wolfson, 1985), SAWM (Johansson and Ronnback, 2015), and Digit Symbol Coding (DSC) (Wechsler, 2010), were performed. The sequence was repeated once. Between the two blocks, an 8 min sustained-attention test and the self-report of MFS was done, with the intention to induce even more fatigue. The test procedure lasted for approximately 2½ h.

To measure brain activity, functional near-infrared spectroscopy (fNIRS) was used. Similar to fMRI, fNIRS measures the hemodynamic response to neural activity. fNIRS is a noninvasive optical brain imaging technique that uses near-infrared light to measure the relative concentration of oxygenated (oxy-Hb) and deoxygenated (deoxy-Hb) hemoglobin (Jo Bsis-Vandervliet, 1999). By applying light emitting sources on the scalp the fNIRS can detect hemodynamic change that occur to a depth of 1.5–2 cm into the cortex (Jo Bsis-Vandervliet, 1999; Obrig, 2014). Compared to other imaging techniques, fNIRS is more robust to movement artifacts (Balardin et al., 2017). Thus, fNIRS is well-suited to studies in natural environments (Kopton and Kenning, 2014), and has been used in psychiatric studies (Ehlis et al., 2014), and for cognitive assessment (Irani et al., 2007; Ferrari and Quaresima, 2012; Ehlis et al., 2014). MF has been investigated by means of fNIRS in patients with multiple sclerosis, and the level of self-reported fatigue correlated with neural activity in the dorsolateral prefrontal cortex (DLPFC) during a working memory task (Borragán et al., 2018). To the best of our knowledge, no previous study has used fNIRS to study MF resulting from TBI. There are, however, a few cognitive studies using fNIRS in subjects with TBI. Most of these studies are exploratory, with few participants (Merzagora et al., 2011; Hibino et al., 2013; Kontos et al., 2014; Rodriguez Merzagora et al., 2014; Sawamura et al., 2014; Helmich et al., 2015; Plenger et al., 2016). With the exception of one study (Rodriguez Merzagora et al., 2014), fNIRS measurements show decreased activity in the DLPFC for the TBI group compared to controls for cognitive performance (Merzagora et al., 2011; Hibino et al., 2013; Kontos et al., 2014; Sawamura et al., 2014; Helmich et al., 2015; Plenger et al., 2016). Other studies on healthy adults applying fNIRS while performing the conflict processing Stroop test have reported increased activity in the DLPFC (Schroeter et al., 2002, 2004; Leon-Carrion et al., 2008; Hyodo et al., 2012; Endo et al., 2013; Lague-Beauvais et al., 2013; Byun et al., 2014; Yasumura et al., 2014). We opted to investigate brain activity using the Stroop–Simon task (Egner et al., 2007) adapted to fNIRS in a cohort with TBI-MF.

We hypothesized that, during performance of the Stroop–Simon test, the TBI-MF group would show less activity in the DLPFC, as compared to controls. In addition, individuals with TBI-MF may demonstrate altered brain activity in the frontal cortex between the first and second test sessions. This hypothesis was not directed, meaning that we did not know based on previous literature if the alteration would be an increased or decreased in oxygen consumption, as compared to controls. We also hypothesized that the TBI-MF

group would perform less well in the second test session, as compared to the first.

MATERIALS AND METHODS

Study Participants and Protocol

Twenty individuals with long-term TBI-MF (minimum 5 months after injury) were recruited from the Department of Neurology, Sahlgrenska University Hospital, Gothenburg. Inclusion criteria were as follows: diagnosed with mild TBI according to the definition proposed by The World Health Organization Collaborating Centre for Neurotrauma Task Force (Carroll et al., 2004); scoring above the cut-off score of 10.5 on the Mental Fatigue Scale (MFS) (Johansson and Rönnbäck, 2014); aged 20–65 years and not suffering from any other psychiatric or neurological disorders. All participants had recovered well, were independent in their daily living, with the exception of their prolonged MF. Twenty-one healthy controls who neither suffered from MF (below 10.5 points on MFS), nor did they have any psychiatric or neurological disorders, were recruited at the request of the general community. The study was approved by the regional Ethical Review Board in Gothenburg (reference number: 028-16). The participants gave their informed written consent before the assessment and were told that they could withdraw at any time.

Experimental Design

The participant was seated in a chair next to a table with a computer screen. All tests were performed sitting in the same location, whereas the tasks differed with respect to the response type, such as pen and paper task, verbal response tasks or computerized tasks where the participant used the computer mouse, tablet or a gamepad. The fNIRS cap with optodes attached was carefully placed on the participant's head and was worn throughout the whole experimental sessions. To minimize ambient light reaching the scalp during the test procedure, the fNIRS cap was covered by another stretchable cap. The experiment consisted of two identical test sessions with 6 individual tests performed in the same sequence (**Figure 1A**): (1) Stroop–Simon (Egner et al., 2007); (2) Symbol Search (SS, WAIS-IV) (Wechsler, 2010); (3). Digit Span (DS, WAIS-IV) (Wechsler, 2010); (4) Parallel Serial Mental Operations (PaSMO) (Reitan and Wolfson, 1985); (5) a computerized test combining Speed, divided Attention and Working Memory simultaneously (SAWM) (Johansson and Ronnback, 2015), and (6) Digit Symbol Coding (DSC, WAIS-IV) (Wechsler, 2010). The two sessions were separated by once presenting a sustained-attention test with an 8 min one-back task (OPATUS-CPTA) and completing the MFS (**Figure 1A**). MFS is invariant to age, gender and education (Johansson et al., 2010; Johansson and Ronnback, 2014). In total, the test procedure took 2½ h. Participants were allowed to take a short break and drink water or stand up and stretch their legs between tests, while keeping the fNIRS cap on. Before start of the experimental procedure and after completion of all tests, the participants were asked to rate their energy level on a visual analog scale (VAS). They specified their energy level on a continuous line (10 cm) indicating a position between the two end-points, "full of energy" and "totally exhausted, no energy left."

Cognitive Tests

The Stroop–Simon test was used to measure both the Stroop effect (conflict between semantic meaning and ink color) and the Simon effect (conflict between stimulus location and response hand) (Egner, 2008; Forster and Cho, 2014). The participant was asked to fixate on the cross located in the middle of the screen. The word RED or BLUE – either in red or blue ink – was presented to the left or right side of the cross (5 cm). The participant was asked to respond to the ink color by pressing a button on a gamepad with either the left thumb for red, or the right thumb for blue (see **Figure 1B**). The response to stimulus interval was randomly assigned to be between 7 and 11 s, and the participants had 3 s to respond. This created four different types of trials and each trial had two dimensions; Stroop congruent and Simon congruent (CC), Stroop congruent and Simon incongruent (CI), Stroop incongruent and Simon congruent (IC), or Stroop incongruent and Simon incongruent (II) (see **Figure 1B**). There was a total of 164 stimuli, semi-randomized with a 30 s pause after half of the stimuli. Reaction time, errors made and omissions were used as raw scores.

Symbol Search (SS) and Digit Symbol Coding (DSC) are subtests within the Processing Speed Index in WAIS-IV (Wechsler, 2010) that were used to measure attention, speed of mental and psychomotor operation and visual discrimination. In both tests, the subject is asked to perform as many symbols as possible during 2 min. Raw score is the number of correct symbols performed.

Digit Span (DS) from WAIS-IV (Wechsler, 2010) was used to assess working memory. Raw scores were reported as the number of correctly repeated strings of digits.

The PaSMO (Reitan and Wolfson, 1985) was used to measure mental control and tracking in a task similar to the Trail Making Test (Reitan and Wolfson, 1985). In PaSMO, the participants were asked to say the whole alphabet with the corresponding digits, i.e., A1, B2, C3, and so forth, as fast as possible. Performance was measured in time (seconds) with a faster time indicating a better performance.

The SAWM test was used for simultaneous assessment of Speed, divided Attention and Working Memory (Johansson and Ronnback, 2015). The test measured number of mouse clicks in four squares, located in each corner of a larger square on the computer screen, and was performed in a clockwise order. At the same time, the subject was asked to count how many instances of a specific digit were shown (seen in the square located to the upper right). Another digit, between zero and nine was randomly chosen for each run. The digits to be counted were randomly displayed for 1 s in a square located to the upper left. After 30 s, the subject was asked to report how many of the specific digits he/she had seen. The answer was compared with the correct number of the digits presented, and the numbers of errors made in each run was analyzed. The number of clicks was simultaneously recorded. Each session lasted for 30 s and was repeated five times. All participants had the opportunity

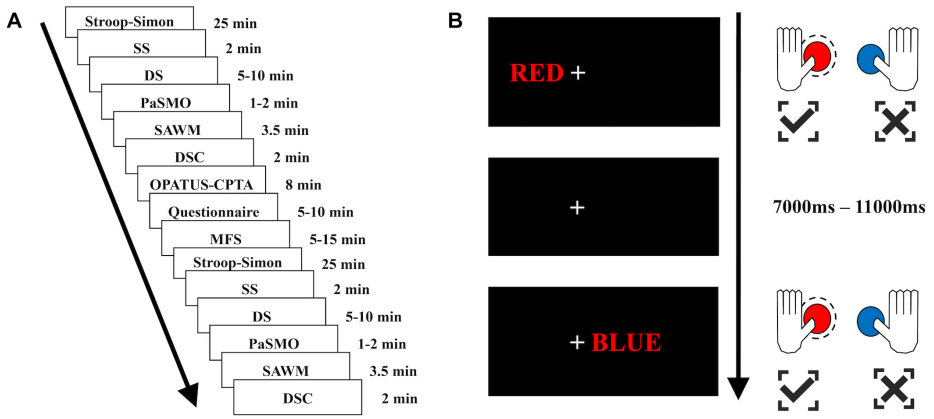

FIGURE 1 | Test sequence and illustration of the Stroop–Simon test. **(A)** The test sequence consisted of 6 tests – Stroop–Simon, SS (Symbol Search), DS (Digit Span), PaSMO (Parallel Serial Mental Operation), SAWM (Speed, divided Attention and Working Memory), DSC (Digit Symbol Coding) – which were repeated once after the OPATUS-CPTA (one-back sustained attention task), and MFS, Mental Fatigue Scale questionnaire were applied. The time indicates the length of each test, not including practice and preparation for each test. **(B)** Examples of stimulus-responses for the Stroop–Simon test. When a word written in red color is presented, the correct response is to press the left button (marked in red on the game pad), irrespective of the placement (Simon effect – left or right) or meaning of the word (Stroop effect – "RED" or "BLUE"). Both examples (top and bottom) require to press the left (red) button. Top example: a Stroop(word)-congruent/Simon(place) -congruent stimulus, bottom example: a Stroop(word)-incongruent/Simon(place)-incongruent stimulus. All stimuli were presented 7,000–11,000 ms apart.

to rehearse the task before starting the assessment to ensure that they had understood the task instructions displayed on the computer screen. The raw scores used for analysis were the mean scores of errors and number of successful responses from the second to fifth run.

The continuous performance test with a one-back task (OPATUS-CPTA) was used as a measure of sustained attention. The 8 min OPATUS-CPTA task was delivered on a mini tablet, and the participant was asked to tap the screen when the same symbol as the one previously shown appeared on the screen. Triangles pointing up/down/left/right and appeared in two colors: yellow or blue, stimuli duration was 150 ms, inter stimuli interval was 2000 ms, target rate was 20% and the number of trials was 240. Reaction time, errors made and omissions were used as raw scores.

fNIRS Data Acquisition

The fNIRS measurements were performed using a continuous wave system (NTS) Optical Imaging System, Gowerlabs Ltd., United Kingdom (Everdell et al., 2005) using two wavelengths (780 and 850nm) to measure changes in the concentration of oxygenated hemoglobin (oxy-Hb), deoxygenated hemoglobin (deoxy-Hb) and their sum total hemoglobin (tot-Hb). The system has 16 dual-wavelength sources and 16 detectors. The array used provided 50 standard fNIRS channels (i.e., source/detector pairs) plus two short-separation channels. There were 44 channels with a source-detector distance of 30 mm and 6 channels with 45 mm distance. The six longer channels connected the two hemispheres, but the signal quality was too low for the data to be included in our analysis. The distance for the short-separation channels was 10 mm, as suggested in previous studies (Gagnon et al., 2011; Brigadoi and Cooper, 2015). Short separation channels are only sensitive to hemodynamics in the scalp. Since the regular separation channels measure signals originating in both the brain and the scalp, the use of short-separation channels allowed us to regress out the scalp signal from regular-separation signals with the aim to improve the brain specificity of the fNIRS measurement (Gagnon et al., 2011; Brigadoi and Cooper, 2015). The placement of the optodes was designed to encompass five regions of interest (ROIs) on each hemisphere covering areas of the frontal cortex, previously reported to be involved in executive function and cognitive control tasks (Roberts and Hall, 2008). The ROIs were left and right frontal polar area (FPA) or Brodmann area (BA) 10; DLPFC or BA 9 and 46; dorsal motor cortex (DMC) BA 6 and 8; ventral lateral prefrontal cortex (VLPFC) BA 44 and 45 and ventral motor cortex VMC BA 6 and 44 (see **Figure 2**). Data were acquired at a sampling frequency of 10 Hz.

fNIRS Data Analysis

The fNIRS data were preprocessed using MATLAB 2014a (MATLAB, 2014) and the MATLAB based fNIRS-processing package HomER2 (Huppert et al., 2009). The processing pipeline started with pruning the raw data such as that channels were rejected if their mean intensity was below the noise floor of the instrument (5e-4 A.U.). The raw data was then converted to optical density (OD). The HomER2 functions enPCAFilter, hmrMotionArtifact and hmrMotionCorrectSpline were used to correct for motion artifacts. A high band-pass filter of 0.03 was used to correct for drift and a low band-pass 0.5 filter to remove pulse and respiration. To calculate the hemodynamic response function (HRF) the GLM_HRF_Drift_SS function in HomER2, which estimates the HRF by applying a General Linear Model (GLM), was used. To solve the GLM, a least square fit of a convolution model in which the HRF at each channel and chromophore was modeled as a series of Gaussian basis

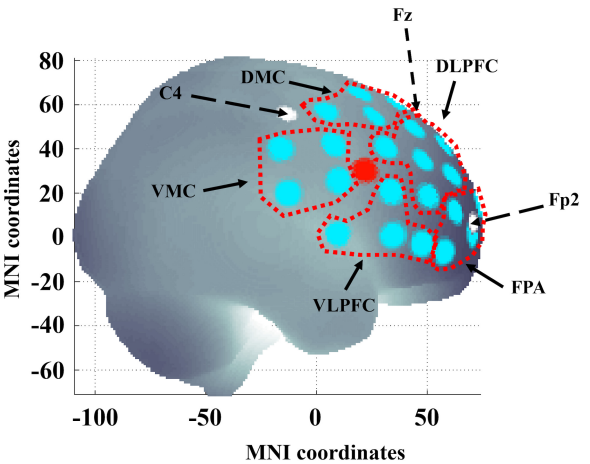

FIGURE 2 | Channel locations in the right hemisphere. Areas delineated with a red dotted line indicate the regions of interest (ROIs): left and right frontal polar area (FPA) corresponding to Brodmann area (BA) 10; dorsolateral prefrontal cortex (DLPFC) corresponding to BA 9 and 46; dorsal motor cortex (DMC) corresponding to BA 6 and 8; ventrolateral prefrontal cortex (VLPFC) corresponding to BA 44 and 45 and ventral motor cortex (VMC) corresponding to BA 6 and 44. The large red dot indicates the location of the short separation channel. Dashed black arrows and white dots indicate 10/20 reference points C4, Fp2, and Fz. The brain template was generated from a MATLAB-based toolbox (Singh et al., 2005). x- and y-axis refer to MNI (Montreal Neurological Institute) coordinate system.

function, with a spacing and standard deviation of 0.5 s (Ye et al., 2009). The model included polynomial drift regressors up to the 3rd order. The regression time length was −2–12 s. The short channels selected for regression for each long channel was those with the highest correlation to the regular channel. The analysis of the Stroop–Simon data was analyzed with pre-determined ROIs. A visual analysis of each channel was done and the channels that remained too noisy were removed, but not to the exclusion of any ROI. On average, 0.65 channels per ROI was excluded after the pruning function and manual removal.

Since the combination of wavelengths used (780, 850 nm) is more sensitive to oxy-Hb compared to deoxy-HB, only the oxy-Hb data were statistically analyzed (Uludag et al., 2004; Sato et al., 2013). The deoxy-HB did not add any further information to this study and is not included. For the Stroop–Simon test the maximum peak between 3 and 9 s after each stimulus was identified. One second around the peak value was averaged.

Statistics

A two-way repeated ANOVA with within-subject factor *Time* (first and second test session) and the between-subject factor *Group* for each particular test was used. For items having both a group and an interaction effect, independent *t*-tests as *post hoc* test were used for interpreting the main result. For the Stroop–Simon test a four-way repeated ANOVA was performed with the following within-subject factors; (i) Time (first and seconds sessions); (ii) Stroop (congruent and incongruent); (iii) Simon (congruent and incongruent); and (iv) the between-subject factor Group (patients and controls). For the Stroop–Simon test, mean reaction time was used for each stimulus type for each participant. This excluded omissions (more than 3 s after stimulus without an answer), error trials, the trial set after the error and condition-specific outlier values that were greater than 2 SDs from the mean.

fNIRS data acquired during the Stroop–Simon test were analyzed within each ROI and only for the Stroop effect. A three-way repeated ANOVA with within-subject factor, Time (first and second test sessions) and Stroop (congruent and incongruent) and the between-subject factor, Group for each ROI was used. The CC trials were used as congruent and the average of the IC and II trials were used as incongruent. *T*-test, chi-square and Pearson's correlation was used for demographic data, *post hoc* analysis and OPATIS-CPTA. To correct for multiple comparisons with the neuropsychological test and the fNIRS, a false discovery rate (FDR) was used with the *q*-value set to 0.05 in order to keep the false positive rate at 5% (Singh and Dan, 2006). Parametric tests were done using SPSS version 25 and Matlab statistical toolbox (MATLAB, 2014). The datasets generated in the current study are available from the corresponding author on reasonable request.

RESULTS

Demographics

Demographical and clinical characteristics of the study population are presented in **Table 1**. One control subject was excluded due to failure to follow instruction to remain

TABLE 1 | Background data for the TBI-MF and the control group.

	TBI-MF group	Control group	*p*-values
Age (years)	42.1 ± 10.2	39.3 ± 11.9	0.285
Range (years)	24–64	24–61	
Sex, females/males (n)	13/7	12/8	0.744
MFS score	21.3 ± 5.4	3.3 ± 2.9	<0.001
Education, upper secondary school/university (n)	3/17	4/16	0.677
Time elapsed since TBI exposure (months)	27.8 ± 21.2		
Range (months)	5–85		
Exposed to one/more than one mild TBI (n)	12/8		
Employment status at time of the study (n)			
100%	1	19	
75%	1	0	
50%	7	1 (of free choice)	
25%	1	0	
0%	10	0	
Preinjury employment status (n)			
100%	19		
50%	1		
Have undergone neuropsychological testing previously (Yes/No)	8/12	6/14	0.520

Data are presented as Mean ± SD unless otherwise noted.

seated and physically calm during the fNIRS session. The mean time since injury was 28 (±21) months. The only variable that differed significantly between groups was the MFS score, that was rated significantly higher in the TBI-MF group as compared to controls ($p < 0.001$). No correlation between time since injury and MFS was found ($r = 0.21$, $p = 0.35$). Eight of the individuals with MF-TBI (40%) had experienced two or more mild TBI, but no significant difference was found in any tests or rating on MFS in these individuals compared to those who had suffered only one mild TBI. Six individuals with TBI-MF (30%) received methylphenidate drug treatment but had suspended the treatment 1 week prior to the assessment. No significant differences with respect to the cognitive test results and ratings on MFS were detected between these six individuals compared to the other individuals with TBI-MF.

A significant interaction effect was detected with respect to the subjective experience of mental energy (**Table 2**). Prior to start of the experiment the experienced energy level did not differ between groups ($t = 0.792$, FDR adjusted $p > 0.05$, with a Cohen's d of 0.26), whereas after the experiment, the TBI-MF group rated their energy level significantly lower than controls ($t = 5.769$, FDR adjusted $p < 0.05$, with a Cohen's d of 1.37) (**Figure 3A**).

TABLE 2 | Repeated ANOVA for the behavioral test results.

	TBI	Control	Df	Time vs. Group FDR | F | η_p^2	Group FDR | F | η_p^2
VAS (cm)			1,36	FDR = **	FDR = **
Before	3.13 (2.0)	2.66 (1.5)		$F = 17.812$	$F = 14.912$
After	7.27 (1.7)	4.12 (1.6)		$\eta_p^2 = 0.331$	$\eta_p^2 = 0.293$
Stroop–Simon RT			1,37	FDR = ns	FDR = **
Test 1	918 (271)	717 (143)		$F = 7.685$	$F = 12.117$
Test 2	1019 (345)	716 (157)		$\eta_p^2 = 0.172$	$\eta_p^2 = 0.247$
Stroop–Simon error			1,37	FDR = ns	FDR = ns
Test 1	0.02 (0.02)	0.01 (0.01)		$F = 0.139$	$F = 0.714$
Test 2	0.02 (0.02)	0.02 (0.02)		$\eta_p^2 = 0.004$	$\eta_p^2 = 0.019$
Stroop–Simon			1,37	FDR = ns	FDR = ns
omission Test 1	0.65 (1.5)	0.1 (0.3)		$F = 4.867$	$F = 4.933$
Test 2	3.95 (7.3)	0.4 (0.8)		$\eta_p^2 = 0.116$	$\eta_p^2 = 0.118$
Symbol search (SS)			1,38	FDR = ns	FDR = ***
Test 1	30.8 (5.9)	37.3 (6.4)		$F = 5.697$	$F = 21.343$
Test 2	32.4 (6.7)	42.5 (5.4)		$\eta_p^2 = 0.130$	$\eta_p^2 = 0.360$
Digit span (DS)			1,38	FDR = ns	FDR = ns
Test 1	24.4 (5.4)	26.8 (4.3)		$F = 0.589$	$F = 2.707$
Test 2	26.2 (5.9)	29.0 (4.8)		$\eta_p^2 = 0.015$	$\eta_p^2 = 0.066$
PaSMO			1,36	FDR = ns	FDR = *
Test 1	88.2 (43.3)	63.4 (13–6)		$F = 0.402$	$F = 6.471$
Test 2	84.4 (48.6)	55.7 (12.4)		$\eta_p^2 = 0.011$	$\eta_p^2 = 0.152$
PaSMO error			1,36	FDR = ns	FDR = ns
Test 1	1.16 (2.0)	0.95 (1.3)		$F = 0.041$	$F = 0.193$
Test 2	0.47 (1.0)	0.37 (0.8)		$\eta_p^2 = 0.001$	$\eta_p^2 = 0.005$
SAWM			1,38	FDR = ns	FDR = *
Test 1	36.6 (5.6)	41.9 (8.3)		$F = 2.099$	$F = 7.996$
Test 2	36.8 (6.0)	43.9 (8.4)		$\eta_p^2 = 0.052$	$\eta_p^2 = 0.174$
SAWM error			1,38	FDR = ns	FDR = ns
Test 1	0.35 (0.6)	0.60 (1.0)		$F = 3.055$	$F = 0.107$
Test 2	1.00 (1.0)	0.60 (0.8)		$\eta_p^2 = 0.074$	$\eta_p^2 = 0.003$
DSC			1,38	FDR = *	FDR = *
Test 1	65.6 (11.7)	72.2 (10.9)		$F = 13.942$	$F = 6.423$
Test 2	67.0 (15.6)	80.4 (12.4)		$\eta_p^2 = 0.268$	$\eta_p^2 = 0.145$

*VAS, Energy level on a visual analog scale of 0–10 cm; RT, reaction time; PaSMO, Parallel Serial Mental Operation; SAWM, Speed, divided Attention and Working Memory; DSC, Digit Symbol Coding, FDR, p-value after adjustment with false discovery rate; ***$p < 0.001$, **$p < 0.01$, *$p < 0.05$, $^{ns}p > 0.05$; η_p^2, partial eta-squared effect size.*

Cognitive Tests

Interaction Effect

Significant interaction effects between *Time* and *Group* were detected for DSC. The TBI-MF group did not improve their speed during the second DSC test, whereas the controls became faster (**Figure 3K**). No other *Time* and *Group* interaction was found for the other tests (**Table 2**). There was no interaction for the *Stroop* and *Group* [$F(1, 37) = 4, 725$; FDR adjusted $p > 0.05$, $\eta_p^2 = 0.113$]. Nor were any *Simon* and *Group* interactions found [$F(1, 37) = 0.003$; FDR adjusted $p > 0.05$, $\eta_p^2 < 0.001$].

Group Effect

The TBI-MF group was significantly slower than the control group on SS, PaSMO, SAWM, Stroop–Simon, and DSC (**Table 2** and **Figures 3B,F,H,J,L**). The additional *post hoc* t-test for the DSC did not show any difference between the groups during the first test session ($t = -1.859$, FDR adjusted $p > 0.05$, with a Cohen's d of 0.57), while the TBI-MF was significantly slower in the second test session ($t = -2.988$, FDR adjusted $p < 0.05$, with a Cohen's d of 0.86). No differences in reaction time nor errors made were found between the groups for the OPATUS-CPTA, but the rate of omissions was significantly higher in the TBI-MF group, as compared to controls ($t = 2.472$, FDR adjusted $p < 0.05$). No difference was found between groups with respect to Digit Span, and errors made in any of the tests (SAWM, PaSMO, and Stroop–Simon). For comparison, data adjusted to age according to WAIS-IV manual, DSC, SS, and DS were within the normal range for both groups.

fNIRS Result

Stroop–Simon

No *Group* and *Time* interactions were found for any of the ROIs (**Figure 4** and **Table 3**). There was a *Group* effect in bilateral FPA, bilateral VMC and left DLPFC, with the TBI-MF group having lower concentrations of oxy-Hb compared to controls in the mentioned ROIs (see **Figure 4** and **Supplementary Figures S1–S4** for the hemodynamic response curves for each ROI and for single channels). A *Stroop* and *Group* interaction was found in the left VLPFC showing that the TBI-MF group did have the same oxy-Hb concentration for both congruent and incongruent trials, whereas the controls had more oxy-Hb in the incongruent trial, compared to the congruent trial. To explore the Stroop effect (the oxy-Hb difference between incongruent and congruent trials) in the left VLPFC, we

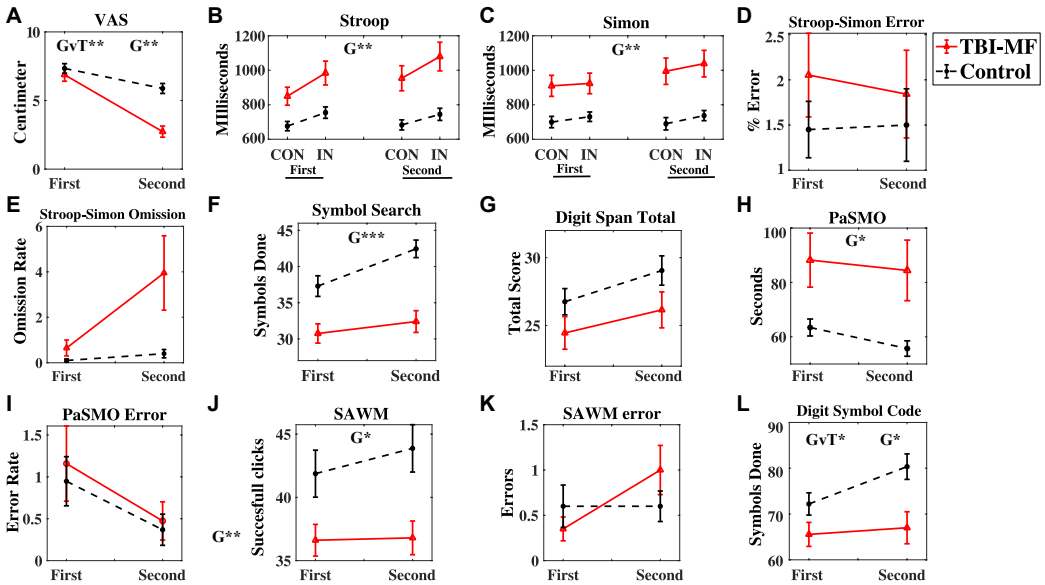

FIGURE 3 | Behavioral test results. **(A)** Energy level measured by the VAS scale (0–10 cm visual analog scale), **(B–E)** Stroop-Simon test, **(B)** Stroop effect reaction time, **(C)** Simon effect reaction time, **(D)** Error rate Stroop-Simon, **(E)** Omission rate Stroop–Simon, **(F)** Symbol Search – number of correct symbols done, **(G)** Digit Span total score, **(H)** PaSMO performance in seconds, **(I)** PaSMO – number of errors, **(J)** SAWM total successful responses, **(K)** SAWM – number of errors, **(L)** Digit Symbol Coding – number of correct symbols done. In **(B)** *CON* represent the congruent stimuli, and *IN* the incongruent stimuli. Both stimulus types are illustrated in **Figure 1B** and described in the Materials and Methods section. Error bars represent standard error of mean. Significant effects are indicated for Group (G) and Group-Time interaction (GvT). ***FDR adjusted $p < 0.001$, **FDR adjusted $p < 0.01$, *FDR adjusted $p < 0.05$.

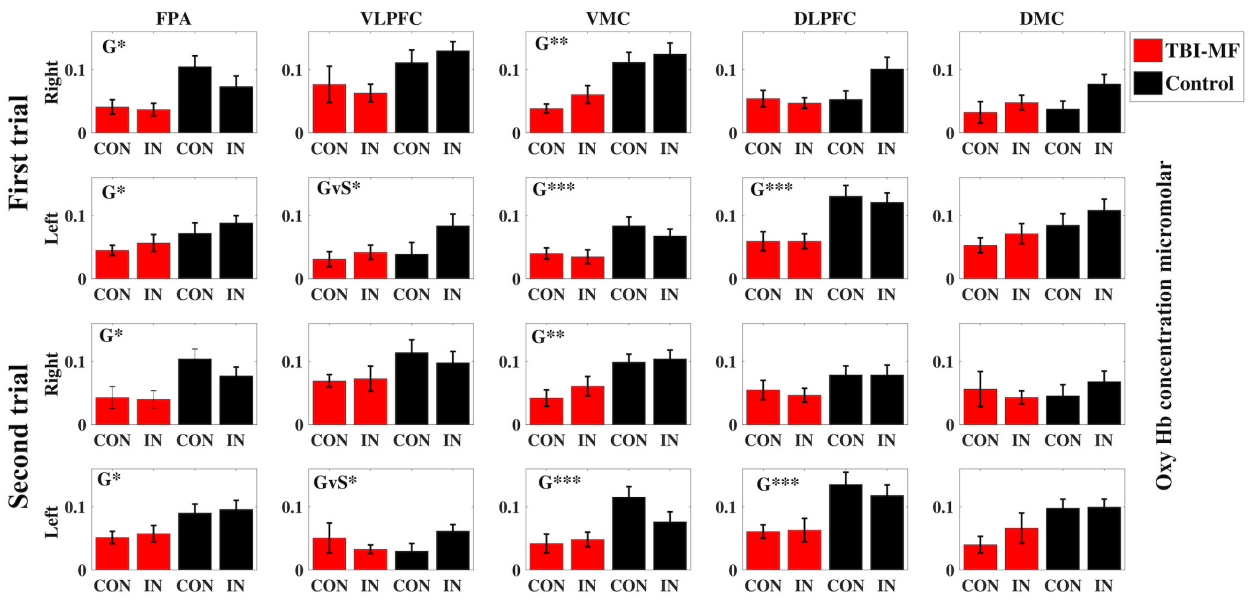

FIGURE 4 | Concentration of oxygenated hemoglobin (micromolar) during fNIRS imaging of the Stroop–Simon test separated by test sessions (First and Second) and hemispheres (Right and Left) for all regions of interest (FPA, frontal polar area; VLPFC, ventral lateral prefrontal cortex; VMC, ventral motor cortex; DLPFC, dorsolateral prefrontal cortex; DMC, dorsal motor cortex). The red columns indicate data for the TBI-MF group, the black columns for healthy controls. *CON* refers to Stroop congruent trials, and *IN* refers to Stroop incongruent trials, as described in the Materials and Methods section. The error bars indicate standard error of mean. Significant effects are indicated for Group (G) or Group-Stroop interaction (GvS). ***FDR adjusted $p < 0.001$, **FDR adjusted $p < 0.01$, *FDR adjusted $p < 0.05$.

conducted a Pearson's correlation between the Stroop effect and the first VAS, the second VAS, the difference between the first and second VAS as well as MFS. None of the correlation with VAS was significant with the first VAS ($r = -0.04$, FDR adjusted $p > 0.05$), the second VAS ($r = -0.282$, FDR adjusted $p > 0.05$) and the VAS difference ($r = -0.234$, FDR adjusted

$p > 0.05$). The correlation with MFS was found to be significant ($r = -0.399$, FDR adjusted $p < 0.05$), showing that higher MFS scores were associated with lower oxy-Hb concentrations (see **Supplementary Figure S5**).

DISCUSSION

The present study examined how prolonged mental activity affects cognitive performance and its neural correlates in individuals with TBI-MF. The TBI-MF group demonstrated lower event-related activity in the FPA, VLPFC, and DLPFC, compared to controls. Group difference in brain activity was detected already during the first test session. No difference in brain activity between the two test sessions was found, and this was the case for both groups.

The TBI-MF participants had difficulty utilizing the left VLPFC in the conflict processing, with no difference in oxy-Hb between congruent and incongruent trials. This was not the case for the controls, who had higher levels of oxy-Hb for the incongruent than congruent trials, indicating a capacity to recruit more activation when the task was more demanding. The left VLPFC, involving inferior frontal gyrus, is known to be involved in semantic conflict processing in Stroop (Egner and Hirsch, 2005; Yasumura et al., 2014; Musz and Thompson-Schill, 2017). A correlation between increased difficulties in utilizing the left VLPFC for the semantic conflict and higher rating on the MFS, was detected. This correlation should, however, be interpreted with caution since a score above 10.5 was an inclusion criterion for the TBI-MF group. This is in line with previous findings by Berginstrom and colleagues, where a modified version of Symbol Digit Modality Test (SDMT) was used, and a correlation between self-assessed fatigue and decreased brain activity in the right inferior and middle frontal gyrus was reported (Berginstrom et al., 2017). We also hypothesized that we would detect this difference in the DLPFC, an area important for cognitive control (Vanderhasselt et al., 2009). We found a difference as indicated by the high *F*-value for the interaction between group and the Stroop effect in the right DLPFC (see **Table 3**), but it did not reach statistical significance after correcting for multiple tests.

To our knowledge, this is the first fNIRS study focusing on MF after mild TBI. There is one previous study by Plenger et al. that used fNIRS while performing a Stroop test in a cohort of individuals with moderate to severe TBI (Plenger et al., 2016). Their results suggest impaired frontal cortex conflict processing indicated by no difference in oxy-Hb concentration levels between the simple dot-color naming task and the more demanding incongruent task. Several other fNIRS studies with moderate to severer TBI have reported a reduced brain activity for a variety of cognitive tasks such as visual discrimination, attention and working memory, especially in DLPFC (Merzagora et al., 2011; Hibino et al., 2013; Kontos et al., 2014; Sawamura et al., 2014; Helmich et al., 2015) but also in VLPFC (Hibino et al., 2013). However, fatigue was not assessed in these fNIRS studies, and, in contrast to our sample, they studied individuals with moderate to severe TBI, whereas we included individuals with mild TBI in our study. A recent fNIRS study, including participants with post-concussion symptoms (PCS) after a mild TBI, showed reduced connectivity for the mild TBI group compared to controls and a correlation between reduced coherence and increased symptom severity (Hocke et al., 2018). In their study, fatigue was not reported, despite the fact that fatigue is one of the symptoms included in the PCS.

TABLE 3 | Repeated ANOVA for the Stroop fNIRS data.

	Group			Time vs. Group			Stroop Effect vs. Group		
	F	FDR	η_p^2	F	FDR	η_p^2	F	FDR	η_p^2
rFPA	9.342	*	0.202	0.002	ns	0.000	5.303	ns	0.125
lFPA	5.630	*	0.132	0.455	ns	0.012	0.026	ns	0.001
rVLPFC	4.030	ns	0.098	0.525	ns	0.014	0.125	ns	0.003
lVLPFC	1.112	ns	0.029	0.612	ns	0.016	10.876	*	0.227
rVMC	12.761	**	0.256	1.152	ns	0.030	1.391	ns	0.036
lVMC	15.588	***	0.296	0.211	ns	0.006	7.218	ns	0.163
rDLPFC	4.632	ns	0.111	0.005	ns	0.000	5.199	ns	0.123
lDLPFC	19.619	***	0.347	0.005	ns	0.000	0.558	ns	0.015
rDMC	0.552	ns	0.015	0.174	ns	0.005	4.437	ns	0.107
lDMC	4.912	ns	0.117	0.260	ns	0.007	0.620	ns	0.016

*FDR, p-value after adjustment with false discovery rate, ***$p < 0.001$, **$p < 0.01$, *$p < 0.05$, $^{ns}p > 0.05$; η_p^2, partial eta-squared effect size; r, right; l, left; FPA, frontal polar area; VLPFC, ventral lateral prefrontal cortex; VMC, ventral motor cortex; DLPFC, dorsolateral prefrontal cortex; DMC, dorsal motor cortex.*

In previous fMRI studies, changes in brain activity have been reported to be related to fatigue. During the performance of a Symbol Digit Modalities Test task, Kohl et al. (2009) found increased brain activity during the 30 min test period among participants who had suffered a moderate to severe TBI. In contrast, a decreased activity was reported for the controls in several brain regions, including middle frontal gyrus, superior parietal cortex, basal ganglia and anterior cingulate (Kohl et al., 2009). Another study using the same task reported decreased brain activity in deeper brain structures, in particular in the basal ganglia, primarily caudate nucleus, the thalamus and anterior insula in the TBI group (mild, moderate, severe) as compared to controls (Berginstrom et al., 2017). The activity of the controls decreased across the 27 min test session, whereas the TBI participants remained on a similar lower activity level (Berginstrom et al., 2017). A recent fMRI study measuring fatigue among individuals who had suffered a moderate to severe TBI, found an interaction between brain activity and cognitive tasks, in the tail of the caudate nucleus (Wylie et al., 2017). Fatigue after mild TBI also correlated with abnormal functional connectivity in the thalamus and middle frontal cortex (Nordin et al., 2016). Altered cerebral blood flow in mild TBI was also reported, mainly in the frontal cortex and thalamic networks (Moller et al., 2017).

A difference was found in the DSC task of processing speed with the controls improving their performance during

the second test session, whereas the TBI-MF group did not. Similarly, improved performance over time for controls has been reported, with a better performance over time, and with no change in speed for TBI patients (Ashman et al., 2008; Johansson and Ronnback, 2015; Jonasson et al., 2018). This indicated a fatiguing effect with reduced efficiency for those suffering from mental fatigue during a longer cognitive activity. However, the relationship between effectiveness and efficiency needs to be interpreted, e.g., a low effectiveness (more errors) may be due to a high efficiency (fast response time). In this study, the controls and TBI-MF did not differ in their effectiveness, which was measured by error rate in the cognitive tests. In contrast, a difference was reported in efficiency, measured in terms of response time, with controls improving during the second test session, while the TBI-MF participants remained at a similar level as during the first test session.

Regarding performance in cognitive tests, the TBI-MF group was slower than the control group on SS, PaSMO, SAWM, DSC and Simon-Stoop and made more omissions on OPATUS-CPTA, while no difference in working memory (DS) was found. Related to the omission of the OPATUS-CPTA, there was a high rate of omissions in the Stroop–Simon test for the TBI-MF group as indicated by the high *F*-value (see **Table 2**). It did, however, not reach statistical significance after correcting for multiple tests. The higher rate of omissions is an indicator of the problem of keeping a sustained attention for the TBI-MF group. The performance on the WAIS-IV tests included in this study (SS, DSC, DS) was within normal range for all participants, even though the TBI-MF group suffered from MF, as indicated by their rating on the MFS. Differences in cognitive performance at a group level have been reported previously and it has been proposed that cognitive decline is related to fatigue among people who had suffered a mild TBI (Azouvi et al., 2004; Ziino and Ponsford, 2006a; Ashman et al., 2008; Belmont et al., 2009; Johansson et al., 2009). The TBI-MF group was less efficient, and the participants' decreased experience of mental energy from start to the end of the test session suggest an objective and subjective fatigability due to the mental load they were exposed for during 2½ h.

The difference in brain activity between the groups was reported during the first test session using the VAS scale, but no differences were reported as to how they experienced their energy level at start of the test procedure. This may have implications for the ability to adapt to a balanced activity level in daily living for the TBI-MF group. From years of clinical experience, most people suffering from TBI-MF report that finding a sustainable daily activity level is challenging. They rest when they feel fatigued, which is natural, but it is difficult to learn to take rests more regularly during the day if they do not feel the need to do so. Many subjects also report about overdoing activities when they temporarily feel "normal," but they later suffer from severe exhaustion. This finding also fits in with the discrepancy between subjective experience and actual brain function.

LIMITATIONS

The Stroop–Simon test adopted for fNIRS had an average stimulus-response time of 9 s in this study. Because the hemodynamic response normally takes 12 s to return to baseline, a shorter time interval could result in the oxy-Hb not returning to baseline. Since change in the oxy-Hb and deoxy-Hb concentration is calculated from a relative baseline, this shorter interval could possibly affect the sensitivity of oxy-Hb as a measure of brain activity. However, no additive increase of oxy-Hb was found, implying that the lower frontal cortex activity for the TBI-MF group cannot be explained by their hemodynamic concentration levels not returning to baseline after 9 s (see the **Supplementary Material**, **Supplementary Figure S6**). A longer stimulus-response time would have enabled us to also measure other properties of the hemodynamic response, e.g., time-to-peak or time-to-baseline. It was not possible to analyze fNIRS Simon effect due to coding problems. Due to the design of our Stroop–Simon test, we are also lacking hemodynamic response data for easier trials as used by Plenger et al. (2016), where naming a color dot represents an easier task as compared to our study using congruent and incongruent stimulus-response pairs. It is possible that the long recording of the Stroop–Simon task could have induced artifacts to the data. However, since we presume this to create random error in the data and the main question related to between-group differences, this should not affect the interpretation of the data.

Additional analysis with the deoxy-Hb could have yielded complementary information. However, the wavelength of the fNIRS system used was better suited for oxy-Hb, and since we did not find any additional information from the basic analysis of deoxy-Hb, we chose to exclusively analyze oxy-Hb. Further analysis would also have led to more corrections which, in turn could have led to more type II errors.

Correction for multiple testing could have obscured true differences, i.e., a type II error. However, *t*- and *F*-values, degrees of freedom and effect sizes are reported here for assessing results. Because we did not have a second control group with mild TBI without MF we are not able to discriminate between effects of mental fatigue and the effects of mild TBI. Since we focused on studying conflict processing, processing speed, attention, working memory and mental control, we did not include additional measurements of learning or memory. Therefore, we cannot discriminate to what degree the deterioration in the performance on the DSC for the TBI-MF is due to an associated memory problem.

CONCLUSION

We found indications that individuals with TBI-MF have a reduced efficiency of neuronal activity in the frontal cortex. This may result both in deterioration of cognitive function and the experience of a mental fatigue after extended mental activity.

ETHICS STATEMENT

This study was carried out in accordance with the recommendations of Ethical Review Board in Gothenburg with written informed consent from all subjects. All subjects gave written informed consent in accordance with the Declaration of Helsinki. The protocol was approved by the Ethical Review Board in Gothenburg.

AUTHOR CONTRIBUTIONS

BJ and SS conceived, planned, and carried out the experiments. BJ, HK, and SS analyzed the data. BJ and SS took the lead in writing the manuscript. All authors made significant contribution to the writing of the manuscript.

FUNDING

The study was funded by grants from The Local Research and Development Council Göteborg and Södra Bohuslän. HK was supported by the Swedish Research Council (Vetenskapsrådet 721-2014-2468 and 521-2014-3224), Swedish Childhood Cancer Foundation (Barncancerfonden MT2017-0013) and by a grant from the Swedish state under the ALF agreement (ALFGBG-726541).

ACKNOWLEDGMENTS

We want to thank Robert Cooper at UCL for using some of his Matlab scripts. We deeply appreciate OPATUS and Petter Knagenhjelm for letting us use the OPATUS-CPTA test for free and for all the technical support we have got. We want also to thank William Hedley Thompson and Niklas Klasson for valuable input and support.

SUPPLEMENTARY MATERIAL

The Supplementary Material for this article can be found online at: https://www.frontiersin.org/articles/10.3389/fnhum.2019.00145/full#supplementary-material

FIGURE S1 | The oxy-Hb and deoxy-Hb concentration for the incongruent trials in the Stroop-Simon test for all five regions of interest in each hemisphere (FPA – frontal polar area, VLPFC – ventral lateral prefrontal cortex, VMC – ventral motor cortex, DLPFC – dorsolateral prefrontal cortex, DMC – dorsal motor cortex). fNIRS activity for the TBI-MF group is depicted with solid lines and controls with dashed lines. The oxy-Hb concentration in indicated in red and the deoxy-Hb in blue. All y-axis are presented as μ molar concentrations of oxy-Hb and deoxy-Hb. Significant effects are indicated for Group (G) or Group-Stroop interaction (GvS). ***FDR adjusted $p < 0.001$, **FDR adjusted $p < 0.01$, *FDR adjusted $p < 0.05$.

FIGURE S2 | fNIRS channel locations viewed from above.

FIGURE S3 | Oxy-Hb and deoxy-Hb concentration with short separation regression for Stroop incongruent trials in the Stroop-Simon test for one channel from each of the ten regions of interest. The TBI-MF group activity is depicted with the solid lines and the dashed lines represent the controls. Red lines indicate oxy-Hb concentrations and blue lines deoxy-Hb concentrations.

FIGURE S4 | Oxy-Hb and deoxy-Hb concentration without short separation regression for Stroop incongruent trials in the Stroop-Simon test for one channel from each of the ten regions of interest. The TBI-MF group activity is depicted with the solid lines and the dashed lines represent the controls. Red lines indicate oxy-Hb concentrations and blue lines deoxy-Hb concentrations.

FIGURE S5 | Pearson's correlation between the mental fatigue scale (MFS) and Stroop effect in the left VLPFC. The Stroop effect is calculated in the fNIRS data as the oxy-Hb difference between incongruent and congruent trials in the Stroop dimension. **(A)** Correlation of $r = -0.399$, a possible outlier is highlighted with a rectangle. **(B)** Correlation of $r = -0.442$, the association is still present with the potential outlier removed. Both correlations are statistically significant with an FDR adjusted $p < 0.05$.

FIGURE S6 | The oxy-Hb concentration for the complete first Stroop-Simon test session (23 min) for all ten ROI. The black curves indicate controls and the red curves the TBI-MF group. If the smaller oxy-Hb response of TBI-MF group were due to a maximum ceiling effect, we would predict a steady increase for the red curves. Since we did not observe such increase, we propose that the shortened stimulus-stimulus interval of 7-11 seconds had not affected the oxy-Hb levels of the TBI-MF group more than the controls.

REFERENCES

Ahman, S., Saveman, B. I., Styrke, J., Bjornstig, U., and Stalnacke, B. M. (2013). Long-term follow-up of patients with mild traumatic brain injury: a mixed-method study. *J. Rehabil. Med.* 45, 758–764. doi: 10.2340/16501977-1182

Ashman, T. A., Cantor, J. B., Gordon, W. A., Spielman, L., Egan, M., Ginsberg, A., et al. (2008). Objective measurement of fatigue following traumatic brain injury. *J. Head. Trauma Rehabil.* 23, 33–40. doi: 10.1097/01.htr.0000308719.70288.22

Azouvi, P., Couillet, J., Leclercq, M., Martin, Y., Asloun, S., and Rousseaux, M. (2004). Divided attention and mental effort after severe traumatic brain injury. *Neuropsychologia* 42, 1260–1268. doi: 10.1016/j.neuropsychologia.2004.01.001

Balardin, J. B., Zimeo Morais, G. A., Furucho, R. A., Trambaiolli, L., Vanzella, P., Biazoli, C., et al. (2017). Imaging brain function with functional near-infrared spectroscopy in unconstrained environments. *Front. Hum. Neurosci.* 11:258. doi: 10.3389/fnhum.2017.00258

Belmont, A., Agar, N., and Azouvi, P. (2009). Subjective fatigue, mental effort, and attention deficits after severe traumatic brain injury. *Neurorehabil. Neural Repair* 23, 939–944. doi: 10.1177/1545968309340327

Berginstrom, N., Nordstrom, P., Ekman, U., Eriksson, J., Andersson, M., Nyberg, L., et al. (2017). Using functional magnetic resonance imaging to detect chronic fatigue in patients with previous traumatic brain injury: changes linked to altered striato-thalamic-cortical functioning. *J. Head. Trauma Rehabil.* 33, 266–274. doi: 10.1097/htr.0000000000000340

Borragán, G., Gilson, M., Atas, A., Slama, H., Lysandropoulos, A., De Schepper, M., et al. (2018). Cognitive fatigue, sleep and cortical activity in multiple sclerosis disease. a behavioral, polysomnographic and functional near-infrared spectroscopy investigation. *Front. Hum. Neurosci.* 12:378. doi: 10.3389/fnhum.2018.00378

Brigadoi, S., and Cooper, R. J. (2015). How short is short? Optimum source-detector distance for short-separation channels in functional near-infrared spectroscopy. *Neurophotonics* 2:025005. doi: 10.1117/1.NPh.2.2.025005

Byun, K., Hyodo, K., Suwabe, K., Ochi, G., Sakairi, Y., Kato, M., et al. (2014). Positive effect of acute mild exercise on executive function via arousal-related prefrontal activations: an fNIRS study. *Neuroimage* 98, 336–345. doi: 10.1016/j.neuroimage.2014.04.067

Cantor, J. B., Ashman, T., Gordon, W., Ginsberg, A., Engmann, C., Egan, M., et al. (2008). Fatigue after traumatic brain injury and its impact on participation and quality of life. *J. Head. Trauma Rehabil.* 23, 41–51. doi: 10.1097/01.HTR.0000308720.70288.af

Carroll, L. J., Cassidy, J. D., Peloso, P. M., Borg, J., von Holst, H., Holm, L., et al. (2004). Prognosis for mild traumatic brain injury: results of the WHO collaborating centre task force on mild traumatic brain injury. *J. Rehabil. Med.* 43(Suppl.), 84–105.

Chaudhuri, A., and Behan, P. O. (2004). Fatigue in neurological disorders. *Lancet* 363, 978–988. doi: 10.1016/s0140-6736(04)15794-2

Dux, P. E., and Marois, R. (2009). The attentional blink: a review of data and theory. *Atten. Percept. Psychophys.* 71, 1683–1700. doi: 10.3758/app.71.8.1683

Egner, T. (2008). Multiple conflict-driven control mechanisms in the human brain. *Trends Cogn. Sci.* 12, 374–380. doi: 10.1016/j.tics.2008.07.001

Egner, T., Delano, M., and Hirsch, J. (2007). Separate conflict-specific cognitive control mechanisms in the human brain. *Neuroimage* 35, 940–948. doi: 10.1016/j.neuroimage.2006.11.061

Egner, T., and Hirsch, J. (2005). The neural correlates and functional integration of cognitive control in a Stroop task. *Neuroimage* 24, 539–547. doi: 10.1016/j.neuroimage.2004.09.007

Ehlis, A. C., Schneider, S., Dresler, T., and Fallgatter, A. J. (2014). Application of functional near-infrared spectroscopy in psychiatry. *Neuroimage* 85, 478–488. doi: 10.1016/j.neuroimage.2013.03.067

Endo, K., Matsukawa, K., Liang, N., Nakatsuka, C., Tsuchimochi, H., Okamura, H., et al. (2013). Dynamic exercise improves cognitive function in association with increased prefrontal oxygenation. *J. Physiol. Sci.* 63, 287–298. doi: 10.1007/s12576-013-0267-6

Everdell, N. L., Gibson, A. P., Tullis, I. D. C., Vaithianathan, T., Hebden, J. C., and Delpy, D. T. (2005). A frequency multiplexed near-infrared topography system for imaging functional activation in the brain. *Rev. Sci. Instru.* 76:093705. doi: 10.1063/1.2038567

Ferrari, M., and Quaresima, V. (2012). A brief review on the history of human functional near-infrared spectroscopy (fNIRS) development and fields of application. *Neuroimage* 63, 921–935. doi: 10.1016/j.neuroimage.2012.03.049

Forster, S. E., and Cho, R. Y. (2014). Context specificity of post-error and post-conflict cognitive control adjustments. *PLoS One* 9:e90281. doi: 10.1371/journal.pone.0090281

Frencham, K. A., Fox, A. M., and Maybery, M. T. (2005). Neuropsychological studies of mild traumatic brain injury: a meta-analytic review of research since 1995. *J. Clin. Exp. Neuropsychol.* 27, 334–351. doi: 10.1080/13803390490520328

Gagnon, L., Perdue, K., Greve, D. N., Goldenholz, D., Kaskhedikar, G., and Boas, D. A. (2011). Improved recovery of the hemodynamic response in diffuse optical imaging using short optode separations and state-space modeling. *Neuroimage* 56, 1362–1371. doi: 10.1016/j.neuroimage.2011.03.001

Haber, S. N., and Calzavara, R. (2009). The cortico-basal ganglia integrative network: the role of the thalamus. *Brain Res. Bull.* 78, 69–74. doi: 10.1016/j.brainresbull.2008.09.013

Hawthorne, G., Gruen, R. L., and Kaye, A. H. (2009). Traumatic brain injury and long-term quality of life: findings from an Australian study. *J. Neurotrauma* 26, 1623–1633. doi: 10.1089/neu.2008-073510.1089/neu.2008.0735

Helmich, I., Saluja, R. S., Lausberg, H., Kempe, M., Furley, P., Berger, A., et al. (2015). Persistent postconcussive symptoms are accompanied by decreased functional brain oxygenation. *J. Neuropsychiatr. Clin. Neurosci.* 27, 287–298. doi: 10.1176/appi.neuropsych.14100276

Hibino, S., Mase, M., Shirataki, T., Nagano, Y., Fukagawa, K., Abe, A., et al. (2013). Oxyhemoglobin changes during cognitive rehabilitation after traumatic brain injury using near infrared spectroscopy. *Neurol. Med. Chir.* 53, 299–303.

Hocke, L. M., Duszynski, C. C., Debert, C. T., Dleikan, D., and Dunn, J. F. (2018). Reduced functional connectivity in adults with persistent post-concussion symptoms: a functional near-infrared spectroscopy study. *J. Neurotrauma* 35, 1224–1232. doi: 10.1089/neu.2017.5365

Huppert, T. J., Diamond, S. G., Franceschini, M. A., and Boas, D. A. (2009). HomER: a review of time-series analysis methods for near-infrared spectroscopy of the brain. *Appl. Opt.* 48, D280–D298.

Hyodo, K., Dan, I., Suwabe, K., Kyutoku, Y., Yamada, Y., Akahori, M., et al. (2012). Acute moderate exercise enhances compensatory brain activation in older adults. *Neurobiol. Aging* 33, 2621–2632. doi: 10.1016/j.neurobiolaging.2011.12.022

Irani, F., Platek, S. M., Bunce, S., Ruocco, A. C., and Chute, D. (2007). Functional near infrared spectroscopy (fNIRS): an emerging neuroimaging technology with important applications for the study of brain disorders. *Clin. Neuropsychol.* 21, 9–37. doi: 10.1080/13854040600910018

Jo Bsis-Vandervliet, F. F. (1999). Discovery of the near-infrared window into the body and the early development of near-infrared spectroscopy. *J. Biomed. Opt.* 4, 392–396. doi: 10.1117/1.429952

Johansson, B., Berglund, P., and Ronnback, L. (2009). Mental fatigue and impaired information processing after mild and moderate traumatic brain injury. *Brain Inj.* 23, 1027–1040. doi: 10.3109/02699050903421099

Johansson, B., and Ronnback, L. (2014). Evaluation of the mental fatigue scale and its relation to cognitive and emotional functioning after traumatic brain injury or stroke. *Int. J. Phys. Med. Rehabil.* 2, 572–573. doi: 10.4172/2329-9096.1000182

Johansson, B., and Rönnbäck, L. (2014). "Long-lasting mental fatigue after traumatic brain injury – a major problem most often neglected diagnostic criteria, assessment, relation to emotional and cognitive problems, cellular background, and aspects on treatment," in *Traumatic Brain Injury*, ed. F. Sadaka (Rijeka: InTech).

Johansson, B., and Ronnback, L. (2015). Novel computer tests for identification of mental fatigue after traumatic brain injury. *Neurorehabilitation* 36, 195–202. doi: 10.3233/nre-151207

Johansson, B., Starmark, A., Berglund, P., Rodholm, M., and Ronnback, L. (2010). A self-assessment questionnaire for mental fatigue and related symptoms after neurological disorders and injuries. *Brain Inj.* 24, 2–12. doi: 10.3109/02699050903452961

Jonasson, A., Levin, C., Renfors, M., Strandberg, S., and Johansson, B. (2018). Mental fatigue and impaired cognitive function after an acquired brain injury. *Brain Behav.* 8:e01056. doi: 10.1002/brb3.1056

King, N. S., Crawford, S., Wenden, F. J., Moss, N. E., and Wade, D. T. (1995). The Rivermead post concussion symptoms questionnaire: a measure of symptoms commonly experienced after head injury and its reliability. *J. Neurol.* 242, 587–592.

Kohl, A. D., Wylie, G. R., Genova, H. M., Hillary, F. G., and Deluca, J. (2009). The neural correlates of cognitive fatigue in traumatic brain injury using functional MRI. *Brain Inj.* 23, 420–432. doi: 10.1080/02699050902788519

Kontos, A. P., Huppert, T. J., Beluk, N. H., Elbin, R. J., Henry, L. C., French, J., et al. (2014). Brain activation during neurocognitive testing using functional near-infrared spectroscopy in patients following concussion compared to healthy controls. *Brain Imaging Behav.* 8, 621–634. doi: 10.1007/s11682-014-9289-9

Kopton, I. M., and Kenning, P. (2014). Near-infrared spectroscopy (NIRS) as a new tool for neuroeconomic research. *Front. Hum. Neurosci.* 8:549. doi: 10.3389/fnhum.2014.00549

Kraus, J. F., Hsu, P., Schafer, K., and Afifi, A. A. (2014). Sustained outcomes following mild traumatic brain injury: results of a five-emergency department longitudinal study. *Brain Inj.* 28, 1248–1256. doi: 10.3109/02699052.2014.916420

Lague-Beauvais, M., Brunet, J., Gagnon, L., Lesage, F., and Bherer, L. (2013). A fNIRS investigation of switching and inhibition during the modified Stroop task in younger and older adults. *Neuroimage* 64, 485–495. doi: 10.1016/j.neuroimage.2012.09.042

Lannsjo, M., Af Geijerstam, J. L., Johansson, U., Bring, J., and Borg, J. (2009). Prevalence and structure of symptoms at 3 months after mild traumatic brain injury in a national cohort. *Brain Inj.* 23, 213–219. doi: 10.1080/02699050902748356

Leon-Carrion, J., Damas-Lopez, J., Martin-Rodriguez, J. F., Dominguez-Roldan, J. M., Murillo-Cabezas, F., Barroso, Y. M. J. M., et al. (2008). The hemodynamics of cognitive control: the level of concentration of oxygenated hemoglobin in the superior prefrontal cortex varies as a function of performance in a modified Stroop task. *Behav. Brain Res.* 193, 248–256. doi: 10.1016/j.bbr.2008.06.013

Lindqvist, G., and Malmgren, H. (1993). Organic mental disorders as hypothetical pathogenetic processes. *Acta Psychiatr. Scand. Suppl.* 373, 5–17.

MATLAB (2014). *MATLAB*. Massachusetts, MA: The MathWorks, Inc.

McInnes, K., Friesen, C. L., MacKenzie, D. E., Westwood, D. A., and Boe, S. G. (2017). Mild traumatic brain injury (mTBI) and chronic cognitive impairment: a scoping review. *PLoS One* 12:e0174847. doi: 10.1371/journal.pone.0174847

Merzagora, A. C., Schultheis, M. T., Onaral, B., and Izzetoglu, M. (2011). Functional near-infrared spectroscopy-based assessment of attention impairments after traumatic brain injury. *J. Innovat. Opt. Health Sci.* 4, 251–260. doi: 10.1142/S1793545811001551

Moller, M. C., Nordin, L. E., Bartfai, A., Julin, P., and Li, T. Q. (2017). Fatigue and cognitive fatigability in mild traumatic brain injury are correlated with altered neural activity during vigilance test performance. *Front. Neurol.* 8:496. doi: 10.3389/fneur.2017.00496

Musz, E., and Thompson-Schill, S. L. (2017). Tracking competition and cognitive control during language comprehension with multi-voxel pattern analysis. *Brain Lang.* 165, 21–32. doi: 10.1016/j.bandl.2016.11.002

Nguyen, R., Fiest, K. M., McChesney, J., Kwon, C. S., Jette, N., Frolkis, A. D., et al. (2016). The international incidence of traumatic brain injury: a systematic review and meta-analysis. *Can. J. Neurol. Sci.* 43, 774–785. doi: 10.1017/cjn.2016.290

Nordin, L. E., Moller, M. C., Julin, P., Bartfai, A., Hashim, F., and Li, T. Q. (2016). Post mTBI fatigue is associated with abnormal brain functional connectivity. *Sci. Rep.* 6:21183. doi: 10.1038/srep21183

Obrig, H. (2014). NIRS in clinical neurology - a 'promising' tool? *Neuroimage* 85(Pt 1), 535–546. doi: 10.1016/j.neuroimage.2013.03.045

Park, N. W., Moscovitch, M., and Robertson, I. H. (1999). Divided attention impairments after traumatic brain injury. *Neuropsychologia* 37, 1119–1133.

Plenger, P., Krishnan, K., Cloud, M., Bosworth, C., Qualls, D., and Marquez de la Plata, C. (2016). fNIRS-based investigation of the Stroop task after TBI. *Brain Imaging Behav.* 10, 357–366. doi: 10.1007/s11682-015-9401-9

Ponsford, J., Cameron, P., Fitzgerald, M., Grant, M., and Mikocka-Walus, A. (2011). Long-term outcomes after uncomplicated mild traumatic brain injury: a comparison with trauma controls. *J. Neurotrauma* 28, 937–946. doi: 10.1089/neu.2010.1516

Reitan, R. M., and Wolfson, D. (1985). *The Halstead-Reitan Neuropsychological test Battery: Theory and Clinical Interpretation*. Tucson: Neuropsychology Press.

Roberts, K. L., and Hall, D. A. (2008). Examining a supramodal network for conflict processing: a systematic review and novel functional magnetic resonance imaging data for related visual and auditory stroop tasks. *J. Cogn. Neurosci.* 20, 1063–1078. doi: 10.1162/jocn.2008.20074

Rodriguez Merzagora, A. C., Izzetoglu, M., Onaral, B., and Schultheis, M. T. (2014). Verbal working memory impairments following traumatic brain injury: an fNIRS investigation. *Brain Imaging Behav.* 8, 446–459. doi: 10.1007/s11682-013-9258-8

Sato, H., Yahata, N., Funane, T., Takizawa, R., Katura, T., Atsumori, H., et al. (2013). A NIRS-fMRI investigation of prefrontal cortex activity during a working memory task. *Neuroimage* 83, 158–173. doi: 10.1016/j.neuroimage.2013.06.043

Sawamura, D., Ikoma, K., Yoshida, K., Inagaki, Y., Ogawa, K., and Sakai, S. (2014). Active inhibition of task-irrelevant sounds and its neural basis in patients with attention deficits after traumatic brain injury. *Brain Inj.* 28, 1455–1460. doi: 10.3109/02699052.2014.919531

Schroeter, M. L., Zysset, S., Kupka, T., Kruggel, F., and Yves von Cramon, D. (2002). Near-infrared spectroscopy can detect brain activity during a color-word matching Stroop task in an event-related design. *Hum. Brain Mapp.* 17, 61–71. doi: 10.1002/hbm.10052

Schroeter, M. L., Zysset, S., Wahl, M., and von Cramon, D. Y. (2004). Prefrontal activation due to Stroop interference increases during development–an event-related fNIRS study. *Neuroimage* 23, 1317–1325. doi: 10.1016/j.neuroimage.2004.08.001

Singh, A. K., and Dan, I. (2006). Exploring the false discovery rate in multichannel NIRS. *Neuroimage* 33, 542–549. doi: 10.1016/j.neuroimage.2006.06.047

Singh, A. K., Okamoto, M., Dan, H., Jurcak, V., and Dan, I. (2005). Spatial registration of multichannel multi-subject fNIRS data to MNI space without MRI. *Neuroimage* 27, 842–851. doi: 10.1016/j.neuroimage.2005.05.019

Uludag, K., Steinbrink, J., Villringer, A., and Obrig, H. (2004). Separability and cross talk: optimizing dual wavelength combinations for near-infrared spectroscopy of the adult head. *Neuroimage* 22, 583–589. doi: 10.1016/j.neuroimage.2004.02.023

Vanderhasselt, M. A., De Raedt, R., and Baeken, C. (2009). Dorsolateral prefrontal cortex and Stroop performance: tackling the lateralization. *Psychon. Bull. Rev.* 16, 609–612. doi: 10.3758/pbr.16.3.609

Wechsler, D. (2010). *Wechsler Adut Intelligence Scale - Fourth Edition, Swedish Edition*. Stockholm: Pearson Assessment.

Wylie, G. R., Dobryakova, E., DeLuca, J., Chiaravalloti, N., Essad, K., and Genova, H. (2017). Cognitive fatigue in individuals with traumatic brain injury is associated with caudate activation. *Sci. Rep.* 7:8973. doi: 10.1038/s41598-017-08846-6

Yasumura, A., Kokubo, N., Yamamoto, H., Yasumura, Y., Nakagawa, E., Kaga, M., et al. (2014). Neurobehavioral and hemodynamic evaluation of Stroop and reverse Stroop interference in children with attention-deficit/hyperactivity disorder. *Brain Dev.* 36, 97–106. doi: 10.1016/j.braindev.2013.01.005

Ye, J. C., Tak, S., Jang, K. E., Jung, J., and Jang, J. (2009). NIRS-SPM: statistical parametric mapping for near-infrared spectroscopy. *Neuroimage* 44, 428–447. doi: 10.1016/j.neuroimage.2008.08.036

Ziino, C., and Ponsford, J. (2006a). Selective attention deficits and subjective fatigue following traumatic brain injury. *Neuropsychology* 20, 383–390. doi: 10.1037/0894-4105.20.3.383

Ziino, C., and Ponsford, J. (2006b). Vigilance and fatigue following traumatic brain injury. *J. Int. Neuropsychol. Soc.* 12, 100–110. doi: 10.1017/s1355617706060139

Conflict of Interest Statement: The authors declare that the research was conducted in the absence of any commercial or financial relationships that could be construed as a potential conflict of interest.

frontiers in Human Neuroscience

ORIGINAL RESEARCH
published: 26 June 2019
doi: 10.3389/fnhum.2019.00186

An MRI Study of the Metabolic and Structural Abnormalities in Obsessive-Compulsive Disorder

Juliana B. de Salles Andrade[1,2], Fernanda Meireles Ferreira[1], Chao Suo[3], Murat Yücel[3], Ilana Frydman[1,4], Marina Monteiro[1], Paula Vigne[1,4], Leonardo F. Fontenelle[1,3,4]† and Fernanda Tovar-Moll[1,2]*†*

[1]D'Or Institute for Research and Education (IDOR), Rio de Janeiro, Brazil, [2]Institute of Biomedical Sciences (ICB), Federal University of Rio de Janeiro, Rio de Janeiro, Brazil, [3]Turner Institute for Brain and Mental Health and School of Psychological Sciences, Monash University, Clayton, VIC, Australia, [4]Obsessive, Compulsive, and Anxiety Spectrum Research Program, Institute of Psychiatry, Federal University of Rio de Janeiro, Rio de Janeiro, Brazil

OPEN ACCESS

Edited by:
Guido van Wingen,
University of Amsterdam,
Netherlands

Reviewed by:
Siyan Fan,
VU University Amsterdam,
Netherlands
Kathrin Koch,
Technical University of Munich,
Germany
Chris Vriend,
VU University Medical Center,
Netherlands

***Correspondence:**
Leonardo F. Fontenelle
lfontenelle@gmail.com
Fernanda Tovar-Moll
fernanda.tovarmoll@idor.org

†These authors have contributed equally to this work

Received: 23 January 2019
Accepted: 21 May 2019
Published: 26 June 2019

Citation:
Salles Andrade JB, Ferreira FM, Suo C, Yücel M, Frydman I, Monteiro M, Vigne P, Fontenelle LF and Tovar-Moll F (2019) An MRI Study of the Metabolic and Structural Abnormalities in Obsessive-Compulsive Disorder. Front. Hum. Neurosci. 13:186. doi: 10.3389/fnhum.2019.00186

Obsessive-compulsive disorder (OCD) is a neuropsychiatric illness characterized by obsessions and/or compulsions. Its pathophysiology is still not well understood but it is known that the cortico-striatal-thalamic-cortical (CSTC) circuitry plays an important role. Here, we used a multi-method MRI approach combining proton magnetic resonance spectroscopy (H1-MRS) and diffusion tensor imaging (DTI) techniques to investigate both the metabolic and the microstructural white matter (WM) changes of the anterior cingulate cortex (ACC) in OCD patients as compared to healthy controls. Twenty-three OCD patients and 21 age-, sex-, and education-matched healthy volunteers participated in the study. Our 1H-MRS findings show increased levels of Glx in ACC in OCD. Further, significantly lower fractional anisotropy (FA) values were observed in OCD patients' left cingulate bundle (CB) as compared to healthy controls. Finally, there was a negative correlation between FA in the left CB and level of obsessions, as well as the duration of the illness. Our findings reinforce the involvement of CSTC bundles in pathophysiology of OCD, pointing to a specific role of glutamate (glutamine) and WM integrity.

Keywords: obsessive-compulsive disorder, HMRS, DTI, anterior cingulate cortex, cingulate bundle

INTRODUCTION

Obsessive-compulsive disorder (OCD) is a neuropsychiatric illness characterized by obsessions and/or compulsions. Obsessions are recurrent, persistent, and unwanted thoughts, urges, or images that generate anxiety and/or distress that are alleviated transiently by compulsions, i.e., repetitive and ritualized behaviors (such as checking, washing, and ordering) or mental acts (such as counting, praying, or repeating words silently; American Psychiatric Association, 2013). Current first-line treatments for OCD include exposure and response prevention (ERP) and serotonin reuptake inhibitors (SRIs; Sookman and Fineberg, 2015). However, as not all patients respond satisfactorily to these treatments, other augmenting drugs (such as glutamate-modulating agents, among others) may need to be added to SRIs (Fineberg et al., 2006; Simpson et al., 2013; Modarresi et al., 2018). Clearly, to develop more effective treatments for OCD, a greater understanding of its etiology and pathophysiology is required.

Although the etiology of OCD remains unclear, research has revealed changes in the cortico-striatal-thalamic-cortical (CSTC) circuits of OCD patients (Pittenger et al., 2011). These circuits link areas that have important roles in the executive function and regulation of behavior (Saxena et al., 2001) and may be well implicated in the mediation of OCD symptoms (Chamberlain et al., 2005). They include cortical and subcortical regions and the white matter (WM) tracts that link them. The cingulate bundle (CB), for example, interconnects the cingulate cortex with limbic regions such as the prefrontal cortex, striatum, and thalamus, and has already been implicated in other neuropsychiatric disorders (Sun et al., 2003; Catheline et al., 2010). The importance of the cingulum in OCD has been highlighted by its use as a target of deep brain stimulation and ablative procedures of treatment refractory OCD patients (Rauch, 2003).

Diffusion tensor imaging (DTI) is a method that allows the measurement of the diffusion characteristics of water molecules *in vivo*. This approach is widely used to investigate WM integrity in psychiatric disorders (Thomason and Thompson, 2011). Although decreased fractional anisotropy (FA) seems disseminated to several brain regions of individuals with OCD, such as the corpus callosum, the longitudinal superior and inferior fasciculus, and the anterior limb of the internal capsule (Szeszko et al., 2005; Bora et al., 2011; Nakamae et al., 2011; Admon et al., 2012), the existing DTI literature suggests the CB to be one of the tracts most consistently affected by decreased WM integrity in adult samples (Piras et al., 2013; Koch et al., 2014). For instance, a recent systematic review found abnormalities in the cingulum in 10 out of the 17 studies (Piras et al., 2013), mostly decreased FA or increased mean diffusivity (MD; consistent with decreased WM integrity; Garibotto et al., 2010; Nakamae et al., 2011). Another proxy for decreased WM integrity was also found in the corticospinal tract, internal capsule, and superior longitudinal fasciculus (Fontenelle et al., 2011).

Glutamate is the principal excitatory neurotransmitter in the brain and a primary neurotransmitter in CSTC circuitry (Shepherd, 2004). It is synthesized from glutamine supplied by astrocytes (Ramadan et al., 2013). Once glutamate is released into the synaptic cleft, it is re-uptaken by astrocytes and converted into glutamine, which will again be used as a precursor of glutamate (Ramadan et al., 2013). Studies using different methods suggest that OCD patients might have a dysfunctional glutamatergic neurotransmission (Carlsson, 2001; Pittenger et al., 2006; Ting and Feng, 2008). For instance, genetic association studies have reported that specific SNPs in or near gene SLC1A1 (which codes for a neural glutamate transporter) such as *rs301443*, rs10491734, and rs7856675 are associated with OCD (Shugart et al., 2009; Samuels et al., 2011). GRIN2B, a gene that codes for a subunit of *N*-methyl-D-aspartate (NMDA) receptors, has also been associated with OCD (Arnold et al., 2009; Kohlrausch et al., 2016). Two studies found elevated cerebrospinal fluid glutamate levels in OCD patients compared to controls (Chakrabarty et al., 2005; Bhattacharyya et al., 2009). There is now evidence of the efficacy of glutamatergic drugs in OCD (Grados et al., 2013; Rodriguez et al., 2013; Marinova et al., 2017). Finally, mice with knocked OUT glutamatergic genes present OCD-like (grooming) behavior (Pittenger et al., 2011).

Perhaps one of the most disseminated methods to assess glutamate and other metabolite levels in the brain is the proton magnetic resonance spectroscopy (H1-MRS). H1-MRS is a noninvasive method that permits *in vivo* quantification of brain biochemistry and has been applied to investigate glutamate levels on OCD. The molecular structures of glutamate and glutamine, which are very similar, give rise to similar magnetic resonance spectra (Ramadan et al., 2013). As a consequence, the combined glutamate and glutamine (Glx) levels are measured by the H1-MRS. The reports, however, have shown some apparent contradictory results. Studies have demonstrated that unmedicated children with OCD had increased Glx levels in the left caudate nucleus that declined after paroxetine treatment as compared to controls (Rosenberg et al., 2000). In adults, a reduction in the anterior cingulate cortex (ACC) Glx levels was restricted to women and negatively correlated with the severity of OCD symptoms (Yücel et al., 2008). Here, we used a multi-method approach combining H1-MRS and DTI techniques to investigate both the metabolic and the microstructural WM changes in OCD patients as compared to healthy controls.

It is important to investigate the relationships between WM integrity and H1-MRS parameters [e.g., glutamate and *N*-acetylaspartate (NAA)] across different neuropsychiatric disorders. For instance, oligodendrocytes (glial cells largely responsible for WM synthesis) seem vulnerable to glutamate receptor-mediated excitotoxicity (McDonald et al., 1998). There is evidence suggesting that changes in NAA may reflect disturbed myelin synthesis (Chakraborty et al., 2001; Madhavarao et al., 2005; Wang et al., 2009; Arun et al., 2010). In healthy adults, WM NAA explained a significant proportion of variability in the FA values, particularly in the splenium of corpus callosum (Wijtenburg et al., 2013). Although a handful of studies have attempted to correlate WM integrity to H1-MRS profile in schizophrenia (Steel et al., 2001; Tang et al., 2007; Rowland et al., 2009; Chiappelli et al., 2015; Reid et al., 2016), the relationship between WM integrity and brain biochemistry in OCD patients remains understudied (Wang et al., 2017, 2018). In the first combined DTI-MRS study, Wang et al. found a positive correlation between FA in the dorsal ACC and choline. In the second, they investigated the anterior thalamic radiation and found a negative correlation between the mean fiber length in the right and ipsilateral thalamic choline level in patients. So far, the association between structural abnormality in the CB and ACC metabolic profile has not been explored. Given the literature reviewed above, we hypothesized: (i) that OCD patients would exhibit decreased FA values in the CB and increased Glx levels in the ACC; (ii) that these findings would correlate with OCD symptomatology; (iii) that they would be independent from medication status; and (iv) that the Glx levels in ACC will negatively correlate with FA in CB.

MATERIALS AND METHODS

Participants

Patients with OCD who were under treatment in the Obsessive, Compulsive, and Anxiety Research Program of the Federal

University of Rio de Janeiro and age- and sex-matched healthy community controls participated in the study. All patients met clinical criteria for OCD according to the *Diagnostic and Statistical Manual of Mental Disorders* (*DSM-IV-TR*), had their diagnosis confirmed using the Structured Clinical Interview for the *Diagnostic and Statistical Manual of Mental Disorders* (Del-Ben et al., 2001), and had total Yale–Brown Obsessive–Compulsive Scale (YBOCS; Goodman et al., 1989) scores ≥16. OCD patients and controls with mental retardation, previous suicidal attempts, psychotic disorders, antisocial personality, or contraindications to MRI were excluded from the study. Also, controls with history of obsessions and compulsions were excluded. All participants were older than 18 years and provided their written informed consent to participate in the research protocol, which was approved by the D'Or Institute for Research and Education review board.

Clinical Assessments

All participants with OCD were interviewed using the YBOCS to evaluate the severity of OCD symptoms. They were also assessed for age at onset (and consequently duration of illness), severity of depression [with the Beck Depression Inventory (BDI; Cunha, 2001)], and functioning [with the *Global Assessment of Functioning* (*GAF*)]. All patients were undergoing pharmacological treatment.

To rate the relative dose of antipsychotic and SRI or other antidepressants being used, scores were attributed to the therapeutically equivalent doses across different medications. According to this scoring system, a score of 1 corresponded to the minimally effective dose for a given SRI, which is also known to occupy at least 80% of the brain serotonin transporters in the striatum (Meyer et al., 2004). Therefore, we feel that the adopted strategy was clinically and biologically valid. Eventually, each participant received an SRI equivalent score, i.e., zero to patients without medication; one to patients who were taking 20 mg of fluoxetine, paroxetine, or citalopram, 50 mg of sertraline, 100 mg of fluvoxamine, or 75 mg of clomipramine; two to patients taking twice the minimally effective doses; and so on and so forth. The score for relative dose of antipsychotic was based on doses equivalent to 100 mg of chlorpromazine (i.e., 1 for patients taking 2 mg of haloperidol, 2 mg of trifluoperazine, 2 mg of pimozide, 2 mg of risperidone, 5 mg of olanzapine, 7.5 mg of aripiprazole, 75 mg of quetiapine, 100 mg of sulpiride, and 1,000 mg of thioridazine, and so on; Woods, 2003).

Imaging Acquisition

Anatomical images were obtained with an Achieva 3T scanner (Philips Medical Systems, Netherlands), using the following pulse sequences: 3D T1-weighted field echo [repetition time (TR)/echo time (TE)/matrix/field of view (FOV) = 7.2 ms/3.4 ms/240 × 240/240 mm, 170 slices, thickness 60 mm] and fluid attenuate inversion recovery [FLAIR; TR/TE/inversion time (TI)/matrix/FOV = 11,000 ms/125 ms/2,800 ms/288 × 168/230 mm, 26 slices, gap = 1 mm, thickness = 4.5 mm]. Diffusion-weighted images (DWIs) were acquired in axial plane with a single-shot, spin-echo echoplanar sequences: TR/3TE/matrix/FOV = 5,582 ms/65 ms/96 × 95/240 × 240 (mm), slice thickness = 2.5 mm, 60 slices without gap. Diffusion sensitization gradients were applied in 32 non-collinear directions, with a *b* factor of 1,000 s/mm^2. H1-MRS findings were recorded using a point resolved spectroscopy volume selection (PRESS; TE 31 ms/TR 2,000 ms/2,048 points/2 kHz bandwidth). Voxel size was 30 × 30 × 15 mm and placed on the ACC bilaterally (**Figure 1**). Levels of total N-acetyl-aspartate (NAAt), glutamate and glutamine (Glx), choline (Cho), and creatine + phosphocreatine (Cr) were measured.

Diffusion Tensor Imaging Procedures

Prior to analysis, participants' datasets received a numeric code and were divided into controls or OCD patients. All diffusion images were visually inspected for artifacts. Movement artifacts and eddy current distortion effects were corrected. Exclusion criteria included excessive movements and brain lesions. The DTI parameters used to investigate the WM integrity include FA and MD, the frequently used parameters, as they measure the directionality of water diffusion and the magnitude of diffusion, respectively. The diffusion tensor for each voxel was calculated based on the eigenvectors (v1, v2, v3) and eigenvalues (λ1, λ2, λ3). After the FA and MD maps were calculated from the eigenvalues, color-coded maps were generated from the FA values and three vector elements of v1 to visualize the WM tract orientation were performed (DTIFit 2.0, FDT-FMRIB's *Diffusion Toolbox*, FSL). FA and MD were brain-extracted (BET, DTIFit toolbox, part of FSL 5.0.6, FMRIB software; Smith, 2002) and registered to a common space (Montreal Neurological

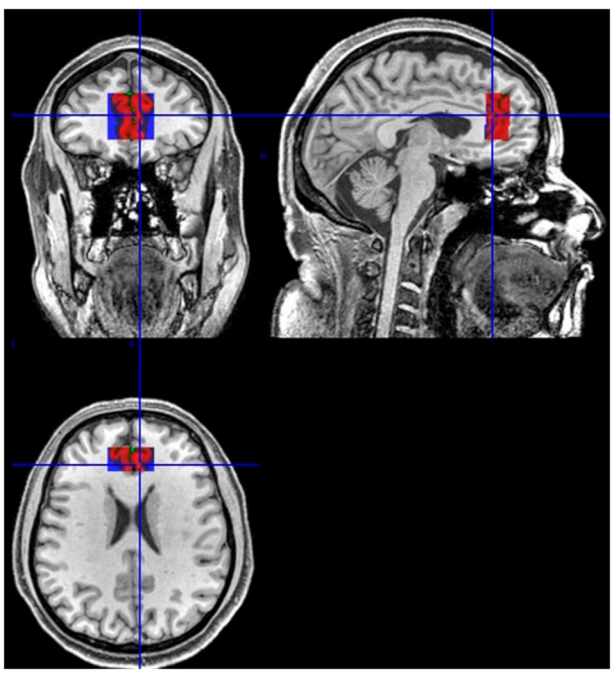

FIGURE 1 | Example of the anatomical reference for the position of the volume of interest (VOI). Sagittal, coronal, and axial views.

Institute Template or MNI152) using constrained nonlinear registration (Image Registration Toolkit; Rueckert et al., 1999). The derived FA and MD data were further analyzed using voxelwise whole-brain Tract based Spatial Statistics (TBSS 1.2, FSL; Smith et al., 2006; Simonyan et al., 2008) and Region of interest (ROI) approaches to explore the WM integrity and differences among groups. ROI analyses were selected according to their relationship with OCD pathology and related anatomical changes previously reported.

Whole-Brain Analysis

Whole-brain voxelwise statistical analysis of FA and MD were performed using TBSS in order to assess the differences in the WM fiber tracts between OCD patients and healthy volunteers. To preserve the intactness of WM structure, a voxelwise-specific tuned nonlinear registration method was used to register FA and MD images into a standard space (Image Registration Toolkit; Rueckert et al., 1999). Aligned FA images were averaged to create the mean FA from all subjects. The mean FA was used to generate the mean FA "skeleton tract," which represents the tracts shared by all subjects (Smith et al., 2006). Registered FA data from each subject were "projected" onto the mean FA skeleton mask to generate the final skeletonized FA data.

A threshold was applied (FA >0.2) to restrict the statistical analysis only to WM voxels that were successfully aligned across subjects, maintaining only the subject's major tract structures. To test for significant local FA and MD differences between controls and OCD, voxelwise cross-subject statistical analysis was carried out using permutation-based non-parametric inference with 10,000 random permutations (FSL Randomize tool) on each voxel of the resulting "mean skeletonized" data (Rueckert et al., 1999) generating the statistical maps The statistical map was "thickened" using spatial smoothing in order to improve visualization.

ROI Analysis

ROIs were placed using a DTI–MRI atlas of human WM from Johns Hopkins University (JHU ICBM-DTI-81 White-Matter Labels and JHU WM Tractography Atlas) in the left and right CB. The ROIs were automatically loaded onto the FA and MD maps and visually checked to confirm their location. FA and MD values were automatically extracted using FSL 5.0.6, FMRIB software. Statistical analysis was performed with $p < 0.05$. Analyses including BDI scores and treatment scores as covariates were carried out to investigate associations between the FA and MD values and OCD severity assessed by Y-BOCS scores.

H1-MRS Procedures

Single-voxel H1-MRS was performed bilaterally and exclusively at the rostral ACC ($30 \times 30 \times 15$ mm^3 fixed). The volume of interest (VOI) was positioned to avoid the skullcap. The anatomical reference for the position of the VOI was the rostrum of the corpus callosum, angulated according to its genu. T2-weighted scans and FLAIR were used to help the placement. Total H1-MRS examination time was approximately 4 min. Eddy current correction was performed for each subject. LCModel (version 6.3- 1H; Provencher, 1993) was used for spectrum quantification. An example of a spectrum is in the **Supplementary Material**. The amplitude (i.e., the area under the spectra) was firstly fitted for the major metabolites, including NAA, Glx, Cr, and Cho. To minimize changes in magnetic field homogeneity, we used Cr signals as the reference, with the results presented as metabolite-to-Cr ratio, because Cr is relatively stable among other metabolites (Govindaraju et al., 2000). Results are presented in arbitrary units (a.u.). The H1-MRS parameters used for the present study provided robust signals for both the healthy controls and OCD groups in the ACC. The output from LCModel includes the signal-to-noise ratio (SNR) and the mean Cramer–Rao lower bound (CRLB), which is a measure of reliability of the fit. We included participants who had CRLB (SD%) <20% and SNR ≥10. Specifically, healthy controls had an ACC SNR of 21.24 (SD 5.09) and a full width at half maximum peak height (FWHM) of 0.06 ppm (SD 0.02). OCD patients had an SNR of 20.96 (SD 4.89) and an FWHM of 0.05 ppm (SD 0.02). None of these measures were different between the two groups (p = 0.86 and 0.26), suggesting that the quality of the data is comparable across the two groups. The CRLB for NAAt, Cr, Cho, and Glx were 5.1%, 3.9%, 4.4%, and 9.5% (SD 2.71, 2.28, 1.89, and 2.73), respectively, for healthy controls, and 4.3%, 3.1%, 3.8%, and 8.3% (SD 2.42, 1.94, 1.69, and 2.29), respectively, for patients.

Statistics

The t-test was used to compare the means of age, schooling, GAF, and BDI among patients and controls. Metabolites were analyzed individually using the SPSS (v.20.0 IBM, Windows). To analyze the associations between H1-MRS metabolite levels and continuous variables (such as the YBOCS, BDI, and GAF scores), Spearman's correlation coefficients were performed. For FA and MD data processed using the FSL tool, statistical analyses of the voxelwise type of the whole brain were made using non-parametric inference based on permutations, with 10,000 random permutations through the FSL randomization tool, in each voxel contained in the map FA and MD skeletonized mean. Results with a p-value of less than 0.05 were considered statistically significant, using family-wise error rate (FWE)-based TFCE (threshold-free cluster enhancement). The r values for FA and MD analysis were obtained from $r = t/\mathrm{sqrt}(t^2 + \mathrm{df})$. t-values were extracted using randomize (TBSS).

RESULTS

Clinical Assessment

A total of 23 OCD patients and 21 healthy volunteers participated in the study. The comparisons between age, sex, years of study, and GAF and BDI scores exhibited by OCD patients and healthy volunteers are shown in **Table 1**. There was no statistically significant difference between OCD patients and the control group in terms of gender (p = 0.239), age (p = 0.561), and years of education (p = 0.367; **Table 1**). However, compared to controls, OCD patients scored higher in the BDI ($p \leq 0.001$) and lower in the GAF ($p \leq 0.001$). Also, all patients were receiving medication for OCD, including clomipramine (n = 10), fluoxetine (n = 8), sertraline (n = 4);

TABLE 1 | Comparison between some sociodemographic and clinical features of obsessive-compulsive disorder (OCD) patients vs. healthy controls.

	OCD (SD)	Controls (SD)	Sig
Age	39.65 (13.7)	37.29 (12.9)	0.561*
Sex (male/female)	15/8	10/11	0.239†
Education	14.39 (2.1)	15.00 (2.3)	0.367*
GAF	47.17 (8.1)	92.19 (4.9)	<0.001*
BDI	20.65 (11.0)	4.10 (4.6)	<0.001*
Y-BOCS total	27.70 (5.7)	-	-
Y-BOCS obsessions	13.78 (3.0)	-	-
Y-BOCS compulsions	13.91 (3.1)	-	-
Disease duration	25.17 (15.9)	-	-

*GAF, Global Assessment of Functioning; BDI, Beck Depression Inventory; SD, standard deviation; Y-BOCS, Yale–Brown Obsessive–Compulsive Scale. Age, education, and disease duration in years. *t-test; †chi-square test.*

paroxetine (n = 3), escitalopram (n = 2), and fluvoxamine (n = 2). An additional 13 patients were receiving concomitant antipsychotics, seven being typical and six atypical. The mean Y-BOCS scores were 13.78 (3.0) for obsessions, 13.91 (3.1) for compulsions, and 27.70 (5.7) for both symptoms (total score). The mean disease duration was 25.17 (15.9) years.

H1-MRS Findings

In the ACC, NAAt/Cr levels did not significantly differ by group (p = 0.191). There were also no significant group differences in Cho/Cr levels (p = 0.454). However, compared with controls, OCD patients had significantly higher levels of Glx/Cr in the ACC (p = 0.016; **Table 2**, **Figure 2**).

Correlation Between H1-MRS Findings and Clinical Data

A correlational analysis was made to investigate if the higher levels of Glx/Cr found in patients were related to symptom severity or disease duration, but no statistically significant results emerged (p = 0.931 and r = 0.019, and p = 0.15 and r = 0.31, respectively; see **Supplementary Material**). As our OCD sample was under pharmacotherapy at the time of the scans, a medication score was created for each group of medication (i.e., SRIs and antipsychotics) according to the equivalent dosage administrated. Then, a correlation analysis was performed between the metabolic ratios and the scores for each patient on each group of medication. Although we were unable to find any significant correlation between different metabolic ratios and the OCD patients' SRI (p = 0.088 and r = 0.373 for NAAt/Cr, p = 0.119 and r = 0.342 for Cho/Cr, and p = 0.17 and r = 0.303 for Glx/Cr) and antipsychotics' scores (p = 0.073 and r = −0.381 for NAAt/Cr, p = 0.106 and r = 0.346 for Cho/Cr, and p = 0.726 and r = 0.077 for Glx/Cr), two trends were particularly noticeable, i.e., a positive correlation between the NAAt/Cr and the SRI's scores (p = 0.088 and r = 0.373) and a negative correlation between NAAt/Cr levels and antipsychotics' score (p = 0.073 and r = 0.381; **Supplementary Material**). However, these findings did not survive statistical correction. Lack of relationships with medication use was confirmed by comparing the metabolic ratios in the ACC of OCD patients using SRI minus (SRI − ANP) vs. SRI plus antipsychotic (SRI + ANP; see **Supplementary Material**).

TABLE 2 | Comparison between metabolites' concentration in OCD vs. healthy controls in anterior cingulate cortex (ACC).

Metabolite	OCD (n = 23)	Controls (n = 21)	Sig.
NAAt/Cr	1.18 (0.16)	1.11 (0.16)	0.191
Cho/Cr	0.29 (0.05)	0.28 (0.04)	0.454
Glx/Cr	1.51 (0.27)	1.32 (0.23)	0.016*

*NAAt, N-acetyl-aspartate total; Cho, choline; Glx, glutamate–glutamine; Cr, creatine + phosphocreatine. t-test *p < 0.05.*

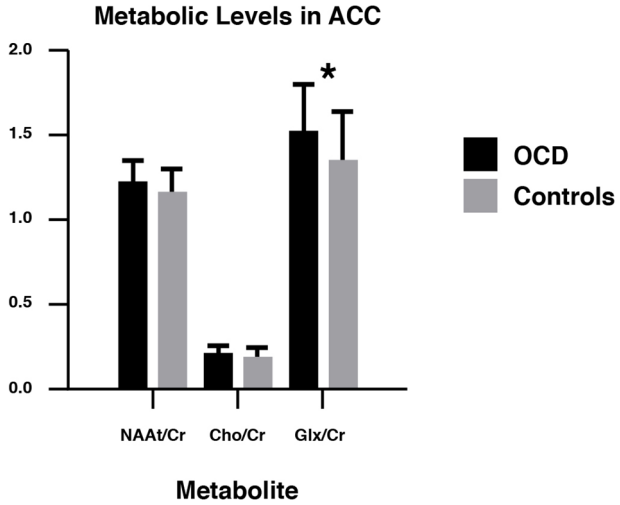

FIGURE 2 | NAAt/Cr, Cho/Cr, and Glx/Cr concentrations in obsessive-compulsive disorder (OCD) patients and healthy controls in the ACC. NAAt, Total *N*-acetyl-aspartate; Cho, choline; Glx, glutamate–glutamine; Cr, creatine + phosphocreatine. ACC, anterior cingulate cortex. *p < 0.05.

Diffusion Tensor Imaging Findings

Voxelwise analysis showed no differences in FA and MD between OCD patients and healthy volunteers. However, ROI analysis showed lower FA in the left CB (p = 0.034, **Figure 3**) of OCD patients compared to healthy controls. Values of MD did not differ significantly between groups.

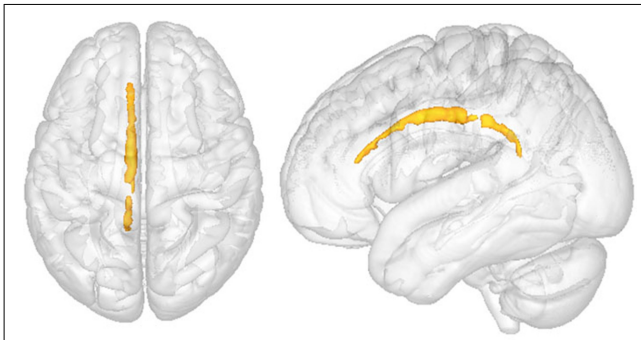

FIGURE 3 | Comparison between OCD patients and healthy controls in the left cingulate bundle (CB). Region of interest (ROI) analysis between groups. Clusters of voxels significantly different (p < 0.05) are shown in red for fractional anisotropy (FA) in the white matter (WM). p = 0.034.

Diffusion Tensor Imaging Findings and Clinical Data

Significant correlations were found between the severity of symptoms and WM integrity. We found a significant negative correlation between Y-BOCS total score and FA value in left CB (p = 0.044 and r = 0.510), but it failed to survive the adjustments for depression and treatment score. We also found a significant negative correlation between Y-BOCS obsession subscore and FA value in right CB (p = 0.032 and r = 0.498) that also failed to survive the covariation analysis. Further, we found a significant negative correlation between Y-BOCS obsession subscore and FA value in left CB (r = 0.458; **Figure 4**). This correlation remained significant after depression (p = 0.039), antipsychotics (p = 0.010), and SRI scores (p = 0.014) were statistically controlled. Regarding the duration of the illness, we found a significant negative correlation with FA values and CB (both left p = 0.033 and r = 0.494 and right p = 0.048 and r = 0.551) and positive correlations between MD value and right CB (significant p = 0.005 and r = 0.498) and left CB (trend p = 0.057; **Figure 5**).

Correlation Between Structural and Metabolic Data

We investigated the association between Glx/Cr levels in ACC with FA values in the CB but failed to find any

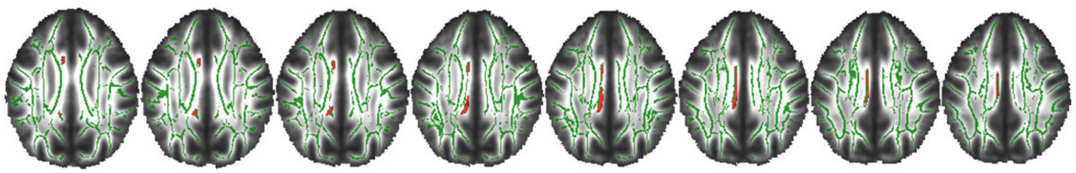

FIGURE 4 | Negative correlation between Y-BOCS obsession score and FA in the left CB. Axial slices. Clusters of voxels significantly different ($p < 0.05$) are shown in red for FA in the WM. p = 0.009.

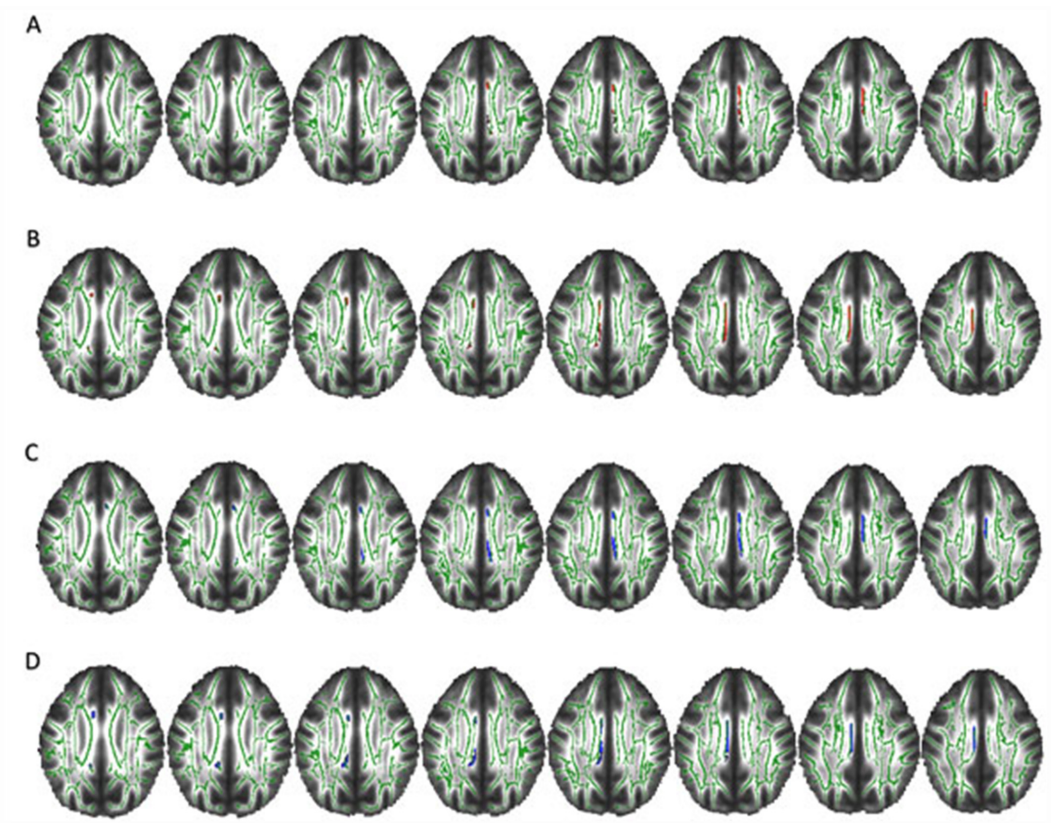

FIGURE 5 | Correlations between FA and mean diffusivity (MD) values and the duration of the illness. Axial slices. Clusters of voxels significantly different ($p < 0.05$) are shown in red for FA and in blue for MD in the WM. **(A,B)** Negative correlation between FA value and years of disease in right (p = 0.048) and left (p = 0.033) CB. **(C,D)** Positive correlation between MD value and years of disease in right CB (p = 0.005) and a trend in left CB (p = 0.057).

significant results (p = 0.794 and r = −0.041 for left CB; and p = 0.560 and r = 0.090 for right CB; see **Supplementary Information**).

DISCUSSION

We performed a novel and simultaneous investigation of metabolic and structural alterations in OCD patients using 1H-MRS and DTI, respectively. First, metabolic ratios in the ACC in 23 OCD patients and 21 healthy volunteers were compared. The findings revealed higher concentrations of Glx/Cr in OCD patients' ACC compared to healthy controls (p = 0.016). However, Glx/Cr did not correlate with the severity of the symptoms (YBOCS score; p = 0.931) or with the duration of the illness (p = 0.15). Similarly, two previous studies reported significantly higher Glx levels in unmedicated OCD patients as compared to controls, one in the orbitofrontal cortex (Whiteside et al., 2006) and the other in the ACC (Gnanavel et al., 2014). Thus, 1H-MRS findings in the CB seem to be consistent with the hyperglutamatergic model of OCD, which describes high levels of glutamate in other parts of the CSTC system, such as the orbitofrontal and striatal regions (Rosenberg et al., 2000; Brennan et al., 2013). Indeed, in light of glutamate dysregulation in OCD, there is clinical evidence for the therapeutic utility of glutamate-modulating drugs as an augmentation or monotherapy in OCD patients. These drugs include memantine, anti-convulsant drugs, riluzole, and ketamine (Marinova et al., 2017). Among these, memantine appears to have greater potential (Sheshachala and Narayanaswamy, 2019).

We have also investigated the integrity of the WM in OCD patients compared to healthy controls, firstly by assessing FA and MD through whole-brain TBSS in all WM of OCD patients and controls, and then by placing ROIs on CB (a critical region of the CSTC loop) of the same research subjects. Similarly to previous studies in children and adolescents (Jayarajan et al., 2012; Silk et al., 2013), our whole-brain analysis did not find significant differences between adult patients and controls in FA or MD measurement. However, significantly lower FA values were observed in OCD patients' left CB as compared to healthy controls in the ROI analysis (p = 0.034). Accordingly, reductions of FA in the left anterior cingulate have been reported in both male and female (Lázaro et al., 2014) or just male OCD patients (Ha et al., 2009). Reduced FA values in patients with OCD may indicate changes in myelination or disorganization of fibers within the bundle. Regions that are interconnected by CBs include the prefrontal cortex, the parahippocampal areas, and the striatum (Lochner et al., 2012; Radua et al., 2014). These data suggest microstructural abnormalities in CSTC loops encompassing ACC.

Importantly, we found a negative correlation between FA and severity of obsessions in the left CB (p = 0.009), suggesting that the more severe the obsessive symptoms, the lower the integrity of this bundle. Although we could not perform a direct cause-and-effect analysis, this correlation could support the role of the CB (and its related circuits) in the neurobiology of OCD. Reinforcing the involvement of this circuitry in OCD, we also found that the longer the duration of the illness, the lower the FA in CB (p = 0.048 for the right CB and p = 0.033 for the left CB), suggesting that bundle disorganization is either a consequence of or a risk factor for long-standing OCD. In the same line, disease duration also positively correlated with MD in right CB and, on a trend level, in left CB (p = 0.005 and p = 0.057, respectively). In addition, the previous report of the lack of WM impairment in younger OCD samples (Jayarajan et al., 2012; Silk et al., 2013) may be consistent with the duration-related impairment of this circuitry in OCD.

Then, we sought to explore whether CB integrity was related to regional neurochemistry. We hypothesized that abnormalities in WM integrity (i.e., reduced FA) would be negatively correlated with higher levels of Glx in patients. More specifically, we predicted that elevated levels of glutamate could lead to excitotoxicity that could influence the integrity of their axons or their connections. However, in contrast to our initial hypothesis, the Glx levels did not correlate with the FA in the CB. A possible reason for the absence of correlation between these parameters is that the increase in Glx may not have been sufficiently large to be neurotoxic.

In order to evaluate the influence of the medication on the metabolic concentrations of the ACC and WM integrity, a dose equivalence score was created for both SRIs and antipsychotics followed by a correlation analysis with the metabolic ratios and DTI values. The analysis showed no significant correlation between the scores and the imaging results. In addition, the sample of patients was separated into two groups: those who used SRIs and those who, besides using SRIs, were also on antipsychotics. Metabolic ratios in the ACC between patient groups were compared, and no meaningful differences were found that could prove the influence of these substances in the metabolite's ratios. That is, pharmacological treatment with antipsychotics did not seem to affect the H1-MRS variables in our OCD patients, a finding that had already been reported in previous studies in OCD children and adolescents (Ortiz et al., 2015).

Our study has some limitations. First, our OCD patients were under active treatment. Although the inclusion of medicated OCD patients can be considered a major drawback of our study, our analyses took into account the relative dose of medications being used in an attempt to control the effect of SRIs and antipsychotics. Second, possible patients' comorbidities were not addressed. Therefore, some could ascribe part of our findings to a higher severity of depressive symptoms in OCD patients as compared to healthy controls. However, in contrast to our findings in this OCD cohort, meta-analysis of MRS studies in patients with depression did not show increased but rather decreased glutamate levels in ACC (Luykx et al., 2012). Third, we did not distinguish between glutamate and glutamine levels when using the Glx measure. Yet, the fact that we used a 3.0-T machine, which has greater accuracy in the quantification of metabolites, has probably minimized the effects of this limitation (Paiva et al., 2013).

Finally, the fact that metabolic concentrations were corrected for Cr levels, instead of being absolutely quantified, could also be seen as a systematic limitation. Although the latter methodology is very widely applied and useful for clinical diagnosis (Jansen et al., 2006), metabolic concentrations corrected for Cr levels assume that there are no differences in the levels of Cr between patients and healthy volunteers, a premise that may not necessarily be true, since changes in Cr concentrations have already been reported in other psychiatric disorders such as schizophrenia and bipolar disorder (Ongür et al., 2009).

CONCLUSION

Thus, summing up, our findings reinforce the involvement of CSTC and bundles that connect areas within the circuitry in pathophysiology of OCD. Further researches are needed with larger samples taking into account the dimensions of OCD to better understand how these changes correlate with the heterogeneous clinical/phenotypic presentations of OCD.

ETHICS STATEMENT

This study was carried out in accordance with the recommendations of the local ethics guidelines, with written informed consent from all subjects. All subjects gave written informed consent in accordance with the Declaration of Helsinki. The protocol was approved by the ethics committee from D'Or Institute for Research and Education.

AUTHOR CONTRIBUTIONS

FT-M, LF, and MY designed the study. IF, PV, JSA, and FF acquired the data, which MM, FF, and CS analyzed. JSA, IF, and FT-M wrote the article, which all authors reviewed and approved for publication.

FUNDING

This work was supported by Conselho Nacional de Desenvolvimento Científico e Tecnológico (CNPq; LF, grant number 302526/2018-8), Fundação de Amparo à Pesquisa do Estado do Rio de Janeiro (FAPERJ; LF, grant number CNE E-26/203.052/2017), as well as by intramural grants from D'Or Institute for Research and Education (IDOR). This study was financed in part by the Coordenação de Aperfeiçoamento de Pessoal de Nível Superior–Brasil (CAPES)–Finance Code 001. MY has received funding from Monash University and Australian Government funding bodies such as the National Health and Medical Research Council (NHMRC; including Fellowship #APP1117188), the Australian Research Council (ARC), and the Department of Industry, Innovation and Science. He has also received philanthropic donations from the David Winston Turner Endowment Fund, as well as payment from law firms in relation to court and/or expert witness reports. The funding sources had no role in study design, data analysis, and result interpretation.

ACKNOWLEDGMENTS

We are thankful to Débora Oliveira and all the technical team for their support in different parts of the study and data acquisition. We also thank all volunteers for their participation in the study.

SUPPLEMENTARY MATERIAL

The Supplementary Material for this article can be found online at: https://www.frontiersin.org/articles/10.3389/fnhum.2019.00186/full#supplementary-material

REFERENCES

Admon, R., Bleich-Cohen, M., Weizmant, R., Poyurovsky, M., Faragian, S., and Hendler, T. (2012). Functional and structural neural indices of risk aversion in obsessive-compulsive disorder (OCD). *Psychiatry Res.* 203, 207–213. doi: 10.1016/j.pscychresns.2012.02.002

American Psychiatric Association. (2013). *Diagnostic and Statistical Manual of Mental Disorders.* Arlington, VA: American Psychiatric Publishing.

Arnold, P. D., Macmaster, F. P., Hanna, G. L., Richter, M. A., Sicard, T., Burroughs, E., et al. (2009). Glutamate system genes associated with ventral prefrontal and thalamic volume in pediatric obsessive-compulsive disorder. *Brain Imaging Behav.* 3, 64–76. doi: 10.1007/s11682-008-9050-3

Arun, P., Madhavarao, C. N., Moffett, J. R., Hamilton, K., Grunberg, N. E., Ariyannur, P. S., et al. (2010). Metabolic acetate therapy improves phenotype in the tremor rat model of Canavan disease. *J. Inherit. Metab. Dis.* 33, 195–210. doi: 10.1007/s10545-010-9100-z

Bhattacharyya, S., Khanna, S., Chakrabarty, K., Mahadevan, A., Christopher, R., and Shankar, S. K. (2009). Anti-brain autoantibodies and altered excitatory neurotransmitters in obsessive-compulsive disorder. *Neuropsychopharmacology* 34, 2489–2496. doi: 10.1038/npp.2009.77

Bora, E., Harrison, B. J., Fornito, A., Cocchi, L., Pujol, J., Fontenelle, L. F., et al. (2011). White matter microstructure in patients with obsessive-compulsive disorder. *J. Psychiatry Neurosci.* 36, 42–46. doi: 10.1503/jpn.100082

Brennan, B. P., Rauch, S. L., Jensen, J. E., and Pope, H. G. Jr. (2013). A critical review of magnetic resonance spectroscopy studies of obsessive-compulsive disorder. *Biol. Psychiatry* 73, 24–31. doi: 10.1016/j.biopsych.2012.06.023

Carlsson, M. L. (2001). On the role of prefrontal cortex glutamate for the antithetical phenomenology of obsessive compulsive disorder and attention deficit hyperactivity disorder. *Prog. Neuropsychopharmacol. Biol. Psychiatry* 25, 5–26. doi: 10.1016/s0278-5846(00)00146-9

Catheline, G., Periot, O., Amirault, M., Braun, M., Dartigues, J. F., Auriacombe, S., et al. (2010). Distinctive alterations of the cingulum bundle during aging and Alzheimer's disease. *Neurobiol. Aging* 31, 1582–1592. doi: 10.1016/j.neurobiolaging.2008.08.012

Chakrabarty, K., Bhattacharyya, S., Christopher, R., and Khanna, S. (2005). Glutamatergic dysfunction in OCD. *Neuropsychopharmacology* 30, 1735–1740. doi: 10.1038/sj.npp.1300733

Chakraborty, G., Mekala, P., Yahya, D., Wu, G., and Ledeen, R. W. (2001). Intraneuronal N-acetylaspartate supplies acetyl groups for myelin lipid synthesis: evidence for myelin-associated aspartoacylase. *J. Neurochem.* 78, 736–745. doi: 10.1046/j.1471-4159.2001.00456.x

Chamberlain, S. R., Blackwell, A. D., Fineberg, N. A., Robbins, T. W., and Sahakian, B. J. (2005). The neuropsychology of obsessive compulsive disorder:

the importance of failures in cognitive and behavioural inhibition as candidate endophenotypic markers. *Neurosci. Biobehav. Rev.* 29, 399–419. doi: 10.1016/j.neubiorev.2004.11.006

Chiappelli, J., Hong, L. E., Wijtenburg, S. A., Du, X., Gaston, F., Kochunov, P., et al. (2015). Alterations in frontal white matter neurochemistry and microstructure in schizophrenia: implications for neuroinflammation. *Transl. Psychiatry* 5:e548. doi: 10.1038/tp.2015.43

Cunha, J. A. (2001). *Manual da Versão em Português das Escalas Beck*. São Paulo: Casa do Psicólogo.

Del-Ben, C. M., Vilela, J. A., Crippa, J. A., Hallaka, J. E., Labate, C. M., and Zuardi, A. W. (2001). Reliability of the structured clinical interview for DSM-IV—clinical version translated into Portuguese. *Rev. Bras. Psiquiatr.* 23, 156–159. doi: 10.1590/s1516-44462001000300008

Fineberg, N. A., Stein, D. J., Premkumar, P., Carey, P., Sivakumaran, T., Vythilingum, B., et al. (2006). Adjunctive quetiapine for serotonin reuptake inhibitor-resistant obsessive-compulsive disorder: a meta-analysis of randomized controlled treatment trials. *Int. Clin. Psychopharmacol.* 21, 337–343. doi: 10.1097/01.yic.0000215083.57801.11

Fontenelle, L. F., Bramati, I. E., Moll, J., Mendlowicz, M. V., de Oliveira-Souza, R., and Tovar-Moll, F. (2011). White matter changes in OCD revealed by diffusion tensor imaging. *CNS Spectr.* 16, 101–109. doi: 10.1017/S1092852912000260

Garibotto, V., Scifo, P., Gorini, A., Alonso, C. R., Brambati, S., Bellodi, L., et al. (2010). Disorganization of anatomical connectivity in obsessive compulsive disorder: a multi-parameter diffusion tensor imaging study in a subpopulation of patients. *Neurobiol. Dis.* 37, 468–476. doi: 10.1016/j.nbd.2009.11.003

Gnanavel, S., Sharan, P., Khandelwal, S., Sharma, U., and Jagannathan, N. R. (2014). Neurochemicals measured by (1)H-MR spectroscopy: putative vulnerability biomarkers for obsessive compulsive disorder. *MAGMA* 27, 407–417. doi: 10.1007/s10334-013-0427-y

Goodman, W. K., Price, L. H., Rasmussen, S. A., Mazure, C., Fleischmann, R. L., Hill, C. L., et al. (1989). The Yale-Brown obsessive compulsive scale I. Development, use and reliability. *Arch. Gen. Psychiatry* 46, 1006–1011. doi: 10.1001/archpsyc.1989.01810110048007

Govindaraju, V., Young, K., and Maudsley, A. A. (2000). Proton NMR chemical shifts and coupling constants for brain metabolites. *NMR Biomed.* 13, 129–153. doi: 10.1002/1099-1492(200005)13:3<129::aid-nbm619>3.3.co;2-m

Grados, M. A., Specht, M. W., Sung, H. M., and Fortune, D. (2013). Glutamate drugs and pharmacogenetics of OCD: a pathway-based exploratory approach. *Expert Opin. Drug Discov.* 8, 1515–1527. doi: 10.1517/17460441.2013.845553

Ha, T. H., Kang, D. H., Park, J. S., Jang, J. H., Jung, W. H., Choi, J. S., et al. (2009). White matter alterations in male patients with obsessive-compulsive disorder. *Neuroreport* 20, 735–739. doi: 10.1097/WNR.0b013e32832ad3da

Jansen, J. F., Backes, W. H., Nicolay, K., and Kooi, M. E. (2006). ^{1}H MR spectroscopy of the brain: absolute quantification of metabolites. *Radiology* 240, 318–332. doi: 10.1148/radiol.2402050314

Jayarajan, R. N., Venkatasubramanian, G., Viswanath, B., Janardhan Reddy, Y. C., Srinath, S., Vasudev, M. K., et al. (2012). White matter abnormalities in children and adolescents with obsessive-compulsive disorder: a diffusion tensor imaging study. *Depress Anxiety* 29, 780–788. doi: 10.1002/da.21890

Koch, K., Reeß, T., Rus, G., Zimmer, C., and Zaudig, M. (2014). Diffusion tensor imaging (DTI) studies in patients with obsessive-compulsive disorder (OCD): a review. *J. Psychiatr. Res.* 54, 26–35. doi: 10.1016/j.jpsychires.2014.03.006

Kohlrausch, F. B., Giori, I. G., Melo-Felippe, F. B., Vieira-Fonseca, T., Velarde, L. G., de Salles Andrade, J. B., et al. (2016). Association of GRIN2B gene polymorphism and obsessive compulsive disorder and symptom dimensions: a pilot study. *Psychiatry Res.* 243, 152–155. doi: 10.1016/j.psychres.2016.06.027

Lázaro, L., Calvo, A., Ortiz, A. G., Ortiz, A. E., Morer, A., Moreno, E., et al. (2014). Microstructural brain abnormalities and symptom dimensions in child and adolescent patients with obsessive-compulsive disorder: a diffusion tensor imaging study. *Depress Anxiety* 31, 1007–1017. doi: 10.1002/da.22330

Lochner, C., Fouche, J. P., du Plessis, S., Spottiswoode, B., Seedat, S., Fineberg, N., et al. (2012). Evidence for fractional anisotropy and mean diffusivity white matter abnormalities in the internal capsule and cingulum in patients with obsessive-compulsive disorder. *J. Psychiatry Neurosci.* 37, 193–199. doi: 10.1503/jpn.110059

Luykx, J. J., Laban, K. G., van den Heuvel, M. P., Boks, M. P., Mandl, R. C., Kahn, R. S., et al. (2012). Region and state specific glutamate downregulation in major depressive disorder: a meta-analysis of (1)H-MRS findings. *Neurosci. Biobehav. Rev.* 36, 198–205. doi: 10.1016/j.neubiorev.2011.05.014

Madhavarao, C. N., Arun, P., Moffett, J. R., Szucs, S., Surendran, S., Matalon, R., et al. (2005). Defective N-acetylaspartate catabolism reduces brain acetate levels and myelin lipid synthesis in Canavan's disease. *Proc. Natl. Acad. Sci. U S A* 102, 5221–5226. doi: 10.1073/pnas.0409184102

Marinova, Z., Chuang, D. M., and Fineberg, N. (2017). Glutamate-modulating drugs as a potential therapeutic strategy in obsessive-compulsive disorder. *Curr. Neuropharmacol.* 15, 977–995. doi: 10.2174/1570159x15666170320104237

McDonald, J. W., Althomsons, S. P., Hyrc, K. L., Choi, D. W., and Goldberg, M. P. (1998). Oligodendrocytes from forebrain are highly vulnerable to AMPA/kainate receptor-mediated excitotoxicity. *Nat. Med.* 4, 291–297. doi: 10.1038/nm0398-291

Meyer, J. H., Wilson, A. A., Sagrati, S., Hussey, D., Carella, A., Potter, W. Z., et al. (2004). Serotonin transporter occupancy of five selective serotonin reuptake inhibitors at different doses: an [11C]DASB positron emission tomography study. *Am. J. Psychiatry* 161, 826–835. doi: 10.1176/appi.ajp.161.5.826

Modarresi, A., Sayyah, M., Razooghi, S., Eslami, K., Javadi, M., and Kouti, L. (2018). Memantine augmentation improves symptoms in serotonin reuptake inhibitor-refractory obsessive-compulsive disorder: a randomized controlled trial. *Pharmacopsychiatry* 51, 263–269. doi: 10.1055/s-0043-120268

Nakamae, T., Narumoto, J., Sakai, Y., Nishida, S., Yamada, K., Nishimura, T., et al. (2011). Diffusion tensor imaging and tract-based spatial statistics in obsessive-compulsive disorder. *J. Psychiatr. Res.* 45, 687–690. doi: 10.1016/j.jpsychires.2010.09.016

Ongür, D., Prescot, A. P., Jensen, J. E., Cohen, B. M., and Renshaw, P. F. (2009). Creatine abnormalities in schizophrenia and bipolar disorder. *Psychiatry Res.* 172, 44–48. doi: 10.1016/j.pscychresns.2008.06.002

Ortiz, A. E., Ortiz, A. G., Falcon, C., Morer, A., Plana, M. T., Bargalló, N., et al. (2015). ^{1}H-MRS of the anterior cingulate cortex in childhood and adolescent obsessive-compulsive disorder: a case-control study. *Eur. Neuropsychopharmacol.* 25, 60–68. doi: 10.1016/j.euroneuro.2014.11.007

Paiva, F. F., Otaduy, M. C. G., de Oliveira-Souza, R., Moll, J., Bramati, I. E., Oliveira, L., et al. (2013). Comparison of human brain metabolite levels using 1H MRS at 1.5T and 3.0T. *Dement. Neuropsychol.* 7, 216–220. doi: 10.1590/S1980-57642013DN70200013

Piras, F., Piras, F., Caltagirone, C., and Spalletta, G. (2013). Brain circuitries of obsessive-compulsive disorder: a systematic review and meta-analysis of tensor imaging studies. *Neurosci. Biobehav. Rev.* 37, 2856–2877. doi: 10.1016/j.neubiorev.2013.10.008

Pittenger, C., Bloch, M. H., and Williams, K. (2011). Glutamate abnormalities in obsessive compulsive disorder: neurobiology, pathophysiology, and treatment. *Pharmacol. Ther.* 132, 314–332. doi: 10.1016/j.pharmthera.2011.09.006

Pittenger, C., Krystal, J. H., and Coric, V. (2006). Glutamate-modulating drugs as novel pharmacotherapeutic agents in the treatment of obsessive-compulsive disorder. *NeuroRx* 3, 69–81. doi: 10.1016/j.nurx.2005.12.006

Provencher, S. W. (1993). Estimation of metabolite concentrations from localized *in vivo* proton NMR spectra. *Magn. Reson. Med.* 30, 672–679. doi: 10.1002/mrm.1910300604

Radua, J., Grau, M., van den Heuvel, O. A., Thiebaut de Schotten, M., Stein, D. J., Canales-Rodriguez, E. J., et al. (2014). Multimodal voxel-based meta-analysis of white matter abnormalities in obsessive-compulsive disorder. *Neuropsychopharmacology* 39, 1547–1557. doi: 10.1038/npp.2014.5

Ramadan, S., Lin, A., and Stanwell, P. (2013). Glutamate and glutamine: a review of *in vivo* MRS in the human brain. *NMR Biomed.* 26, 1630–1646. doi: 10.1002/nbm.3045

Rauch, S. L. (2003). Neuroimaging and neurocircuitry models pertaining to the neurosurgical treatment of psychiatric disorders. *Neurosurg. Clin. N. Am.* 14, 213–223. doi: 10.1016/s1042-3680(02)00114-6

Reid, M. A., White, D. M., Kraguljac, N. V., and Lahti, A. C. (2016). A combined diffusion tensor imaging and magnetic resonance spectroscopy study of patients with schizophrenia. *Schizophr. Res.* 170, 341–350. doi: 10.1016/j.schres.2015.12.003

Rodriguez, C. I., Kegeles, L. S., Levinson, A., Feng, T., Marcus, S. M., Vermes, D., et al. (2013). Randomized controlled crossover trial of ketamine in obsessive-compulsive disorder: proof-of-concept. *Neuropsychopharmacology* 38, 2475–2483. doi: 10.1038/npp.2013.150

Rosenberg, D. R., MacMaster, F. P., Keshavan, M. S., Fitzgerald, K. D., Stewart, C. M., and Moore, G. J. (2000). Decrease in caudate glutamatergic concentrations in pediatric obsessive-compulsive disorder patients taking paroxetine. *J. Am. Acad. Child Adolesc. Psychiatry* 39, 1096–1103. doi: 10.1097/00004583-200009000-00008

Rowland, L. M., Spieker, E. A., Francis, A., Barker, P. B., Carpenter, W. T., and Buchanan, R. W. (2009). White matter alterations in deficit schizophrenia. *Neuropsychopharmacology* 34, 1514–1522. doi: 10.1038/npp.2008.207

Rueckert, D., Sonoda, L. I., Hayes, C., Hill, D. L., Leach, M. O., and Hawkes, D. J. (1999). Nonrigid registration using free-form deformations: application to breast MR images. *IEEE Trans. Med. Imaging* 18, 712–721. doi: 10.1109/42.796284

Samuels, J., Wang, Y., Riddle, M. A., Greenberg, B. D., Fyer, A. J., McCracken, J. T., et al. (2011). Comprehensive family-based association study of the glutamate transporter gene SLC1A1 in obsessive-compulsive disorder. *Am. J. Med. Genet. B Neuropsychiatr. Genet.* 156B, 472–477. doi: 10.1002/ajmg.b.31184

Saxena, S., Bota, R. G., and Brody, A. L. (2001). Brain-behavior relationships in obsessive-compulsive disorder. *Semin. Clin. Neuropsychiatry* 6, 82–101. doi: 10.1053/scnp.2001.21833

Shepherd, G. M. (2004). *The Synaptic Organization of the Brain.* 5th Edn. New York, NY: Oxford University Press.

Sheshachala, K., and Narayanaswamy, J. C. (2019). Glutamatergic augmentation strategies in obsessive-compulsive disorder. *Indian J. Psychiatry* 61, S58–S65. doi: 10.4103/psychiatry.indianjpsychiatry_520_18

Shugart, Y. Y., Wang, Y., Samuels, J. F., Grados, M. A., Greenberg, B. D., Knowles, J. A., et al. (2009). A family-based association study of the glutamate transporter gene SLC1A1 in obsessive-compulsive disorder in 378 families. *Am. J. Med. Genet. B Neuropsychiatr. Genet.* 150B, 886–892. doi: 10.1002/ajmg.b.30914

Silk, T., Chen, J., Seal, M., and Vance, A. (2013). White matter abnormalities in pediatric obsessive-compulsive disorder. *Psychiatry Res.* 213, 154–160. doi: 10.1016/j.pscychresns.2013.04.003

Simonyan, K., Tovar-Moll, F., Ostuni, J., Hallett, M., Kalasinsky, V. F., Lewin-Smith, M. R., et al. (2008). Focal white matter changes in spasmodic dysphonia: a combined diffusion tensor imaging and neuropathological study. *Brain* 131, 447–459. doi: 10.1093/brain/awm303

Simpson, H. B., Foa, E. B., Liebowitz, M. R., Huppert, J. D., Cahill, S., Maher, M. J., et al. (2013). Cognitive-behavioral therapy vs. risperidone for augmenting serotonin reuptake inhibitors in obsessive-compulsive disorder: a randomized clinical trial. *JAMA Psychiatry* 70, 1190–1199. doi: 10.1001/jamapsychiatry.2013.1932

Smith, S. M. (2002). Fast robust automated brain extraction. *Hum. Brain Mapp.* 17, 143–155. doi: 10.1002/hbm.10062

Smith, S. M., Jenkinson, M., Johansen-Berg, H., Rueckert, D., Nichols, T. E., Mackay, C. E., et al. (2006). Tract-based spatial statistics: voxelwise analysis of multi-subject diffusion data. *Neuroimage* 31, 1487–1505. doi: 10.1016/j.neuroimage.2006.02.024

Sookman, D., and Fineberg, N. A. (2015). Specialized psychological and pharmacological treatments for obsessive-compulsive disorder throughout the lifespan: a special series by the Accreditation Task Force (ATF) of The Canadian Institute for Obsessive Compulsive Disorders (CIOCD, www.ciocd.ca). *Psychiatry Res.* 227, 74–77. doi: 10.1016/j.psychres.2014.12.002

Steel, R. M., Bastin, M. E., McConnell, S., Marshall, I., Cunningham-Owens, D. G., Lawrie, S. M., et al. (2001). Diffusion tensor imaging (DTI) and proton magnetic resonance spectroscopy (1H MRS) in schizophrenic subjects and normal controls. *Psychiatry Res.* 106, 161–170. doi: 10.1016/s0925-4927(01)00080-4

Sun, Z., Wang, F., Cui, L., Breeze, J., Du, X., Wang, X., et al. (2003). Abnormal anterior cingulum in patients with schizophrenia: a diffusion tensor imaging study. *Neuroreport* 14, 1833–1836. doi: 10.1097/01.wnr.0000094529.75712.48

Szeszko, P. R., Ardekani, B. A., Ashtari, M., Malhotra, A. K., Robinson, D. G., Bilder, R. M., et al. (2005). White matter abnormalities in obsessive-compulsive disorder: a diffusion tensor imaging study. *Arch. Gen. Psychiatry* 62, 782–790. doi: 10.1001/archpsyc.62.7.782

Tang, C. Y., Friedman, J., Shungu, D., Chang, L., Ernst, T., Stewart, D., et al. (2007). Correlations between Diffusion Tensor Imaging (DTI) and Magnetic Resonance Spectroscopy (1H MRS) in schizophrenic patients and normal controls. *BMC Psychiatry* 7:25. doi: 10.1186/1471-244x-7-25

Thomason, M. E., and Thompson, P. M. (2011). Diffusion imaging, white matter, and psychopathology. *Annu. Rev. Clin. Psychol.* 7, 63–85. doi: 10.1146/annurev-clinpsy-032210-104507

Ting, J. T., and Feng, G. (2008). Glutamatergic synaptic dysfunction and obsessive-compulsive disorder. *Curr. Chem. Genomics* 2, 62–75. doi: 10.2174/1875397300802010062

Wang, R., Fan, Q., Zhang, Z., Chen, Y., Tong, S., and Li, Y. (2017). White matter integrity correlates with choline level in dorsal anterior cingulate cortex of obsessive-compulsive disorder patients: a combined DTI-MRS study. *Conf. Proc. IEEE Eng. Med. Biol. Soc.* 2017, 3521–3524. doi: 10.1109/embc.2017.8037616

Wang, R., Fan, Q., Zhang, Z., Chen, Y., Zhu, Y., and Li, Y. (2018). Anterior thalamic radiation structural and metabolic changes in obsessive-compulsive disorder: a combined DTI-MRS study. *Psychiatry Res. Neuroimaging* 277, 39–44. doi: 10.1016/j.pscychresns.2018.05.004

Wang, J., Leone, P., Wu, G., Francis, J. S., Li, H., Jain, M. R., et al. (2009). Myelin lipid abnormalities in the aspartoacylase-deficient tremor rat. *Neurochem. Res.* 34, 138–148. doi: 10.1007/s11064-008-9726-5

Whiteside, S. P., Port, J. D., Deacon, B. J., and Abramowitz, J. S. (2006). A magnetic resonance spectroscopy investigation of obsessive-compulsive disorder and anxiety. *Psychiatry Res.* 146, 137–147. doi: 10.1016/j.pscychresns.2005.12.006

Wijtenburg, S. A., McGuire, S. A., Rowland, L. M., Sherman, P. M., Lancaster, J. L., Tate, D. F., et al. (2013). Relationship between fractional anisotropy of cerebral white matter and metabolite concentrations measured using (1)H magnetic resonance spectroscopy in healthy adults. *Neuroimage* 66, 161–168. doi: 10.1016/j.neuroimage.2012.10.014

Woods, S. W. (2003). Chlorpromazine equivalent doses for the newer atypical antipsychotics. *J. Clin. Psychiatry* 64, 663–667. doi: 10.4088/jcp.v64n0607

Yücel, M., Wood, S. J., Wellard, R. M., Harrison, B. J., Fornito, A., Pujol, J., et al. (2008). Anterior cingulate glutamate-glutamine levels predict symptom severity in women with obsessive-compulsive disorder. *Aust. N. Z. J. Psychiatry* 42, 467–477. doi: 10.1080/00048670802050546

Conflict of Interest Statement: The authors declare that the research was conducted in the absence of any commercial or financial relationships that could be construed as a potential conflict of interest.

frontiers in Human Neuroscience

ORIGINAL RESEARCH
published: 06 September 2019
doi: 10.3389/fnhum.2019.00317

Evaluation of Neural Degeneration Biomarkers in the Prefrontal Cortex for Early Identification of Patients With Mild Cognitive Impairment: An fNIRS Study

Dalin Yang[1], Keum-Shik Hong[1,2], So-Hyeon Yoo[1] and Chang-Soek Kim[2]*

[1] School of Mechanical Engineering, Pusan National University, Busan, South Korea, [2] Department of Cogno-Mechatronics Engineering, Pusan National University, Busan, South Korea

Mild cognitive impairment (MCI), a condition characterizing poor cognition, is associated with aging and depicts early symptoms of severe cognitive impairment, known as Alzheimer's disease (AD). Meanwhile, early detection of MCI can prevent progression to AD. A great deal of research has been performed in the past decade on MCI detection. However, availability of biomarkers for MCI detection requires greater attention. In our study, we evaluated putative and reliable biomarkers for diagnosing MCI by performing different mental tasks (i.e., *N*-back task, Stroop task, and verbal fluency task) using functional near-infrared spectroscopy (fNIRS) signals on a group of 15 MCI patients and 9 healthy control (HC). The 15 digital biomarkers (i.e., five means, seven slopes, peak, skewness, and kurtosis) and two image biomarkers (*t*-map, correlation map) in the prefrontal cortex (PFC) (i.e., left PFC, middle PFC, and right PFC) between the MCI and HC groups were investigated by the statistical analysis, linear discriminant analysis (LDA), and convolutional neural network (CNN) individually. The results reveal that the statistical analysis using digital biomarkers (with a p-value < 0.05) could not distinguish the MCI patients from the HC over 60% accuracy. Therefore, the current statistical analysis needs to be improved to be used for diagnosing the MCI patients. The best accuracy with LDA was 76.67% with the *N*-back and Stroop tasks. However, the CNN classification results trained by image biomarkers showed a high accuracy. In particular, the CNN results trained via *t*-maps revealed the best accuracy (90.62%) with the *N*-back task, whereas the CNN result trained by the correlation maps was 85.58% with the *N*-back task. Also, the results illustrated that investigating the sub-regions (i.e., right, middle, left) of the PFC for detecting MCI would be better than examining the whole PFC. The *t*-map (or/and the correlation map) is conclusively recommended as an image biomarker for early detection of AD. The combination of CNN and image biomarkers can provide a reliable clinical tool for diagnosing MCI patients.

Keywords: functional near-infrared spectroscopy (fNIRS), mild cognitive impairment (MCI), linear discriminant analysis (LDA), convolutional neural network (CNN), neural degeneration

OPEN ACCESS

Edited by:
Chang-Hwan Im,
Hanyang University, South Korea

Reviewed by:
Hendrik Santosa,
University of Pittsburgh, United States
Yingchun Zhang,
University of Houston, United States

****Correspondence:***
Keum-Shik Hong
kshong@pusan.ac.kr

Specialty section:
This article was submitted to Health, a section of the journal Frontiers in Human Neuroscience

Received: *08 May 2019*
Accepted: *26 August 2019*
Published: *06 September 2019*

Citation:
Yang D, Hong K-S, Yoo S-H and Kim C-S (2019) Evaluation of Neural Degeneration Biomarkers in the Prefrontal Cortex for Early Identification of Patients With Mild Cognitive Impairment: An fNIRS Study. Front. Hum. Neurosci. 13:317. doi: 10.3389/fnhum.2019.00317

INTRODUCTION

Alzheimer's disease (AD) is a degenerative brain disorder of unknown etiology, a common form of dementia, which begins in middle-aged or older adults (Ieracitano et al., 2018). AD results in progressive memory loss, thinking impairment, disorientation, changes in personality and mood (Niu et al., 2013). In the final stages of AD, people lose the ability to communicate or respond to their environment. They need assistance in all their activities of daily living, and they may even lose their ability to swallow. As reported via the Alzheimer's Association, by 2050 one new case of AD is expected to develop every 33 s resulting in nearly 1 million new cases per year (Alzheimer's Association, 2018). In addition, in 2017, more than 16 million family members and other unpaid caregivers, a contribution valued at more than $232 billion, were devoting toward the care of Alzheimer's patients. Such findings highlight the requirement for solutions to prevent dementia-related costs from jeopardizing the health and financial security of the families of people with Alzheimer's related diseases.

However, there is a relative mild condition of cognitive impairment before the onset of AD, known as mild cognitive impairment (MCI), a stage at which treatment can reduce the chance for developing to AD (Yeung et al., 2016b; Fang et al., 2018; Valenzuela et al., 2018). MCI patients are divided into two categories; amnestic and non-amnestic. In the case of amnestic MCI patients, the memory is affected primarily. For the case of non-amnestic MCI, the patients have difficulty with thought process such as planning and completing complex tasks such as balancing a checkbook or making a judgment in a risky situation (Marmarelis et al., 2017). There are various methods to diagnose an MCI patient. Primarily, the diagnosis in a clinic relies on the patient's medical history and clinical rating scores, such as clinical dementia rate or Mini-Mental State Examination (MMSE) (Li R. et al., 2018). However, it is known that the MMSE performance is influenced by education and age, and the clinical evaluation and diagnosis through MMSE requires an experienced clinician (Nguyen et al., 2008). To cope with these issues, the biomedical examination methods using brain signals have been introduced, such as the transcranial Doppler ultrasonography (Keage et al., 2012), functional near-infrared spectroscopy (fNIRS) (Vermeij et al., 2017), functional magnetic resonance imaging (fMRI) (Khazaee et al., 2017; Katzorke et al., 2018), and positron emission tomography (Beishon et al., 2017). fNIRS is a relatively new optical imaging technology that uses light in the near infrared range to monitor the hemodynamic responses non-invasively: A neural firing increases blood flow in the neighboring capillary network, and fNIRS measures the concentration changes of the oxyhemoglobin (ΔHbO) and deoxyhemoglobin (ΔHbR) in the cerebral cortex (Boas et al., 2014; Hong et al., 2014; Zafar and Hong, 2018). fNIRS is known for its portability, non-invasiveness, low cost, and high temporal resolution (compared with fMRI) (Ferrari and Quaresima, 2012; Hong and Santosa, 2016; Pinti et al., 2018). Recently, the possibility of improving the spatial and temporal resolutions using a bundled-optodes configuration and the initial dip was demonstrated in the process of brain-computer-interfaces (Nguyen and Hong, 2016; Zafar and Hong, 2017; Hong and Zafar, 2018). Therefore, fNIRS has distinct advantages over other modalities (Ghafoor et al., 2017; Yap et al., 2017).

The difficulty in diagnosing the causes of diseases has a severe frustration on patients if they do not receive an appropriate care in a timely manner. Therefore, robust and sensitive biomarkers for a prompt monitoring of cognitive or biological changes between healthy elderly and MCI patients is required (Nestor et al., 2004). A number of studies have examined the feasibility of using fNIRS to diagnose MCI and other types of dementia using different biomarkers (Niu et al., 2013; Katzorke et al., 2017, 2018; Perpetuini et al., 2017; Vermeij et al., 2017; Yap et al., 2017; Halliday et al., 2018; Stuart et al., 2018). Appropriate biomarkers may provide a reliable diagnosis for patients with MCI before the onset of AD. **Table 1** lists the existing biomarkers examined in the previous fNIRS studies.

As shown in **Table 1**, there are a number of studies that have applied different mental tasks in various brain regions to assess meaningful biomarkers. Li R. et al. (2018) asked the subjects to perform a cognitive task (digit verbal span task) while brain signals were measured from the frontal and bilateral lobes. The results showed that the mean value of ΔHbO (i.e., MHbO) and the slope of ΔHbO (i.e., SHbO) were higher in healthy control (HC) than the MCI group during the time window of 3–12 s. Katzorke et al. (2018) also evaluated the biomarker of MHbO and the mean value of ΔHbR (i.e., MHbR) when the subjects performed a verbal fluency task (VFT). A slight decrease in the hemodynamic response was observed in the inferior frontotemporal cortex in the MCI group. Some of the studies have employed a quantitative analysis of multiscale entropy: The results demonstrated that the resting-state brain signal complexity was decreased in the MCI group (Perpetuini et al., 2017; Li X. et al., 2018). Yap et al. (2017) employed biomarkers such as active channels, MHbO, time response of ΔHbO to reach the peak, and SHbO for detecting a patient with MCI or AD. The results illustrated that MCI exhibited a greater mean activation (than AD and HC) for both the right and left prefrontal cortex (PFC) when the subjects performed VFT (see **Figure 5B**). The results using the time to reach the peak and SHbO presented a meaningful difference between the left and right PFC (see **Figures 5C,D**). The biomarker of using activated channels did not show a significant difference among various brain regions. The authors also claimed that the difference in the hemoglobin responses in the left and right PFC was caused by neural compensation, and that the capacity for such neural compensation was inversely proportional to the severity of neurodegeneration (Price and Friston, 2002). **Figure 1** summarizes the existing biomarkers, categories of mental tasks, and brain regions that have been used in the fNIRS studies for diagnosing the patients with MCI.

Even there exist a number of biomarkers in the fNIRS area as in **Table 1**. Most of the studies prefer to conduct the statistical analysis for seeking the group difference between the MCI and HC. However, the high standard deviations (SD) illustrate that the method of using statistical analysis is not useful in establishing a confident diagnosis of individual patients for clinical purposes (Labaer, 2005). To the best of authors' knowledge, there is no result on the evaluation the existing biomarkers, brain

TABLE 1 | List of fNIRS biomarkers, mental tasks, and brain regions used in various studies.

No.	Author (Year)	Biomarkers	Mental Task	Brain Region
1	Li R. et al., 2018	Mean, Slope of ΔHbO	Digital verbal span	Frontal and bilateral parietal
2	Jung et al., 2018	Clinical assessment	Working memory	Prefrontal
3	Katzorke et al., 2018	Mean ΔHbO	Verbal fluency	Prefrontal
4	Li X. et al., 2018	Multi-scale entropy	Resting state	All scalp
5	Perpetuini et al., 2017	Entropy	Working memory	Prefrontal
6	Yap et al., 2017	No. active chs., Mean, Slope, Peak time	Verbal fluency	Prefrontal
7	Katzorke et al., 2017	Mean ΔHbO	Verbal fluency	Inferior frontal
8	Vermeij et al., 2017	Mean ΔHbO, Mean ΔHbR	Working memory	Prefrontal
9	Marmarelis et al., 2017	Cerebral autoregulation	Resting state	Prefrontal
10	Uemura et al., 2016	Mean ΔHbO	Memory retrieval	Prefrontal
11	Yeung et al., 2016b	Mean ΔHbO	Working memory	Frontal and temporal
12	Yeung et al., 2016a	Mean ΔHbO of active channels	Category fluency	Prefrontal
13	Haworth et al., 2016	Reaction time	Trail making	None
14	Heinzel et al., 2013	Mean ΔHbO	Verbal fluency	Frontal and bilateral parietal
15	Doi et al., 2015	Mean ΔHbO	Dual-task walking	Prefrontal
16	Niu et al., 2013	Mean and *t*-map of ΔHbO	Working memory	Frontal and Temporal
17	Arai et al., 2006	Mean ΔHbO	Verbal fluency	Frontal and bilateral parietal

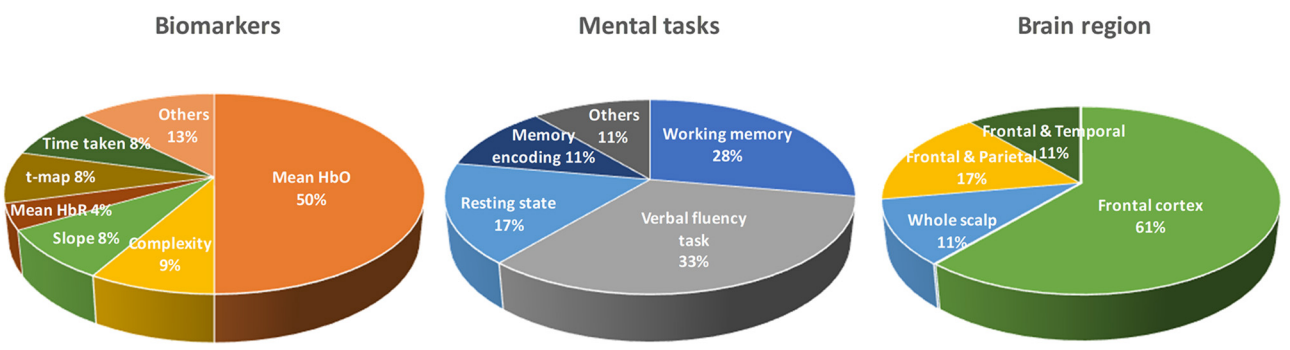

FIGURE 1 | Summary of widely used biomarkers, categories of mental tasks, and brain regions used in various fNIRS studies for diagnosing of MCI patients (the total number of fNIRS articles was 17).

regions, and time durations. Cotelli et al. (2008) and Park and Reuter-Lorenz (2009) suggested the right PFC as one of the functional compensatory regions in cognitively impaired individuals. Additionally, the selection of a proper biomarker will directly influence the results on classification and diagnosis of the disease. Therefore, the evaluation of the digital biomarkers, brain regions, and time intervals in obtaining biomarkers is necessary, and it would become a reference for the future research.

In this study, we investigate 15 digital biomarkers and 2 image biomarkers generated from the fNIRS hemodynamic responses for 15 MCI patients and 9 HC. The digital biomarkers take the form of mean, slope, peak, skewness, and kurtosis for a certain interval of time, and the two image biomarkers include *t*-map and correlation map. Finally, a conclusive result suggesting how to combine a biomarker and a classification method will be demonstrated, which turns out to be the combination of *t*-map and CNN classification. In the study, the used headset in **Figure 2** covers the entire PFC (i.e., left PFC, middle PFC, and right PFC) making 204 channels. However, only 48 channels with sufficient emitter-detector distances (3 cm) are utilized. The performed three mental tasks include the *N*-back task, Stroop task, and VFT.

MATERIALS AND METHODS

Participants

Twenty-four volunteers, who were right-handed and were able to communicate in Korean, were chosen for this study, comprising of fifteen patients with MCI (1 male and 14 females) and nine HC (2 males and 7 females) of similar age and educational background. MCI patients were recruited from the Pusan National University Hospital, Busan, Republic of Korea. The HC were selected from the local community on a voluntary basis. In addition, the mental state of each subject was examined using a Korean-Mini-Mental State Examination (K-MMSE), which is a 30-points questionnaire providing a quantitative measure of cognitive impairment (Han et al., 2008). The demographic information for all the volunteers including age (mean ± SD), gender, education background (mean ± SD),

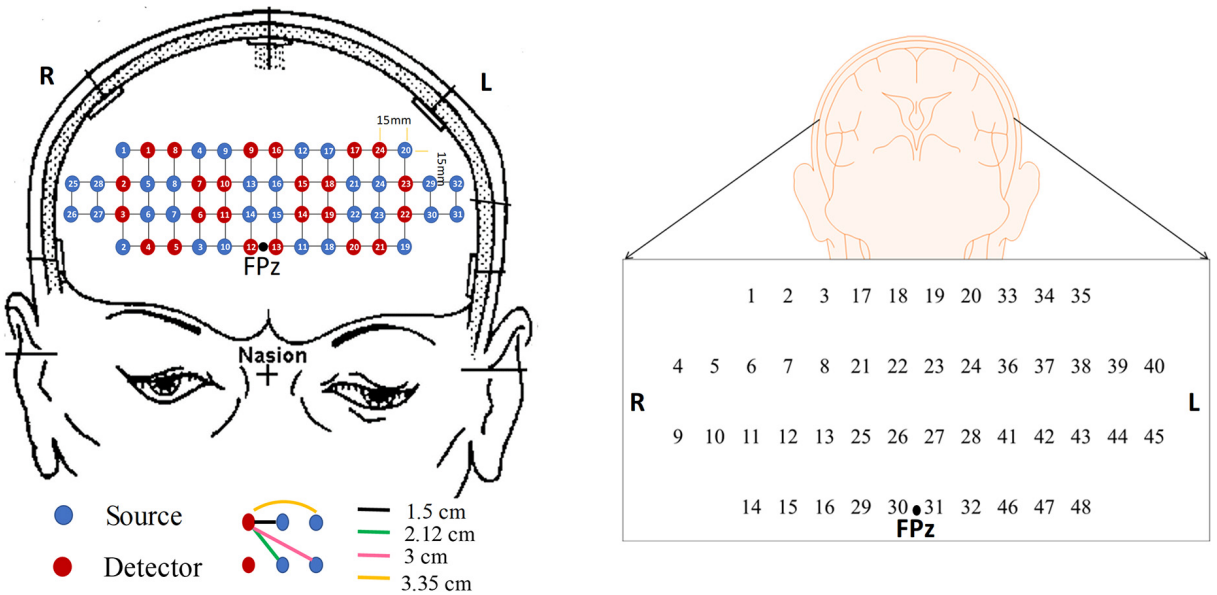

FIGURE 2 | The configuration of the headset employed during the experiment, which consists of 24 emitters and 32 detectors **(left)** and the channels used in this paper **(right)**.

K-MMSE scores (mean ± SD), and statistical information are summarized in **Table 2**. This experiment was conducted in accordance with the latest Declaration of Helsinki upon the approval of the Pusan National University Institutional Review Board (General Assembly of the World Medical Association, 2014). All volunteers were given a detailed description of the experimental procedure prior to the beginning of the experiment, and they provided written consent agreeing to the experiments.

Channel Configuration

In this study, a near-infrared multi-channel continuous wave system (NIRSIT, OBELAB Inc., Rep. of Korea) with 8.138 Hz sampling rate was employed to measure the brain signals via 24 emitters and 32 detectors. The device has an active detection sensor with a total capacity of 204 channels out of which 48 channels were used in this study, which covered the entire PFC area. Channel 1 to channel 16 were placed in the right PFC, channel 17 to channel 32 in the middle PFC, and channel 33 to channel 48 in the left PFC. **Figure 2** shows the locations of emitters and detectors with a reference point FPz (left) and the 48 channels in this study (right). The wavelengths used for detecting two chromophores (HbO, HbR) were 780 and 850 nm, respectively. As reported in Strangman et al. (2013), fNIRS is more sensitive to the gray matter and even a large source detector separation (up to ∼4.5 cm) can be used. Considering the spatial resolution and the differential path length factors into account, the pairs having the source detector distance of 3 cm were used.

TABLE 2 | The demographic information of all participants.

Characteristics	MCI (*n* = 15)	HC (*n* = 9)	*p*-value
Gender (Male/Female)	1/14	2/7	0.44
Education [years]	11.2 (±4.81)	10.56 (±2.88)	0.36
Age [years]	69.27 (±7.09)	68.33 (±4.69)	0.36
K-MMSE Score	25.13 (±2.33)	27.22 (±1.98)	0.49

K-MMSE, Korea Mini-Mental State Examination.

Experimental Paradigm

Participants seated on a comfortable chair and were instructed to avoid movement as much as possible. First, all subjects took a 10 min resting state. Subjects in each group participated in three sessions, which consisted of the *N*-back task, Stroop task, and semantic VFT. Each task took 60 s and was performed three times with a 30 s rest between tasks. **Figure 3** illustrates the experimental paradigm for all three tasks. The *N*-back task evaluates the working memory (Kane et al., 2007) and, in our study, a two-back task was performed and one-digit numbers between 1–9 were displayed on the monitor. The subjects were asked to press the keyboard when the current number on the display matched the second-last number displayed before. The Stroop test is a measurement of widely used executive function and is known as a measurement of mental control and response flexibility. The Stroop task requires new reactions while suppressing the dominant response, such as letter reading conditions and color reading conditions, etc. In this study, the Korean-Color Word Stroop test (K-CWST) was used. The subjects were requested to read the color of letters when letters were written in red, blue, yellow, and black colors within a limited time (Byeon et al., 2017). The semantic VFT is a task to generate as many words (related to the given semantic category) as possible within a limited time (Whiteside et al., 2016). The task measures how much information can be retrieved from the categorization and memory repository of text for 1 min.

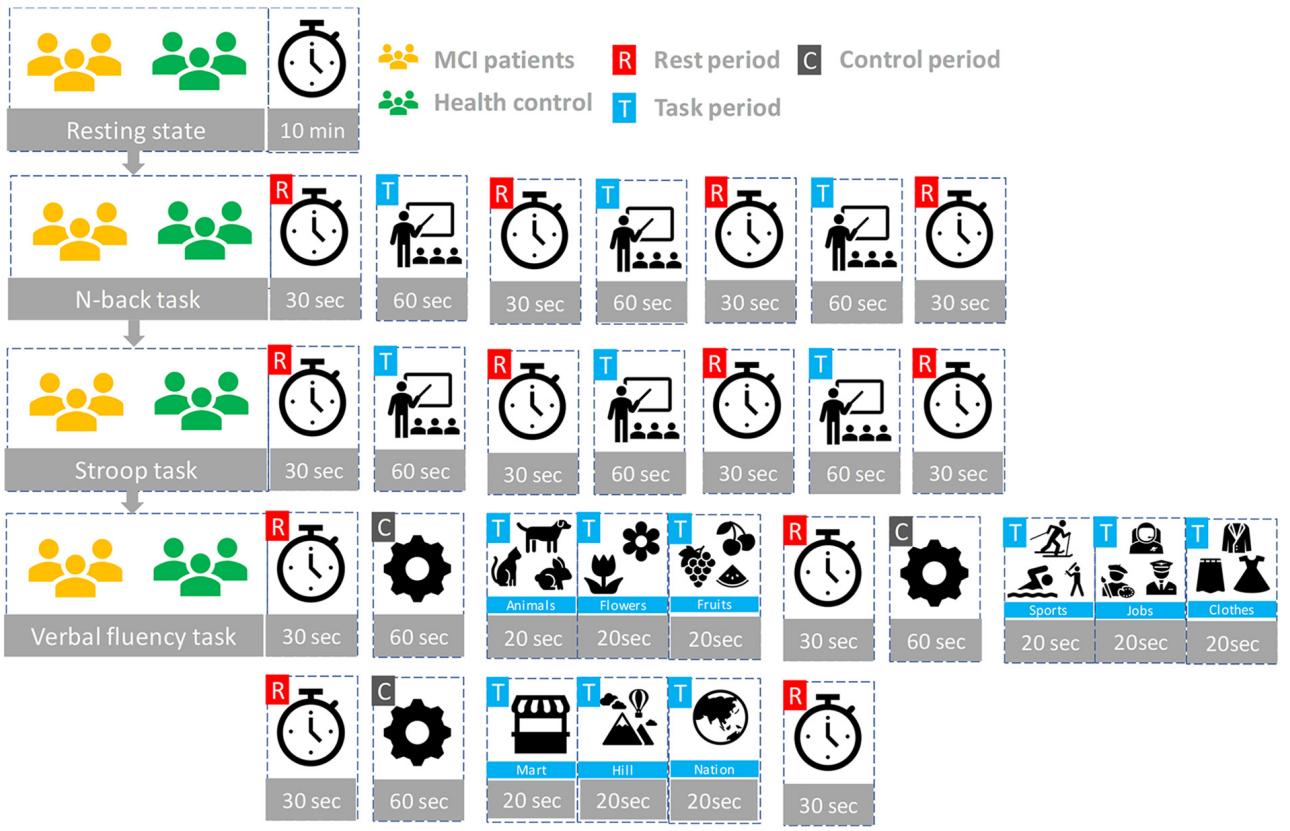

FIGURE 3 | The experiment paradigms: Three tasks (*N*-back, Stroop, and verbal fluency) having three trials.

Data Pre-processing

The fNIRS data were pre-processed and analyzed for each subject using MATLAB^{TM}. The optical intensity signals were first transformed into the time series of HbO and HbR concentration changes using the modified Beer-Lambert law (MBLL) (Sassaroli and Fantini, 2004). The data were digitally bandpass-filtered to remove the physiological noises (respiration, cardiac activity, and low-frequency drift signals): For this, two fourth-order Butterworth filters (low and high-pass) with cutoff frequencies of 0.1 and 0.001 Hz, respectively, were used to filter off the noises from the converted hemodynamic signals (Khan and Hong, 2015, 2017). In this study, we analyzed both ΔHbO and ΔHbR signals for the evaluation of biomarkers, even though HbO signals are robust and more sensitive.

The previous comparison study between MCI and HC investigated by Li R. et al. (2018) indicated that utilizing the region of interest (ROI) strategy could provide the satisfying results with the averaged means and slope changes of ΔHbO. In this study, we implemented two strategies to identify the ROI; (i) *t*-value analysis and (ii) visual inspection (Privitera and Stark, 2000). In the first case, the active channels (i.e., $t > 1.6469$ and p-value < 0.05) were selected by using the MATLAB^{TM} function (*robustfit*), which becomes the ROI. In the second case, all the HbO signals were inspected visually, and those signals having the desired pattern were selected manually (i.e., visual inspection).

Feature Extraction

Diverse biomarkers were evaluated, as a possible candidate, for an early identification of MCI. The considered digital biomarkers include the MHbO, SHbO, MHbR, SHbR, time to peak in the hemodynamic response, skewness, and kurtosis. In addition. we considered two image biomarkers: The *t*-map of all the channels and the correlation map of all the channels.

Digital Biomarkers

The HbO mean value change between the rest and task periods is represented as follows.

$$MHbO = \frac{Avg(\Delta HbO_{t=t_1:t_2}) - Avg(\Delta HbO_{t=-10:0})}{Avg(\Delta HbO_{t=-10:0})} \quad (1)$$

where t_1 and t_2 are the starting and ending time in the selected time window, $t = -10$ indicates 10 s before the onset time, and $t = 0$ is the onset time of the task execution. The mean change of HbR concentration is computed as follows.

$$MHbR = \frac{Avg(\Delta HbR_{t=t_1:t_2}) - Avg(\Delta HbR_{t=-10:0})}{Avg(\Delta HbR_{t=-10:0})} \quad (2)$$

We employed the *polyfit* function in MATLAB^{TM} to calculate the slope of HbO (i.e., SHbO) and the slope of HbR change (i.e., SHbR). The location of the peak, skewness, and kurtosis

were conducted by using MATLAB^{TM} functions of *findpeaks*, *skewness*, and *kurtosis*, respectively.

Activation Map (*t*-Map)

To quantify cortical hemodynamic activities during the mental tasks, the general linear model (GLM, a model-based statistical analysis tool) was utilized (Pinti et al., 2017; Salis-Perales and Barajas-Ramirz, 2017). In GLM, the desired hemodynamic response function (dHRF) is used to serve as a reference to estimate the changes in HbO signals (Yennu et al., 2016). The formula is as follows:

$$z(t) = \beta f(t) + \varepsilon \tag{3}$$

$$f(t) = h(t) \otimes s(t) \tag{4}$$

where $z(t)$ represents the temporal profile of the measured ΔHbO or ΔHbR, β is the estimated amplitude of ΔHbO/ΔHbR, and ε represents the residual owing to the difference between the measured signals and the predicted model. $f(t)$ is the stimulation-specific predicated response, which is expected to match the temporal profiles of the measured hemodynamic signal (i.e., dHRF); $h(t)$ represent the canonical hemodynamic response function, and $s(t)$ is the stimulation-specific boxcar function for a given task. Thus, after fitting equation (3), a statistical t-value representing a statistical significance of the brain activation with respect to the baseline at each respective channel was obtained. Moreover, the t-values were derived from *robustfit* for individual channels and were used to generate the t-map for a topographic image (Liu and Hong, 2017).

Channel-by-Channel Correlation Map

Comparing to fMRI, fNIRS has a significant advantage in temporal resolution. This advantage could provide convenience for investigating the functional connectivity of the prefrontal lobe by exploiting the temporal correlations channel by channel (Tak and Ye, 2014). The correlation map was calculated by using the MATLAB^{TM} correlation function (*corr*).

Classification

In this study, the digital biomarkers were classified using the linear discriminant analysis (LDA) (Naseer et al., 2016) available as *classify* function in MATLAB^{TM}. The tenfold cross validation method was used to estimate the classification performance of the predictive LDA model. The sample size in analyzing each digital biomarker becomes the number of subjects $\times$ the number of trials $\times$ the number channels in the ROI. The convolutional neural network (CNN) was utilized to conduct the classification of image biomarkers. CNN is highly capable of learning appropriate features automatically from the input data by optimizing the weight parameters in individual layer by using forward and backward propagation to minimize classification errors (Ding et al., 2017; Hamadache and Lee, 2017; Kim et al., 2017; Moon et al., 2018; Trakoolwilaiwan et al., 2019). The networks in this paper consist of four layers, including two convolutional layers and two fully connected layers. In the convolutional layers, a convolutional filter whose width is equal to the dimension of the input, and the kernel size of h is convolved with the input data, where the output of the i'th filter is represented as follows.

$$output_i = w \cdot x[i : i + h - 1] \tag{5}$$

$$f(output_i) = ReLU(output_i) \tag{6}$$

$$ReLU(x) = Max(o, x) \tag{7}$$

where w is the weights of the matrix and $x[i{:}j]$ is the submatrix of the input from row i to j. Then the output of the first convolutional layer f (*output*) is converted by an activation function Re$LU(x)$ to build the feature map. To enhance the performance, additional subsampling operation, max-pooling, and dropout (avoiding overfitting) are employed in this subsampling layer. To obtain an appropriate predictive model, the hyper-parameters such as the learning rate, batch size, and the number of epochs should be considered. In our study, the size of input data was 48 $\times$ 48. To maintain the original feature completely, we set up the batch size by 4. The grid search (Ou et al., 2019) and Adam optimization algorithm (β_1 = 0.9, β_2 = 0.1, and $\varepsilon = 10^{-8}$; Tang et al., 2019) were utilized to choose the learning rate and the parameters in gradient descent optimization.

RESULTS

Comparison of Hemodynamic Responses

Figure 4 shows the hemodynamic responses of ΔHbO from three brain regions (i.e., right, middle, and left PFC) of MCI patients and HC for three mental tasks (i.e., *N*-back task, Stroop task, and VFT). The purpose behind this strategy is to observe any visual differences between the MCI patients and HC. The figures plot the average HbOs of individual groups. MCI Patients are denoted by red color, whereas the corresponding SDs are shown with red shadows. HC are marked with blue color with its respective shadow in blue showing the SD. In the left brain region, the averaged concentration change of HbO for HC group is higher than that of MCI group in all three mental tasks. In addition, HC shows an earlier increase than MCI patients. But the middle and right PFCs do not show such a significant difference between two groups. The plots reveal that the brain regions have unique patterns of ΔHbO fluctuations. However, the averaged hemodynamic responses cannot tell the existence of improvement in cognition for the MCI patients, since their SDs were too large. Thus, the examination of the hemodynamic responses of ΔHbO is not sufficient to distinguish an individual from MCI or HC group. This leads us to the second technique, in which we will evaluate the digital biomarkers at using appropriate time intervals for statistical analysis.

Statistical Analysis of Digital Biomarkers

To evaluate the digital biomarkers such as MHbO/MHbR, SHbO/SHbR, peak location, skewness, and kurtosis for the hemodynamic responses, we divided the PFC into three areas (i.e., left, middle and right PFC) and applied different time

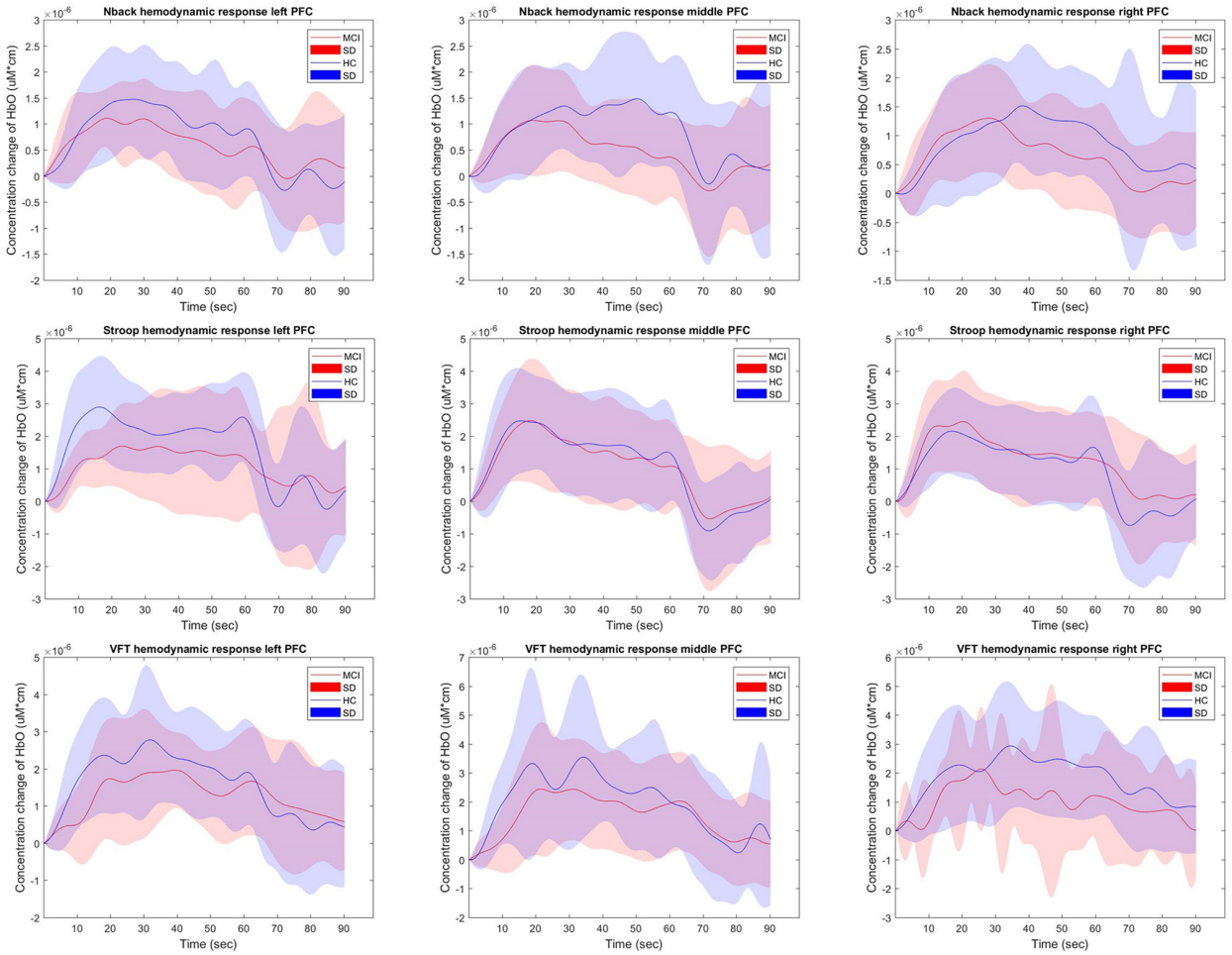

FIGURE 4 | The average HbOs in three brain regions (**left, middle,** and **right** PFCs) of MCI patients and HC after performing three mental tasks.

intervals for three mental tasks (i.e., *N*-back, Stroop and VFT), respectively. The statistical values of all the biomarkers obtained from the ROI channels ($t > 1.6469$) for three mental tasks are shown in **Tables 3–5**. **Tables 6–8** present the statistical information of the biomarkers obtained from those channels selected by visual inspection. In this study, the task duration was set to 60 s. This is to see where the MCI patients can focus on the verbal fluency task for a somewhat long time period of time. Also, for comparison purposes, the task durations for *N*-back and Stroop tasks were to 60 s as well. The reason, why we considered the time period between 5 and 65 s, was due to the time delay (3–5 s) of the hemodynamic response (Naseer and Hong, 2015). The time interval of 5–25 s was selected since the initial peak time for hemodynamic response is nearly located in the first 20 s period. The slope features (i.e., SHbO/SHbR) were considered from three intervals of the hemodynamic response: First, the initial increasing interval of ΔHbO (i.e., from 5 to 15 s), the plateau period of ΔHbO during the task (i.e., from 20 to 60 s), and the final decreasing interval of ΔHbO (i.e., from 60 to 70 s). We expect that the MCI patients would have a light decline of ΔHbO during the second interval while performing the mental tasks if they cannot focus on the tasks, as seen in **Figure 4**. The time to peak (i.e., from 0 to the peak time) is to see when the peak value of the hemodynamic response occurs owing to the provided stimulation. Lastly, two biomarkers, skewness (from 5 to 65 s) and kurtosis (from 5 to 65 s) are to examine whether the overall profile of the hemodynamic responses of a MCI patient is different from that of HC. The entire biomarkers are summarized as follows.

Biomarker 1: MHbO in the interval of 5∼65 s
Biomarker 2: MHbR in the interval of 5∼65 s
Biomarker 3: MHbO in the interval of 5∼25 s
Biomarker 4: MHbR in the interval of 5∼25 s
Biomarker 5: MHbO in the interval of 0 – Peak
Biomarker 6: SHbO from 5 to 15 s
Biomarker 7: SHbR from 5 to 15 s
Biomarker 8: SHbO from 20 to 60 s
Biomarker 9: SHbR from 20 to 60 s
Biomarker 10: SHbO from 60 to 70 s
Biomarker 11: SHbR from 60 to 70 s
Biomarker 12: SHbO from 0 to the peak
Biomarker 13: Peak time of ΔHbO

TABLE 3 | Statistical data of *N*-back task (based upon ROI channels).

Biomarkers		Left PFC			Middle PFC			Right PFC		
		Avg.	***SD***	***p*-value**	**Avg.**	***SD***	***p*-value**	**Avg.**	***SD***	***p*-value**
MHbO (5–65 s)	MCI	7.35e−07	4.80e−06	0.1511	1.29e−07	2.61e−06	0.3811	7.88e−07	2.92e−06	**0.0211**
	HC	4.37e−07	2.05e−06		8.25e−08	1.11e−06		4.59e−07	1.08e−06	
MHbR (5–65 s)	MCI	−2.56e−08	8.90e−07	0.6407	−6.60e−08	3.55e−07	0.9996	−1.69e−08	9.69e−07	0.0868
	HC	−1.18e−08	3.96e−07		−1.08e−08	2.00e−07		−7.02e−08	3.12e−07	
MHbO (5–25 s)	MCI	7.24e−07	3.67e−06	0.4381	3.01e−07	2.45e−06	0.4697	7.65e−07	2.91e−06	0.0491
	HC	6.87e−07	1.89e−06		2.90e−07	1.01e−06		5.06e−07	8.85e−07	
MHbR (5–25 s)	MCI	2.14e−08	1.33e−06	0.1062	−4.67e−08	5.53e−07	0.9690	8.33e−08	1.56e−06	**0.0148**
	HC	−5.17e−08	6.46e−07		5.10e−09	3.85e−07		−5.56e−08	5.39e−07	
MHbO (0–Peak seconds)	MCI	4.36e−07	5.61e−06	0.7752	2.32e−07	2.16e−06	0.6413	5.54e−07	2.41e−06	0.1252
	HC	5.61e−07	1.76e−06		2.75e−07	7.42e−07		4.08e−07	6.28e−07	
SHbO (5–15 s)	MCI	8.03e−09	6.11e−08	0.1840	2.33e−09	2.18e−08	0.6180	8.16e−09	4.52e−08	0.0283
	HC	4.55e−09	3.11e−08		2.77e−09	1.30e−08		3.50e−09	1.42e−08	
SHbR (5–15 s)	MCI	−1.09e−09	3.88e−08	0.3311	−2.43e−10	1.30e−08	0.3528	1.33e−09	4.40e−08	0.1437
	HC	−1.91e−09	2.49e−08		−4.61e−10	6.51e−09		−5.00e−10	1.06e−08	
SHbO (20–60 s)	MCI	−1.63e−09	1.46e−08	0.3163	−1.44e−09	3.51e−09	0.4562	−1.35e−09	1.28e−08	0.8269
	HC	−2.07e−09	7.31e−09		−1.20e−09	3.74e−09		−6.80e−10	4.88e−09	
SHbR (20–60 s)	MCI	4.29e−10	1.11e−08	0.4641	1.32e−10	2.45e−09	0.2921	−3.01e−10	1.24e−08	0.7714
	HC	3.88e−10	3.84e−09		1.22e−11	4.13e−09		7.21e−11	3.94e−09	
SHbO (60–70 s)	MCI	−1.68e−08	1.07e−07	0.4975	−1.13e−08	2.57e−08	0.0842	−1.84e−08	6.49e−08	0.8426
	HC	−1.69e−08	3.62e−08		−1.39e−08	1.96e−08		−1.49e−08	2.29e−08	
SHbR (60–70 s)	MCI	1.50e−09	8.36e−08	0.3460	2.44e−09	2.96e−08	0.0605	−6.23e−10	6.01e−08	0.7577
	HC	5.73e−11	3.96e−08		1.81e−10	1.97e−08		1.13e−09	2.31e−08	
SHbO (0–Peak seconds)	MCI	1.81e−08	6.91e−08	0.2161	8.80e−09	2.65e−08	0.0842	1.97e−08	5.82e−08	**0.0011**
	HC	1.46e−08	3.75e−08		9.16e−09	1.58e−08		1.03e−08	1.51e−08	
Peak time (seconds)	MCI	1.50e+01	5.62e+00	0.8265	1.47e+01	4.93e+00	**0.0245**	1.56e+01	5.36e+00	0.1738
	HC	1.51e+01	5.36e+00		1.38e+01	5.53e+00		1.50e+01	5.36e+00	
Skewness	MCI	−8.02e−02	6.42e−01	0.3731	−1.05e−01	6.65e−01	0.5418	−1.66e−01	6.45e−01	**0.0015**
	HC	−1.01e−01	7.61e−01		−9.73e−02	8.99e−01		−3.52e−01	8.40e−01	
Kurtosis	MCI	2.26e+00	9.64e−01	0.4155	2.18e+00	8.96e−01	0.5462	2.19e+00	7.74e−01	0.9987
	HC	2.33e+00	9.81e−01		2.23e+00	8.77e−01		2.40e+00	8.70e−01	

Biomarker 14: Skewness of ΔHbO for the duration of 5 – 65 s
Biomarker 15: Kurtosis of ΔHbO for the duration of 5 – 65 s

This study employed two-sample independent *t*-test to conduct the statistical analysis with the significance level of 0.05. The *p*-value lower than 0.05 indicates the existence of significance difference between two groups. As demonstrated in **Tables 3**–**8**, the biomarkers with *p*-value < 0.05 are considered as ones with significant differences between the MCI and HC groups, which are marked bold. The appearance of significant biomarkers was random. It is remarked that the obtained biomarkers were not repeated for all three tasks or brain regions. Only Biomarker 14 (skewness) revealed a significant difference for all three brain regions when performing the Stroop task in the case of ROI channels, see **Table 4**. Although a few biomarkers showed some difference (similarly to Section "Comparison of Hemodynamic Responses"), the group statistical analysis was difficult to permit a meaningful diagnostic result for the individuals. This leads to our third strategy, Section "Classification of Digital Biomarkers": Evaluating the individual classification accuracy using digital biomarkers for three mental tasks and different brain regions.

Classification of Digital Biomarkers

The selection of the time intervals for Biomarkers 1–15 has already been discussed in Section "Statistical Analysis of Digital Biomarkers." **Figure 5** depicts the entire classification accuracies between MCI and HC based upon ROI channels for (i) three mental tasks, (ii) three brain regions, and (iii) fifteen biomarkers. LDA was used as a classifier. On the other hand, for the channels manually selected, **Figure 6** shows the comparative data for **Figure 5**. In agreement with the previous results (Yap et al., 2017), ΔHbO shows better classification results compared to ΔHbR (see Biomarkers 1 and 2 of *N*-back and Stoop tasks in **Figures 5A,B**). Therefore, in the case of manually selected channels, the analysis of ΔHbR is omitted and only ΔHbO is focused. Surprisingly, Biomarker 1 in the middle PFC when channels were selected manually showed the higher classification result than the case of ROI channels. It is remarked that the biomarkers showing significant difference in **Tables 3**–**8** are not necessarily going to have the same satisfactory classification results with LDA: For instance, Biomarkers 6 and 10 showed a good classification results in **Table 6**, but it is not so in **Figure 6A**. Even though the best accuracy of 76.67% (i.e., Biomarker 11 of

TABLE 4 | Statistical data of Stroop task (based upon ROI channels).

Biomarkers		Left PFC			Middle PFC			Right PFC		
		Avg.	*SD*	*p*-value	Avg.	*SD*	*p*-value	Avg.	*SD*	*p*-value
MHbO (5–65 s)	MCI	8.43e−07	3.65e−06	0.5778	4.15e−07	2.44e−06	0.0644	9.03e−07	3.51e−06	0.3884
	HC	9.26e−07	4.72e−06		8.50e−07	2.43e−06		8.30e−07	2.78e−06	
MHbR (5–65 s)	MCI	3.96e−07	9.66e−07	0.9089	2.06e−07	4.42e−07	0.1575	3.98e−07	8.00e−07	0.1772
	HC	4.07e−07	9.07e−07		2.65e−07	4.45e−07		3.32e−07	6.49e−07	
MHbO (5–25 s)	MCI	1.05e−06	3.47e−06	0.6053	7.23e−07	2.41e−06	**0.0298**	1.21e−06	3.97e−06	0.1971
	HC	1.16e−06	4.89e−06		1.21e−06	2.15e−06		9.85e−07	2.39e−06	
MHbR (5–25 s)	MCI	2.49e−07	1.36e−06	0.7795	1.70e−07	5.45e−07	0.5652	2.90e−07	1.21e−06	0.1860
	HC	3.37e−07	1.05e−06		1.99e−07	4.88e−07		2.08e−07	6.92e−07	
MHbO (0–Peak seconds)	MCI	9.37e−07	2.99e−06	0.3400	5.44e−07	1.71e−06	**0.0057**	8.78e−07	3.13e−06	0.3101
	HC	8.00e−07	3.63e−06		9.78e−07	1.39e−06		7.80e−07	1.77e−06	
SHbO (5–15 s)	MCI	3.27e−09	5.52e−08	0.9798	6.83e−09	2.78e−08	0.0919	1.81e−08	9.39e−08	**0.0083**
	HC	1.16e−08	3.37e−08		4.03e−09	1.87e−08		6.03e−09	2.06e−08	
SHbR (5–15 s)	MCI	8.57e−09	4.05e−08	**0.0344**	1.98e−09	1.54e−08	0.1172	1.49e−08	9.84e−08	0.0192
	HC	3.10e−09	2.37e−08		−4.08e−10	1.70e−08		2.39e−09	1.51e−08	
SHbO (20–60 s)	MCI	−1.33e−09	9.82e−09	0.1610	−2.08e−09	6.75e−09	0.6976	−1.82e−09	1.71e−08	0.9298
	HC	2.04e−11	1.04e−08		−1.81e−09	4.44e−09		−4.28e−10	5.18e−09	
SHbR (20–60 s)	MCI	3.37e−10	8.87e−09	0.8996	−8.35e−11	2.48e−09	**0.0149**	5.42e−10	9.60e−09	0.2607
	HC	2.33e−10	7.89e−09		4.84e−10	2.46e−09		1.19e−10	4.00e−09	
SHbO (60–70 s)	MCI	−3.14e−08	1.01e−07	**0.0045**	−3.04e−08	7.63e−08	**0.0061**	−2.70e−08	9.68e−08	**0.0029**
	HC	−6.23e−08	1.32e−07		−5.83e−08	1.27e−07		−5.13e−08	1.10e−07	
SHbR (60–70 s)	MCI	−2.22e−08	7.17e−08	0.7094	−7.05e−09	1.71e−08	**0.0014**	−2.18e−08	6.91e−08	0.8339
	HC	−1.88e−08	5.78e−08		−1.40e−08	2.93e−08		−1.65e−08	4.36e−08	
SHbO (0–Peak seconds)	MCI	2.69e−08	7.96e−08	0.0859	1.37e−08	4.30e−08	0.9788	2.81e−08	7.13e−08	**0.0008**
	HC	1.87e−08	5.08e−08		2.08e−08	3.32e−08		1.48e−08	3.07e−08	
Peak time (seconds)	MCI	1.41e+01	5.80e+00	0.0775	1.51e+01	5.85e+00	0.9238	1.47e+01	5.60e+00	0.2485
	HC	1.50e+01	5.21e+00		1.52e+01	6.43e+00		1.52e+01	5.76e+00	
Skewness	MCI	−1.36e−01	8.97e−01	**0.0045**	−6.57e−02	8.64e−01	**0.0032**	−3.61e−02	8.88e−01	**0.0002**
	HC	−4.06e−01	1.14e+00		−3.53e−01	1.17e+00		−3.43e−01	1.13e+00	
Kurtosis	MCI	2.48e+00	1.06e+00	0.9423	2.48e+00	1.07e+00	0.6990	2.52e+00	1.17e+00	0.3557
	HC	2.67e+00	1.26e+00		2.44e+00	1.06e+00		2.43e+00	1.15e+00	

N-back task and Biomarker 10 of Stroop task) was achieved by using LDA, it is still considered low to be implemented for clinical applications. As previously mentioned, these 15 biomarkers were chosen based on the existing studies and our own experiences. But, the low classification result using LDA necessitates a further pursuit toward a reliable biomarker for MCI patients based on the hemodynamic response. We therefore consider using the whole or selected hemodynamic responses in combination with a machine learning method, CNN.

CNN Classification of Hemodynamic Responses

In this section, we investigate the CNN method for automatic learning of the useful features from the hemodynamic responses between MCI and HC. We regard that most of the valuable features appearing in the digital biomarkers are already contained in the non-linear feature form in the CNN model. As demonstrated in **Figure 7**, the CNN classification results trained by the concentration changes of the ΔHbO of the *N*-back task show approximately similar accuracies in the three brain regions (i.e., whole PFC: 64.21%, right PFC: 72.46%, and middle PFC 74.03%) except for the left PFC, which has the lowest accuracy than other regions. The classification accuracies with the Stroop task ranged from a minimum of 73.36% (right PFC) to a maximum of 75.77% (left PFC). In the VFT case, the middle PFC obtained a good classification accuracy (78.94%) in comparison to the whole PFC, left PFC, and right PFC. The classification accuracies were improved in comparison to the LDA results obtained by the digital biomarkers. Even the best accuracy in the case of CNN results trained by hemodynamic response was nearly 80% (i.e., 78.94% in **Figure 7C**), the potential to increase the accuracy still exists. To push the boundary for a better classification accuracy, we employ the *t*-map and the correlation map as biomarkers for classifying the MCI patients from HC.

CNN Classification Results of Imaging Biomarkers

The *t*-map and correlation map are widely used as an image biomarker in the field of fMRI. **Figure 8** shows the group averaged *t*-maps of three mental tasks. The numbers shown in **Figure 8** represent the channel numbers on the PFC. The top

TABLE 5 | Statistical data of VFT (based upon ROI channels).

Biomarkers		Left PFC			Middle PFC			Right PFC		
		Avg.	*SD*	*p*-value	Avg.	*SD*	*p*-value	Avg.	*SD*	*p*-value
MHbO (5–65 s)	MCI	9.54e−07	4.05e−06	0.7156	3.04e−06	3.04e−06	0.8332	1.34e−06	5.09e−06	0.6294
	HC	1.09e−06	2.06e−06		1.04e−06	2.39e−06		1.43e−06	2.09e−06	
MHbR (5–65 s)	MCI	3.52e−07	9.62e−07	**0.0032**	1.55e−07	4.80e−07	0.0907	3.10e−07	8.44e−07	**0.0000**
	HC	1.75e−07	3.74e−07		1.08e−07	2.45e−07		1.03e−07	2.39e−07	
MHbO (5–25 s)	MCI	9.27e−07	3.21e−06	0.8961	3.07e−06	3.07e−06	0.9405	1.29e−06	5.49e−06	0.6196
	HC	1.20e−06	2.37e−06		1.21e−06	2.49e−06		1.39e−06	1.85e−06	
MHbR (5–25 s)	MCI	2.65e−07	1.38e−06	0.5851	2.23e−07	8.54e−07	0.2009	3.34e−07	1.82e−06	0.1186
	HC	2.87e−07	7.17e−07		1.73e−07	3.87e−07		1.98e−07	5.84e−07	
MHbO (0–Peak seconds)	MCI	7.63e−07	2.59e−06	0.6852	2.63e−06	2.63e−06	0.7594	7.56e−07	4.85e−06	0.8759
	HC	8.44e−07	1.78e−06		8.40e−07	1.86e−06		1.06e−06	1.53e−06	
SHbO (5–15 s)	MCI	6.80e−09	1.04e−07	0.6619	5.04e−08	5.04e−08	0.9667	1.93e−08	1.25e−07	**0.0393**
	HC	9.12e−09	2.77e−08		1.12e−08	3.22e−08		7.43e−09	3.61e−08	
SHbR (5–15 s)	MCI	1.08e−08	5.56e−08	**0.0347**	3.82e−09	2.71e−08	0.2267	1.58e−09	1.09e−07	0.4574
	HC	3.37e−09	2.98e−08		2.37e−09	1.33e−08		8.90e−10	1.30e−08	
SHbO (20–60 s)	MCI	8.45e−10	1.26e−08	**0.0002**	1.12e−08	1.12e−08	0.4277	−1.08e−10	2.02e−08	0.1714
	HC	−1.92e−09	7.42e−09		−1.70e−09	4.83e−09		−1.15e−09	6.04e−09	
SHbR (20–60 s)	MCI	−1.42e−11	1.01e−08	0.0922	−5.89e−10	4.50e−09	0.1039	7.31e−10	1.47e−08	**0.044**
	HC	−9.76e−10	5.00e−09		−9.98e−10	2.24e−09		−8.23e−10	3.83e−09	
SHbO (60–70 s)	MCI	−1.65e−08	7.67e−08	0.8321	1.12e−08	4.82e−08	0.429	−2.18e−08	9.44e−08	0.6000
	HC	−1.22e−08	3.45e−08		−6.72e−09	3.22e−08		−2.04e−08	4.50e−08	
SHbR (60–70 s)	MCI	−1.75e−08	6.75e−08	0.9888	−2.68e−09	1.46e−08	0.1605	−1.01e−08	8.96e−08	0.8797
	HC	−7.53e−09	2.23e−08		−4.73e−09	1.42e−08		−3.83e−09	1.46e−08	
SHbO (0–Peak seconds)	MCI	2.41e−08	7.05e−08	0.1679	4.82e−08	3.55e−08	0.9989	4.05e−08	1.25e−07	**0.0098**
	HC	2.02e−08	3.02e−08		2.34e−08	2.68e−08		2.44e−08	3.99e−08	
Peak time (seconds)	MCI	1.54e+01	5.55e+00	0.3332	5.68e+00	5.68e+00	**0.0051**	1.56e+01	5.20e+00	0.0624
	HC	1.50e+01	5.44e+00		1.40e+01	5.73e+00		1.47e+01	5.66e+00	
Skewness	MCI	−4.01e−02	6.38e−01	0.6858	6.97e−01	6.97e−01	0.9286	−7.38e−02	7.17e−01	0.2114
	HC	3.08e−02	6.86e−01		−2.59e−02	7.78e−01		−1.47e−01	7.29e−01	
Kurtosis	MCI	2.29e+00	9.39e−01	0.3276	2.28e+00	1.08e+00	0.4949	2.29e+00	1.02e+00	0.2745
	HC	2.36e+00	9.26e−01		2.28e+00	7.88e−01		2.25e+00	8.25e−01	

three figures in **Figure 8** (i.e., **A–C**) present the *t*-maps generated by MCI group with the *N*-back task, Stroop task, and VFT, respectively, and the lower three maps represent those of HC (i.e., **Figures 8D–F**). The results reveal that the activated regions between MCI patients and HC are different. **Figure 9**, portrays the correlation maps of three mental tasks for MCI (**Figures 9A–C**) and HC (**Figures 9D–F**). Finally, the CNN results trained by *t*-map and correlation map are compared in **Figure 10**. All the CNN results (accuracy) trained by both image biomarkers were higher than 82.05%, except for the VFT task and *t*-map (71.59%). Particularly, the CNN result trained by *t*-map with the *N*-back task showed a highest accuracy of 90.62%.

DISCUSSION

In this paper, our goal is to propose the best biomarker for diagnosing the MCI patients for clinical usage. For this, 15 digital biomarkers (5 means and 7 slopes of ΔHbO/ΔHbR, peak time, skewness, kurtosis), three PFC regions, and two image biomarkers (*t*-map, correlation map) were investigated for detecting neural degeneration in the MCI patients. This study also aims at developing a novel method for diagnosing the MCI patients from the elderly in their everyday environment using fNIRS. To the best of the authors' knowledge, this is the first work for evaluating the digital biomarkers in relation to MCI/AD with fNIRS. The obtained results can become a reference for utilizing appropriate biomarkers for neural information detection, and may provide a new tool to diagnose MCI patients in a harmless, non-invasive and portable manner.

(i) Statistical analysis and individual classification: In **Figure 4** and **Tables 3–8**, the existence of differences of hemodynamic responses between two groups (MCI, HC) is shown. Most biomarkers in **Tables 3–8** as well as the differences in HbOs in **Figure 4** reveal the existence. This is consistent with the former studies (Katzorke et al., 2017; Vermeij et al., 2017; Yap et al., 2017; Li R. et al., 2018). However, the LDA classification accuracies based up the biomarkers shown in **Figure 5** are too low for clinical applications. That means that the statistical analysis approach is not reliable for the detection of an MCI patient clinically. Beyond the current method, a new method

TABLE 6 | Statistical data of *N*-back task (manually selected channels).

Biomarkers		Left PFC			Middle PFC			Right PFC		
		Avg.	***SD***	***p*-value**	**Avg.**	***SD***	***p*-value**	**Avg.**	***SD***	***p*-value**
MHbO (5–65 s)	MCI	7.99e−07	6.54e−07	0.0827	6.44e−07	6.76e−07	**0.0108**	7.78e−07	5.65e−07	0.5999
	HC	1.05e−06	6.93e−07		9.70e−07	7.08e−07		8.35e−07	6.62e−07	
MHbO (5–25 s)	MCI	9.23e−07	6.23e−07	0.7490	8.25e−07	7.61e−07	0.2285	8.16e−07	5.81e−07	**0.0047**
	HC	1.03e−06	9.00e−07		7.03e−07	9.99e−07		4.85e−07	8.46e−07	
MHbO (0–Peak seconds)	MCI	6.62e−07	4.92e−07	0.9820	8.25e−07	5.20e−07	0.1477	4.94e−07	4.81e−07	**0.0056**
	HC	6.65e−07	7.56e−07		3.64e−07	8.60e−07		2.00e−07	6.65e−07	
SHbO (5–15 s)	MCI	5.94e−09	8.40e−09	**0.0025**	8.59e−09	1.20e−08	0.5788	1.06e−08	1.33e−08	0.7049
	HC	1.24e−08	1.04e−08		9.79e−09	1.15e−08		9.71e−09	1.29e−08	
SHbO (20–60 s)	MCI	−2.45e−09	2.58e−09	0.4853	−2.52e−09	3.58e−09	**0.0002**	−2.49e−09	3.82e−09	**0.0002**
	HC	−2.48e−09	4.16e−09		3.22e−10	4.40e−09		3.00e−10	4.41e−09	
SHbO (60–70 s)	MCI	−6.43e−09	1.41e−08	**0.0128**	−8.51e−09	1.75e−08	**0.0040**	−7.55e−09	1.46e−08	0.7138
	HC	−1.58e−08	1.90e−08		−1.83e−08	1.91e−08		−5.36e−09	2.86e−08	
SHbO (0–Peak seconds)	MCI	1.28e−08	1.09e−08	0.7124	1.29e−08	9.43e−09	0.4330	1.29e−08	8.34e−09	0.1379
	HC	1.20e−08	8.63e−09		1.15e−08	9.47e−09		1.04e−08	1.01e−08	
Peak time (seconds)	MCI	1.65e+01	5.07e+00	0.1711	1.62e+01	4.90e+00	0.5788	1.61e+01	5.16e+00	0.2327
	HC	1.79e+01	4.83e+00		1.66e+01	5.36e+00		1.72e+01	5.03e+00	
Skewness	MCI	−8.92e−02	6.39e−01	0.6745	−9.64e−02	6.60e−01	0.1374	−7.30e−02	6.90e−01	**0.0067**
	HC	−3.88e−02	4.93e−01		−2.95e−01	7.98e−01		−4.37e−01	7.91e−01	
Kurtosis	MCI	2.28e+00	9.35e−01	0.3903	2.26e+00	1.05e+00	**0.0121**	2.32e+00	8.19e−01	0.7654
	HC	2.46e+00	9.53e−01		2.73e+00	9.78e−01		2.44e+00	1.06e+00	

TABLE 7 | Statistical data of Stroop task (manually selected channels).

Biomarkers		Left PFC			Middle PFC			Right PFC		
		Avg.	***SD***	***p*-value**	**Avg.**	***SD***	***p*-value**	**Avg.**	***SD***	***p*-value**
MHbO (5–65 s)	MCI	1.40e−06	1.33e−06	**0.0129**	1.60e−06	1.39e−06	0.6469	1.68e−06	1.23e−06	0.5993
	HC	2.27e−06	1.29e−06		1.75e−06	1.44e−06		1.52e−06	1.24e−06	
MHbO (5–25 s)	MCI	1.27e−06	8.05e−07	0.9999	2.00e−06	1.50e−06	0.7069	2.10e−06	1.29e−06	0.2326
	HC	2.47e−06	1.42e−06		2.13e−06	1.48e−06		1.76e−06	1.10e−06	
MHbO (0–Peak seconds)	MCI	9.21e−07	6.42e−07	**0.0009**	1.42e−06	1.04e−06	0.7069	1.46e−06	9.74e−07	0.2140
	HC	1.67e−06	1.01e−06		1.51e−06	1.08e−06		1.20e−06	8.01e−07	
SHbO (5–15 s)	MCI	1.27e−08	1.38e−08	0.0555	2.13e−08	1.85e−08	0.9113	1.97e−08	1.75e−08	0.3121
	HC	1.99e−08	1.47e−08		2.09e−08	1.53e−08		1.81e−08	1.22e−08	
SHbO (20–60 s)	MCI	−9.36e−10	4.49e−09	0.3268	−3.66e−09	3.27e−09	0.1450	−3.00e−09	3.49e−09	0.9623
	HC	7.47e−11	3.22e−09		−2.64e−09	2.50e−09		−1.81e−09	2.25e−09	
SHbO (60–70 s)	MCI	−8.95e−09	2.01e−08	**0.0000**	−2.19e−08	3.76e−08	**0.0471**	−1.17e−08	1.82e−08	**0.0001**
	HC	−3.98e−08	1.74e−08		−3.27e−08	2.05e−08		−3.43e−08	2.62e−08	
SHbO (0–Peak seconds)	MCI	1.53e−08	9.22e−09	0.9999	2.26e−08	1.57e−08	0.8587	2.67e−08	1.83e−08	0.2631
	HC	3.29e−08	2.12e−08		2.78e−08	2.34e−08		2.23e−08	1.43e−08	
Peak time (seconds)	MCI	1.82e+01	6.33e+00	**0.0104**	1.71e+01	4.07e+00	0.6153	1.68e+01	5.41e+00	0.9528
	HC	1.50e+01	3.67e+00		1.76e+01	5.51e+00		1.68e+01	4.61e+00	
Skewness	MCI	−4.56e−01	7.31e−01	0.3755	−1.09e−01	9.53e−01	0.1087	−2.62e−01	9.96e−01	0.7460
	HC	−2.90e−01	7.03e−01		−4.49e−01	8.28e−01		−3.34e−01	9.03e−01	
Kurtosis	MCI	3.00e+00	1.32e+00	0.6991	2.53e+00	9.36e−01	0.6885	2.61e+00	1.11e+00	0.6029
	HC	3.14e+00	1.50e+00		2.63e+00	1.23e+00		2.47e+00	1.32e+00	

of using the averaged hemodynamic responses of MCI patients and HC should be investigated, for instance, adaptive estimation algorithms (Iqbal et al., 2018; Nguyen et al., 2018; Yazdani et al., 2018; Yi et al., 2018) or advanced signal processing (Chen et al., 2018; Hong et al., 2018a).

(ii) Better results in local PFCs: In the literature, Goh and Park (2009) proposed the scaffolding theory for aging and cognition. Similar results (Cabeza et al., 2002; Katzorke et al., 2018) also verified that a neural compensatory mechanism exists and an additional neural passageway is recruited to support the

TABLE 8 | Statistical data of VFT (manually selected channels).

Biomarkers		Left PFC			Middle PFC			Right PFC		
		Avg.	*SD*	*p*-value	Avg.	*SD*	*p*-value	Avg.	*SD*	*p*-value
MHbO (5–65 s)	MCI	1.56e−06	9.50e−07	**0.0371**	1.60e−06	1.39e−06	0.6469	1.24e−06	7.60e−07	1.0000
	HC	2.12e−06	1.06e−06		1.75e−06	1.44e−06		2.21e−06	1.59e−06	
MHbO (5–25 s)	MCI	1.09e−06	1.26e−06	**0.0004**	2.00e−06	1.50e−06	0.7069	1.18e−06	9.32e−07	0.9934
	HC	2.29e−06	1.23e−06		2.13e−06	1.48e−06		1.82e−06	1.62e−06	
MHbO (0–Peak seconds)	MCI	7.33e−07	8.93e−07	**0.0001**	1.42e−06	1.04e−06	0.7069	6.98e−07	5.18e−07	0.9993
	HC	1.79e−06	9.83e−07		1.51e−06	1.08e−06		1.24e−06	1.11e−06	
SHbO (5–15 s)	MCI	8.50e−09	1.99e−08	0.2225	2.13e−08	1.85e−08	0.9113	1.97e−08	2.29e−08	0.8179
	HC	1.41e−08	1.42e−08		2.09e−08	1.53e−08		1.84e−08	2.74e−08	
SHbO (20–60 s)	MCI	−7.78e−10	5.29e−09	0.1965	−3.66e−09	3.27e−09	0.1450	−3.39e−09	7.52e−09	0.9903
	HC	−2.42e−09	4.26e−09		−2.64e−09	2.50e−09		−9.40e−11	5.40e−09	
SHbO (60–70 s)	MCI	−4.39e−09	2.14e−08	0.0597	−2.19e−08	3.76e−08	**0.0471**	−6.18e−09	1.40e−08	**0.0126**
	HC	−1.37e−08	1.49e−08		−3.27e−08	2.05e−08		−1.45e−08	1.73e−08	
SHbO (0–Peak seconds)	MCI	1.26e−08	1.46e−08	**0.0110**	2.26e−08	1.57e−08	0.8587	1.46e−08	1.91e−08	**0.0145**
	HC	2.34e−08	1.74e−08		2.78e−08	2.34e−08		2.55e−08	2.30e−08	
Peak time (seconds)	MCI	1.84E+01	4.47E+00	0.9834	1.71E+01	4.07E+00	0.6153	1.71E+01	4.07E+00	0.4011
	HC	1.84E+01	3.76E+00		1.76E+01	5.51E+00		1.76E+01	5.51E+00	
Skewness	MCI	−6.96e−02	5.60e−01	0.7028	−1.09e−01	9.53e−01	0.1087	1.55e−02	4.91e−01	**0.0409**
	HC	−1.22e−01	4.90e−01		−4.49e−01	8.28e−01		−2.31e−01	6.38e−01	
Kurtosis	MCI	2.12E+00	6.62e−01	0.9957	2.53E+00	9.36e−01	0.6885	1.90E+00	1.04E+00	0.9623
	HC	2.75E+00	1.05E+00		2.63E+00	1.23E+00		2.25E+00	7.70e−01	

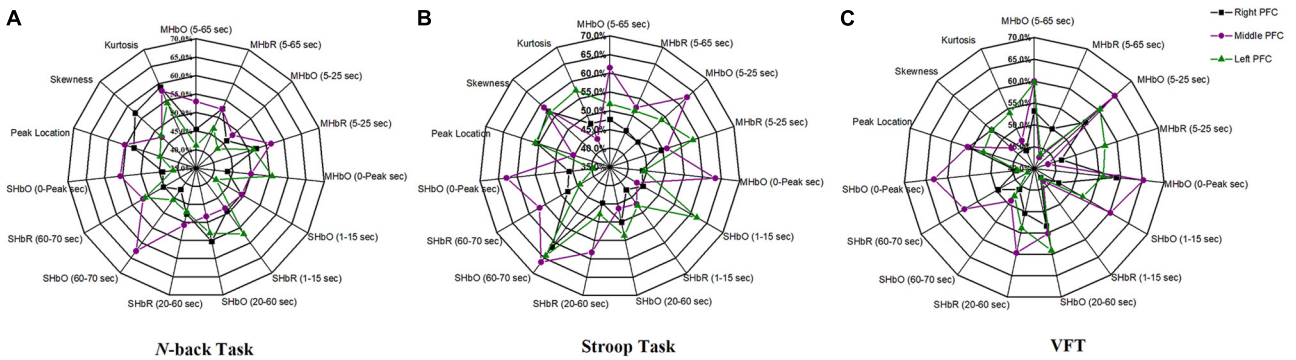

FIGURE 5 | Panels **(A–C)** are the LDA classification results of 15 digital biomarkers based upon ROI channels with N-back, Stroop, and VFT task, respectively.

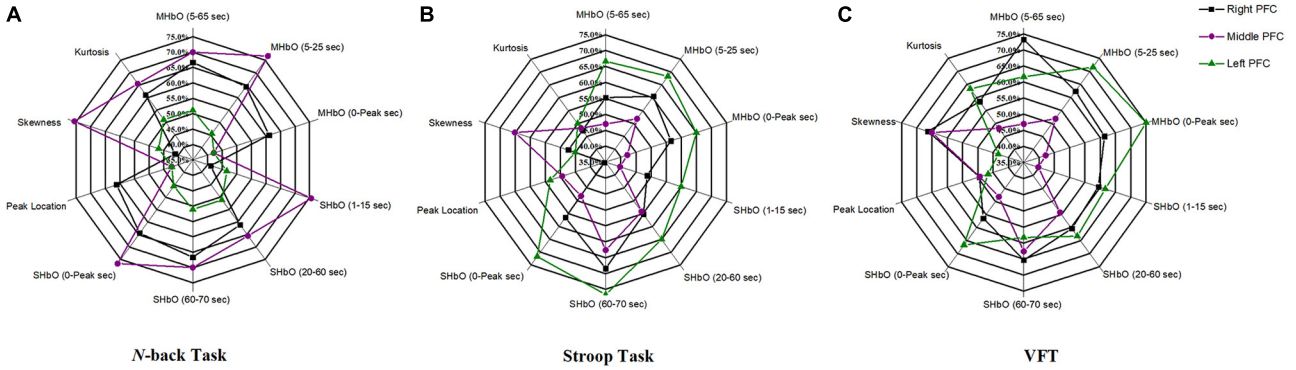

FIGURE 6 | Panels **(A–C)** are the LDA classification results of 10 digital biomarkers based upon manually selected ROI channels with N-back, Stroop, and VFT task, respectively.

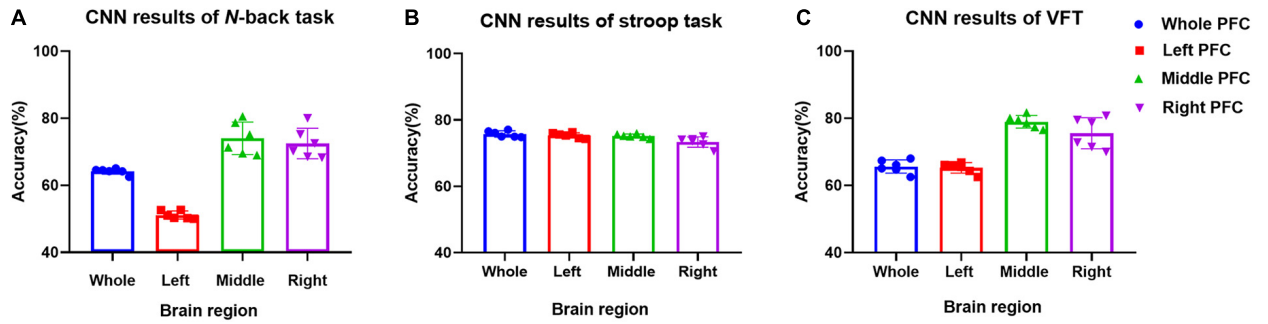

FIGURE 7 | Classification results by CNN (repeated six times) using the HbO data in the ROI.

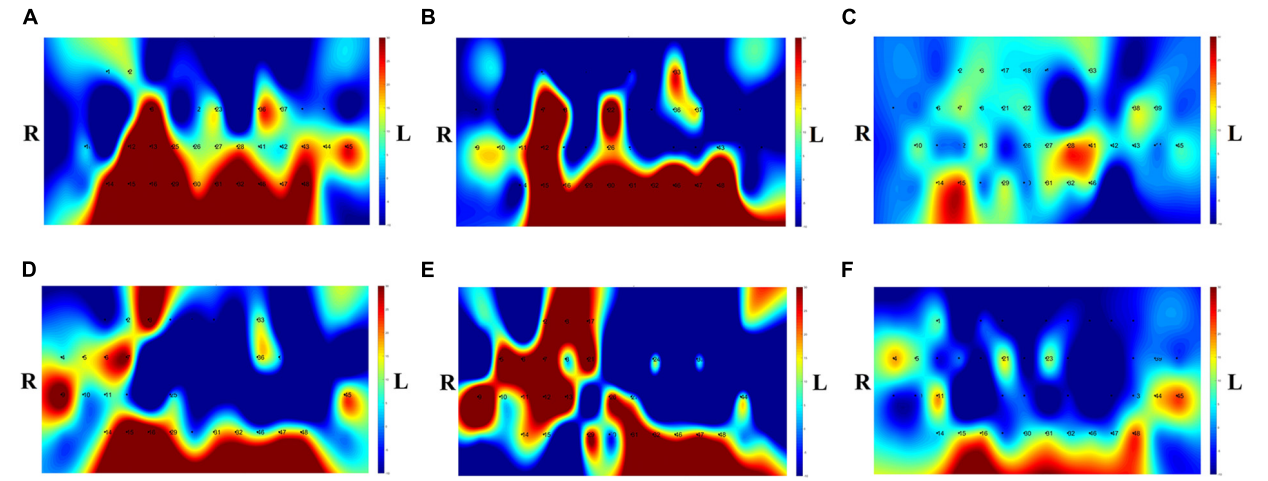

FIGURE 8 | Comparison of average *t*-maps between MCI and HC for three mental tasks: **(A)** *N*-back MCI, **(B)** Stroop MCI, **(C)** VFT MCI, **(D)** *N*-back HC, **(E)** Stroop HC, and **(F)** VFT HC.

declining brain function if it becomes inefficient. Similar with this compensation theory, the ΔHbO of HC in the left PFC (shown in **Figure 3**) appeared higher than that of MCI, but this was not obvious in the right and middle PFCs. This result is consistent with the work of Reuter-Lorenz et al. (2000), which claims that the contralateral right PFC of the patients with MCI can increase recruitment of both working memory and episodic encoding. Also, the higher classification result when using the middle PFC, as seen in **Figure 7**, indicates that the middle brain activity got decreased in the MCI patients. This may coincide with the fact that the gray matter in the middle PFC gets reduced during the process of aging (Minkova et al., 2017).

(iii) ROI strategy: Two strategies for selecting the signals for analysis were evaluated; *t*-value based selection and manual selection by visual examination. The *t*-value based ROI selection is widely employed in the bio-signal processing areas (Plichta et al., 2006), since it has the advantage of being convenient and consumes lesser time. However, in this study, we found that the automatic ROI selection with $t > t_{crit}$ included many data with high noise oscillations. As revealed in **Figures 5**, **6** and **Tables 3**–**8**, the results obtained by using the manually selected active channels showed a better performance than the automatic ROI selection. It reveals that the channel selection is very sensitive to the final result because the poor performance could be caused by the wrong selection of ROI channels algorithmically. In light of the above-mentioned advantage, the automatic ROI selection would be convenient when analyzing a big data set.

(iv) Mental tasks: Three mental tasks (*N*-back, Stroop, VFT) were employed to classify the MCI patients from HC. Based on the hemodynamic response of ΔHbO, the statistical digital biomarkers analysis, and digital/image biomarkers classification, the *N*-back task showed a robust and stable performance in contrast to the Stroop task and VFT. Especially, the CNN result using the *t*-map data obtained the accuracy over 90% by performing the *N*-back task. This might be an indication that the memory-related neural degeneration is more apparent in the MCI patients when compared with the other mental functions. It will be interesting to apply another deep learning technique such as the recurrent neural network (RNN) (Sanchez et al., 2017; Li X. F. et al., 2018; Liu, 2018).

A number of different time intervals were evaluated in line with the statistical digital biomarkers in this study. As shown in **Figures 5**, **6** and **Tables 3**–**8**, the significant results (i.e., accuracy > 60% or *p*-value < 0.05) occurred randomly. It was

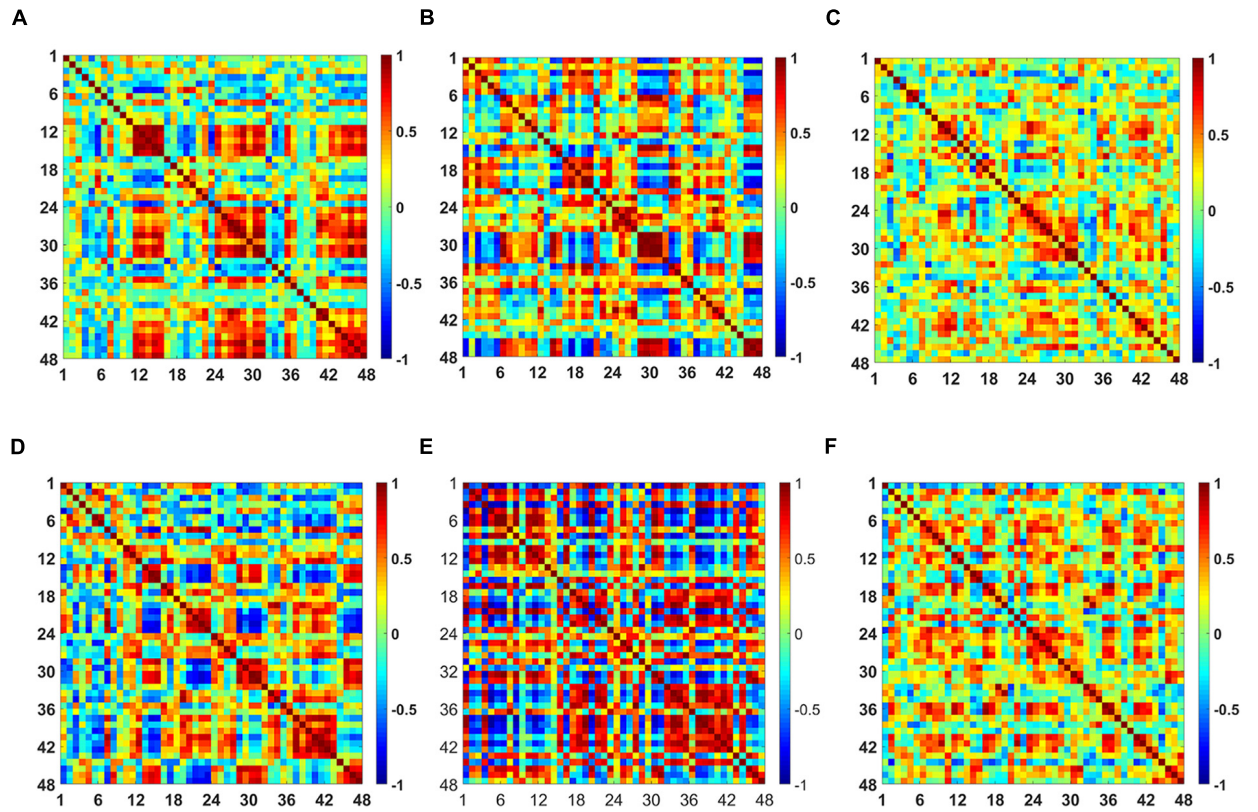

FIGURE 9 | Comparison of the correlation maps between MCI and HC for three mental tasks: **(A)** *N*-back MCI, **(B)** Stroop MCI, **(C)** VFT MCI, **(D)** *N*-back HC, **(E)** Stroop HC, and **(F)** VFT HC (the color bar in the right shows the correlation coefficient from –1 to 1).

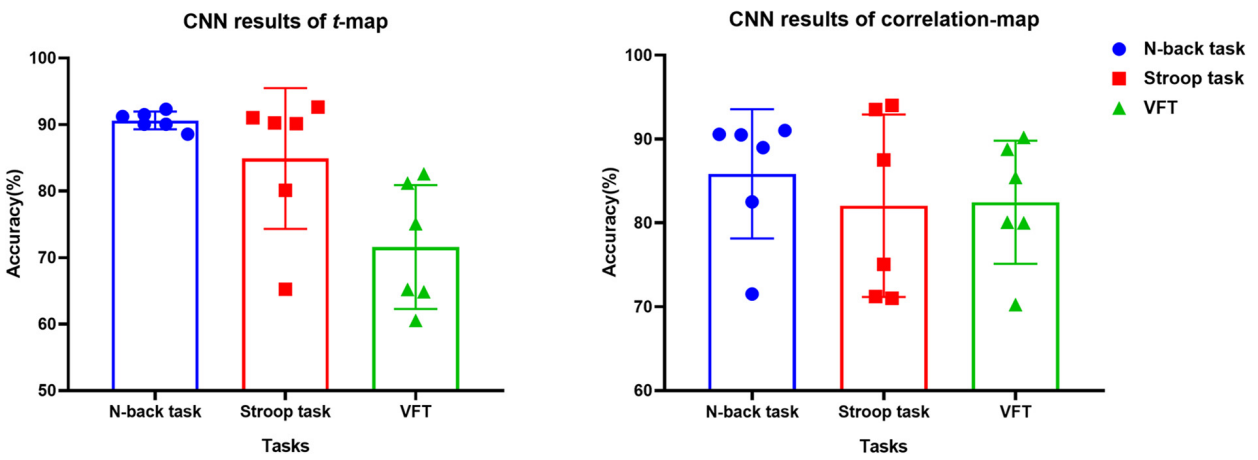

FIGURE 10 | Classification results of *t*-maps and correlation maps by CNN (repeated six times) for three mental tasks.

difficult to conclude the best time interval for MCI detection. In addition, most of the studies (as listed in **Table 1**) prefer to conduct the statistical analysis using the entire task period between the groups of MCI and HC. However, as per the obtained results, the biomarkers were not consistent to make a satisfactory classification result. Therefore, the statistical analysis is not recommended to detect the early stage of AD. Therefore, as shown in **Figure 9**, the combined technique (deep learning and an imaging biomarker) shows a promising advantage for detecting the MCI patients from HC in the fNIRS field.

Since the present study accessed a relatively small number of MCI patients, no attempt was made to exclude patients based on other criteria. To substantiate the findings, research with a larger sample size would help ensuring that participants with secondary

comorbidities can be excluded. In addition, a study with more participants will allow assessing separately, participants with different subtypes of MCI. In this study, we considered only the prefrontal lobes for our investigation, as PFC is widely (>90%) used for diagnosing MCI in the fNIRS area. Another issue for improvement can be found from the used headset. NIRSIT has a specific channel configuration for the PFC. It cannot be used over the entire brain. Meanwhile, several former studies claimed that MCI patients have a reduced activation in the hippocampus and PFC (Johnson et al., 2006; Dannhauser et al., 2008). A broader brain region than the PFC might give the better opportunity for examining more effective biomarkers. In the future, the whole brain with a hybrid technique including EEG and fNIRS (Khan et al., 2014, 2018; Hong et al., 2018b) with a greater number of subjects will be pursued hoping that more effective and reliable biomarkers for diagnosing the early stage of AD are disclosed.

CONCLUSION

For the purpose of diagnosing MCI patients using fNIRS, we investigated three approaches (statistical analysis, LDA, CNN) in classifying the measured fNIRS signals. Fifteen digital biomarkers (i.e., 5 means and 7 slopes of ΔHbO/ΔHbR, peak time, skewness, kurtosis) in combination of LDA and two image biomarkers (t-map, correlation map) in combination with CNN were analyzed. It appears that the classical statistical analysis method is not reliable for clinical application, because the biomarkers ($p < 0.05$) that provided good LDA classification results (> 60%) were not consistent throughout the trials. However, the CNN classification result using the t-map input data provided the best classification accuracy (90.62%) between MCI and HC. Secondly, the local analyses in the PFC (left PFC, or middle PFC, or right PFC) provided better classification accuracies than examining the entire PFC. This leads to the conclusion that the task-related brain activity in the PFC may be localized per person, and the use of a few channels of fNIRS may be acceptable for MCI diagnosis. Finally, the N-back task presented a robust and accurate performance than the Stroop or VF tasks when the image biomarkers with CNN were analyzed.

DATA AVAILABILITY

The datasets generated for this study are available on request to the corresponding author.

ETHICS STATEMENT

This experiment was conducted in accordance with the latest Declaration of Helsinki upon the approval of the Pusan National University Institutional Review Board. All volunteers were given a detailed description of the experimental procedure prior to the beginning of the experiment, and they provided written consent agreeing to these experiments.

AUTHOR CONTRIBUTIONS

DY carried out the data processing and wrote the first draft of the manuscript. K-SH suggested the theoretical aspects of the current study, corrected the manuscript, and supervised the entire process leading to the manuscript generation. S-HY participated in collecting experimental data. C-SK has examined the data. All authors have approved the final manuscript.

FUNDING

This work was supported by the National Research Foundation (NRF) of Korea under the auspices of the Ministry of Science and ICT, Republic of Korea (Grant Nos. NRF-2017R1A2A1A17069430 and NRF-2017R1A4A1015627).

REFERENCES

Alzheimer's Association, (2018). 2018 Alzheimer's disease facts and figures. *Alzheimers Dement.* 14, 367–429. doi: 10.1016/j.jalz.2016.03.001

Arai, H., Takano, M., Miyakawa, K., Ota, T., Takahashi, T., Asaka, H., et al. (2006). A quantitative near-infrared spectroscopy study: a decrease in cerebral hemoglobin oxygenation in Alzheimer's disease and mild cognitive impairment. *Brain Cogn.* 61, 189–194. doi: 10.1016/j.bandc.2005.12.012

Beishon, L., Haunton, V. J., Panerai, R. B., and Robinson, T. G. (2017). Cerebral hemodynamics in mild cognitive impairment: a systematic review. *J. Alzheimers Dis.* 59, 369–385. doi: 10.3233/JAD-170181

Boas, D. A., Elwell, C. E., Ferrari, M., and Taga, G. (2014). Twenty years of functional near-infrared spectroscopy: introduction for the special issue. *Neuroimage* 85, 1–5. doi: 10.1016/J.NEUROIMAGE.2013.11.033

Byeon, H., Jin, H., and Cho, S. (2017). Development of Parkinson's disease dementia prediction model based on verbal memory, visuospatial memory, and executive function. *J. Med. Imag. Heal. Inform.* 7, 1517–1521. doi: 10.1166/jmihi.2017.2196

Cabeza, R., Anderson, N. D., Locantore, J. K., and McIntosh, A. R. (2002). Aging gracefully: compensatory brain activity in high-performing older adults. *Neuroimage* 17, 1394–1402. doi: 10.1006/nimg.2002.1280

Chen, H. T., Jiang, B., and Lu, N. Y. (2018). A multi-mode incipient sensor fault detection and diagnosis method for electrical traction systems. *Int. J. Control Autom. Syst.* 16, 1783–1793. doi: 10.1007/s12555-017-0533-0

Cotelli, M., Manenti, R., Cappa, S. F., Zanetti, O., and Miniussi, C. (2008). Transcranial magnetic stimulation improves naming in Alzheimer disease patients at different stages of cognitive decline. *Eur. J. Neurol.* 15, 1286–1292. doi: 10.1111/j.1468-1331.2008.02202.x

Dannhauser, T. M., Shergill, S. S., Stevens, T., Lee, L., Seal, M., Walker, R. W., et al. (2008). An fMRI study of verbal episodic memory encoding in amnestic mild cognitive impairment. *Cortex* 44, 869–880. doi: 10.1016/j.cortex.2007.04.005

Ding, Z. Y., Chen, Y. M., Chen, Y. L., and Wu, X. Y. (2017). Similar hand gesture recognition by automatically extracting distinctive features. *Int. J. Control Autom. Syst.* 15, 1770–1778. doi: 10.1007/s12555-015-0403-6

Doi, T., Shimada, H., Park, H., Makizako, H., Tsutsumimoto, K., Uemura, K., et al. (2015). Cognitive function and falling among older adults with mild cognitive impairment and slow gait. *Geriatr. Gerontol. int.* 15, 1073–1078. doi: 10.1111/ggi.12407

Fang, C., Li, C. F., Cabrerizo, M., Barreto, A., Andrian, J., Rishe, N., et al. (2018). Gaussian discriminant analysis for optimal delineation of mild cognitive impairment in Alzheimer's disease. *Int. J. Neural. Syst.* 28:1850017. doi: 10.1142/S012906571850017X

Ferrari, M., and Quaresima, V. (2012). A brief review on the history of human functional near-infrared spectroscopy (fNIRS) development and fields of application. *Neuroimage* 63, 921–935. doi: 10.1016/j.neuroimage.2012.03.049

General Assembly of the World Medical Association, (2014). World medical association declaration of helsinki: ethical principles for medical research involving human subjects. JAMA-J. *Am. Med. Assoc.* 310, 2191–2194. doi: 10.1001/jama.2013.281053

Ghafoor, U., Kim, S., and Hong, K.-S. (2017). Selectivity and longevity of peripheral-nerve and machine interfaces: a review. *Front. Neurorobot.* 11:59. doi: 10.3389/fnbot.2017.00059

Goh, J. O., and Park, D. C. (2009). Neuroplasticity and cognitive aging: the scaffolding theory of aging and cognition. *Restor. Neurol. Neurosci.* 27, 391–403. doi: 10.3233/RNN-2009-0493

Halliday, D. W. R., Hundza, S. R., Garcia-Barrera, M. A., Klimstra, M., Commandeur, D., Lukyn, T. V., et al. (2018). Comparing executive function, evoked hemodynamic response, and gait as predictors of variations in mobility for older adults. *J. Clin. Exp. Neuropsychol.* 40, 151–160. doi: 10.1080/13803395.2017.1325453

Hamadache, M., and Lee, D. (2017). Principal component analysis-based signal-to-noise ratio improvement for inchoate faulty signals: application to ball bearing fault detection. *Int. J. Control Autom. Syst.* 15, 506–517. doi: 10.1007/s12555-015-0196-7

Han, C., Jo, S., Jo, I., Kim, E., Park, M., Kang, Y., et al. (2008). An adaptation of the korean mini-mental state examination (K-MMSE) in elderly koreans: demographic influence and population-based norms (the AGE study). *Arch. Gerontol. Geriatr.* 47, 302–310. doi: 10.1016/j.archger.2007.08.012

Haworth, J., Phillips, M., Newson, M., Rogers, P. J., Torrens-Burton, A., and Tales, A. (2016). Measuring information processing speed in mild cognitive impairment: clinical versus research dichotomy. *J. Alzheimers Dis.* 51, 263–275. doi: 10.3233/JAD-150791

Heinzel, S., Haeussinger, F. B., Hahn, T., Ehlis, A.-C., Plichta, M. M., and Fallgatter, A. J. (2013). Variability of (functional) hemodynamics as measured with simultaneous fNIRS and fMRI during intertemporal choice. *Neuroimage* 71, 125–134. doi: 10.1016/j.neuroimage.2012.12.074

Hong, K.-S., Khan, M. J., and Hong, M. J. (2018b). Feature extraction and classification methods for hybrid fNIRS-EEG brain-computer interfaces. *Front. Hum. Neurosci.* 12:246. doi: 10.3389/fnhum.2018.00246

Hong, K.-S., Aziz, N., and Ghafoor, U. (2018a). Motor-commands decoding using peripheral nerve signals: a review. *J. Neural. Eng.* 15:031004. doi: 10.1088/1741-2552/aab383

Hong, K.-S., Naseer, N., and Kim, Y. H. (2014). Classification of prefrontal and motor cortex signals for three-class fNIRS-BCI. *Neurosci. Lett.* 587, 87–92. doi: 10.1016/j.neulet.2014.12.029

Hong, K.-S., and Santosa, H. (2016). Decoding four different sound-categories in the auditory cortex using functional near-infrared spectroscopy. *Hear. Res.* 333, 157–166. doi: 10.1016/j.heares.2016.01.009

Hong, K.-S., and Zafar, A. (2018). Existence of initial dip for BCI: an illusion or reality. *Front. In Neurorobot.* 12:69. doi: 10.3389/fnbot.2018.00069

Ieracitano, C., Mammone, N., Bramanti, A., Hussain, A., and Morabito, F. C. (2018). A convolutional neural network approach for classification of dementia stages based on 2D-spectral representation of EEG recordings. *Neurocomputing* 323, 96–107. doi: 10.1016/j.neucom.2018.09.071

Iqbal, M., Rehan, M., and Hong, K.-S. (2018). Robust adaptive synchronization of ring configured uncertain chaotic fitzhugh-nagumo neurons under direction-dependent coupling. *Front. Neurorobot.* 12:6. doi: 10.3389/fnbot.2018.00006

Johnson, S. C., Schmitz, T. W., Moritz, C. H., Meyerand, M. E., Rowley, H. A., Alexander, A. L., et al. (2006). Activation of brain regions vulnerable to Alzheimer's disease: the effect of mild cognitive impairment. *Neurobiol. Aging* 27, 1604–1612. doi: 10.1016/j.neurobiolaging.2005.09.017

Jung, E. S., Lee, J. H., Kim, H. T., Park, S. S., Kim, J. E., Kim, J. E., et al. (2018). Effect of acupuncture on patients with mild cognitive impairment assessed using functional near-infrared spectroscopy on week 12 (close-out): a pilot study protocol. *Integr. Med. Res.* 7, 287–295. doi: 10.1016/j.imr.2018.06.002

Kane, M. J., Conway, A. R. A., Miura, T. K., and Colflesh, G. J. H. (2007). Working memory, attention control, and the n-back task: a question of construct validity. *J. Exp. Psychol. Learn. Mem. Cogn.* 33, 615–622. doi: 10.1037/0278-7393.33.3.615

Katzorke, A., Zeller, J. B. M., Müller, L. D., Lauer, M., Polak, T., Deckert, J., et al. (2018). Decreased hemodynamic response in inferior frontotemporal regions in elderly with mild cognitive impairment. *Neuroimaging* 274, 11–18. doi: 10.1016/j.pscychresns.2018.02.003

Katzorke, A., Zeller, J. B. M., Müller, L. D., Lauer, M., Polak, T., Reif, A., et al. (2017). Reduced activity in the right inferior frontal gyrus in elderly APOE-E4 carriers during a verbal fluency task. *Front. Hum. Neurosci.* 11:46. doi: 10.3389/fnhum.2017.00046

Keage, H. A. D., Churches, O. F., Kohler, M., Pomeroy, D., Luppino, R., Bartolo, M. L., et al. (2012). Cerebrovascular function in aging and dementia: a systematic review of transcranial doppler studies. *Dement. Geriatr. Cogn. Dis. Extra.* 2, 258–270. doi: 10.1159/000339234

Khan, M. J., Ghafoor, U., and Hong, K.-S. (2018). Early detection of hemodynamic responses using EEG: a hybrid EEG-fNIRS study. *Front. Hum. Neurosci.* 12:479. doi: 10.3389/fnhum.2018.00479

Khan, M. J., and Hong, K.-S. (2015). Passive BCI based on drowsiness detection: an fNIRS study. *Biomed. Opt. Express.* 6, 4063–4078. doi: 10.1364/BOE.6.004063

Khan, M. J., and Hong, K.-S. (2017). Hybrid EEG-fNIRS-based eight-command decoding for BCI: application to quadcopter control. *Front. Neurorobot.* 11:6. doi: 10.3389/fnbot.2017.00006

Khan, M. J., Hong, M. J., and Hong, K.-S. (2014). Decoding of four movement directions using hybrid NIRS-EEG brain-computer interface. *Front. Hum. Neurosci.* 244:8. doi: 10.3389/fnhum.2014.00244

Khazaee, A., Ebrahimzadeh, A., and Babajani-Feremi, A. (2017). Classification of patients with MCI and AD from healthy controls using directed graph measures of resting-state fMRI. *Behav. Brain Res.* 322, 339–350. doi: 10.1016/J.BBR.2016.06.043

Kim, H. H., Park, J. K., Oh, J. H., and Kang, D. J. (2017). Multi-task convolutional neural network system for license plate recognition. *Int. J. Control Autom. Syst.* 15, 2942–2949. doi: 10.1007/s12555-016-0332-z

Labaer, J. (2005). So, you want to look for biomarkers - (Introduction to the special biomarkers issue). *J. Proteome Res.* 4, 1053–1059. doi: 10.1021/pr0501259

Li, R., Rui, G., Chen, W., Li, S., Schulz, P. E., and Zhang, Y. (2018). Early detection of Alzheimer's disease using non-invasive near-infrared spectroscopy. *Front. Aging Neurosci.* 10:366. doi: 10.3389/fnagi.2018.00366

Li, X., Zhu, Z., Zhao, W., Sun, Y., Wen, D., Xie, Y., et al. (2018). Decreased resting-state brain signal complexity in patients with mild cognitive impairment and Alzheimer's disease: a multi-scale entropy analysis. *Biomed. Opt. Express.* 9, 1916–1929. doi: 10.1364/BOE.9.001916

Li, X. F., Fang, J. A., and Li, H. Y. (2018). Exponential synchronization of stochastic memristive recurrent neural networks under alternate state feedback control. *Int. J. Control Autom. Syst.* 16, 2859–2869. doi: 10.1007/s12555-018-0225-4

Liu, P. L. (2018). Further improvement on delay-range-dependent stability criteria for delayed recurrent neural networks with interval time-varying delays. *Int. J. Control Autom. Syst.* 16, 1186–1193. doi: 10.1007/s12555-016-0359-1

Liu, X., and Hong, K.-S. (2017). Detection of primary RGB colors projected on a screen using fNIRS. *J. Innov. Opt. Health Sci.* 10:1750006. doi: 10.1142/s1793545817500067

Marmarelis, V. Z., Shin, D. C., Tarumi, T., and Zhang, R. (2017). Comparison of model-based indices of cerebral autoregulation and vasomotor reactivity using transcranial doppler versus near-infrared spectroscopy in patients with amnestic mild cognitive impairment. *J. Alzheimers Dis.* 56, 89–105. doi: 10.3233/JAD-161004

Minkova, L., Habich, A., Peter, J., Kaller, C. P., Eickhoff, S. B., and Klöppel, S. (2017). Gray matter asymmetries in aging and neurodegeneration: a review and meta-analysis. *Hum. Brain Mapp.* 38, 5890–5904. doi: 10.1002/hbm.23772

Moon, J., Kim, H., and Lee, B. (2018). View-point invariant 3d classification for mobile robots using a convolutional neural network. *Int. J. Control Autom. Syst.* 16, 2888–2895. doi: 10.1007/s12555-018-0182-y

Naseer, N., and Hong, K.-S. (2015). fNIRS-based brain-computer interfaces: a review. *Front. Hum. Neurosci.* 9:172. doi: 10.3389/fnhum.2015.00003

Naseer, N., Noori, F. M., Qureshi, N. K., and Hong, K.-S. (2016). Determining optimal feature-combination for LDA classification of functional near-infrared spectroscopy signals in brain-computer interface application. *Front. Hum. Neurosci.* 10:237. doi: 10.3389/fnhum.2016.00237

Nestor, P. J., Scheltens, P., and Hodges, J. R. (2004). Advances in the early detection of Alzheimer's disease. *Nat. Med.* 10, S34–S41. doi: 10.1038/nrn1433

Nguyen, C. T., Couture, M. C., Alvarado, B. E., and Zunzunegui, M. V. (2008). Life course socioeconomic disadvantage and cognitive function among the elderly population of seven capitals in latin america and the Caribbean. *J. Aging Health* 20, 347–362. doi: 10.1177/0898264308315430

Nguyen, H.-D., and Hong, K.-S. (2016). Bundled-optode implementation for 3D imaging in functional near-infrared spectroscopy. *Biomed. Opt. Express.* 7, 3491–3507. doi: 10.1364/BOE.7.003491

Nguyen, Q. C., Piao, M., and Hong, K.-S. (2018). Multivariable adaptive control of the rewinding process of a roll-to-roll system governed by hyperbolic partial differential equations. *Int. J. Control Autom. Syst.* 16, 2177–2186. doi: 10.1007/s12555-017-0205-0

Niu, H. J., Li, X., Chen, Y. J., Ma, C., Zhang, J. Y., and Zhang, Z. J. (2013). Reduced frontal activation during a working memory task in mild cognitive impairment: a non-invasive near-infrared spectroscopy study. *CNS Neurosci. Ther.* 19, 125–131. doi: 10.1109/SIBGRAPI.2001.963071

Ou, M., Wei, H., Zhang, Y., and Tan, J. (2019). A dynamic adam based deep neural network for fault diagnosis of oil-immersed power transformers. *Energies* 12:995. doi: 10.3390/en12060995

Park, D. C., and Reuter-Lorenz, P. (2009). The adaptive brain: aging and neurocognitive scaffolding. *Annu. Rev. Psychol.* 60, 173–196. doi: 10.1146/annurev.psych.59.103006.093656

Perpetuini, D., Bucco, R., Zito, M., and Merla, A. (2017). Study of memory deficit in Alzheimer's disease by means of complexity analysis of fNIRS signal. *Neurophotonics* 5:011010. doi: 10.1117/1.NPh.5.1.011010

Pinti, P., Merla, A., Aichelburg, C., Lind, F., Power, S., Swingler, E., et al. (2017). A novel GLM-based method for the automatic identification of functional events (AIDE) in fNIRS data recorded in naturalistic environments. *Neuroimage* 155, 291–304. doi: 10.1016/j.neuroimage.2017.05.001

Pinti, P., Tachtsidis, I., Hamilton, A., Hirsch, J., Aichelburg, C., Gilbert, S., et al. (2018). The present and future use of functional near-infrared spectroscopy (fNIRS) for cognitive neuroscience. *JPN. Psychol. Res.* 60, 347–373. doi: 10.1111/nyas.13948

Plichta, M. M., Herrmann, M. J., Baehne, C. G., Ehlis, A. C., Richter, M. M., Pauli, P., et al. (2006). Event-related functional near-infrared spectroscopy (fNIRS): are the measurements reliable? *Neuroimage* 31, 116–124. doi: 10.1016/j.neuroimage.2005.12.008

Price, C. J., and Friston, K. J. (2002). Degeneracy and cognitive anatomy. *Trends Cogn. Sci.* 6, 416–421. doi: 10.1016/S1364-6613(02)01976-9

Privitera, C. M., and Stark, L. W. (2000). Algorithms for defining visual regions-of-lnterest: comparison with eye fixations. *IEEE Trans. Pattern Anal. Mach. Intell.* 22, 970–982. doi: 10.1109/34.877520

Reuter-Lorenz, P. A., Jonides, J., Smith, E. E., Hartley, A., Miller, A., Marshuetz, C., et al. (2000). Age differences in the frontal lateralization of verbal and spatial working memory revealed by PET. *J. Cogn. Neurosci.* 12, 174–187. doi: 10.1162/089892900561814

Salis-Perales, G., and Barajas-Ramirz, J. G. (2017). Activation of neuronal ensembles via controlled synchronization. *Int. J. Control Autom. Syst.* 15, 122–128. doi: 10.1007/s12555-015-0203-z

Sanchez, E. N., Rodriguez-Castellanos, D. I., Chen, G., and Ruiz-Cruz, R. (2017). Pinning control of complex network synchronization: a recurrent neural network approach. *Int. J. Control. Autom. Syst.* 15, 1405–1414. doi: 10.1007/s12555-016-0364-4

Sassaroli, A., and Fantini, S. (2004). Comment on the modified Beer–Lambert law for scattering media. *Phys. Med. Biol.* 49, N255–N257. doi: 10.1088/0031-9155/49/14/N07

Strangman, G. E., Li, Z., and Zhang, Q. (2013). Depth sensitivity and source-detector separations for near infrared spectroscopy based on the colin27 brain template. *PLoS One* 8:e66319. doi: 10.1371/journal.pone.0066319

Stuart, S., Vitorio, R., Morris, R., Martini, D. N., Fino, P. C., and Mancini, M. (2018). Cortical activity during walking and balance tasks in older adults and in people with Parkinson's disease: a structured review. *Maturitas* 113, 53–72. doi: 10.1016/j.maturitas.2018.04.011

Tak, S., and Ye, J. C. (2014). Statistical analysis of fNIRS data: a comprehensive review. *Neuroimage* 85, 72–91. doi: 10.1016/J.NEUROIMAGE.2013.06.016

Tang, W., Cha, H., Wei, M., Tian, B., and Ren, X. (2019). An atmospheric refractivity inversion method based on deep learning. *Results Phys.* 12, 582–584. doi: 10.1016/j.rinp.2018.12.014

Trakoolwilaiwan, T., Lee, J., Choi, J., Trakoolwilaiwan, T., Behboodi, B., Lee, J., et al. (2019). Convolutional neural network for high-accuracy functional near- infrared spectroscopy in a brain – computer interface: three-class classification of rest, right-, and left- hand motor execution functional near-infrared spectroscopy in. *Neurophotonics* 5:011008. doi: 10.1117/1.NPh.5.1.011008

Uemura, K., Doi, T., Shimada, H., Makizako, H., Park, H., and Suzuki, T. (2016). Age-related changes in prefrontal oxygenation during memory encoding and retrieval. *Geriatr Gerontol Int.* 16, 1296–1304. doi: 10.1111/ggi.12642

Valenzuela, O., Jiang, X. J., Carrillo, A., and Rojia, I. (2018). Multi-objective genetic algorithms to find most relevant volumes of the brain related to Alzheimer's disease and mild cognitive impairment. *Int. J. Neural Syst.* 28:1850022. doi: 10.1142/S0129065718500223

Vermeij, A., Kessels, R. P. C., Heskamp, L., Simons, E. M. F., Dautzenberg, P. L. J., and Claassen, J. A. H. R. (2017). Prefrontal activation may predict working-memory training gain in normal aging and mild cognitive impairment. *Brain Imaging Behav.* 11, 141–154. doi: 10.1007/s11682-016-9508-7

Whiteside, D. M., Kealey, T., Semla, M., Luu, H., Rice, L., Basso, M. R., et al. (2016). Verbal fluency: language or executive function measure? *Appl. Neuropsychol. Adult* 23, 29–34. doi: 10.1080/23279095.2015.1004574

Yap, K. H., Ung, W. C., Ebenezer, E. G. M., Nordin, N., Chin, P. S., Sugathan, S., et al. (2017). Visualizing hyperactivation in neurodegeneration based on prefrontal oxygenation: a comparative study of mild Alzheimer's disease, mild cognitive impairment, and healthy controls. *Front. Aging Neurosci.* 9:287. doi: 10.3389/fnagi.2017.00287

Yazdani, M., Salarieh, H., and Foumani, M. S. (2018). Bio-inspired decentralized architecture for walking of a 5-link biped robot with compliant knee joints. *Int. J. Control Autom. Syst.* 16, 2935–2947. doi: 10.1007/s12555-017-0578-0

Yennu, A., Tian, F., Gatchel, R. J., and Liu, H. (2016). Prefrontal hemodynamic mapping by functional near-infrared spectroscopy in response to thermal stimulations over three body sites. *Neurophotonics* 3:045008. doi: 10.1117/1.NPh.3.4.045008

Yeung, M. K., Sze, S. L., Woo, J., Kwok, T., Shum, D. H. K., Yu, R., et al. (2016b). Reduced frontal activations at high working memory load in mild cognitive impairment: near-infrared spectroscopy. *Dement. Geriatr. Cogn. Disord.* 42, 278–296. doi: 10.1159/000450993

Yeung, M. K., Sze, S. L., Woo, J., Kwok, T., Shum, D. H. K., Yu, R., et al. (2016a). Altered frontal lateralization underlies the category fluency deficits in older adults with mild cognitive impairment: a near-infrared spectroscopy study. *Front. Aging Neurosci.* 8:59. doi: 10.3389/fnagi.2016.00059

Yi, G., Mao, J. X., Wang, Y. N., Guo, S. Y., and Miao, Z. Q. (2018). Adaptive tracking control of nonholonomic mobile manipulators using recurrent neural networks. *Int. J. Control Autom. Syst.* 16, 1390–1403. doi: 10.1007/s12555-017-0309-6

Zafar, A., and Hong, K.-S. (2017). Detection and classification of three-class initial dips from prefrontal cortex. *Biomed. Opt. Express.* 8, 367–383. doi: 10.1364/BOE.8.000367

Zafar, A., and Hong, K.-S. (2018). Neuronal activation detection using vector phase analysis with dual threshold circles: a functional near-infrared spectroscopy study. *Int. J. Neural Syst.* 28:1850031. doi: 10.1142/S0129065718500314

Conflict of Interest Statement: The authors declare that the research was conducted in the absence of any commercial or financial relationships that could be construed as a potential conflict of interest.

frontiers in Human Neuroscience

ORIGINAL RESEARCH
published: 19 September 2019
doi: 10.3389/fnhum.2019.00318

An Investigation of Neurochemical Changes in Chronic Cannabis Users

Sharlene D. Newman[1,2], Hu Cheng[1,2], Ashley Schnakenberg Martin[1], Ulrike Dydak[3,4], Shalmali Dharmadhikari[3,4], William Hetrick[1] and Brian O'Donnell[1]*

[1] Department of Psychological and Brain Sciences, Indiana University, Bloomington, IN, United States, [2] Program in Neuroscience, Indiana University, Bloomington, IN, United States, [3] School of Health Sciences, Purdue University, West Lafayette, IN, United States, [4] Department of Radiology and Imaging Sciences, Indiana University School of Medicine, Indianapolis, IN, United States

With the legalization of recreational cannabis (CB) the characterization of how it may impact brain chemistry is essential. Magnetic resonance spectroscopy (MRS) was used to examine neurometabolite concentrations in the dorsal anterior cingulate (dACC) in chronic CB users (N = 26; 10 females) and controls (N = 24; 10 females). The concentrations of glutamate (Glu), total creatine (tCr), choline (Cho), total N-acetylaspartate (tNAA), and myo-inositol (mI) were estimated using LCModel. The ANCOVAs failed to show significant differences between controls and CB users. Regression analyses were then performed on the CB group to model each neurometabolite to determine its relationship to monthly CB use, sex, the interaction between CB use and sex. tCr was found to be predicted by both monthly CB use and sex. While the regression model was not significant the relationship between monthly CB use and Glu appears to be modulated by sex with the effect of monthly use (dose) being stronger in males. tNAA failed to show an effect of CB use but did reveal an effect of sex with females showing larger tNAA levels. Although the results presented are preliminary due to the small sample size they do guide future research. The results presented provide direction for further studies as they suggest that dose may significantly influence the observance of CB effects and that those effects may be modulated by sex. Studies with significantly larger sample sizes designed specifically to examine individuals with varying usage as well as sex effects are necessary.

Keywords: cannabis, magnetic resonance spectroscopy, creatine, glutamate, anterior cingualte cortex

OPEN ACCESS

Edited by:
Dieter J. Meyerhoff, University of California, San Francisco, United States

Reviewed by:
Anne Marije Kaag, University of Amsterdam, Netherlands
Joseph O'Neill, University of California, Los Angeles, United States
James J. Prisciandaro, Medical University of South Carolina, United States

****Correspondence:***
Sharlene D. Newman
sdnewman@indiana.edu

Specialty section:
This article was submitted to Health, a section of the journal Frontiers in Human Neuroscience

Received: *05 May 2019*
Accepted: *29 August 2019*
Published: *19 September 2019*

Citation:
Newman SD, Cheng H, Schnakenberg Martin A, Dydak U, Dharmadhikari S, Hetrick W, O'Donnell B (2019) An Investigation of Neurochemical Changes in Chronic Cannabis Users. Front. Hum. Neurosci. 13:318. doi: 10.3389/fnhum.2019.00318

INTRODUCTION

The use of cannabis (CB) has increased over the past decade in the United States, and past-year prevalence of CB use exceeds 10% (Grucza et al., 2016) with few users seeking treatment (Brown et al., 2003). However, delta-9-tetrahydrocannabinol (THC), the compound responsible for the psychoactive effects of CB, has been found to alter neurochemistry (Sneider et al., 2013; Colizzi et al., 2016) which may interact with the development of psychiatric disorders such as schizophrenia and depression (Auer et al., 2012; Egerton and Stone, 2012). In terms of the impact on neurochemistry, the few studies using magnetic resonance spectroscopy (MRS) to measure neurometabolites in humans have reported CB related modulations in glutamate (Glu), creatine (Cr), N-acetylaspartate (NAA), myo-Inositol (mI) and choline (Cho) (Sneider et al., 2013).

CB use impacts an array of neurochemicals with human studies reporting that CB exposure interacts with NAA, Cr, mI and Cho in addition to Glu (Cowan et al., 2009; Sneider et al., 2013; Bitter et al., 2014). For example, in a review Sneider et al. (2013) found that CB users had lower NAA (found in 6 out of 8 studies) than did controls. They also reported that frequency or duration of CB use was associated with lower levels of NAA, Cho and mI. NAA is an indicator of neuronal health (Chawla et al., 2014); therefore, the lower levels of NAA suggest that CB use may have a toxic effect on neurons. Additionally, Hermann et al. (2007) found that recreational male CB users had lower NAA/tCr than control non-users and Yücel et al. (2016) found lower levels of NAA in the hippocampus in CB users. It should be noted that the reports reviewed measured NAA from different brain regions and often reported NAA as a ratio making replication studies important.

As mentioned, CB use, particularly heavy use, has been linked to psychiatric disorders (Moore et al., 2007; Lev-Ran et al., 2014). A meta- analysis of longitudinal studies examining the relationship between CB use and depression found a moderate association between heavy CB use (defined as at least weekly use) and increased risk of developing depression (Lev-Ran et al., 2014). Additionally, a recent study using genome-wide data from the International Cannabis Consortium and the Psychiatric Genomics Consortium (Gage et al., 2017) found a small causal effect of CB use on the development of schizophrenia and a large effect of the reverse – schizophrenia risk predicts CB use. Regardless of the direction of causation, there is a clear relationship between CB use and psychosis.

Neurochemistry may be the key to understanding the relationship between CB use and psychiatric disorders. In a recent review it was found that NAA, Glu and Cr were systematically found to be altered in psychosis patients (Li et al., 2018). Creatine which plays a role in regulating energy metabolism as a neuromodulator has been linked to psychiatric disorders including schizophrenia (Volz et al., 1998; Allen, 2012) and mood disorders (depression and anxiety) (Agren and Niklasson, 1988; Coplan et al., 2006; Mirza et al., 2006; Allen, 2012). NAA is linked to neuronal integrity and mitochondrial dysfunction (Moffett et al., 2007; Larabi et al., 2017). Li et al. (2018) also found in their review that NAA appears to be downregulated in psychosis which they argue is consistent with studies suggesting myelination abnormalities in psychosis (Flynn et al., 2003; Mighdoll et al., 2015). Finally, Glu is the most abundant excitatory neurotransmitter in the brain and has also been linked to psychiatric disorders. For example, a recent study found that ACC Glu levels were higher in symptomatic compared to remitted schizophrenia patients (Egerton and Stone, 2012) while reductions in Glu were found in the ACC of patients with major depression (Auer et al., 2012). In a recent study by Rigucci et al. (2018) examining prefrontal Glu in early psychosis patients who use CB and non-CB users found that Glu was lower in early psychosis users compared to both controls and early psychosis non-users but there were no differences between the non-user early psychosis group and controls. However, a greater decline in Glu with age was found in the early psychosis users compared to the two non-user groups suggesting that CB use may interact with disease progression. In sum, given that CB use has been found previously to be correlated with changes in NAA, Cr and Glu levels and these same neurochemicals are linked to psychiatric disorders, disorders that have also been associated with CB use, it is important to further explore these relationships.

The primary aim of the current study was to examine the relationship between chronic CB use and neurochemistry in humans using MRS. The target of investigation was the dorsal anterior cingulate (dACC) cortex. The ACC has also been found to have high CB1 receptor density (Glass et al., 1997; Tsou et al., 1998) suggesting that CB is likely to have an impact on the processing and neurochemistry of the region. It should also be noted that the ACC is a heterogeneous region with a number of subregions that have different cytoarchitecture and connectivity patterns. The current study focuses on the dACC which has been linked to inhibitory control processes and has been shown previously to have Glu concentration differences in CB users (Prescot et al., 2011, 2013). Additionally, because the region has been examined previously it allows for extension and replication of previous studies.

Differential effects of CB use as a function of sex have been reported previously in humans as well as in animal models (Calakos et al., 2017). For example, male CB users exhibit higher circulating levels of delta9-tetrahydrocannabinol (THC), the psychoactive component of CB (Jones et al., 2013); show larger cardiovascular and subjective effects than female users (Leatherdale et al., 2007); display more withdrawal symptoms; and are less likely to be CB-only users (Hasin et al., 2008). Preclinical studies in rats have found that males are more sensitive to the hyperphagic and hypophagic effects of the CB1 receptor agonists and antagonists, respectively (Diaz et al., 2009) and to their hypothermic and hyperthermic effects (Farhang et al., 2009); females show greater catalepsy, antinociception and locomotor effects (Tseng and Craft, 2004); and decreases in both exploratory behavior and emotionality/anxiety levels (Biscaia et al., 2003). The previous research strongly suggests that females are different from males in their response to cannabinoids. However, there are very few studies examining neurochemical sex differences in humans. Those few studies that examine effects of sex show sex differences. For example, a study examining sex differences in CB users as a secondary aim found that female users had higher levels of mI and lower levels of Glu + glutamine (Glx) in the dorsal striatum than control females, while male users failed to show any effect (Muetzel et al., 2013). Also, Wiers et al. (2016) using PET found that frontal dopamine signaling is impaired in female CB users but not males. A secondary analysis performed in the current study was designed to examine the interaction between sex and CB use on neurochemistry. It was predicted that CB use has a greater impact on female users than male users.

It should be noted that differences in neurochemistry between CB users and non-users in humans have not been consistently observed (Cousijn et al., 2018). For example, in the Sneider et al. (2013) review two of the 8 studies failed to show an effect of CB use on NAA. There are a number of potential explanations for the discrepant findings including that the effects of CB use may be dependent upon age of participants, duration of use, and

brain region examined. An additional explanation for discrepant findings is the variation in the definition of chronic CB use. Currently there is no consistency across studies regarding the CB use criterion within the chronic CB user group [e.g., 10 uses in past 12 months (Wright et al., 2016) to 5 times a week in the past 12 months (Muetzel et al., 2013)]. In the current study we examined whether CB dosage, defined here as monthly instances of use, predicts neurometabolite levels and hypothesized that higher CB use will be correlated with neurometabolite levels.

MATERIALS AND METHODS

Participants

A total of 69 current users and non-users participated in the study. Subjects were recruited by local advertisements. After detailed description of the study, written and verbal informed consent was obtained from each participant. Subjects were asked to refrain from alcohol or CB use the day prior to the MRI scan. This study was carried out in accordance with the recommendations of and approved by Indiana University's Institutional Review Board for the protection of human subjects. All subjects gave written informed consent in accordance with the Declaration of Helsinki.

The exclusion criteria include: younger than 18 years or older than 40; presence of any neurological disorder; history of head trauma with loss of consciousness greater than 10 min; learning disability; diagnosed psychological disorders including major depression, panic disorder, or psychosis; use of illicit drugs (other than CB); alcohol dependence; and contraindication to MRI. For the CB user group an additional exclusion criteria was CB use less than one instance per week.

Participants completed a battery of assessments including the Structured Clinical Interview for DSM-IV-TR (SCID-IV-TR), Research Version (First et al., 2002); a written drug use questionnaire; a 6-month time line follow back assessment to estimate current and past use of CB and alcohol; the short Michigan alcohol screening test (SMAST); Fagerstrom Test for Nicotine Dependence (FTND); and the Wechsler Abbreviated Scale of Intelligence (WASI; Wechsler, 1999). The control subjects had no history of substance dependence, a negative urine screen for CB and other substances, and no use of CB in the past 3 months. Groups did not significantly differ in age, IQ score, sex, days since last alcohol use at the time of screening, or drinks per week ($p > 0.1$). Additionally, when examining just the CB group, there were no sex differences in age, age of CB use onset, monthly CB use, or lifetime CB use ($p > 0.1$); females were similar to males. CB use disorder was not a requirement for the CB user group.[1]

[1]Based on the SCID 10 of the CB users failed to meet criteria for CUD. In order to meet criteria for diagnosis for abuse/dependence participants had to endorse impairment and/or withdrawal symptoms from use. Given that no collateral reports were obtained and that participants often deny or lack insight about potential impairment we argue for the use of amount of use versus diagnostic categorization. Additionally, when comparing the 2 groups of users – those with and without CUD diagnosis – there were no significant or marginally significant group differences for any of the measures with the exception of age of CB initiation (M = 17 for non-CUD; M = 15 for CUD).

MRI Acquisition

Image acquisition was performed on a 3T Siemens Tim-Trio MRI scanner. Foam pads were used to minimize head motion for all participants. High-resolution T1-weighted anatomical images were acquired in the sagittal plane using an MP-RAGE sequence (TR = 1.8 s; TE = 2. 67 ms; inversion time = 0.9 s; flip angle 9°; imaging matrix = 256 × 256; 192 slices; voxel size = 1 × 1 × 1 mm^3). MRS was performed using a single-voxel PRESS sequence (TR/TE = 2000/30 ms, bandwidth = 2000 Hz, 2048 data points, 120 averages, scan time = 4 min), followed by a water reference scan (8 averages). Each voxel measurement began with the FASTMAP shimming method twice (Gruetter, 1993; Gruetter and Tkác, 2000). FASTMAP is a pulse sequence that samples the magnetic field along a group of radial columns and then adjusts the first order and second order shims. Each run of FASTMAP is one iteration. Manual shimming was performed only if FASTMAP did not give a good shimming result. The full width at half maximum (FWHM) of the linewidths of the water peak was all below 14 Hz after these procedures. All scans were visually checked to ensure acceptable MRI quality.

Voxel Placement

The MR spectroscopy voxel was positioned in the dACC using the T1-weighted image. The voxel was positioned in the following way: locate the mid-slice of the corpus callosum on the sagittal slice, then place the voxel directly above the superior and posterior genu of the corpus callosum with the long axis aligned with them (see **Figure 1**). The voxel size was 15 × 20 × 25 mm^3.

MRS Analysis

The MRS data were processed with LCModel (version 6.2-0R)[2] using default settings for water attenuation, estimated water concentration and baseline modeling. LCModel was used to fit each spectrum as a weighted linear combination of a basis set of *in vitro* spectra from individual metabolite solutions. The basis set was provided by LCModel for TE 30 ms and 123 MHz. The water reference signal was used for eddy current correction and scaling the metabolite concentrations. The concentrations of glutamate (Glu), total creatine (tCr), choline (Cho), total *N*-acetylaspartate (tNAA) and myo-inositol (mI) were expressed in institutional units. LCModel also reports an estimated relative standard deviation (%SD) for each fitted component, which is equivalent to the Crame'r-Rao lower bounds (CRLB). Subjects were excluded if the sum of CRLB values of creatine and phosphocreatine was greater than 17%. This threshold was chosen based on the visual check of spectrum quality. It is stricter than that used in the previous literature, which was normally set to 20% for any individual metabolite. As a matter of fact, the CRLB values were all smaller than 20% for Glu and other metabolites for the remaining subjects in our study.

The neurometabolite concentrations were normalized using a method described by Gussew et al. (2012). This method controls for MRS signal differences in tissue composition within the measured voxel across subjects. The high-resolution structural scan acquired to position the voxel during data acquisition was

[2]http://www.s-provencher.com/

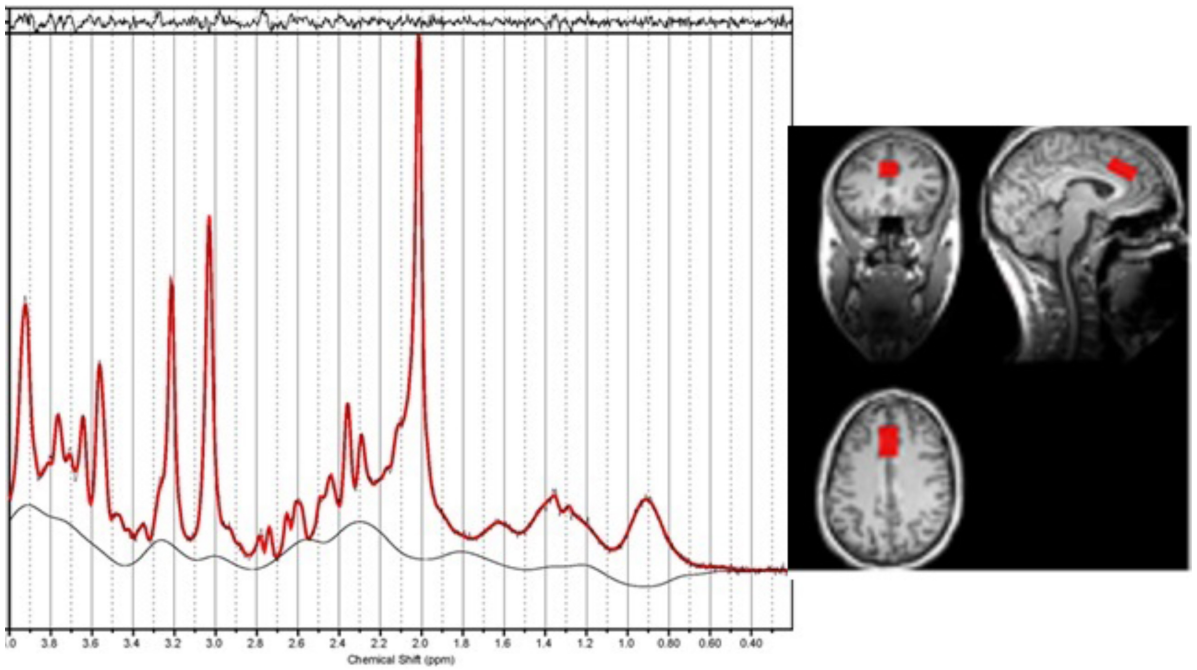

FIGURE 1 | An example of the location of the voxel for Magnetic resonance spectroscopy (MRS) in the dorsal anterior cingulate along with the resultant spectrum processed by LCModel. The fitted spectrum (red) is superimposed on the original spectrum (black); the residual of fitting is on the top while the baseline is at the bottom. The linewidth is 0.033 ppm.

used to determine the tissue composition. The T1-weighted image was segmented for gray matter, white matter, and CSF with SPM12[3]. The corresponding fraction of tissue volumes in the MRS voxel was calculated and used to correct for neurometabolite concentration with respect to heterogeneous tissue compositions according to equation 2 in the paper by Gussew et al. (2012). Additional parameters for the correction included the T1 and T2 relaxation time of water in GM (1.82/0.10 s), WM (1.08/0.07 s), and CSF (4.16/0.50 s) (Lin et al., 2001; Stanisz et al., 2005; Piechnik et al., 2009), relative water contents in GM (0.78), WM (0.65) and CSF (1.0) (Ernst et al., 1993), and T1 and T2 of Glu in the GM (1.27/0.16 s) and WM (1.17/0.17) (Ernst et al., 1993; Mlynárik et al., 2001), respectively. Thus, corrected metabolite concentrations are given in institutional units. Because tCr was found to be predicted by CB use we did not normalize other metabolites to tCr. An analysis examining the ratio of neurometabolites with tCr was performed to make comparisons with previous studies easier. Those results can be found in the **Supplementary Table S7** and **Supplementary Figure S2**.

Statistical Analyses

A correlation analysis was performed to explore the relationship between measures. Secondly, a 2 (group) by 2 (sex) ANOVA was performed on each MRS measure to examine group and sex effects. Finally, a two-step multiple regression analysis was performed with only the CB users to determine the impact of monthly use on metabolite measures. In the first step monthly use, and sex were entered into the model. In the second step the interaction between sex and monthly CB use was included (an analysis with alcohol and nicotine use measures entered in the model can be found in the **Supplementary Material**). Analyses were performed using SAS version 9.4. Multiple comparison correction was performed using Bonferroni correction. For the model statistics an alpha of 0.025 (0.05/2) and for the parameter estimates an alpha of 0.05/#of predictors were used to determine significance.

RESULTS

Of the 69 participants, six were removed due to a history of alcohol use disorder, 4 were removed due to an axis I psychiatric disorder, 2 due to insufficient CB use, 5 due to noisy MRS data, and 2 due to neurological disorders. Data from fifty participants were included in the final analyses – twenty-six current (CB) users and 24 healthy non-user controls (see **Table 1**).

Voxel Tissue Composition

The majority of the MRS voxel was composed of gray matter in both groups. An independent samples *t*-test was performed and the gray matter concentration did not differ between groups (p = 0.75; control group 89% gray matter; user group 85% gray matter). White matter concentration was found to be different between groups with the user group having a larger concentration of white matter (p = 0.04). The tissue fractions

[3]http://www.fil.ion.ucl.ac.uk/spm/software/spm12/

were then used to correct for the concentrations as indicated by Gussew et al. (2012). The analysis was also performed with the ratio of GM/WM included as a covariate (see **Supplementary Table S8**).

Data Quality

The FWHM and S/R from the LCModel Miscellaneous Output are measures of the linewidth and signal-to-noise ratio (SNR) of the *in vivo* spectra. Independent samples *t*-tests were used to examine measures of data quality. No differences were found between the user and control groups in linewidth (p = 0.44; control: 0.0347 ± 0.0042; CB: 0.0335 ± 0.006) or SNR (p = 0.63; control: 63.8 ± 10.1; CB: 62.6 ± 7.5).

Correlation Analyses

The correlation results are shown in **Tables 2**, **3**. As shown, the CB user group shows significant positive correlations between tNAA and tCr, Glu and mI while the control group does not show such significant correlations between those metabolites. Additionally, in the CB user group there is a negative correlation between monthly CB use and drinks per week such that those who drink more use CB less.

TCr

The ANOVA failed to show an effect of group or sex ($F < 1$); additionally the interaction was also not significant [$F(1,49) = 1.87$, $p = 0.18$]. Both regression models were significant (see **Table 4** and **Figure 2**). CB monthly use significantly predicted tCr levels in both the model with and without the interaction term. Sex was marginally significant in the model without the interaction term but significant in the model with the term.

TABLE 1 | Demographics.

	Controls	CB Users
N	24	26
#Males	10	10
Age	21.5 ± 2.3 (18–26 years)	21.4 ± 4.5 (18–39 years)
Age of CB initiation	n/a	16.4 ± 2.5 years
Average monthly CB use		33.1 ± 27.2 instances/month*
	0	19.7 ± 9.1 days/month*
Lifetime CB use (instances)	1 ± 2.7	1442.1 ± 2115.5*
Average days since last CB use (prior to scan)	n/a	1 ± 1.8 days
Average days since last alcohol use (prior to scan)	138.9 ± 403.2	22.2 ± 59.4
Average drinks per week	2.2 ± 2.9	3.3 ± 3.2
FNTD	0 ± 0	0.77 ± 0.27
% have used nicotine in month prior to scan	4%	19%
WASI	113.7 ± 11.1	110.7 ± 9.2

** indicates significant difference between CB users and controls, based on 2-tailed t-test.*

Glu

The ANOVA failed to show an effect of group or sex ($F < 1$); additionally the interaction was also not significant [$F(1,49) = 2.53$, $p = 0.12$]. Both regression failed to reach significance (see **Table 5** and **Figure 2**). When examining each predictor variable the parameter estimate for monthly use appears to be modulated by the introduction of the interaction term to the model (although the factor is not significant when corrected for multiple comparisons) suggesting that the effect of monthly CB use is different for males and females. However, these results should be interpreted with great caution given the small sample size and small effect size.

tNAA

The ANOVA failed to show an effect of group or an interaction between group and sex ($F < 1$). However, there was a significant effect of sex [$F(1,49) = 7.44$, $p = 0.009$]; females had a higher level of tNAA than did males. Neither regression model was significant (see **Supplementary Table S5**, **Supplementary Figure S1**, and **Figure 2**). When examining the predictor variables sex approached significance.

mI

The ANOVA failed to show an effect of group or sex ($F < 1$); additionally the interaction was also not significant [$F(1,49) = 2.7$, $p = 0.11$]. Neither regression model was significant (see **Supplementary Tables S1, S4**, **Supplementary Figure S1**, and **Figure 2**).

TABLE 2 | Correlation analysis for control group.

	CBmonth	Drinks	FNTD	tCr	Glu	tNAA	mI	Cho
CBmonth	.	.	.	.	.	.	.	.
drinks		1	.	0.24	0.04	−0.17	0.14	0.04
FNTD				.	.	.	.	.
tCr				1	0.02	0.18	**0.45**	0.39
Glu					1	−0.3	0.14	−0.3
tNAA						1	0.04	0.09
mI							1	**0.55**
Cho								1

Bolded values indicate statistical significance.

TABLE 3 | Correlation analysis for CB user group.

	CBmonth	Drinks	FNTD	tCr	Glu	tNAA	mI	Cho
CBmonth	1	**−0.55**	−0.26	**0.47**	0.25	0.34	0.28	0.09
drinks		1	−0.17	−0.12	−0.23	0.02	−0.13	−0.16
FNTD			1	−0.21	−0.04	−0.36	0.16	−0.005
tCr				1	0.38	**0.66**	**0.4**	0.29
Glu					1	**0.46**	**0.49**	−0.09
tNAA						1	**0.61**	0.22
mI							1	0.38
Cho								1

Bolded values indicate statistical significance.

TABLE 4 | Regression analysis with tCr as the dependent variable for the CB users only.

Variable	DF	Parameter estimate	Standard error	*t*	Pr > |*t*|	Standardized estimate	Variance inflation	95% Confidence limits	
Without interaction term: F(2,26) = *7.16*, p = *0.0036*, R^2 = *0.37*, Bayes Factor = *6.58*									
Sex	1	−0.16	0.072	−2.32	***0.029***	−0.38	1.01	−0.32	−0.018
CBmonth	1	0.0037	0.0011	3.23	**0.0035**	0.53	1.01	0.0013	0.006
With the interaction term: F(3,23) = *5.43*, p = *0.0057*, R^2 = *0.4145*, Bayes Factor = *3.1*									
Sex	1	−0.22	0.83	−2.66	**0.014**	−0.50	1.36	−0.39	−0.049
CBmonth	1	0.003	0.0013	2.42	***0.024***	0.43	1.24	0.00043	0.0056
CBmonth*Sex	1	0.0034	0.0027	1.27	0.22	0.26	1.64	−0.0022	0.009

Bolded values indicate statistical significance.

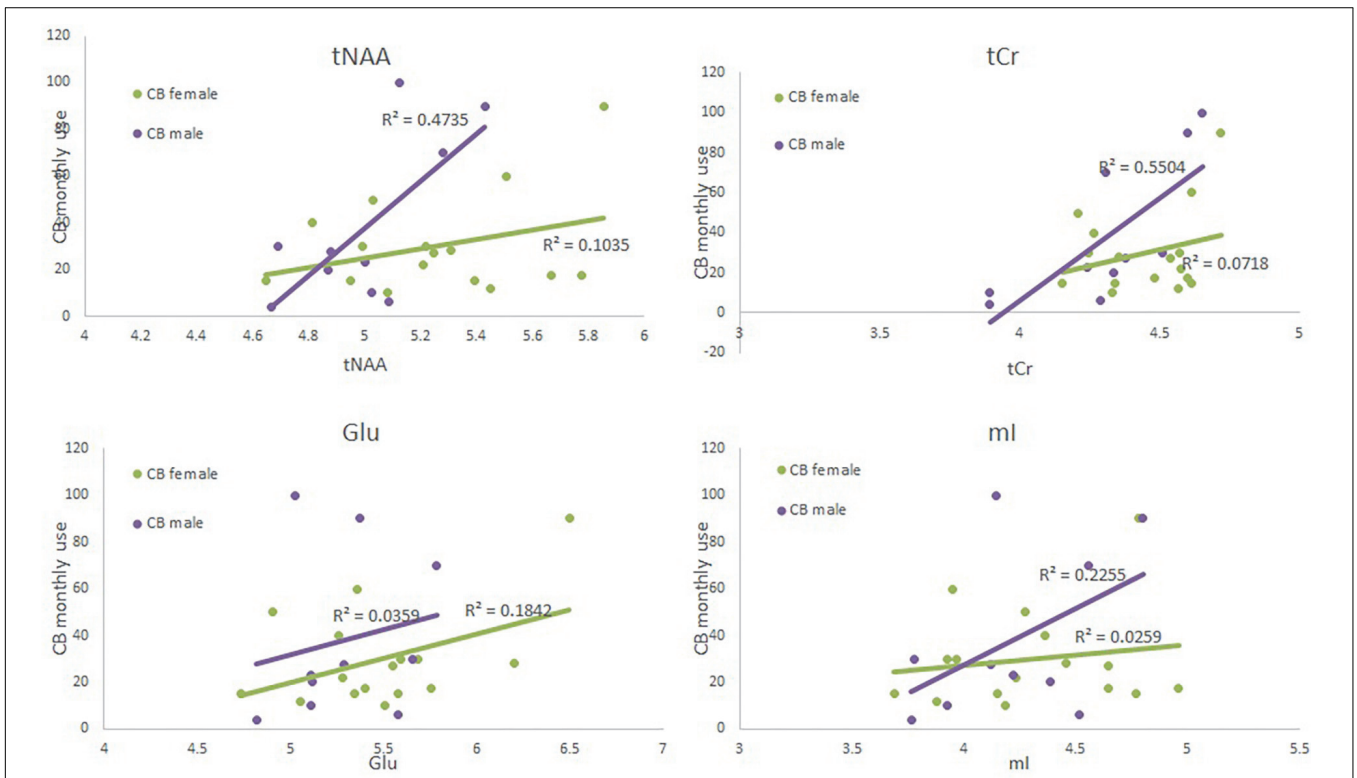

FIGURE 2 | Scatter plots depicting each neurometabolite level (*x*-axis), monthly CB use (*y*-axis) and sex (green = CB user females, and purple = CB user male4).

Cho

The ANOVA failed to show an effect of group [$F(1,49) = 2.12$, $p = 0.15$], sex ($F < 1$), or an interaction [$F(1,49) = 1.01$, $p = 0.32$]. Neither regression model was significant (see **Supplementary Table S6** and **Supplementary Figure S1**).

DISCUSSION

The goal of the current study was to examine the relationship between chronic CB use and neurochemistry in humans. Neurometabolite concentrations in the dACC were measured using MRS. Unlike in some previous studies, the current study failed to show significant differences between the control and CB user group. However, when using regression models to examine the factors that may contribute to the variance in neurometabolite concentrations within the CB user group two major observations were reported. First, monthly CB use consistently predicted total creatine in the CB user group regardless of the other factors entered into the regression model. Second, sex was a consistent predictor of total NAA in the CB group and it was a significant factor in the ANOVA.

Total creatine is considered to have stable concentrations and, as mentioned above, has been widely used as an internal reference such that many MRS studies report concentrations of other metabolites as a ratio of tCr. In the current study, tCr was consistently found to be predicted by monthly CB use regardless of the other measures included in the regression model. The finding that tCr is modulated by CB use has been reported previously (Prescot et al., 2011). Prescot et al. (2011) found

TABLE 5 | Regression analysis with Glu as the dependent variable for the CB users only.

Variable	DF	Parameter estimate	Standard error	*t*	Pr > |*t*|	Standardized estimate	Variance inflation	95% Confidence limits	
Without interaction term: F(2,24) = *2.31*, p = *0.12*, R^2 = *0.16*, Bayes Factor = *0.21*									
Sex	1	−0.23	0.15	−1.49	0.15	−0.28	1.0	−0.54	0.087
CBmonth	1	0.0041	0.0024	1.7	0.1	0.32	1.0	−0.00087	0.009
With the interaction term: F(3,23) = *2.08*, p = *0.13*, R^2 = *0.21*, Bayes Factor = *0.12*									
Sex	1	−0.12	0.18	−0.67	0.51	−0.15	1.36	−0.48	0.24
CBmonth	1	0.0055	0.0026	2.08	***0.048***	0.43	1.24	0.000043	0.011
Sex*CBmonth	1	−0.007	0.0057	−1.23	0.23	−0.29	1.64	−0.019	0.0048

Bolded values indicate statistical significance.

that tCr levels decreased in adolescent CB users compared to controls. As a result of this modulation of tCr by CB use the measures presented in the current study were not normalized to it and instead all measures were normalized to tissue water and corrected for tissue composition.

Recently it has been reported that Cr has neuroprotective properties with it potentially being used to treat a number of disorders. For example, Cr was given to children and adolescents with traumatic brain injury and was shown to improve cognitive performance (Sakellaris et al., 2006). Creatine kinase and its substrates creatine and phosphocreatine are part of the cellular energy buffering and transport system that connects sites of energy production (mitochondria) to sites of energy consumption (Hemmer and Wallimann, 1993). Previous studies have found that Cr administration increases brain concentrations of phosphocreatine and inhibits mitochondrial permeability transition, both of which may exert neuroprotective effects (Hemmer and Wallimann, 1993; O'Gorman et al., 1996; Ferrante et al., 2000). Phosphocreatine has also been found to stimulate synaptic Glu uptake, reducing extracellular Glu (Xu et al., 1996), thereby providing an additional neuroprotective pathway. Another potential neuroprotective mechanism of Cr is related to its relationship with NAA. Ferrante et al. (2000) found a correlation between Cr and NAA in Cr treated transgenic Huntington's mice but not untreated mice. NAA has been shown previously to be an indicator of neuronal health (Chawla et al., 2014). Interestingly, in the current study a positive correlation between tNAA and tCr was found for the CB users (r = 0.66) but not the controls (r = 0.18). Although the variance in both tNAA and tCr in the CB user group can be explained partially by CB monthly use, the correlation between tNAA and tCr remains significant when partialing out the impact of monthly CB use (r = 0.6, p = 0.001). These results suggest that the young adult users examined in this study may have increased brain concentrations of tCr as a mechanism to protect itself from damage caused by an increase in exogenous cannabinoids. This is different from the results reported by Prescot et al. (2011) which shows that adolescents show decreases in tCr. This discrepancy may be due to differences in the subject population. The population examined in this study is a high functioning chronic CB user group with normal to high IQ. Further studies examining how age of CB initiation, cognitive capacity and years of use may interact with tCr are necessary.

A second finding of the study is a sex differences in tNAA levels such that women had a higher level of tNAA than men. While there are few studies examining sex differences in tNAA one recent study reported similar results. Silaidos et al. (2018) examined NAA as a proxy for mitochondrial dysfunction. There they found that female participants had higher NAA levels in both gray and white matter than male participants did; a similar finding to that reported in the current study. While there was no interaction between sex and CB use for the NAA measure, this sex difference and how it may interact with the effects of CB use warrants further study.

Glutamate is one of the brain's primary excitatory neurotransmitters whose concentration is tightly controlled due to its potential toxic properties. Although previous studies have found a relationship between CB use and Glu the current study failed to show a strong effect. However, the results do advocate for future studies with a much larger sample size in order to fully explore factors that may interact with the relationship between CB use and Glu levels. For example, the current results show that monthly CB use begins to approach significance when the interaction between monthly use and sex is included in the model suggesting that Glu levels may be dependent on the amount of CB use and that the relationship between Glu and CB use may be modulated by sex. The potential influence of sex on the relationship between CB dose and Glu levels support previous reports in preclinical studies and previous studies in humans by Muetzel et al. (2013) and Prescot et al. (2011). In fact, Prescot et al. (2011) had a very similar result in that the effect of Glu was increased when sex was included in the model. Again, while the interpretation of this effect should be considered with caution, they clearly indicate a direction for future research.

In addition, more fully examining the interaction between CB use and other substance use including alcohol and nicotine on neurometabolite levels is important. The current study attempted to control for the use of other substances, however, both alcohol and nicotine are used in higher rates in the CB user population than the non-user in the current study. Additionally, a recent study by Schulte et al. (2017) found that differences in dACC Glx (glutamate + glutamine) were not dependent on the type of substance used whether it be nicotine or polysubstance users.

It should be noted that our results are contradictory to those reported previously by Prescot et al. (2011) and Muetzel et al. (2013) in that both of these previous studies reported a decrease

in neurometabolite levels in the ACC of adolescents and in the striatum of college-aged individuals, respectively, while we show increases in college-aged individuals. There are a number of reasons for these discrepant results. First, most studies, including Muetzel et al. (2013), use tCr to normalize neurometabolite concentrations and report a ratio with tCr. Because we observed CB effects of tCr we do not report concentrations in terms of a ratio. Second, in the current study we normalized the differing effects of gray and white matter on the MRS signal which was not performed in the previous studies. Finally, there were differences in the LCModel processing and the version of the software used to perform quantification. For instance, the analysis window was set to 0.2–4.0 ppm in our study in contrast to 0.5–4.5 ppm by Prescot et al. (2011, 2013). The latter three reasons may account for different results even using the ratio to tCr (**Supplementary Table S7** and **Supplementary Figure S2**). These differences in the analysis makes direct comparison across studies difficult. Even with these differences, the relationship between CB use and sex are very similar across studies.

Limitations

The results presented should be interpreted with caution. There were some limitations regarding the participants. The number of participants, while larger than some previous studies, is rather small, particularly when examining the effect of current CB use and sex. In addition, the results of the current study suggest that a larger sample size with a range of CB use levels (dosage) as well as better characterization of CB use is necessary to characterize the impact of CB on neurochemistry. Again, although we do not have adequate power to properly address our research questions we do feel that the study is important in that it clearly directs future work and highlights the importance of fully characterizing and controlling factors such as sex and CB dose.

Currently there is no consistency across studies regarding the CB use criterion within the chronic CB user group. The concentration of THC being consumed is not controlled in human studies as it is in preclinical studies making it impossible to control dose. The results reported in the current study demonstrate that the amount of CB use is an important factor to consider when characterizing the impact of CB on neurochemistry. In the current study there was a wide range of monthly CB use with the monthly use having a standard deviation of 27 instances per month. As expected the range of lifetime use is also large with few participants on the far end of the use spectrum. It will be important in future research to ensure an equal distribution of dose in order to examine its effect on neurochemistry.

Another source of variation across studies regarding CB consumption is variability of THC content across geographic regions. The THC products available vary across different regions of the country which likely impact the effects of CB use on neural processing. Unfortunately, we were unable to determine the THC content of the products used by our study participants. However, future studies should consider this issue.

Cannabis use tends to be co-morbid with some psychological disorders like depression and anxiety (Auer et al., 2012) as well as with the use of other drugs like alcohol and nicotine (Blanco et al., 2018). Also, these co-morbidities may also interact with neurochemistry making it difficult to determine the relationship between CB use and brain function, structure and neurochemistry. In the current study we have attempted to control for other substance use and psychological disorders. However, while there are no statistically significant differences between groups it is still possible that they may interact with brain processing differently in the two groups. This requires more extensive research examining poly-substance users as well as those with psychological disorders.

Magnetic resonance spectroscopy is a non-invasive technique that allows for the measurement of a number of molecules including Glu. Glutamate levels in humans have been reliably reported at 3T (Hurd et al., 2004; Cohen-Gilbert et al., 2014; Yasen et al., 2017). While sophisticated 3D MRS sequences are available, single voxel MRS allows for a focus on discreet regions with the higher spatial and spectral resolution necessary for regions with susceptibility issues related to field inhomogeneities like those close to the sinuses (Cohen-Gilbert et al., 2014) (e.g., the nucleus accumbens). The measurement of Glu is complicated by the overlapping resonances of glutamine (Gln). There is some debate as to whether Glu can be reliably separated from Gln at 3T (Mayer and Spielman, 2005; Wijtenburg and Knight-Scott, 2011; Ende, 2015) and it is very likely that our Glu measurements are contaminated by Gln. Also, while MRS technology has advanced to the point that neurometabolites can be reliably measured in humans making it a powerful tool in the study of addiction, the metabolite levels measured by MRS include both intracellular and extracellular components. This is different from methods used in preclinical studies; microlysis in animal studies primarily measure extracellular concentrations. This difference in measures makes the direct comparison to the preclinical literature difficult.

CONCLUSION

Cannabis (CB) use is becoming more prevalent with it being legalized for recreational use in a number of states across the United States and countries around the world. Therefore, it is increasingly important to characterize the effect of CB use on brain chemistry, structure and function as it impacts the behavioral and cognitive consequences of use. The current study, even with its limitations, shows that chronic CB use is related to differences in brain chemistry and that those differences may be affected by sex and dose. Understanding these sex differences may be important in the design and implementation of prevention and treatment programs for young users. Additionally, there is the potential to use cannabinoid agonists or antagonists for the treatment of neuropathic pain, glaucoma, multiple sclerosis, migraine, movement disorders and eating/appetite disorders; therefore, understanding the sex differences in cannabinoid pharmacological effects is necessary. Future studies designed to fully characterize the impact of chronic CB use on neurochemistry that accounts for CB dose including THC content, sex, age, age of CB initiation and use of other substances are essential to developing an accurate model of the interaction of CB use and brain chemistry.

DATA AVAILABILITY

The datasets generated for this study are available on request to the corresponding author.

ETHICS STATEMENT

The research protocol was approved by Indiana University's Institutional Review Board for the protection of human subjects.

AUTHOR CONTRIBUTIONS

SN wrote the manuscript and designed the study. HC was responsible for data analysis and quality. AS was involved in data acquisition, subject recruitment and data management. UD assisted with MRS protocol development and analysis. SD assisted with MRS protocol development. WH contributed to study design. BO'D was involved in the study design.

FUNDING

This study was supported by the National Institute on Drug Abuse (NIDA) Grant #5R21DA035493 (BFO/SDN), the National Institute of Mental Health (NIMH) Grant #2R01MH074983 (WPH), a National Science Foundation Graduate Research Fellowship Grant #1342962 (AMSM), NIDA T32 Predoctoral Fellowship Grant #T32DA024628 (AMSM) and NIDA 1R01DA048012-01 (WPH). Any opinions, findings, and conclusions or recommendations expressed in this material are those of the authors and do not necessarily reflect the views of the NIDA, NIMH, or the National Science Foundation.

SUPPLEMENTARY MATERIAL

The Supplementary Material for this article can be found online at: https://www.frontiersin.org/articles/10.3389/fnhum.2019.00318/full#supplementary-material

REFERENCES

Agren, H., and Niklasson, F. (1988). Creatinine and creatine in CSF: indices of brain energy metabolism in depression. *J. Neural. Transm.* 74, 55–59. doi: 10.1007/bf01243575

Allen, P. J. (2012). Creatine metabolism and psychiatric disorders: does creatine supplementation have therapeutic value? *Neurosci. Biobehav. Rev.* 36, 1442–1462. doi: 10.1016/j.neubiorev.2012.03.005

Auer, D. P., Pütz, B., Kraft, E., Lipinski, B., Schill, J., and Holsboer, F. (2012). Reduced glutamate in the anterior cingulate cortex in depression: an *in vivo* proton magnetic resonance spectroscopy study. *Biol. Psychiatry* 47, 305–313. doi: 10.1016/s0006-3223(99)00159-6

Biscaia, M., Marín, S., Fernández, B., Marco, E. M., Rubio, M., Guaza, C., et al. (2003). Chronic treatment with CP 55,940 during the peri-adolescent period differentially affects the behavioural responses of male and female rats in adulthood. *Psychopharmacology* 170, 301–308. doi: 10.1007/s00213-003-1550-7

Bitter, S. M., Weber, W. A., Chu, W. J., Adler, C. M., Eliassen, J. C., Strakowski, S. M., et al. (2014). N-acetyl aspartate levels in adolescents with bipolar and/or cannabis use disorders. *J. Dual Diagn.* 10, 39–43. doi: 10.1080/15504263.2013.869077

Blanco, C., Flórez-Salamanca, L., Secades-Villa, R., Wang, S., and Hasin, D. S. (2018). Predictors of initiation of nicotine, alcohol, cannabis, and cocaine use: results of the National Epidemiologic Survey on Alcohol and Related Conditions (NESARC). *Am. J. Addict.* 27, 477–484. doi: 10.1111/ajad.12764

Brown, T. M., Brotchie, J. M., and Fitzjohn, S. M. (2003). Cannabinoids decrease corticostriatal synaptic transmission via an effect on glutamate uptake. *J. Neurosci.* 23, 11073–11077. doi: 10.1523/jneurosci.23-35-11073.2003

Calakos, K. C., Bhatt, S., Foster, D. W., and Cosgrove, K. P. (2017). Mechanisms underlying sex differences in cannabis use. *Cur. Addict. Rep.* 4, 439–453. doi: 10.1007/s40429-017-0174-7

Chawla, S., Wang, S., Kim, S., Sheriff, S., Lee, P., Rengan, R., et al. (2014). Radiation injury to the normal brain measured by 3D-Echo-planar spectroscopic imaging and diffusion tensor imaging: initial experience. *J. Neuroimaging* 25, 97–104. doi: 10.1111/jon.12070

Cohen-Gilbert, J. E., Jensen, J. E., and Silveri, M. M. (2014). Contributions of magnetic resonance spectroscopy to understanding development: potential applications in the study of adolescent alcohol use and abuse. *Dev. Psychopathol.* 26, 405–423. doi: 10.1017/S0954579414000030

Colizzi, M., McGuire, P., Pertwee, R. G., and Bhattacharyya, S. (2016). Effect of cannabis on glutamate signalling in the brain: a systematic review of human and animal evidence. *Neurosci. Biobehav. Rev.* 64, 359–381. doi: 10.1016/j.neubiorev.2016.03.010

Coplan, J. D., Mathew, S. J., Mao, X., Smith, E. L., Hof, P. R., Coplan, P. M., et al. (2006). Decreased choline and creatine concentrations in centrum semiovale in patients with generalized anxiety disorder: relationship to IQ and early trauma. *Psychiatry Res. Neuroimaging* 147, 27–39. doi: 10.1016/j.pscychresns.2005.12.011

Cousijn, J., Núñez, A. E., and Filbey, F. M. (2018). Time to acknowledge the mixed effects of cannabis on health: a summary and critical review of the NASEM 2017 report on the health effects of cannabis and cannabinoids. *Addiction* 113, 958–966. doi: 10.1111/add.14084

Cowan, R. L., Joers, J. M., and Dietrich, M. S. (2009). N-acetylaspartate (NAA) correlates inversely with cannabis use in a frontal language processing region of neocortex in MDMA (Ecstasy) polydrug users: a 3 T magnetic resonance spectroscopy study. *Pharmacol. Biochem. Behav.* 92, 105–110. doi: 10.1016/j.pbb.2008.10.022

Diaz, S., Farhang, B., Hoien, J., Stahlman, M., Adatia, N., Cox, J. M., et al. (2009). Sex differences in the cannabinoid modulation of appetite, body temperature and neurotransmission at POMC synapses. *Neuroendocrinology* 89, 424–440. doi: 10.1159/000191646

Egerton, A., and Stone, J. M. (2012). The glutamate hypothesis of schizophrenia: neuroimaging and drug development. *Curr. Pharm. Biotechnol.* 13, 1500–1512. doi: 10.2174/138920112800784961

Ende, G. (2015). Proton magnetic resonance spectroscopy: relevance of glutamate and GABA to neuropsychology. *Neuropsychol. Rev.* 25, 315–325. doi: 10.1007/s11065-015-9295-8

Ernst, T., Kreis, R., and Ross, B. (1993). Absolute quantitation of water and metabolites in the human brain I Compartments and water. *J. Magn. Reson. B* 102, 1–8. doi: 10.1006/jmrb.1993.1055

Farhang, B., Diaz, S., Tang, S. L., and Wagner, E. J. (2009). Sex differences in the cannabinoid regulation of energy homeostasis. *Psychoneuroendocrinology* 34, S237–S246. doi: 10.1016/j.psyneuen.2009.04.007

Ferrante, R. J., Andreassen, O. A., Jenkins, B. G., Dedeoglu, A., Kuemmerle, S., Kubilus, J. K., et al. (2000). Neuroprotective effects of creatine in a transgenic mouse model of Huntington's disease. *J. Neurosci.* 20, 4389–4397. doi: 10.1523/jneurosci.20-12-04389.2000

First, M. B., Spitzer, R. L., Gibbon, M., and Williams, J. B. W. (2002). *Structured Clinical Interview for DSM-IV-TR Axis I Disorders - Non-patient Edition (SCID-I/NP 1/2010 revision)*. New York, NY: Biometrics Research Department New York State Psychiatric Institute.

Flynn, S. W., Lang, D. J., Mackay, A. L., Goghari, V., Vavasour, I. M., Whittall, K. P., et al. (2003). Abnormalities of myelination in schizophrenia detected *in vivo*

with MRI, and post-mortem with analysis of oligodendrocyte proteins. *Mol. Psychiatry* 38, 811–820. doi: 10.1038/sj.mp.4001337

Gage, S. H., Jones, H. J., Burgess, S., Bowden, J., Davey Smith, G., Zammit, S., et al. (2017). Assessing causality in associations between cannabis use and schizophrenia risk: a two-sample Mendelian randomization study. *Psychol. Med.* 47, 971–980. doi: 10.1017/S0033291716003172

Glass, M., Faull, R. L. M., and Dragunow, M. (1997). Cannabinoid receptors in the human brain: a detailed anatomical and quantitative autoradiographic study in the fetal neonatal and adult human brain. *Neuroscience* 77, 299–318. doi: 10.1016/s0306-4522(96)00428-9

Grucza, R. A., Agrawal, A., Krauss, M. J., Cavazos-Rehg, P. A., and Bierut, L. J. (2016). Recent trends in the prevalence of marijuana use and associated disorders in the United States. *JAMA Psychiatry.* 73, 300–301.

Gruetter, R. (1993). Automatic localized in Vivo adjustment of all first-and second-order shim coils. *Magn. Reson. Med.* 29, 804–811. doi: 10.1002/mrm.1910290613

Gruetter, R., and Tkác, I. (2000). Field mapping without reference scan using asymmetric echo-planar techniques. *Magn. Reson. Med.* 43, 319–323. doi: 10.1002/(sici)1522-2594(200002)43:2<319::aid-mrm22>3.0.co;2-1

Gussew, A., Erdtel, M., Hiepe, P., Rzanny, R., and Reichenbach, J. R. (2012). Absolute quantitation of brain metabolites with respect to heterogeneous tissue compositions in 1H-MR spectroscopic volumes. *MAGMA* 25, 321–333. doi: 10.1007/s10334-012-0305-z

Hasin, D. S., Keyes, K. M., Alderson, D., Wang, S., Aharonovich, E., and Grant, B. F. (2008). Cannabis withdrawal in the United States: a general population study. *J. Clin. Psychiatry* 69, 1354–1363. doi: 10.4088/jcp.v69n0902

Hemmer, W., and Wallimann, T. (1993). Functional aspects of creatine kinase in brain. *Dev. Neurosci.* 15, 249–260. doi: 10.1159/000111342

Hermann, D., Sartorius, A., Welzel, H., Walter, S., Skopp, G., Ende, G., et al. (2007). Dorsolateral prefrontal cortex N-acetylaspartate/total creatine (NAA/tCr) loss in male recreational cannabis users. *Biol. Psychiatry* 61, 1281–1289. doi: 10.1016/j.biopsych.2006.08.027

Hurd, R., Sailasuta, N., Srinivasan, R., Vigneron, D. B., Pelletier, D., and Nelson, S. J. (2004). Measurement of brain glutamate using TE-averaged PRESS at 3T. *Magn. Reson. Med.* 51, 435–440. doi: 10.1002/mrm.20007

Jones, J., Mosher, W., and Daniels, K. (2013). "Current contraceptive use in the united states, 2006-2010, and changes in patterns of use since 1995," in *Sexual Statistics: Select Reports from the National Center for Health Statistics*, ed. E. A. Thomas, (New York, NY: Nova Science Publishers, Inc.).

Larabi, D. I., Liemburg, E. J., Pijnenborg, G. H., Sibeijn-Kuiper, A., de Vos, A. E., and Bais, L. (2017). Association between prefrontal N-acetylaspartate and insight in psychotic disorders. *Schizophrenia Res.* 179, 112–118. doi: 10.1016/j.schres.2016.09.018

Leatherdale, S. T., Hammond, D. G., Kaiserman, M., and Ahmed, R. (2007). Marijuana and tobacco use among young adults in Canada: are they smoking what we think they are smoking? *Cancer Causes Control* 18, 391–397. doi: 10.1007/s10552-006-0103-x

Lev-Ran, S., Roerecke, M., Le Foll, B., George, T. P., McKenzie, K., and Rehm, J. (2014). The association between cannabis use and depression: a systematic review and meta-analysis of longitudinal studies. *Psychol. Med.* 44, 797–810. doi: 10.1017/S0033291713001438

Li, C., Wang, A., Wang, C., Ramamurthy, J., Zhang, E., Guadagno, E., et al. (2018). Metabolomics in patients with psychosis: a systematic review. *Am. J. Med. Genet. Part B Neuropsychiatr. Genet.* 177, 580–588. doi: 10.1002/ajmg.b.32662

Lin, C., Bernstein, M., Huston, J., and Fain, S. (2001). Measurements of T1 relaxation times at 30: implications for clinical MRA. *Proc. Int. Soc. Magn. Reson. Med.* 9:1391.

Mayer, D., and Spielman, D. M. (2005). Detection of glutamate in the human brain at 3 T using optimized constant time point resolved spectroscopy. *Magn. Reson. Med.* 54, 439–442. doi: 10.1002/mrm.20571

Mighdoll, M. I., Tao, R., Kleinman, J. E., and Hyde, T. M. (2015). Myelin, myelin-related disorders, and psychosis. *Schizophrenia Res.* 161, 85–93. doi: 10.1016/j.schres.2014.09.040

Mirza, Y., O'neill, J., Smith, E. A., Russell, A., Smith, J. M., Banerjee, S. P., et al. (2006). Increased medial thalamic creatine-phosphocreatine found by proton magnetic resonance spectroscopy in children with obsessive-compulsive disorder versus major depression and healthy controls. *J. Child Neurol.* 21, 106–111. doi: 10.1177/08830738060210020201

Mlynárik, V., Gruber, S., and Moser, E. (2001). Proton T1 and T2 relaxation times of human brain metabolites at 3 Tesla. *NMR Biomed.* 14, 325–331.

Moffett, J. R., Ross, B., Arun, P., Madhavarao, C. N., and Namboodiri, A. M. (2007). N-Acetylaspartate in the CNS: from neurodiagnostics to neurobiology. *Prog. Neurobiol.* 81, 89–131. doi: 10.1016/j.pneurobio.2006.12.003

Moore, T. H., Zammit, S., Lingford-Hughes, A., Barnes, T. R., Jones, P. B., Burke, M., et al. (2007). Cannabis use and risk of psychotic or affective mental health outcomes: a systematic review. *Lancet* 370, 319–328. doi: 10.1016/s0140-6736(07)61162-3

Muetzel, R. L., Marjaska, M., Collins, P. F., Becker, M., Valabrègue, R., Auerbach, E. J., et al. (2013). In vivo 1 H magnetic resonance spectroscopy in young-adult daily marijuana users. *Neuroimage Clin.* 2, 581–589. doi: 10.1016/j.nicl.2013.04.011

O'Gorman, E., Beutner, G., Wallimann, T., and Brdiczka, D. (1996). Differential effects of creatine depletion on the regulation of enzyme activities and on creatine-stimulated mitochondrial respiration in skeletal muscle heart and brain. *Biochim. Biophys. Acta BBA Bioenerget.* 1276, 161–170. doi: 10.1016/0005-2728(96)00074-6

Piechnik, S. K., Evans, J., Bary, L. H., Wise, R. G., and Jezzard, P. (2009). Functional changes in CSF volume estimated using measurement of water T2 relaxation. *Magn Reson Med.* 61, 579–586. doi: 10.1002/mrm.21897

Prescot, A. P., Locatelli, A. E., Renshaw, P. F., and Yurgelun-Todd, D. A. (2011). Neurochemical alterations in adolescent chronic marijuana smokers: a proton MRS study. *Neuroimage.* 57, 69–75. doi: 10.1016/j.neuroimage.2011.02.044

Prescot, A. P., Renshaw, P. F., and Yurgelun-Todd, D. A. (2013). Amino butyric acid and glutamate abnormalities in adolescent chronic marijuana smokers. *Drug Alcohol Depend* 129, 232–239. doi: 10.1016/j.drugalcdep.2013.02.028

Rigucci, S., Xin, L., Klauser, P., Baumann, P. S., Alameda, L., Cleusix, M., et al. (2018). Cannabis use in early psychosis is associated with reduced glutamate levels in the prefrontal cortex. *Psychopharmacology* 235, 13–22. doi: 10.1007/s00213-017-4745-z

Sakellaris, G., Kotsiou, M., Tamiolaki, M., Kalostos, G., Tsapaki, E., Spanaki, M., et al. (2006). Prevention of complications related to traumatic brain injury in children and adolescents with creatine administration: an open label randomized pilot study. *J. Trauma Acute Care Surg.* 61, 322–329. doi: 10.1097/01.ta.0000230269.46108.d5

Schulte, M. H., Kaag, A. M., Wiers, R. W., Schmaal, L., van den Brink, W., Reneman, L., et al. (2017). Prefrontal Glx and GABA concentrations and impulsivity in cigarette smokers and smoking polysubstance users. *Drug Alcohol Depend* 179, 117–123. doi: 10.1016/j.drugalcdep.2017.06.025

Silaidos, C., Pilatus, U., Grewal, R., Matura, S., Lienerth, B., Pantel, J., et al. (2018). Sex-associated differences in mitochondrial function in human peripheral blood mononuclear cells (PBMCs) and brain. *Biol. Sex Differ.* 9:34. doi: 10.1186/s13293-018-0193-7

Sneider, J. T., Mashhoon, Y., and Silveri, M. M. (2013). A review of magnetic resonance spectroscopy studies in marijuana using adolescents and adults. *J. Addict. Res. Ther. Suppl.* 4:010.

Stanisz, G. J., Odrobina, E. E., Pun, J., Escaravage, M., Graham, S. J., Bronskill, M. J., et al. (2005). T1 T2 relaxation and magnetization transfer in tissue at 3T. *Magn Reson Med.* 54, 507–512. doi: 10.1002/mrm.20605

Tseng, A. H., and Craft, R. M. (2004). CB1 receptor mediation of cannabinoid behavioral effects in male and female rats. *Psychopharmacology* 172, 25–30. doi: 10.1007/s00213-003-1620-x

Tsou, K., Brown, S., Sanudo-Pena, M. C., Mackie, K., and Walker, J. M. (1998). Immunohistochemical distribution of cannabinoid CB1 receptors in the rat central nervous system. *Neuroscience* 83, 393–411. doi: 10.1016/s0306-4522(97)00436-3

Volz, H. P., Rzanny, R., Riehemann, S., May, S., Hegewald, H., Preussler, B., et al. (1998). 31 P magnetic resonance spectroscopy in the frontal lobe of major depressed patients. *Eur. Arch. Psychiatry Clin. Neurosci.* 248, 289–295. doi: 10.1007/s004060050052

Wechsler, D. (1999). *Wechsler Abbreviated Intelligence Scale*. San Antonio, TX: The Psychological Corporation.

Wiers, C. E., Shokri-Kojori, E., Wong, C. T., Abi-Dargham, A., Demiral, Ş. B., Tomasi, D., et al. (2016). Cannabis abusers show hypofrontality and

blunted brain responses to a stimulant challenge in females but not in males. *Neuropsychopharmacology* 41, 2596–2605. doi: 10.1038/npp.2016.67

Wijtenburg, S. A., and Knight-Scott, J. (2011). Very short echo time improves the precision of glutamate detection at 3T in 1H magnetic resonance spectroscopy. *J. Magn. Reson. Imaging* 34, 645–652. doi: 10.1002/jmri.22638

Wright, N. E., Scerpella, D., and Lisdahl, K. M. (2016). Marijuana use is associated with behavioral approach and depressive symptoms in adolescents and emerging adults. *PLoS One* 11:e0166005. doi: 10.1371/journal.pone.0166005

Xu, C. J., Klunk, W. E., Kanfer, J. N., Xiong, Q., Miller, G., and Pettegrew, J. W. (1996). Phosphocreatine-dependent glutamate uptake by synaptic vesicles a comparison with ATP-dependent glutamate uptake. *J. Biol. Chem.* 271, 13435–13440. doi: 10.1074/jbc.271.23.13435

Yasen, A. L., Smith, J., and Christie, A. D. (2017). Reliability of glutamate and GABA quantification using proton magnetic resonance spectroscopy. *Neurosci. Lett.* 643, 121–124. doi: 10.1016/j.neulet.2017.02.039

Yücel, M., Lorenzetti, V., Suo, C., Zalesky, A., Fornito, A., Takagi, M. J., et al. (2016). Hippocampal harms, protection and recovery following regular cannabis use. *Transl. psychiatry* 6:e710. doi: 10.1038/tp.2015.201

Conflict of Interest Statement: The authors declare that the research was conducted in the absence of any commercial or financial relationships that could be construed as a potential conflict of interest.

frontiers in Human Neuroscience

ORIGINAL RESEARCH
published: 13 December 2019
doi: 10.3389/fnhum.2019.00441

Gender Differences in Objective and Subjective Measures of ADHD Among Clinic-Referred Children

Ortal Slobodin[1]* *and Michael Davidovitch*[2]

[1]Department of Education, Ben-Gurion University, Beer-Sheva, Israel, [2]Medical Department and Research Institute, Maccabi Healthcare Services, Tel Aviv, Israel

OPEN ACCESS

Edited by:
Juliana Yordanova,
Institute of Neurobiology (BAS),
Bulgaria

Reviewed by:
Mariya Cherkasova,
University of British Columbia,
Canada
Axel Hutt,
German Weather Service,
Germany

***Correspondence:**
Ortal Slobodin
ortal.slobodin@gmail.com

Specialty section:
This article was submitted to Health, a section of the journal Frontiers in Human Neuroscience

Received: 27 June 2019
Accepted: 02 December 2019
Published: 13 December 2019

Citation:
Slobodin O and Davidovitch M (2019) Gender Differences in Objective and Subjective Measures of ADHD Among Clinic-Referred Children. Front. Hum. Neurosci. 13:441. doi: 10.3389/fnhum.2019.00441

Attention deficit hyperactivity disorder (ADHD), one of the most prevalent childhood disorders today, is generally more likely to be diagnosed and treated in boys than in girls. However, gender differences in ADHD are currently poorly understood, partly because previous research included only a limited proportion of girls and relied mainly on subjective measures of ADHD, which are highly vulnerable to reporter's bias. To further examine gender differences in ADHD and to address some of the shortcomings of previous studies, this study examined gender differences in subjective and objective measures of ADHD among clinic-referred children with ADHD. Participants were 204 children aged 6–17 years-old with ADHD (129 boys, 75 girls). A retrospective analysis was conducted using records of a clinical database. Obtained data included parent and teacher forms of the Conners ADHD rating scales, Child Behavior Checklist (CBCL), Teacher's Report Form (TRF), and child's continuous performance test (CPT) scores. Results showed that according to parents' and teachers' reports of ADHD-related symptoms (Conners ADHD rating scales), girls had more inattention problems than boys, but no differences were identified in the level of hyperactivity and impulsivity symptoms. CPT data, however, revealed higher impulsivity among boys. We did not find gender differences in the level of distractibility during CPT performance. Specifically, the effects of distractors type (visual environmental stimuli, auditory stimuli, or a combination of them) and distractors load (one or two distracting stimuli at a time) on CPT performance did not differ between boys and girls with ADHD. These findings suggest that gender effects on ADHD symptoms may differ between subjective and objective measures. Understanding gender differences in ADHD may lead to improved identification of girls with the disorder, helping to reduce the gender gap in diagnosis and treatment.

Keywords: attention, ADHD, CPT, distractibility, gender, impulsivity

INTRODUCTION

Attention deficit hyperactivity disorder (ADHD) is one of the most prevalent childhood disorders today (Barkley, 2015), with an estimated worldwide prevalence of 7.2% in children under 18 years of age (Thomas et al., 2015). Although gender has been considered a significant factor in ADHD research for many years (Arnold, 1996), gender differences among children with ADHD are not well understood (Hasson and Fine, 2012). Generally, boys are more likely to be referred, diagnosed, and treated for ADHD symptoms than girls. These findings were previously attributed to gender differences in the manifestation of ADHD (e.g., males having more disruptive symptoms; Gaub and Carlson, 1997; Gershon, 2002) as well as to referral bias (Rucklidge, 2008, 2010; Ohan and Visser, 2009). Understanding the role of gender in ADHD care has been historically hindered by methodological issues, such as involving relatively low numbers of girls in research samples, failing to control for possible gender effects, and relying solely on subjective scales which are often subjected to reporter's bias (Quinn and Madhoo, 2014). As a result, literature focusing on ADHD in female subjects, and gender differences in ADHD has been limited (Nadeau and Quinn, 2002; Sassi, 2010). The aim of the current study was, therefore, to examine gender differences in ADHD-related symptoms, using subjective and objective measures, within a clinic-referred sample of 6–17-year-old children with ADHD.

GENDER DIFFERENCES IN ADHD PREVALENCE

Research has consistently shown that boys are more likely to be diagnosed and treated for ADHD-related symptoms than girls (Biederman et al., 2002; Gudjonsson et al., 2014). Male-to-female ratios of ADHD diagnosis ranged from 2:1 to 10:1 (Nøvik et al., 2006; Ramtekkar et al., 2010; Willcutt, 2012), with higher male-to-female ratios found in clinical vs. population-based samples (Skogli et al., 2013).

Research on gender differences in ADHD suggests that girls may be consistently under-identified and underdiagnosed because of differences in the disorder manifestation among boys and girls. Girls diagnosed with ADHD show fewer hyperactive/impulsive symptoms and more inattentive symptoms when compared with boys with the disorder (Biederman et al., 2002; Biederman and Faraone, 2004). Further, girls with ADHD present more commonly with the inattentive subtype than do boys (Hinshaw et al., 2006). In addition, males with ADHD have been found to have more co-existing externalizing disorders (conduct disorder, oppositional defiant disorder) and symptoms (e.g., aggression, rule-breaking) than typically developing boys, while females tend to show more internalizing disorders (e.g., anxiety) in comparison to typically developing girls (Biederman et al., 2010; Hinshaw et al., 2012). Symptoms of inattention and internalization might be less likely to be disruptive in the classroom, resulting in fewer referrals, diagnoses, and treatment of ADHD in girls (Biederman et al., 2002; Diamantopoulou et al., 2007). In a recent Swedish large-scale study, Mowlem et al. (2019) showed that hyperactivity/impulsivity symptoms, as well as conduct problems, were stronger predictors of clinical diagnosis and prescription of pharmacological treatment than other types of ADHD-related symptoms, suggesting that females with ADHD may be more easily missed in the ADHD diagnostic process and less likely to be prescribed medication unless they have prominent externalizing problems.

Another possible reason for underdiagnosis and undertreatment of ADHD in girls is that symptoms of inattention are more likely to be present in a structured educational environment, such as in high school or college, which may delay diagnosis among females (Bruchmüller et al., 2012). Lastly, females with ADHD may develop better-coping strategies than males to compensate for their ADHD-related difficulties, such as working hard to maintain classroom performance. As a result, they can better mitigate or mask the impact of their difficulties (Quinn, 2010). In addition to the gender discrepancies in the expression of ADHD, referral bias may account for the gender differences in ADHD prevalence. Many studies demonstrated that parents, teachers, and professionals are more likely to recognize ADHD-related symptoms in boys than in girls and are more likely to refer boys to treatment (Glass and Wegar, 2000; Bruchmüller et al., 2012). For example, Papageorgiou et al. (2008) conducted a study that collected parent and teacher reports of ADHD behaviors of children and measured the agreement of the parent and teacher reports. The results showed that parents rated boys higher on the hyperactivity scale than girls, but not on emotional problems, conduct problems, and peer problems. Teachers rated boys higher on inattention, hyperactivity, and conduct problems than girls. Likewise, teachers were more likely to refer boys for ADHD treatment, even when showing equal or lower levels of impairment compared to girls (Sciutto et al., 2004; Coles et al., 2012). When gender differences were assessed in a sample of non-referred children (Biederman et al., 2005), boys and girls did not differ in subtypes of ADHD, psychiatric comorbidity, or treatment history. Girls also showed similar levels of cognitive, school, and family functioning. The authors concluded that the clinical correlates of ADHD are not influenced by gender and that gender differences observed in clinical settings may be caused by referral biases.

GENDER DIFFERENCES IN A CONTINUOUS PERFORMANCE TEST (CPT)

Usually, ADHD diagnosis in children and adolescents involves multiple sources of information, including clinical examination, parents' and teachers' reports and self-report scales (Wolraich et al., 2011). The vulnerability of these methods to clinicians and informant biases (Rousseau et al., 2008) may lead to underdiagnosis or overdiagnosis of ADHD, not only in girls but also in other groups such as ethnic minorities (Lambert et al., 2002). Given the limited validity of subjective measures

of ADHD, there has long been an interest in using objective, laboratory-based tools that could provide a norm-referenced measure of ADHD. The CPT is the most frequently used direct measure of ADHD-related inattention, impulsivity, and hyperactivity (Vogt and Williams, 2011). Typically, the test includes a rapid presentation of a sequence of visual or auditory stimuli (numbers, letters, number/letter sequences, or geometric figures). Participants are instructed to respond to the "target" stimulus and to avoid responding to "non-target" stimuli. Responses to non-target stimuli are referred to as "commission errors," and are considered as a measure of impulsivity. An absence of response to target stimuli is referred to as an "omission error" and is assumed to measure inattention. Other common measures of CPT responses include the number of correct responses, response time (RT), and the variability in RT.

The influence of gender on CPT performance among children with ADHD is not clear. Some studies had shown girls to have fewer CPT errors, superior signal detection, and less inattention with longer interstimulus intervals (Arnold, 1996). Other studies, however, failed to identify the gender difference in CPT performance (Yang et al., 2004). A meta-analysis of gender differences in CPT among clinic-referred children indicated that consistent with rating scale studies (Gaub and Carlson, 1997; Gershon, 2002), boys with ADHD committed significantly more commission errors than girls with ADHD. However, no gender differences were found in the rate of omission errors. These findings suggest that inhibitory control, but not attention deficit may be mediated by gender. Alternatively, the lack of gender differences in inattention may be attributed to methodological limitations of the included studies, mainly the inclusion of a low number of studies, which were based on predominantly male samples (Hasson and Fine, 2012).

THE CURRENT STUDY

The gender gap in clinical populations of children with ADHD continues to hinder the correct diagnosis and treatment of girls with the disorder (Skogli et al., 2013). Thus, understanding how gender influences ADHD manifestations may have important clinical, ethical, and public implications. Prior studies have shown that girls with ADHD are under-identified due to sex-specific biases and expectations (Waschbusch and King, 2006; Meyer et al., 2017) and that the threshold for referral and diagnosis of ADHD in girls might be higher than for boys (Mowlem et al., 2019). While these studies were able to identify gender differences on standardized rating scales, differences in gender performances on direct CPT measures have received less attention (Hasson and Fine, 2012). The current study sought to assess gender differences in rating and objective measurements of ADHD as well as in co-occurring problems in a clinic-referred sample of children with ADHD. Based on a relatively balanced female-to-male ratio (1:1.7), the current study examined the gender differences in parent and teacher ADHD rating scales, co-occurring symptoms, and CPT performance indices (attention, timing, impulsivity, and hyperactivity). In addition, we examined gender differences in the level of distractibility and in time-on-task effects during CPT performance. Although increased distractibility is considered one of the core symptoms of ADHD within the inattention domain (American Psychiatric Association, 2013), direct and systematic research on this deficit and how it is differently patterned in males and females is currently very limited. Addressing gender differences in objective and subjective measures of ADHD, as well as in co-occurring symptoms may overcome some of the clinician's and reporter's gender-related biases observed in ADHD rating scales. Furthermore, using different types of measures would increase our understanding of ADHD underdiagnosis in females and whether certain symptoms are more predictive of ADHD referral and diagnosis in males than in females (or vice versa).

MATERIALS AND METHODS

Participants and Procedure

Israel has a socialized healthcare system in which all citizens are free to choose between four health maintenance organizations (HMOs). Patient fees are equivalent across all four HMOs, and all HMOs provide equivalent medical services that are based on national health regulations. The diagnosis of ADHD in Israel is usually given by a psychiatrist or a neurologist and includes the use of the Diagnostic and Statistical Manual of Mental Disorders (DSM) criteria and a formal diagnostic questionnaire for parents and teachers (Hezi, 2010).

The current study included 204 children diagnosed with ADHD (63% boys), referred to an outpatient pediatric neurologic clinic, affiliated with the second-largest HMO. Children were referred to the clinic for ADHD evaluation between January 2014 and December 2017. Participating children and their families were all of Jewish background, lived in rural and urban areas in Northern Israel, and had medium-high or high socioeconomic status, based on a social scale that divides geographic locations into different socioeconomic categories (Israeli Central Bureau of Statistics, 2017).

Children's age ranged between 6 and 17 years (Mean age = 9.44, SD = 2.42). No age differences were found between girls and boys ($t_{(203)} = 1.01$, N.S).

Inclusion criteria were children between 6–17 years, diagnosed with ADHD. The diagnostic procedure was conducted by a certified pediatric neurologist and included an interview with the child and parents, medical/neurological examination, CPT administration, and ADHD diagnostic questionnaires.

Diagnosis of ADHD was considered positive if, based on both parents' and teacher's reports (Conners, 2008), the child scored above the standard clinical cut-offs for ADHD symptoms. Since this is a clinical setting, a more conservative cut-off (+2 Standard deviations and above) for ADHD diagnosis was used (Barkley, 2015).

Exclusion criteria were an intellectual disability, chronic neurological levels (e.g., cerebral palsy, autism spectrum disorder), and psychosis. The protocol for the research project conforms to the provisions of the Declaration of Helsinki, approved by the Institutional Review of Board of Maccabi health services.

Measurements

Background variables included the child's age and gender, ethnicity, socio-economic status, place of residence, and school type.

ADHD-related symptoms were assessed by the parent and teacher forms of the Conners ADHD Index Rating scales, 3rd edition, short-form (Conners 3 AI; Conners, 2008), Hebrew version (Psychtech Ltd, 2012). The Conners 3 is a multi-informant assessment of children between 6 and 18 years of age that takes into account home, social, and school settings and is considered to be a reliable instrument for detecting ADHD problems in children aged 6–18 years.

Co-existing psychiatric symptoms were measured by the Child Behavior Checklist (CBCL), and the Teacher's Report Form (TRF; Achenbach and Rescorla, 2001), Hebrew version (Psychtech Ltd, 2005). These forms include eight DSM-oriented scales consistent with DSM diagnostic categories: Anxious/Depressed, Withdrawn/Depressed, Somatic Complaints, Social Problems, Thought Problems, Attention Problems, Rule-Breaking Behavior, and Aggressive Behavior.

CPT performance—the study employed the MOXO-CPT[1] version (Berger and Goldzweig, 2010), a standardized computerized test designed to diagnose ADHD-related symptoms. Like other CPTs, the MOXO-CPT measures sustained attention, omission and commission errors, and RT. However, as detailed below, it differs from other CPTs in its ability to differentiate between different types of disinhibited responses and between problems in RT and inattention. Importantly, the test incorporates external interfering stimuli (auditory and visual) serving as measurable distractors, a feature that is unique to the MOXO-CPT. The test's validity and utility in distinguishing children and adolescents with ADHD from their typically developing peers were demonstrated in previous studies (Berger and Cassuto, 2014; Berger et al., 2017; Shahaf et al., 2018).

General Description

The test included eight levels (stages); each consisted of 53 trials (33 target and 20 non-target stimuli) and lasted 114.15 s. The total duration of the test was 15.2 min. On each trial, a stimulus (target or non-target) was presented in the middle of the screen for 0.5, 1, or 3 s and was followed by a "void" of the same length (**Supplementary Figure S1**). Each stimulus remained on the screen for the full presentation time, regardless of whether a response was provided or not. This practice allows the measuring of RT as well as its accuracy. The child was instructed to respond to the target stimulus as quickly as possible by pressing the space bar once and only once. In addition, the child was instructed not to respond to any other stimuli but the target, and not to press any other key but the space bar.

Test Stimuli

Target and non-target stimuli were cartoon pictures. Given that ADHD often co-occurs with specific learning disabilities that may be confounded with CPT performance, all stimuli were free of letters or numbers (Seidman et al., 2001). The target stimulus was always a cartoon image of a child's face. Non-target stimuli included five different images of animals.

Distracting Stimuli

To improve the test's ecological validity and to simulate the everyday environment, the MOXO-CPT incorporated visual and auditory distracting stimuli that were not part of the non-target stimuli. Distractors' onset was not synchronized with the onset of the target or the non-target stimuli.

Distractors were short animated video clips with typical elements of the child's everyday life. Overall, six different distractors were presented, each of them could appear as pure visual (e.g., birds moving their wings), pure auditory (e.g., birds singing), or as a combination of visual and auditory stimuli (birds singing and simultaneously moving their wings). Distractor presentation time varied between 3.5 and 14.8 s, with a fixed interval of 0.5 s between two distractors. There were six various visual distractors: a bowling ball (presented for 3.5 s), warrior (Jedi) with a saber, a gong (6.8 s), birds (9.25 s), (14.8 s), saber (6.8 s), and a flying airplane (8.6 s). Auditory distractors included the six corresponding sounds of the visual distractors.

Test Levels

The test included eight levels, each included different distractors set: Levels 1 and 8 did not include any distractors. Levels 2 and 3 included pure visual stimuli, levels 4 and 5 included pure auditory stimuli, and levels 6 and 7 included a combination of visual and auditory stimuli. During levels 2, 4, and 6, only one distractor was presented at a time. During levels 3, 5 and 7, two distractors were presented simultaneously.

Performance indices—The MOXO-CPT measured four performance indices:

(1) Attention: the number of correct responses (pressing the key in response to a target stimulus), which were conducted either during the stimulus presentation or during the void period that followed. This method allows the test to evaluate whether the participant responded correctly to the target (was attentive to the target) independently of his/her RT. The number of omission errors were also calculated (i.e., the number of times that the patient did not respond to a target stimulus). The score in the Attention index was calculated as the average of correct responses throughout the eight test levels.

(2) Timing: the number of correct responses (pressing the key in response to a target stimulus) that were given while the target stimulus was still presented on the screen. This index excluded responses that were performed during the void period (after the stimulus has disappeared). This method allowed the test to differentiate between the overall rate of correct responses (measured by the Attention index) and the rate of correct responses that were given only on the right timing (measured by the Timing index). These two aspects of RT correspond to two different deficits typical to ADHD: difficulty to provide an accurate response and difficulty to respond on time (National Institute of Mental Health, 2012). The score in this index was calculated as the average of correct responses while the target

[1]The term "MOXO" derives from the world of Japanese martial arts and means a "moment of lucidity." It refers to the moments preceding the fight, when the warrior clears his mind from distracting, unwanted thoughts, and feelings.

stimulus was still presented on the screen throughout the eight test levels.

(3) Impulsivity: the number of commission errors performed only when a non-target stimulus was present on the screen. Other types of non-inhibited responses (e.g., pressing the keyboard more than once) were not considered as impulsive responses (as will describe in the next paragraph). Score in this index was calculated as the average of impulsive responses throughout the eight test levels.

(4) Hyperactivity: the total number of commission responses that were not coded as impulsive responses (e.g., multiple responses, random key pressing). Differentiating between commission errors that were conducted due to impulsive behavior and commission errors that were conducted due to motor hyper-responsivity allowed the identification of multiple sources of response disinhibition. The score in this index was calculated as the average of hyperactive responses in the eight test levels.

The MOXO-CPT version for adolescents and adults, that was administered to participants aged 13 and above, differed from the children's version in several aspects. First, in each trial, the stimulus (target/non-target) is presented for 0.5, 1 or 4 s, followed by a "void" period of the same duration. Second, eight different distractors were used instead of six. Distractors were based on adults' and adolescents' everyday life, including car driving, a crying baby, and arguing people. Third, all distractors were presented for 8 s, with a fixed interval of 0.5 s between two distractors. Finally, each level consisted of 59 trials (34 targets and 25 non-targets) and lasted 136.5 s, so that the total duration of the test was longer (18.2 min). All other test's characteristics were identical to the children's version.

Data Analysis

To address gender differences in teachers' and parents' rating scale of child's behavior (TRF and CBSL, respectively), we performed multivariate analysis of variance with covariates (MANCOVA). In these analyses, gender served as the independent variable, and the eight CBCL or TRF subscales were used as dependent variables.

To examine gender differences in teachers' and parents' reports of ADHD symptoms (according to the Conners rating scales for teachers and parents, respectively), we performed two-way repeated-measures ANOVA. Symptom type (inattention or hyperactivity/impulsivity) and informant role (teacher or parent) were the within-subject factors, and gender was the between-subject factor. Of interest were the interaction effects of gender * symptom type, gender * informant role, and the three-way interaction (gender * symptom type * informant role). These effects may provide evidence that gender differences in ADHD symptoms vary as a function of symptom type, informant role or both.

Gender differences in the agreement rates between teacher and parents rating of ADHD-related symptoms were examined with chi-square tests.

Further, we examined gender differences in the four MOXO-CPT performance indices, using a one-way repeated measures ANOVA, with test levels as the within-subject factor and gender as the between-subject factor. In addition, we examined gender effects on the difference between the first and the last test levels (for each CPT index) in order to explore whether boys and girls are differently affected by time on the task.

Finally, to examine gender differences in distractibility levels during CPT performance, we first calculated the difference between the mean score in the no-distractor level (baseline) and the mean score in each distractor type (pure visual, pure auditory, and a combination of visual and auditory distractors). This calculation was conducted separately for each CPT index. The outcome of this calculation is considered a measure of the distractibility level. Next, we conducted two-way repeated-measures ANOVA. Distractor type (visual, auditory, or combined) and distractibility load (low or high distractibility) was the within-subject factors, and gender was the between-subject factor. Of interest were the two-way interactions (gender * distractor type and gender * distractibility load) as well as the three-way interaction (gender * distractor type * distractibility load). Such interactions would provide evidence for differential patterns of sensitivity to environmental distractors between boys and girls. Participants' age served as a covariate in all analyses. Power analysis calculation revealed that using a two-tailed test, $\alpha = 0.05$, and power = 0.80 (Cohen, 1992), a minimum of 51 participants is required in each gender group. Thus, our sample size ($N = 204$) was able to provide adequate power to detect a medium effect size (Cohen $d = 0.5$). All multivariate analyses were followed by posthoc analyses with Bonferroni correction for multiple comparisons. Analyses were conducted with SPSS software for Windows Version 25 (SPSS, Inc., Chicago, IL, USA).

RESULTS

Gender Differences in Co-existing Symptoms

To test gender differences in parents' and teachers' reports of child's behavior we conducted a one-way MACNOVA for the CBCL and the TRF. The total scores in the CBCL and the TRF were the dependent variables, and gender was the independent variable. Age served as a covariate variable. The results of the analyses are presented in **Table 1**.

Overall, MANCOVA results of the CBCL subscales indicated that the effect of gender was not significant, Wilks' Lamda = 0.937, $F_{(8,192)} = 1.62$, $p = 0.12$. MANCOVA results of the TRF subscales yielded a significant overall main effect of gender, Wilks' Lamda = 0.792, $F_{(8,192)} = 6.32$, $p < 0.001$. Univariate comparisons revealed a main effect for gender so that according to teachers' reports, boys had more anxiety/depression symptoms, $F_{(1,199)} = 4.81$, $p = 0.03$, and more rule-breaking behaviors, $F_{(1,199)} = 11.89$, $p = 0.001$ than girls. Girls, on the other hand, were more likely to present attention difficulties/hyperactivity symptoms, $F_{(1,199)} = 5.96$, $p = 0.02$. Because inattention and hyperactivity are included in the same subscale of the TRF, it was impossible to identify whether

TABLE 1 | Parent and teacher rating of child's behavior, by gender.

		Boys (n = 129)		Girls (n = 75)		Gender differences
		Mean score	SD	Mean score	SD	
CBCL parent report						
Anxious/depressed		59.35	8.11	60.49	8.511	$F_{(8,192)} = 1.62$, $p = 0.12$
Withdrawn/depressed		57.10	8.54	55.56	8.896	
Somatic complaints		57.60	8.99	57.33	8.034	
Social problems		58.81	7.42	60.13	9.002	
Thought problems		63.52	63.61	57.70	7.649	
Attention deficit		64.71	7.91	67.53	8.270	
Rule-breaking behavior		57.81	7.60	56.87	6.705	
Aggressive behavior		62.89	9.14	62.60	9.614	
TRF teacher report						
Anxious/depressed		61.75	8.91	59.08	7.62	$F_{(8,192)} = 6.32$, $p < 0.001$
Withdrawn/depressed		58.95	7.24	58.25	8.14	
Somatic complaints		56.98	7.68	55.96	7.15	
Social problems		60.61	8.30	61.17	8.44	
Thought problems		59.59	7.19	58.12	7.69	
Attention deficit and hyperactivity		62.76	5.19	64.77	5.26	
Rule-breaking behavior		59.74	7.69	56.05	6.65	
Aggressive behavior		64.48	10.26	62.84	8.01	
Conners rating scales						
Parent rating of inattention		72.11	11.13	76.25	9.01	$F_{(1,200)} = 10.04$, $p = 0.002$
Teacher rating of inattention		71.12	7.76	76.55	8.08	
Parent rating of hyperactivity/impulsivity		73.47	14.00	76.43	14.26	
Teacher rating of hyperactivity/impulsivity		71.26	12.72	70.88	13.81	
Parent-teacher agreement on inattention symptoms	No report	5	3.8	0	0	$\chi^2_{(2,\ N\ =\ 204)} = 12.08$, $p = 0.002$
	Parent or teacher	38	29.4	9	12	
	Both parent and teacher	86	66.6	66	88	
Parent teacher agreement on hyperactivity/impulsivity symptoms	No report	15	11.6	8	10.7	$\chi^2_{(2,\ N\ =\ 204)} = 2.26$, $p = 0.88$
	Parent or teacher	37	28.7	24	32	
	Both parent and teacher	77	59.6	43	57.3	

Note. Higher scores mean greater pathology.

teachers perceived girls as more inattentive or more hyperactive than boys.

Gender Differences in Parent and Teacher ADHD Rating Scales

To examine gender differences in teachers' and parents' reports of ADHD symptoms (according to the Conners rating scales for teachers and parents, respectively), we performed two-way repeated-measures ANOVA. Symptom type (inattention or hyperactivity/impulsivity) and informant role (teacher or parent) were the within-subject factors, and gender was the between-subject factor. **Table 1** summarizes gender differences in Conners's ADHD scores according to parents' and teachers' reports. Analyses did not find a main effect for symptom type, Wilks' Lamda value = 0.992, $F_{(1,200)} = 1.53$, $p = 0.22$, or for informant role, Wilks' Lamda value = 0.997, $F_{(1,200)} = 0.61$, $p = 0.43$. Gender interacted with symptom type, Wilks' Lamda = 0.981, $F_{(1,200)} = 3.91$, $p = 0.049$, but not with informant role, Wilks' Lamda = 0.997, $F_{(1,200)} = 0.52$, $p = 0.47$. Between subject analysis revealed effect for gender, $F_{(1,200)} = 10.04$, $p = 0.002$. *Post hoc* analysis of the interaction effect yielded a mean difference of 2.99, $p = 0.002$. As depicted in **Supplementary Figure S2**, girls had more inattention problems than boys, but no gender difference was evident in the hyperactivity/impulsivity symptoms.

In order to examine whether gender differences exist in the agreement rates between teacher and parents rating of ADHD-related symptoms, we conducted a chi-square test. Gender differences were found in the rates of agreement on inattention problems $\chi^2_{(2,\ N\ =\ 204)} = 12.08$, $p = 0.002$ so that there were significantly more girls for whom both parent and teacher-reported inattention problems than boys who scored positive on both scales. In contrast, no gender differences were found in the agreement rates on hyperactivity/impulsivity symptoms. $\chi^2_{(2,\ N\ =\ 204)} = 2.26$, $p = 0.88$.

Gender Differences in CPT Performance

To examine gender differences in MOXO-CPT performance, one-way repeated measures ANOVA was conducted, followed by posthoc analyses with Bonferroni correction for multiple comparisons. The eight test levels served as the within-subject factor and gender as the between-subject factor. The results are shown in **Table 2**.

TABLE 2 | Gender differences in the four continuous performance test (CPT) performance indices.

CPT index	Test level	Boys (n = 129)		Girls (n = 75)		Gender differences[c] (between-subject effect)
		Mean score		Mean score		
		M	SD	M	SD	
Attention	Base line	31.85	2.039	31.73	1.710	$F_{(1,193)}$ = 0 0.38, p = 0.54
	Visual[a]	30.59	2.781	29.96	3.482	
	Visual[b]	30.82	2.840	30.58	3.270	
	Auditory[a]	30.63	2.878	30.29	3.238	
	Auditory[b]	30.14	4.096	29.59	3.382	
	Combined[a]	28.96	4.973	28.27	4.718	
	Combined[b]	28.78	4.737	28.51	4.571	
	No distractors	29.48	4.312	28.93	3.717	
Timing	Base line	22.54	4.629	22.18	4.877	$F_{(1,193)}$ = 1.93, p = 0.17
	Visual[a]	19.98	4.346	18.88	3.819	
	Visual[b]	20.68	4.736	19.95	4.447	
	Auditory[a]	21.62	4.733	20.79	4.670	
	Auditory[b]	21.42	5.195	20.00	5.249	
	Combined[a]	19.38	5.698	18.36	5.170	
	Combined[b]	19.54	5.571	17.88	4.936	
	No distractors	21.13	5.118	19.71	5.043	
Hyperactivity	Base line	1.90	2.798	1.44	1.915	
	Visual[a]	3.76	4.940	2.63	2.176	$F_{(1,193)}$ = 2.96, p = 0.09
	Visual[b]	5.90	8.341	4.41	5.838	
	Auditory[a]	4.15	5.252	3.30	3.471	
	Auditory[b]	5.31	7.731	4.53	7.288	
	Combined[a]	6.02	9.115	5.23	10.161	
	Combined[b]	7.25	11.287	4.78	5.197	
	No distractors	4.48	5.759	4.29	6.315	
Impulsivity	Base line	1.81	1.710	1.58	1.363	$F_{(1,193)}$ = 4.63, p = 0.03
	Visual[a]	2.20	2.150	1.45	1.424	
	Visual[b]	2.26	2.003	1.62	1.792	
	Auditory[a]	2.37	2.148	1.88	1.779	
	Auditory[b]	2.88	2.700	2.15	2.961	
	Combined[a]	2.35	2.673	1.90	2.964	
	Combined[b]	2.50	2.417	2.05	2.327	
	No distractors	2.89	2.981	2.51	3.167	

[a]Low distractibility (one distracting stimulus). [b]High distractibility (two distracting stimuli). [c]Based on two-way MANOVA with repeated measures. Note. In the Attention and Timing indices, higher scores mean better performance. In the Hyperactivity and Impulsivity indices, higher scores mean worse performance (increased hyperactive and impulsive responses).

Analyses of within subject effects on the Attention index revealed main effect of test level, Wilks' Lamda = 0.738, $F_{(7,187)}$ = 9.49, $p < 0.001$. Gender did not interact with test level, Wilks' Lamda = 0.986, $F_{(7,187)}$ = 0.39, p = 0.91. Between-subject analyses revealed no effect for gender, $F_{(1,193)}$ = 0 0.38, p = 0.54.

Similar patterns were identified in the Timing and Hyperactivity indices. Analyses of within-subject effects in the Timing index revealed a main effect for test level, Wilks' Lamda = 0.813, $F_{(8,187)}$ = 6.14, $p < 0.001$. Gender did not interact with test level, Wilks' Lamda = 0.969, $F_{(8,187)}$ = 0.84, p = 0.55. Between-subject analyses revealed no effect for gender, $F_{(1,193)}$ = 1.93, p = 0.17.

Analyses within subject effects on the Hyperactivity index revealed main effect for test level, Wilks' Lamda = 0.723, $F_{(8,187)}$ = 10.24, $p < 0.001$. Gender did not interact with test level, Wilks' Lamda = 0.955, $F_{(8,187)}$ = 1.27, p = 0.27. Between-subject analysis revealed no effect for gender, $F_{(1,193)}$ = 2.96, p = 0.09.

Analyses of within-subject effects on the Impulsivity index revealed a main effect for test level, Wilks' Lamda = 0.971, $F_{(1,193)}$ = 5.67, p = 0.018. Gender did not interact with test level, Wilks' Lamda = 0.968, $F_{(2,192)}$ = 0.88, p = 0.52. However, between-subject analysis revealed a main effect of gender, $F_{(1,193)}$ = 4.63, p = 0.03. *Post hoc* analyses with Bonferroni correction for multiple comparisons indicated that boys (M = 2.41, SD = 0.15) conducted more impulsive responses than girls (M = 1.88, SD = 0.20), regardless of test level (p = 0.03).

The effect of the test level that was observed in all CPT indices reflects the variation between levels in the presence, type, or load of distractors. These effects will be described in the next section.

Finally, we wished to examine whether boys and girls were differently affected by time on the task. Therefore, we compared boys and girls on the difference between the first and the last level of every CPT index, using two-way repeated-measures ANOVA. For these analyses, test level (first and last) and CPT index (Attention, Timing, Hyperactivity, and Impulsivity) were the within-subject factors and gender was the between-subject factor.

Within subject analysis revealed a main effect for CPT index, Wilks' Lamda = 0.20, $F_{(3,191)}$ = 250.77, $p < 0.001$ but not for the test level, Wilks' Lamda = 0.998, $F_{(1,193)}$ = 0.34, p = 0.56. Gender did not interact with CPT index, Wilks' Lamda = 0.994, $F_{(3,191)}$ = 0.41, p = 0.75 or with test level, Wilks' Lamda = 0.996, $F_{(1,193)}$ = 0.87, p = 0.35. The three-way interaction was not significant as well, Wilks' Lamda = 0.991, $F_{(3,191)}$ = 0.56, p = 0.64.

The between subject analysis did not reveal a main effect for gender, $F_{(1,193)} = 2.39$, $p = 0.12$.

Gender Differences in Distractibility

To study gender differences in distractibility level during CPT performance, a series of two-way repeated-measures ANOVAs were conducted. Separate analyses were conducted for each one of the four MOXO-CPT performance indices. For these analyses, distractor type (visual, auditory, or combined) and distractibility load (low or high distractibility) was the within-subject factors, and gender was the between-subject factor. The results are shown in **Table 3**.

Analyses of within subject effects on the Attention index revealed main effects of distractor type, Wilks' Lamda = 0.811, $F_{(2,192)} = 22.38$, $p < 0.001$, and distractibility load, Wilks' Lamda = 0.975, $F_{(1,193)} = 4.97$, $p = 0.03$. Gender did not interact with distractor type, Wilks' Lamda = 1.00, $F_{(2,192)} = 0.04$, $p = 0.96$, or with distractibility load, Wilks' Lamda = 0.996, $F_{(1,193)} = 0$ 0.77, $p = 0.38$. The three-way interaction between distractor type, distractibility load and gender was not significant, Wilks' Lamda = 0.995, $F_{(2,192)} = 0$ 0.51, $p = 0.60$. Between-subject analysis revealed no effect for gender, $F_{(1,193)} = 0$ 0.33, $p = 0.57$.

Post hoc analysis with Bonferroni correction of the main effect of distractor type on the Attention index showed that participants were more distracted by the combination of visual and auditory distractors than by the presence of pure visual (mean difference = 1.84, $p < 0.001$) or pure auditory distractors (mean difference = 1.52, $p < 0.001$). *Post hoc* analysis of the effect of distractibility load did not reveal significant differences.

Analyses of within-subject effects on the Timing index revealed a main effect of distractor type, Wilks' Lamda = 0.842, $F_{(2,192)} = 17.97$, $p < 0.001$, but not of distractibility load, Wilks' Lamda = 0.995, $F_{(1,193)} = 0.93$, $p = 0.34$. Gender did not interact with distractor type, Wilks' Lamda = 0.998, $F_{(2,192)} = 0.19$, $p = 0.83$, and not with distractibility load, Wilks' Lamda = 0.996, $F_{(1,193)} = 0$ 0.80, $p = 0.37$. The three-way interaction between distractor type, distractibility load, and gender was not significant, Wilks' Lamda = 0.984, $F_{(2,192)} = 1.51$, $p = 0.22$. Between-subject analysis revealed no effect for gender, $F_{(1,193)} = 2.31$, $p = 0.13$. *Post hoc* analysis with Bonferroni correction of the main effect of distractor type on the Timing index showed that participants were more distracted by the combination of visual and auditory distractors than by pure visual (mean difference = 1.07, $p < 0.001$) or pure auditory (mean difference = 2.16, $p < 0.001$) distractors. Pure visual distractors were more distracting than pure auditory distractors (mean difference = 1.20, $p < 0.001$).

Analyses of within subject effects on the Hyperactivity index revealed main effect of distractibility load, Wilks' Lamda = 0.910, $F_{(1,193)} = 19.06$, $p < 0.001$, but not for distractor type, Wilks' Lamda = 0.990, $F_{(2,192)} = 0.99$, $p = 0.38$. Gender did not interact with distractor type, Wilks' Lamda = 0.993, $F_{(2,192)} = 0.71$, $p = 0.49$ or with distractibility load, Wilks' Lamda = 0.983, $F_{(1,193)} = 3.29$, $p = 0.07$. The three-way interaction between distractor type, distractibility load and gender was not significant, Wilks' Lamda = 0.994, $F_{(2,192)} = 0.54$, $p = 0.58$. Between-subject analysis revealed no effect for gender, $F_{(1,193)} = 2.14$, $p = 0.15$. *Post hoc* analysis with Bonferroni correction of the

TABLE 3 | Gender differences in distractibility during CPT performance.

CPT index	Test level	Boys (n = 129)		Girls (n = 75)		Gender differences[c] (between-subject effect)
		M	SD	M	SD	
Attention	Base line-visual[a]	1.26	2.45	1.77	2.80	$F_{(1,193)} = 0.33$, $p = 0.57$.
	Base line-visual[b]	1.03	2.57	1.16	2.70	
	Base line-auditory[a]	1.23	2.53	1.44	2.45	
	Base line-auditory[b]	1.72	3.91	2.14	2.72	
	Base line-combined[a]	2.89	4.79	3.45	4.32	
	Base line-combined[b]	3.07	4.42	3.22	4.04	
Timing	Base line-visual[a]	2.55	2.91	3.30	3.09	$F_{(1,193)} = 2.31$, $p = 0.13$.
	Base line-visual[b]	1.85	3.73	2.23	3.24	
	Base line-auditory[a]	0.92	3.67	1.38	3.59	
	Base line-auditory[b]	1.11	4.43	2.18	4.20	
	Base line-combined[a]	3.15	4.53	3.82	4.39	
	Base line-combined[b]	3.00	5.03	4.30	4.53	
Hyperactivity	Base line-visual[a]	−1.85	3.34	−1.19	2.49	$F_{(1,193)} = 2.14$, $p = 0.15$
	Base line-visual[b]	−4.00	7.03	−2.97	5.88	
	Base line-auditory[a]	−2.24	4.09	−1.86	3.66	
	Base line-auditory[b]	−3.41	6.60	−3.10	7.17	
	Base line-combined[a]	−4.12	8.16	−3.79	10.16	
	Base line-combined[b]	−5.35	10.51	−3.34	5.18	
Impulsivity	Base line-visual[a]	−0.39	1.717	0.12	1.60	$F_{(1,193)} = 2.40$, $p = 0.12$.
	Base line-visual[b]	−0.45	1.99	−0.04	1.67	
	Base line-auditory[a]	−0.56	1.78	−0.30	1.77	
	Base line-auditory[b]	−1.07	2.61	−0.58	2.84	
	Base line-combined[a]	−0.54	2.66	−0.33	2.83	
	Base line-combined[b]	−0.68	2.56	−0.48	2.34	

[a]*Low distractibility (one distracting stimulus).* [b]*High distractibility (two distracting stimuli).* [c]*Based on two-way MANOVA with repeated measures. Note. In all MOXO-CPT indices, higher scores (in absolute value) mean increased distractibility.*

main effect of distractibility load on the Hyperactivity index showed that CPT performance was worse when two distractors were simultaneously presented than when only one distractor was presented (mean difference = 1.10, $p < 0.001$).

Analyses of within-subject effects on the Impulsivity index revealed a main effect of distractibility load, Wilks' Lamda = 0.971, $F_{(1,193)} = 5.67$, $p = 0.018$, but not of distractor type, Wilks' Lamda, 0.994, $F_{(2,192)} = 0.59$, $p = 0.56$. Gender did not interact with distractor type, Wilks' Lamda = 0.997, $F_{(2,192)} = 0.34$, $p = 0.72$ or with distractibility load, Wilks' Lamda = 0.998, $F_{(1,193)} = 0.23$, $p = 0.79$. The three-way interaction between distractor type, distractibility load, and gender was not significant, Wilks' Lamda = 0.997, $F_{(2,192)} = 0.34$, $p = 0.72$. The between-subject analysis did not reveal a main effect for gender, $F_{(1,193)} = 2.40$, $p = 0.12$. *Post hoc* analysis with Bonferroni correction of the main effect of distractor ability load on the Impulsivity index showed that CPT performance was worse when two distractors were simultaneously presented than when only one distractor was presented (mean difference = 0.21, $p = 0.02$).

DISCUSSION

This study systematically examined gender effects on ADHD manifestations in a clinic-referred sample of children with ADHD aged 6–17 years, as obtained through subjective and objective measures of ADHD symptoms. To reduce a reporter's bias, the current study used the CPT as an objective laboratory-based measure of ADHD symptoms. To the best of our knowledge, this is the first study that focused on gender differences in distractibility in children with ADHD.

Examination of gender differences in parent and teacher reports on ADHD-related symptoms, according to the Conners rating scales, showed that the level of inattention symptoms was higher among referred girls. However, boys and girls were equally impaired in terms of impulsivity and hyperactivity. A similar pattern emerged in the TRF, where teachers reported more inattention problems for girls, but higher levels of depression, anxiety, and rule-breaking behaviors for boys. Consistent with previous studies, these findings suggest that clinically diagnosed males and females showed similar symptom severity except for higher inattention scores in females (Biederman et al., 2002; Biederman and Faraone, 2004; Graetz et al., 2005). In addition, we found that teachers, but not parents, were likely to identify boys as having more psychiatric internalizing (anxiety/depression) and externalizing (rule-breaking) co-occurring symptoms. These findings differ from previous studies, which found more anxious/depressed symptoms in girls than in boys (Quinn, 2008; Liu et al., 2011). Probably, teachers and parents capture different aspects of depression and anxiety (e.g., fear of novel experiences vs. school-related anxiety; Geiser, 2009; Grigorenko et al., 2010). For instance, teachers may be more likely than parents to identify anxiety and depression because ADHD-related social and academic difficulties are more prominent in the school environment (Biederman et al., 1995). Alternatively, it is possible that boys' externalizing symptoms were associated with elevated levels of emotional lability and dysregulation (Martel and Nigg, 2006; Seymour et al., 2014) and therefore were pronounced as anxiety and depression.

While teachers' and parents' ADHD rating scales demonstrated gender differences in the inattention domain, a different pattern of gender differences emerged in the CPT data. Similar to previous studies (McGee et al., 2000; Seidman et al., 2005; Miranda et al., 2012), our results showed that boys conducted more impulsive responses than girls, regardless the presence of distracting stimuli, the type of distractors (visual, auditory or combined) or their load (one or two distracting stimuli at a time). Importantly, gender did not interact with distractors type or with their load, indicating that the effect of environmental distractors on CPT performance did not significantly differ between boys and girls. Our results suggest a possible dissociation between gender and the method of ADHD assessment; while girls with ADHD (but not boys) showed increased inattention symptoms according to teacher and parent report scales, boys (but not girls) showed increased impulsivity according to CPT performance indices. These results indicate that distinct ADHD-related deficits might be evaluated by different assessment methods and might also be differently patterned in males and females.

Nonspecific associations between CPT performance and behavioral measures of ADHD have been well documented in the ADHD literature (Reh et al., 2015; Willard et al., 2016). CPT performance was poorly to moderately correlated with parent and teacher ratings and was often inconsistent with subtypes of ADHD diagnosis (Barkley, 1991; Edwards et al., 2007). Several interpretations were offered for these findings. First, it has been suggested that CPT performance and behavioral measures of ADHD may not converge due to the limited utility and ecological validity of both assessment methods. Some authors have questioned the validity of parent and teacher reports, given their vulnerability to clinician and informant biases (Edwards et al., 2007), reduced reliability for monitoring symptoms over time (Rabiner et al., 2010), and the influences of ethnicity, gender and socioeconomic status on ADHD symptom ratings (Slobodin and Masalha, in press).

On the other hand, several authors have questioned the utility and the ecological validity of the CPT in the diagnosis of ADHD, as it provides only a brief snapshot of a child's attentional capacity in a controlled environment (Barkley, 1991; Netson et al., 2011). A second possible explanation for the low convergent validity of the CPT with other behavioral measures of ADHD is that the magnitude of response achieved on CPT differs from that perceived by parents and teachers. For example, McGee et al. (2000) found that in a sample of clinic-referred children, the CPT was sensitive to behavior ratings only at the highest levels of the behavioral disturbance. The limited sensitivity of the CPT to ADHD-related deficits might be attributed to insufficient cognitive demands of the test (Mahone et al., 2001; Berlin et al., 2004), leading to a ceiling effect in CPT performance (Lasee and Choi, 2013). Third, laboratory and behavioral measures of ADHD may be tapping into qualitatively different aspects of behavior. Behavior ratings are based on

the accumulation of behavior during extended periods that occur in real-life situations. CPT, on the other hand, measures behavior in a particular moment in a laboratory setting (Barkley, 1991). Likewise, the CPT may not capture some aspects of ADHD that are perceived by behavioral ratings, such as hyperactivity (Reh et al., 2015). There is evidence that when a measurement of activity was combined with the CPT, its convergence validity with teacher ratings significantly improved as well its ability to distinguish between ADHD and non-ADHD cases (Reh et al., 2015). Finally, the low correspondence between ratings of behavior and constructs measured by CPT may be related to the fact the CPT fails to demonstrate symptom domain specificity (Epstein et al., 2006; Netson et al., 2011). In a large epidemiological study, Epstein et al. (2006) found that unexpectedly, omission errors were associated with hyperactivity symptoms (and not with inattention symptoms), whereas commission errors were related to impulsivity symptoms, hyperactivity, and inattention symptoms. Likewise, a recent study demonstrated that the levels of hyperactivity or impulsivity during CPT performance might be associated with basic attentional rather than inhibition processes (Vogt et al., 2018). It has been suggested that excessive motoric activity, such as fidgeting during a cognitive performance, reflects efforts to modulate attention and alertness (Hartanto et al., 2016). Thus, children with predominantly inattention problems may demonstrate higher levels of activity during CPT performance than children with predominantly hyperactivity/impulsivity deficits.

The above findings suggest that the limited, nonspecific associations between CPT performance and behavioral measures of ADHD are multi-factorial and may reflect the psychometric properties of both assessment methods as well as the underlying ADHD-related deficits. Given the lack of research on the correlations between gender, ADHD symptomatology, and CPT performance (Sims and Lonigan, 2012), further investigation is needed. Such an examination might assist clinicians in interpreting the similarities and differences in these two sources of data and how they are affected by gender.

A question remains as to whether and how gender differences in CPT performance may vary as a function of the paradigm's requirements. In their meta-analytic study of gender differences in CPT performance, Hasson and Fine (2012) indicated that the type of the included CPTs (i.e., Conners CPT, AX-CPT, and an auditory CPT) did not significantly contribute to their overall findings. However, it was impossible to determine how each CPT version contributed to the overall observed gender differences due to the heterogeneity of CPT paradigms and the different weights imposed on each study. The MOXO-CPT has numerous unique aspects that might have affected our results. First, the MOXO-CPT may pose a higher distractibility load than other CPT paradigms. In most CPTs that involve distracting stimuli, auditory distractors served as background noise while children performed another cognitive task (Abikoff et al., 1996; Pelham et al., 2011). In contrast, distractors in the MOXO-CPT vary in their type, length of presentation and location on the screen. This mode of presentation did not allow adjustment or de-sensitization to the distractors, thus maintaining high distractibility load throughout the test.

Further, while some studies have used neutral stimuli (neutral tone/letter) as distractors (Gordon and Mettelman, 1987; Uno et al., 2006; van Mourik et al., 2007), the MOXO-CPT incorporated ecologically valid stimuli that are typically found in the child's or adolescent's everyday environment. Because patients with ADHD have more difficulties in filtering meaningful distractors than neutral ones (Blakeman, 2000; López-Martín et al., 2013), it is possible that this feature of the test further contributed to its high distractibility load. These increased attention demands may have led to a floor effect in CPT performance of both males and females, thus hindering our ability to observe gender differences on various CPT indices, such as sustained attention and timing. A second aspect of the MOXO-CPT that should be considered when interpreting our results is that the test distinguishes between commission errors associated with impulsivity and hyperactive responses associated with increased activity level. While previous CPT studies consistently showed higher rates of commission responses among boys than girls (Hasson and Fine, 2012), they could not indicate whether these uninhibited responses were associated with impulsivity or with increased activity level (Pettersson et al., 2018). The MOXO-CPT may offer a more nuanced observation of gender differences in these two ADHD-related symptoms, suggesting that boys may be more impulsive but not more active than girls. Finally, the MOXO-CPT may differ from other CPTs in the level of attentional demands over time. Previous studies (Bioulac et al., 2012; Erdodi and Lajiness-O'Neil, 2013) showed decreased attention in children and adolescents with ADHD as the task progressed, probably due to degraded executive functions and/or motivational resources (Baumeister et al., 2007; Inzlicht and Schmeichel, 2012; Dekkers et al., 2017). However, we did not find any differences between participants' CPT scores in the first and the last level of the test, regardless of their gender or the CPT index. One possible explanation for the diversity of our findings may be related to the cognitive complexity of the MOXO-CPT paradigm. Previous research has associated the decreased cognitive performance over time in children and adolescents with ADHD with the increased complexity of the task (Tucha et al., 2009, 2017; Huang-Pollock et al., 2012). For example, in a study with children diagnosed with ADHD, Bioulac et al. (2012) found a deterioration of performances over time in a virtual classroom task but not in the CPT. They suggested that virtual classroom task involved more complex cognitive mechanisms than the CPT, which imposed only minimal working memory load. Although the MOXO-CPT required multiple attentional resources (various inter-stimuli intervals, high burden of distractors, the use of ecologically valid distractors, and various locations and types of stimuli), the first and the last level of the test were always free of distractors and may, therefore, required fewer cognitive demands compared to the other test levels. The fact that order effects confounded with the effects of test conditions (various distractor type and load) may explain why the current study failed to identify time-on-task effects in both genders.

Nevertheless, the interaction between gender and time-on-task effect on CPT performance should be further addressed in future studies.

Several limitations of this study should be considered. The first limitation is associated with the limited generalizability of the study, due to relative ethnic and geographic homogeneity of the sample, its limited size, and the fact that all children were recruited from a single neuro-pediatric clinic. Given that sustained attention is related to socio-cultural factors and even to gender equality in the country (Riley et al., 2016), our sampling method limits our ability to generalize our findings to populations with greater cultural diversity. Another factor that may limit the generalization of our findings is the fact that we included only Israeli patients. Israel is characterized by a dramatic rise in ADHD referral and diagnosis rates, mainly due to increased community knowledge about symptomatology and the benefits of treatment (Davidovitch et al., 2017). The current sample included relatively mild cases of ADHD, thus limiting the generalization of our findings to countries with lower referral rates. Another limitation of the study is our inability to study gender differences separately for children and adolescents due to our limited sample size. Indices of CPT performance, including the level of distractibility, were previously associated with age (Berger et al., 2013; Slobodin et al., 2015). Therefore, it will be worthwhile to study gender effects on developmental trajectories of ADHD. Finally, it should be noted that compared to other well-established CPTs, the MOXO-CPT is a relatively novel tool with more limited empirical support. Further investigation is needed to provide insight into its psychometrical properties in the ADHD evaluation process.

Our results may offer further insight into the various effects of gender on rating and objective measures of ADHD. The current study suggests that attention deficits according to parents' and teacher's rating scales were stronger predictors of ADHD referral among girls, whereas externalization behavior were stronger predictors of ADHD referral among boys. However, when assessed on objective measures of ADHD, boys were more impulsive than girls, but no other gender differences were observed. The fact that boys and girls did not differ on most CPT outcomes, including attention performance, timing, motor activity, distractibility, and time-on-task, may indicate that the severity of their ADHD symptoms is overall similar. These results are in line with previous research in clinically ascertained samples, showing similar levels of ADHD symptoms in boys and girls in ADHD rating scales with the exception of inattention for which females had higher ratings (Gershon, 2002; Mowlem et al., 2019).

Although the utility of the CPT as a stand-alone diagnostic tool for ADHD is currently limited (Berger et al., 2017; Tallberg et al., 2019), it may add valuable information about ADHD-related deficits to support clinical diagnosis. Using an objective laboratory-based measure of ADHD may be especially important among girls, who, due to clinician and informant biases, tend to be underdiagnosed and undertreated for ADHD (Coles et al., 2012). Our findings may encourage clinicians and researchers to consider using gender-specific norms and guidelines when assessing symptoms of ADHD (Hasson and Fine, 2012).

CONCLUSIONS

The present study provides insight into gender differences in ADHD symptoms using subjective and objective measures of ADHD. It demonstrated that parents and teachers were more likely to identify girls as having inattention problems than boys. Teachers were more likely to identify rule-breaking and anxiety/depression symptoms in boys than in girls. CPT analysis revealed higher impulsivity among boys. Gender did not interact with distractors type or load to affect CPT performance, suggesting that deficits in inhibition control and self-regulation might be considered a key aspect of ADHD in both boys and girls (Barkley, 1997, 1999). These findings highlight the need to include multiple sources of information and methods of assessment to reduce the gender gap in referred children.

DATA AVAILABILITY STATEMENT

The datasets generated for this study are available on request to the corresponding author.

ETHICS STATEMENT

The studies involving human participants were reviewed and approved by Ethics Committee of Maccabi Health Services. Written informed consent to participate in this study was provided by the participants' legal guardian/next of kin.

AUTHOR CONTRIBUTIONS

MD recruited the patients and performed clinical evaluations. OS and MD contributed equally to the development of study design, data analysis, integration of findings, and writing the manuscript.

SUPPLEMENTARY MATERIAL

The Supplementary Material for this article can be found online at: https://www.frontiersin.org/articles/10.3389/fnhum.2019.00441/full#supplementary-material.

REFERENCES

Abikoff, H., Courtney, M. E., Szeibel, P. J., and Koplewicz, H. S. (1996). The effects of auditory stimulation on the arithmetic performance of children with ADHD and nondisabled children. *J. Learn. Disabil.* 29, 238–246. doi: 10.1177/002221949602900302

Achenbach, T. M., and Rescorla, L. A. (2001). *Manual for the ASEBA School-Age Forms and Profiles: An Integrated System of Multi-Informant Assessment.*

Burlington, NJ: University of Vermont, Research Center for Children, Youth and Families.

American Psychiatric Association. (2013). *Diagnostic and Statistical Manual of Mental Disorders.* 5th Edn. Washington, DC: American Psychiatric Association.

Arnold, L. E. (1996). Sex differences in ADHD: conference summary. *J. Abnorm. Child Psychol.* 24, 555–569. doi: 10.1007/bf01670100

Barkley, R. A. (1991). The ecological validity of laboratory and analogue assessment methods of ADHD symptoms. *J. Abnorm. Child Psychol.* 19, 149–178. doi: 10.1007/bf00909976

Barkley, R. A. (1997). *ADHD and the Nature of Self-Control.* New York, NY: Guilford Press.

Barkley, R. A. (1999). Response inhibition in attention deficit hyperactivity disorder. *Ment. Retard. Dev. Dis. Res. Rev.* 5, 177–184. doi: 10.1002/(SICI)1098-2779(1999)5:3<177::AID-MRDD3>3.0.CO;2-G

Barkley, R. A. (2015). *Attention-Deficit Hyperactivity Disorder: A Handbook for Diagnosis and Treatment.* 4th Edn. New York, NY: The Guilford Press.

Baumeister, R. F., Vohs, K. D., and Tice, D. M. (2007). The strength model of self-control. *Cur. Dir. Psychol. Sci.* 16, 351–355. doi: 10.1111/j.1467-8721.2007.00534.x

Berger, I., and Cassuto, H. (2014). The effect of environmental distractors incorporation into a CPT on sustained attention and ADHD diagnosis among adolescents. *J. Neurosci. Methods* 222, 62–68. doi: 10.1016/j.jneumeth.2013.10.012

Berger, I., and Goldzweig, G. (2010). Objective measures of attention-deficit/hyperactivity disorder: a pilot study. *Isr. Med. Assoc. J.* 12, 531–535. doi: 10.1016/j.jneumeth.2013.10.012

Berger, I., Slobodin, O., Aboud, M., Melamed, J., and Cassuto, H. (2013). Maturational delay in ADHD: evidence from CPT. *Front. Hum. Neurosci.* 7:691. doi: 10.3389/fnhum.2013.00691

Berger, I., Slobodin, O., and Cassuto, H. (2017). Usefulness and validity of CPT in the diagnosis of ADHD children. *Arch. Clin. Neuropsychol.* 32, 81–93. doi: 10.1093/arclin/acw101

Berlin, L., Bohlin, G., Nyberg, L., and Janols, L. O. (2004). How well do measures of inhibition and other executive functions discriminate between children with ADHD and controls? *Child Neuropsychol.* 10, 1–13. doi: 10.1076/chin.10.1.1.26243

Biederman, J., Faraone, S., Mick, E., and Lelon, E. (1995). Psychiatric comorbidity among referred juveniles with major depression: fact or artifact? *J. Am. Acad. Child Adolesc. Psychiatry* 34, 579–590. doi: 10.1097/00004583-199505000-00010

Biederman, J., and Faraone, S. V. (2004). The massachusetts general hospital studies of gender influences on attention-deficit/hyperactivity disorder in youth and relatives. *Psychiatr. Clin. North Am.* 72, 225–232. doi: 10.1016/j.psc.2003.12.004

Biederman, J., Kwon, A., Aleardi, M., Chouinard, V. A., Marino, T., Cole, H., et al. (2005). Absence of gender effects on attention deficit hyperactivity disorder: findings in nonreferred subjects. *Am. J. Psychiatry* 162, 1083–1089. doi: 10.1176/appi.ajp.162.6.1083

Biederman, J., Mick, E., Faraone, S. V., Braaten, E., Doyle, A., Spencer, T., et al. (2002). Influence of gender on attention deficit hyperactivity disorder in children referred to a psychiatric clinic. *Am. J. Psychiatry* 159, 36–42. doi: 10.1176/appi.ajp.159.1.36

Biederman, J., Petty, C. R., Monuteaux, M. C., Fried, R., Byrne, D., Mirto, T., et al. (2010). Adult psychiatric outcomes of girls with attention deficit hyperactivity disorder: 11-year follow-up in a longitudinal case-control study. *Am. J. Psychiatry* 167, 409–417. doi: 10.1176/appi.ajp.2009.09050736

Bioulac, S., Lallemand, S., Rizzo, A., Philip, P., Fabrigoule, C., and Bouvard, M. P. (2012). Impact of time on task on ADHD patient's performances in a virtual classroom. *Eur. J. Psychiatry* 16, 514–521. doi: 10.1016/j.ejpn.2012.01.006

Blakeman, R. S. (2000). ADHD and distractibility: the role of distractor appeal. *Diss. Abstr. Int. B. Sci. Eng.*, 61:517.

Bruchmüller, K., Margraf, J., and Schneider, S. (2012). Is ADHD diagnosed in accord with diagnostic criteria? Overdiagnosis and influence of client gender on diagnosis. *J. Consult. Clin. Psychol.* 80, 128–138. doi: 10.1037/a0026582

Cohen, J. (1992). A power primer. *Psychol. Bull.* 112, 155–159. doi: 10.1037/0033-2909.112.1.155

Coles, E. K., Slavec, J., Bernstein, M., and Baroni, E. (2012). Exploring the gender gap in referrals for children with ADHD and other disruptive behavior disorders. *J. Atten. Disord.* 16, 101–108. doi: 10.1177/1087054710381481

Conners, C. K. (2008). *Conners.* 3rd Edn. Toronto, Ontario: Multi-Health Systems Inc.

Davidovitch, M., Koren, G., Fund, N., Shrem, M., and Porath, A. (2017). Challenges in defining the rates of ADHD diagnosis and treatment: trends over the last decade. *BMC Pediatr.* 29:218. doi: 10.1186/s12887-017-0971-0

Dekkers, T., Agelink van Rentergem, J. A., Koole, A., van den Wildenberg, W. P. M., Popma, A., Bexkens, A., et al. (2017). Time-on-task effects in children with and without ADHD: depletion of executive resources or depletion of motivation? *Eur. Child Adolesc. Psychiatry* 26, 1471–1481. doi: 10.1007/s00787-017-1006-y

Diamantopoulou, S., Rydell, A. M., Thorell, L. B., and Bohlin, G. (2007). Impact of executive functioning and symptoms of attention deficit hyperactivity disorder on children's peer relations and school performance. *Dev. Neuropsychol.* 31, 521–542. doi: 10.1080/87565640701360981

Edwards, M. C., Gardner, E. S., Chelonis, J. J., Schulz, E. G., Flake, R. A., and Diaz, P. F. (2007). Estimates of the validity and utility of the Conner's CPT in the assessment of inattentive and/or hyperactive impulsive behaviors in children. *J. Abnorm. Child Psychol.* 35, 393–404. doi: 10.1007/s10802-007-9098-3

Epstein, J. N., Conners, C. K., Hervey, A. S., Tonev, S. T., Arnold, L. E., Abikoff, H., et al. (2006). Assessing medication effects in the MTA study using neuropsychological outcomes. *J. Child Psychol. Psychiatry* 47, 446–456. doi: 10.1111/j.1469-7610.2005.01469.x

Erdodi, L. A., and Lajiness-O'Neil, R. (2013). Time-related changes in Conners' CPT-II scores: a replication study. *Appl. Neuropsychol. Adult* 21, 41–50. doi: 10.1080/09084282.2012.724036

Gaub, M., and Carlson, C. I. (1997). Gender differences in ADHD: a meta-analysis and critical review. *J. Am. Acad. Child Adolesc. Psychiatry* 36, 1036–1045. doi: 10.1097/00004583-199708000-00011

Geiser, C. (2009). *Multitrait-Multimethod-Multioccasion Modeling.* München, Germany: AVM.

Gershon, J. (2002). A meta-analytic review of gender differences in ADHD. *J. Atten. Disord.* 5, 143–154. doi: 10.1177/108705470200500302

Glass, C. S., and Wegar, K. (2000). Teacher perceptions of the incidence and management of attention deficit hyperactivity disorder. *Education* 121, 412–420.

Gordon, M., and Mettelman, B. B. (1987). *Technical Guide to the Gordon Diagnostic System.* Syracuse, NY: Gordon Systems.

Graetz, B. W., Sawyer, M. G., and Baghurst, P. (2005). Gender differences among children with DSM-IV ADHD in Australia. *J. Am. Acad. Child Adolesc. Psychiatry* 44, 159–168. doi: 10.1097/00004583-200502000-00008

Grigorenko, E. L., Geiser, C., Slobodskaya, H. R., and Francis, D. J. (2010). Cross-informant symptoms from CBCL, TRF, and YSR: trait and method variance in a normative sample of Russian youths. *Psychol. Assess.* 22, 893–911. doi: 10.1037/a0020703

Gudjonsson, G. H., Sigurdsson, J. F., Sigfusdottir, I. D., and Young, S. (2014). A national epidemiological study of offending and its relationship with ADHD symptoms and associated risk factors. *J. Atten. Disord.* 18, 3–13. doi: 10.1177/1087054712437584

Hartanto, T. A., Krafft, C. E., Iosif, A. M., and Schweitzer, J. B. (2016). A trial-by-trial analysis reveals more intense physical activity is associated with better cognitive control performance in attention-deficit/hyperactivity disorder. *Child Neuropsychology* 22, 618–626. doi: 10.1080/09297049.2015.1044511

Hasson, R., and Fine, J. G. (2012). Gender differences among children with ADHD on continuous performance tests: a meta-analytic review. *J. Atten. Disord.* 16, 190–198. doi: 10.1177/1087054711427398

Hezi, L. (2010). *Criteria for Diagnosing ADHD in Children, Adolescents and Adults.* Israeli Ministry of Health. Available online at: http://www.health.gov.il/hozer/mr40_2010.pdf. Accessed November 20, 2019.

Hinshaw, S. P., Owens, E. B., Sami, N., and Fargeon, S. (2006). Prospective follow-up of girls with attention-deficit/hyperactivity disorder into adolescence: evidence for continuing cross-domain impairment. *J. Consult. Clin. Psychol.* 74, 489–499. doi: 10.1037/0022-006x.74.3.489

Hinshaw, S. P., Owens, E. B., Zalecki, C., Huggins, S. P., Montenegro-Nevado, A. J., Schrodek, E., et al. (2012). Prospective follow-up of girls with attention-deficit/hyperactivity disorder into early adulthood: continuing impairment includes elevated risk for suicide attempts and self-injury. *J. Consult. Clin. Psychol.* 80, 1041–1051. doi: 10.1037/a0029451

Huang-Pollock, C. L., Karalunas, S. L., Tam, H., and Moore, A. N. (2012). Evaluating vigilance deficits in ADHD: a meta-analysis of CPT performance. *J. Abnorm. Psychol.* 121, 360–371. doi: 10.1037/a0027205

Inzlicht, M., and Schmeichel, B. J. (2012). What is ego depletion? Toward a mechanistic revision of the resource model of self-control. *Perspect. Psychol. Sci.* 7, 450–463. doi: 10.1177/1745691612454134

Israeli Central Bureau of Statistics. (2017). *Characterization and Classification of Geographical Units by the Socio-Economic Level of the Population, 2013.* Available online at: https://www.cbs.gov.il/en/publications/Pages/2017/Characterization-and-Classification-of-Geographical-Units-by-the-Socio-Economic-Level-of-the-Population-2013.aspx. Accessed November 20, 2019.

Lambert, M. C., Rowan, G. T., Lyubansky, M., and Russ, C. M. (2002). Do problems of clinic-referred African-American children overlap with the child behavior checklist? *J. Child. Fam. Stud.* 11, 271–285. doi: 10.1023/A:101681600

Lasee, M. J., and Choi, H.-S. (2013). Evidence of Reliability and validity for a children's auditory continuous performance test. *SAGE Open* 3:215824401351182. doi: 10.1177/2158244013511828

Liu, J., Cheng, H., and Leung, P. W. (2011). The application of the preschool Child Behavior Checklist and the caregiver-teacher report form to Mainland Chinese children: syndrome structure, gender differences, country effects, and inter-informant agreement. *J. Abnorm. Child Psychol.* 39, 251–264. doi: 10.1007/s10802-010-9452-8

López-Martín, S., Albert, J., Fernández-Jaén, A., and Carretié, L. (2013). Emotional distraction in boys with ADHD: neural and behavioral correlates. *Brain Cogn.* 83, 10–20. doi: 10.1016/j.bandc.2013.06.004

Mahone, M. E., Pillion, J. P., and Hiemenz, J. R. (2001). Initial development of an auditory continuous performance test for preschoolers. *J. Atten. Disord.* 5, 93–106. doi: 10.1177/108705470100500203

Martel, M. M., and Nigg, J. T. (2006). Child ADHD and personality/temperament traits of reactive and effortful control, resiliency, and emotionality. *J. Child. Psychol. Psychiatry* 47, 1175–1183. doi: 10.1111/j.1469-7610.2006.01629.x

McGee, R. A., Clark, S. E., and Symons, D. K. (2000). Does the conners' continuous performance test aid in ADHD diagnosis? *J. Abnorm. Child Psychol.* 28, 415–424. doi: 10.1023/a:1005127504982

Meyer, B. J., Stevenson, J., and Sonuga-Barke, E. J. S. (2017). Sex differences in the meaning of parent and teacher ratings of ADHD behaviors: an observational study. *J. Atten. Disord.* doi: 10.1177/1087054717723988 [Epub ahead of print].

Miranda, M. C., Rivero, T. S., and Amodeo Bueno, O. F. (2012). Effects of age and gender on performance on Conners' Continuous Performance Test in Brazilian adolescents. *Psychol. Neurosci.* 6, 73–78. doi: 10.3922/j.psns.2013.1.11

Mowlem, F. D., Rosenqvist, M. A., Martin, J., Lichtenstein, P., Asherson, P., and Larsson, H. (2019). Sex differences in predicting ADHD clinical diagnosis and pharmacological treatment. *Eur. Child Adolesc. Psychiatry* 28, 481–489. doi: 10.1007/s00787-018-1211-3

Nadeau, K., and Quinn, P. (2002). "Rethinking the DSM-I," in *Understanding Women with ADHD*, eds K. Nadeau and P. Quinn (Silver Spring: Advantage Books), 2–23.

National Institute of Mental Health. (2012). *Attention Deficit Hyperactivity Disorder.* Available online at: http://www.nimh.nih.gov/health/publications/attention-deficit-hyperactivity-disorder/complete-index.shtml. Accessed June 03, 2019.

Netson, K. L., Conklin, H. M., Ashford, J. M., Kahalley, L. S., Wu, S., and Xiong, X. (2011). Parent and teacher ratings of attention during a year-long methylphenidate trial in children treated for cancer. *J. Pediatr. Psychol.* 36, 438–450. doi: 10.1093/jpepsy/jsq102

Nøvik, T. S., Hervas, A., Ralston, S. J., Dalsgaard, S., Rodrigues Pereira, R., and Lorenzo, M. J. (2006). Influence of gender on attention-deficit/hyperactivity disorder in Europe—ADORE. *Eur. Child Adolesc. Psychiatry* 15, 15–24. doi: 10.1007/s00787-006-1003-z

Ohan, J. L., and Visser, T. A. (2009). Why is there a gender gap in children presenting for attention-deficit/hyperactivity disorder services? *J. Clin. Child Adolesc. Psychol.* 38, 650–660. doi: 10.1080/15374410903103627

Papageorgiou, V., Kalyva, E., Dafoulis, V., and Vostanis, P. (2008). Differences in parents' and teachers' ratings of ADHD symptoms and other mental health problems. *Eur. J. Psychiatry* 22, 200–210. doi: 10.4321/s0213-61632008000400003

Pelham, W. E. Jr., Waschbusch, D. A., Hoza, B., Gnagy, E. M., Greiner, A. R., Sams, S. E., et al. (2011). Music and video as distractors for boys with ADHD in the classroom: comparison with controls, individual differences, and medication effects. *J. Abnorm. Child Psychol.* 39, 1085–1098. doi: 10.1007/s10802-011-9529-z

Pettersson, R., Söderström, S., and Nilsson, K. W. (2018). Diagnosing ADHD in adults: an examination of the discriminative validity of neuropsychological tests and diagnostic assessment instruments. *J. Atten. Disord.* 22, 1019–1031. doi: 10.1177/1087054715618788

Psychtech Ltd. (2005). *Translation of the Achenbach System for Evidence-Based Assessment.* Jerusalem: PsychTech Ltd.

Psychtech Ltd. (2012). *Translation of the Conners 3AI Rating Scales.* Jerusalem: PsychTech Ltd.

Quinn, P. O. (2008). Review Attention-deficit/hyperactivity disorder and its comorbidities in women and girls: an evolving picture. *Curr. Psychiatry Rep.* 10, 419–423. doi: 10.1007/s11920-008-0067-5

Quinn, P. O. (2010). *100 Questions and Answers About Attention Deficit Hyperactivity Disorder (ADHD) in Women and Girls.* Burlington, MA: Jones and Bartlett Learning.

Quinn, P. O., and Madhoo, M. (2014). A review of attention-deficit/hyperactivity disorder in women and girls: uncovering this hidden diagnosis. *Prim. Care Companion CNS Disord.* 16:PCC.13r01596. doi: 10.4088/pcc.13r01596

Rabiner, D. L., Murray, D. W., Skinner, A. T., and Malone, P. S. (2010). A randomized trial of two promising computer-based interventions for students with attention difficulties. *J. Abnorm. Child Psychol.* 38, 131–142. doi: 10.1007/s10802-009-9353-x

Ramtekkar, U., Reiersen, A., Todorov, A., and Todd, R. (2010). Sex and age differences in attention-deficit/hyperactivity disorder symptoms and diagnoses: implications for DSM-V and ICD-11. *J. Am. Acad. Child Adolesc. Psychiatry* 49, 217.e3–228.e3. doi: 10.1016/j.jaac.2009.11.011

Reh, V., Schmidt, M., Lam, L., Schimmelmann, B. G., Hebebrand, J., Rief, W., et al. (2015). Assessment of core ADHD symptoms using the QbTest. *J. Atten. Disord.* 19, 1034–1045. doi: 10.1177/1087054712472981

Riley, E., Okabe, H., Germine, H., Wilmer, J., Esterman, M., and DeGutis, J. (2016). Gender differences in sustained attentional control relate to gender inequality across countries. *PLoS One* 11:e0165100. doi: 10.1371/journal.pone.0165100

Rousseau, C., Measham, T., and Bathiche-Suidan, M. (2008). DSM-IV, culture and child psychiatry. *J. Can. Acad. Child Adolesc. Psychiatry* 17, 69–75.

Rucklidge, J. J. (2008). Gender differences in ADHD: implications for psychosocial treatments. *Expert Rev. Neurother.* 8, 643–655. doi: 10.1586/14737175.8.4.643

Rucklidge, J. J. (2010). Gender differences in attention-deficit/hyperactivity disorder. *Psychiatr. Clin. North Am.* 33, 357–373. doi: 10.1016/j.psc.2010.01.006

Sassi, R. B. (2010). Attention-deficit hyperactivity disorder and gender. *Arch. Womens Ment. Health* 13, 29–31. doi: 10.1007/s00737-009-0121-2

Sciutto, M. J., Nolfi, C. J., and Bluhm, C. (2004). Effects of child gender and symptom type on referrals for ADHD by elementary school teachers. *J. Emot. Behav. Disord.* 12, 247–253. doi: 10.1177/10634266040120040501

Seidman, L. J., Biederman, J., Monuteaux, M., Doyle, A. E., and Faraone, S. V. (2001). Learning disabilities and executive dysfunction in boys with attention-deficit/hyperactivity disorder. *Neuropsychology* 15, 544–556. doi: 10.1037/0894-4105.15.4.544

Seidman, L., Biederman, J., Monuteaux, M., Valera, E., Doyle, A., and Faraone, S. (2005). Impact of gender and age on executive functioning: do girls and boys with and without attention deficit hyperactivity disorder differ neuropsychologically in preteen and teenage years? *Dev. Neuropsychol.* 27, 79–105. doi: 10.1207/s15326942dn2701_4

Seymour, K. E., Chronis-Tuscano, A., Iwamoto, D. K., Kurdziel, G., and Macpherson, L. (2014). Emotion regulation mediates the association between ADHD and depressive symptoms in a community sample of youth. *J. Abnorm. Child Psychol.* 42, 611–621. doi: 10.1007/s10802-013-9799-8

Shahaf, G., Nitzan, U., Erez, G., Meddelovic, S., and Bloch, Y. (2018). Monitoring attention in ADHD with an easy-to-use electrophysiological index. *Front. Hum. Neurosci.* 12:32. doi: 10.3389/fnhum.2018.00032

Sims, D. S., and Lonigan, C. J. (2012). Multi-method assessment of ADHD characteristics in preschool children: relations between measures. *Early Child. Res. Q.* 27, 329–337. doi: 10.1016/j.ecresq.2011.08.004

Skogli, E. W., Teicher, M. H., Anderen, P. N., Hovik, K. T., and Øie, M. (2013). ADHD in girls and boys—gender differences in co-existing symptoms and executive function measures. *BMC Psychiatry* 13:298. doi: 10.1186/1471-244x-13-298

Slobodin, O., Cassuto, H., and Berger, I. (2015). Age-related changes in distractibility: developmental trajectory of sustained attention in ADHD. *J. Atten. Disord.* 22, 1333–1343. doi: 10.1177/1087054715575066

Slobodin, O., and Masalha, R. (in press). Challenges in ADHD care for ethnic minority children: a review of the current literature. *Transcult. Psychiatry*

Tallberg, P., Råstam, M., Wenhov, L., Eliasson, G., and Gustafsson, P. (2019). Incremental clinical utility of continuous performance tests in childhood ADHD—an evidence-based assessment approach. *Scand. J. Psychol.* 60, 26–35. doi: 10.1111/sjop.12499

Thomas, R., Sanders, S., Doust, J., Beller, E. M., and Glasziou, P. (2015). Prevalence of attention-deficit/hyperactivity disorder: a systematic review and meta-analysis. *Pediatrics* 135, e994–e1001. doi: 10.1542/peds.2014-3482

Tucha, L., Fuermaier, A. B., Koerts, J., Buggenthin, R., Aschenbrenner, S., Weisbrod, M., et al. (2017). Sustained attention in adult ADHD: time-on-task effects of various measures of attention. *J. Neural Transm.* 214, 39–53. doi: 10.1007/s00702-015-1426-0

Tucha, L., Tucha, O., Walitza, S., Sontag, T. A., Laufkötter, R., Linder, M., et al. (2009). Vigilance and sustained attention in children and adults with ADHD. *J. Atten. Disord.* 12, 410–421. doi: 10.1177/1087054708315065

Uno, M., Abe, J., Sawai, C., Sakaue, Y., Nishitani, A., Yasuda, Y., et al. (2006). Effect of additional auditory and visual stimuli on continuous performance test (noise-generated CPT) in AD/HD children—usefulness of noise-generated CPT. *Brain Dev.* 28, 162–169. doi: 10.1016/j.braindev.2005.06.007

van Mourik, R., Oosterlaan, J., Heslenfeld, D. J., Konig, C. E., and Sergeant, J. A. (2007). When distraction is not distracting: a behavioral and ERP study on distraction in ADHD. *Clin. Neurophysiol.* 118, 1855–1865. doi: 10.1016/j.clinph.2007.05.007

Vogt, C., and Williams, T. (2011). Early identification of stimulant treatment responders, partial responders and non-responders using objective measures in children and adolescents with hyperkinetic disorder. *Child Adolesc. Ment. Health* 16, 144–149. doi: 10.1111/j.1475-3588.2010.00593.x

Vogt, C., Williams, T., Susi, K., and Harrison, S. (2018). Differences in measurements of hyperactivity between objective testing using infrared motion analysis (QbTest) and behavioural rating scales when comparing problems in alerting functions and response inhibition during the clinical assessment of ADHD. *Psychol. Dis. Res.* 1, 3–6. doi: 10.31487/j.PDR.2018.02.002

Waschbusch, D. A., and King, S. (2006). Should sex-specific norms be used to assess attention-deficit/hyperactivity disorder or oppositional defiant disorder? *J. Consult. Clin. Psychol.* 74, 179–185. doi: 10.1037/0022-006x.74.1.179

Willard, V. M., Conklin, L. H., Huang, L., Zhang, H., and Kahalley, L. S. (2016). Concordance of parent-, teacher- and self-report ratings on the Conners 3 in adolescent survivors of cancer. *Psychol. Assess.* 28, 1110–1118. doi: 10.1037/pas0000265

Willcutt, E. G. (2012). The prevalence of DSM-IV attention-deficit/hyperactivity disorder: a meta-analytic review. *Neurotherapeutics* 9, 490–499. doi: 10.1007/s13311-012-0135-8

Wolraich, M., Brown, L., Brown, R. T., DuPaul, G., Earls, M., and Feldman, H. M. (2011). ADHD: clinical practice guideline for the diagnosis, evaluation, and treatment of attention-deficit/hyperactivity disorder in children and adolescents. *Pediatrics* 128, 1007–1022. doi: 10.1542/peds.2011-2654

Yang, P., Jong, Y., Chung, L., and Chen, C. (2004). Gender differences in a clinic-referred sample of Taiwanese attention-deficit/ hyperactivity disorder children. *Psychiatry Clin. Neurosci.* 58, 619–623. doi: 10.1111/j.1440-1819.2004.01312.x

Conflict of Interest: OS has previously served on the scientific advisory board of NeuroTech Solutions Limited.

The remaining author declares that the research was conducted in the absence of any commercial or financial relationships that could be construed as a potential conflict of interest.

frontiers in Human Neuroscience

ORIGINAL RESEARCH
published: 24 January 2020
doi: 10.3389/fnhum.2019.00470

Saccade Latency Provides Evidence for Reduced Face Inversion Effects With Higher Autism Traits

Robin Laycock[1,2], Kylie Wood[2], Andrea Wright[2], Sheila G. Crewther[2] and Melvyn A. Goodale[3]*

[1]School of Health and Biomedical Sciences, RMIT University, Melbourne, VIC, Australia, [2]School of Psychology and Public Health, La Trobe University, Melbourne, VIC, Australia, [3]The Brain and Mind Institute, The University of Western Ontario, London, ON, Canada

Individuals on the autism spectrum are reported to show impairments in the processing of social information, including aspects of eye-movements towards faces. Abnormalities in basic-level visual processing are also reported. In the current study, we sought to determine if the latency of saccades made towards social targets (faces) in a natural scene as opposed to inanimate targets (cars) would be related to sub-clinical autism traits (ATs) in individuals drawn from a neurotypical population. The effect of stimulus inversion was also examined given that difficulties with processing inverted faces are thought to be a function of face expertise. No group differences in saccadic latency were established for face or car targets, regardless of image orientation. However, as expected, we found that individuals with higher autism-like traits did not demonstrate a saccadic face inversion effect, but those with lower autism-like traits did. Neither group showed a car inversion effect. Thus, these results suggest that neurotypical individuals with high autism-like traits also show anomalies in detecting and orienting to faces. In particular, the reduced saccadic face inversion effect established in these participants with high ATs suggests that speed of visual processing and orienting towards faces may be associated with the social difficulties found across the broader autism spectrum.

Keywords: autism, face processing, face inversion, saccade, eye-movements

OPEN ACCESS

Edited by:
Douglas Owen Cheyne, Hospital for Sick Children, Canada

Reviewed by:
Marianne Latinus, INSERM U1253Imagerie et Cerveau (iBrain), France
Brian C. Coe, Queen's University, Canada

****Correspondence:***
Robin Laycock
robin.laycock@rmit.edu.au

Specialty section:
This article was submitted to Health, a section of the journal Frontiers in Human Neuroscience

Received: *19 July 2019*
Accepted: *23 December 2019*
Published: *24 January 2020*

Citation:
Laycock R, Wood K, Wright A, Crewther SG and Goodale MA (2020) Saccade Latency Provides Evidence for Reduced Face Inversion Effects With Higher Autism Traits. Front. Hum. Neurosci. 13:470. doi: 10.3389/fnhum.2019.00470

INTRODUCTION

A core element of Autism Spectrum Disorder (ASD) is a difficulty in dealing with social situations, including deficits in eye-contact and reading non-verbal social signals. In addition, individuals with ASD often show impairments in attending to social information, spending less time, for example, fixating on the eyes and the central region of faces (Snow et al., 2011). Impairments in identifying emotions from facial expressions (Lozier et al., 2014), and based on eye-tracking studies, in shifting attention towards Guillon et al. (2016), and disengaging attention away from faces (Chawarska et al., 2010; Kikuchi et al., 2011) have also been reported in ASD populations.

Given that nonverbal social cues are usually rapid and dynamic, speed of visual processing and the orienting of attention may be important for developing social-communication skills. For example, the latency of the event-related potential (ERP) associated with early perceptual face processing has been shown to predict emotion recognition in adolescents with ASD (Lerner et al., 2013). In addition, under free-viewing of photographs of natural scenes, individuals with ASD are

slower to first fixate on a person in the scene, and spend less time looking at a person when there are other objects in the scene (Wilson et al., 2010).

In neurotypical populations, faces appear to constitute a unique category of objects that gain priority access to neural processing possibly *via* a direct superior colliculus-pulvinar-amygdala route (McFadyen et al., 2017). For example, faces capture attention in visual search, even when they are irrelevant to the task (Devue and Grimshaw, 2017), and infants also demonstrate preferential looking at faces (Johnson et al., 1991). The salient nature of faces is well illustrated by a saccadic choice reaction time paradigm employed by Crouzet et al. (2010) in which saccade onset times towards photographs of natural scenes presented simultaneously to the left and right of fixation averaged 150 ms when detecting the side containing a face (the express saccade range), compared to more than 180 ms when they were detecting a vehicle. This speed of visual processing for faces is consistent with reports of rapid ventral stream activation (Braeutigam et al., 2001; Eimer and Holmes, 2002; Liu et al., 2002), or may reflect direct subcortical pulvinar pathways to the amygdala that bypass early visual cortex (Johnson, 2005; Méndez-Bértolo et al., 2016; McFadyen et al., 2017). Interestingly, this type of fast processing is likely mediated by the magnocellular system which is also reported to be impaired in ASD (Greenaway et al., 2013). In the present study, we used the Crouzet et al.'s (2010) paradigm to examine the detection of faces vs. cars to disentangle whether the deficit in face detection in ASD is specific to social stimuli such as faces or instead reflects a general deficit in saccadic orienting.

The ASD literature on visually guided saccade tasks has been somewhat inconsistent with regard to latency measures. These studies involve the onset of a single simple target such as a small square [or a more engaging target such as a smiley face or a clown for children participants (Kelly et al., 2013; Kovarski et al., 2019)], triggering a reflexive visually guided saccade, and have found ASD to be associated with slower saccadic onset times (SOTs) towards a target (Goldberg et al., 2002; Miller et al., 2014; Wilkes et al., 2015), whilst others appear to suggest intact (Minshew et al., 1999; Takarae et al., 2004; Luna et al., 2007; Kelly et al., 2013; Zalla et al., 2018) or even faster (Kovarski et al., 2019) saccadic latency in ASD. In the current study however, where two competing photographs were presented, we were interested in the speed of saccadic orienting towards the image that contained the target category. Given that faces are less salient in those with ASD (Chawarska et al., 2010; Kikuchi et al., 2011; Guillon et al., 2016) it would be expected that utilization of a choice reaction time task should be associated with slower saccadic responses to face targets in ASD populations.

In addition, we also examined the effect of face inversion. In typical observers, recognition of inverted faces is reported to be more difficult, possibly due to the disruption of holistic face processing that occurs with inversion (Rossion, 2009). Reduced face inversion effects have been reported in the ASD literature (Rose et al., 2007) and have also been found to predict autism traits (AT) in a neurotypical population (Wyer et al., 2012). A 2012 systematic review argued there is insufficient evidence for reduced inversion effects in ASD (Weigelt et al., 2012). However, while most face inversion studies in those on the autism spectrum have measured identity recognition, only a few have utilized electrophysiological measurements to assess more automatic aspects of face processing, finding reduced inversion effects in ASD (McPartland et al., 2004; Vettori et al., 2019). Here, we measured saccadic latency when participants were detecting upright and inverted faces or cars which may also provide a more reflexive measure of attentional bias towards faces.

As a first step to testing whether or not "reflexive" saccadic mechanisms mediating the rapid detection of faces are compromised in ASD, we adopted the dimensional approach to investigating the autism spectrum (Landry and Chouinard, 2016). Similar to patterns observed in ASD samples, the broader autism phenotype, which includes family members of those with an ASD as well as neurotypical samples with higher ATs, has demonstrated anomalies in a number of cognitive processes, including executive function (Christ et al., 2010), visual processing (Crewther et al., 2015; Cribb et al., 2016), face emotion processing (Palermo et al., 2006; Wallace et al., 2010; Spencer et al., 2011) and in eye-movement patterns towards faces (Davis et al., 2001; Åsberg Johnels et al., 2017). Together, these results suggest that this dimensional approach provides a useful model of ASD, and may shed light on the similarities and dissimilarities between clinical and sub-clinical populations. In the current study, therefore, we tested individuals with high autism-like personality traits drawn from the general population. Such individuals were identified using a self-report scale that treats ASD as one end of a spectrum of behavioral traits extending into the general population (Kanne et al., 2012).

We predicted that individuals with high autism-like traits would exhibit the slower onset of saccadic eye movements than individuals with lower autism-like traits when detecting faces, even though the performance of the two groups might not differ when detecting inanimate objects, such as cars. We also predicted that individuals with high autism-like traits would demonstrate reduced saccadic face inversion effects compared to individuals with low ATs, but neither group would show a "car inversion" effect.

MATERIALS AND METHODS

Participants

Forty-seven participants (32 females, 15 males; mean age = 25.7, *SD* = 6.3) with normal or corrected to normal vision, were tested after providing written informed consent. All procedures were approved by the La Trobe University Human Ethics Committee and carried out in accordance with the approved protocol and relevant regulations. Prior to completing the experiment, participants completed an online version of the Subthreshold Autism Trait Questionnaire (SATQ; Kanne et al., 2012), a 24 item self-report questionnaire assessing a broad range of ATs encompassing social-communication and restricted or repetitive behaviors that has good test-retest reliability, internal consistency and discriminant validity (Nishiyama and Kanne, 2014). A factor analysis revealed five factors (social interaction and enjoyment, oddness, reading facial expressions, expressive language, rigidity). Participants also completed a timed version

TABLE 1 | Demographic information.

	N	Mean age (*SD*)	Mean Raven's raw score (*SD*)	Gender ratio (M:F)	Mean SATQ score (*SD*)
Low autism trait group	15	24.7 (5.2)	48.4 (4.6)	4:11	10.6 (4.5)
High autism trait group	15	27.4 (9.4)	46.4 (5.8)	7:8	32.4 (5.5)

of the standard Raven's Progressive Matrices test (Raven et al., 1996). Thirty participants were initially assigned to either high- or low-AT groups after performing a tertile split in the ranked SATQ scores of the initial pool of 47 participants. The final group characteristics after replacing one participant in the low AT group, and two participants in the high AT group (see below for details) can be seen in **Table 1**. As a comparison to the SATQ scores described in **Table 1**, SATQ scores in the general population have been reported with a mean of 23.1 (*SD* = 7.1), and in a clinical ASD sample with a mean of 40.8 (13.6; Kanne et al., 2012).

A power analysis to determine the sample size, utilizing the GPower package (Faul et al., 2009) was based on Crouzet et al. (2010), Bannerman et al. (2012) and Wilson et al. (2010). First for the within-subject comparison, when an effect size from Crouzet et al. (2010), dz = 2.5 was used, assuming a correlation among repeated measures (face and vehicle targets in saccadic choice reaction time tasks), $r = 0.8$, a sample size of four would be required for getting power of 0.80 with alpha level of 0.05. More conservatively however, when the effect size dz = 0.86 was estimated from Figure 3 of Bannerman et al. (2012) again assuming a correlation among repeated measures (upright and inverted fearful faces in a simple saccadic detection task), $r = 0.8$, a total sample size of 15 was calculated and aimed for in the current study. For the between-subject comparison, although not a saccadic reaction time task, Wilson et al. (2010) report a group effect for time to first fixation towards a face of approximately $d = 1.16$. Using the same assumptions as above, a sample size of 13 per group would be required.

Stimuli and Procedure

Participants viewed stimuli on a PC 24-inch display monitor using Experiment Builder software, and saccades were recorded using the EyeLink 1000 Plus, a video-based eye-tracking system. Participants viewed tasks binocularly, positioned in a chinrest for stability 57 cm from the monitor.

Before commencing each task, a 9-point calibration of the eye movement recording system was carried out. After every 10 trials, a fixation drift-check was made to ensure that the difference between computed fixation position during calibration and the current target is not large.

Task design and procedure closely followed that of Crouzet et al. (2010). Photographs were all grayscale and consisted of 200 natural scenes containing a car, along with 200 natural scenes containing a face, and 200 distractor natural scenes containing neither a face nor a car. The car stimuli were sourced from the internet while the face stimuli and distractor natural scenes were provided by Crouzet et al. (2010). Each image was converted to grayscale, 330 × 330 pixels, and adjusted to a mean luminance value of 128 using Adobe Photoshop. Half the face stimuli were males and half were females. The faces and cars were positioned in different locations within the scene rather than predictably central and were also of varied size and viewpoint (i.e., front/side angle etc.). Most of the face and the car images consisted of close-up views of the target, with approximately 30% (face images) and 35% (car images) taken from mid-stance views. Each photo had a retinal size of 14° by 14° of visual angle and was always positioned 8° left or right of fixation.

Each saccadic choice reaction-time task involved the presentation of two pictures, one on each side of fixation; one picture always contained the target (face or car), and the other was a natural scene that did not contain a target. The same set of 200 natural distractor scenes used for the face tasks were also used as the distractor images for the car tasks. The photo containing the target was randomly presented to the left or right. Initially, a black fixation cross on a white background was presented centrally for a random duration lasting between 800 and 1,600 ms, followed by a blank screen for 200 ms, and then the two images were presented for 400 ms followed again by a blank white screen (see **Figure 1**).

In the upright face task, participants were required to make a saccade towards the picture containing a face and completed 200 trials. Target and distractor images were both randomly

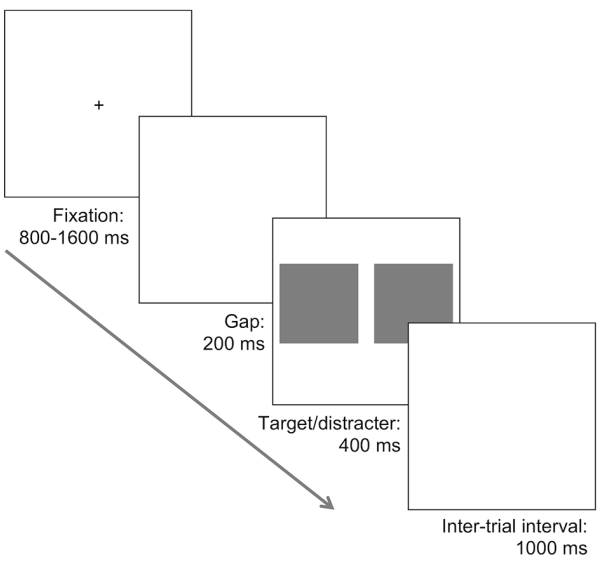

FIGURE 1 | Illustration of the task procedure. A fixation was followed by a 200 ms blank screen, and subsequently two images were presented. In different tasks, one photograph contained a face or a car and was presented alongside a distractor photograph consisting of a natural scene with no car or face. In separate tasks both the target and distractor photographs were presented in an upright orientation, or inverted 180°. Participants were required to make a saccade towards the location of the target, presented randomly to the left or the right, as quickly and accurately as possible.

sampled without replacement. This design was repeated in the inversion task, except that both target and distractor pictures were rotated 180°. Exactly the same procedure was used in the upright and inverted car target tasks. Thus, four separate tasks were completed, with task order counterbalanced between participants. Within each task, participants were allowed a brief break every 50 trials. The whole experiment lasted approximately 75 min.

Data Analysis

Eye-movements were recorded monocularly at 1,000 Hz. Data processing and extraction made use of Eyelink Data Viewer software, before further processing in Excel, with final analyses utilizing SPSS. All saccades were recorded and defined by an eye-movement motion threshold of 0.2°, velocity above 30°/s, and acceleration greater than 8,000°/s^2. An accurate response was defined as an eye movement of 4° or greater in the direction of the photo containing a target. For each participant, we calculated the percent correct trials on each task. Mean SOTs were analyzed for correct trials only, with saccades less than 4° or commencing earlier than 80 ms (i.e., indicating anticipation) excluded from the analysis. One participant in each AT group had missing data for a single task. Box plots for SOTs on each task and also the inversion effects for each target category revealed a high AT participant for face inversion, and a low AT participant for car inversion, both more than two standard deviations above the mean for their group. In order to maintain equal sample sizes, these participants were replaced with the participant next in the ranked SATQ data and formed the final sample for both accuracy and saccadic analyses (see **Table 1**). To analyze the accuracy and SOT data, separate three-way mixed ANOVA's were conducted, including target (face, car) and orientation (upright, inverted) as within-subject factors, and group (low AT, high AT) as a between-group factor. Effect sizes are reported, adopting the convention of small, medium and large effects with partial eta squared values of 0.01, 0.06 and 0.14, respectively.

Given the possibility that apparent discrepancies in the gender balance between AT groups may have influenced the results, further analyses were conducted. Fisher's exact test indicated that gender was not statistically imbalanced between AT groups ($p = 0.45$). Nevertheless, a mixed ANOVA using gender instead of AT group as the between-groups factor to analyze saccadic latencies did not reveal a main effect of gender ($p = 0.219$), nor any interactions including gender (p's > 0.795). Together these analyses suggest that gender does not appear to have influenced saccadic latencies in the current study.

RESULTS

Accuracy

Both groups performed the tasks with a high degree of accuracy (mean accuracy: low AT group—face upright = 98%, face inverted = 95%, car upright = 92%, car inverted 86%; high AT group—face upright = 96%, face inverted = 95%, car upright = 90%, car inverted 87%). A three-way mixed ANOVA revealed a main effect of target, $F_{(1,28)} = 81.56$, $p < 0.001$, $\eta_p^2 = 0.744$, with accuracy higher on face tasks than car tasks; a main effect of orientation, $F_{(1,28)} = 26.75$, $p < 0.001$, $\eta_p^2 = 0.489$, with accuracy higher for upright tasks than inverted tasks; but no effect of group, $F_{(1,28)} = 0.08$, $p = 0.782$, $\eta_p^2 = 0.003$. The only significant interaction was a two-way interaction between orientation and group, $F_{(1,28)} = 5.43$ $p = 0.027$, $\eta_p^2 = 0.162$, with simple effects analyses demonstrating that, although the low AT group was more accurate for upright than inverted stimuli ($p < 0.001$), the high AT group were not more accurate for upright than inverted stimuli ($p = 0.054$), regardless of target category.

Saccadic Onset Times

A three-way mixed ANOVA revealed significant main effects of target, $F_{(1,28)} = 207.54$, $p < 0.001$, $\eta_p^2 = 0.881$, with SOTs to faces faster than those to cars; orientation, $F_{(1,28)} = 8.84$, $p = 0.006$, $\eta_p^2 = 0.24$, with SOTs to upright targets faster than those to inverted targets; but not for group, $F_{(1,28)} = 0.02$, $p = 0.878$, $\eta_p^2 = 0.001$. There were no significant two-way interactions involving the group factor. The three-way interaction, however, was significant, $F_{(1,28)} = 4.97$, $p = 0.034$, $\eta_p^2 = 0.151$ (see **Figure 2A**). Simple main effects analysis used to interpret this interaction demonstrated that it was driven by differences in the inversion effects between groups. The inversion effect was defined as the paired comparison of SOTs between upright and inverted targets separately for each target category. Specifically, the low AT group showed a significant inversion effect for faces ($p < 0.001$) but not for cars ($p = 0.968$), whereas the high AT group did not demonstrate a significant face inversion effect ($p = 0.170$), nor a significant car inversion effect ($p = 0.309$; see **Figure 2B**). A t-test also revealed that the high AT group demonstrated a smaller face inversion effect compared with the low AT group, $t_{(28)} = 2.85$, $p = 0.008$. Although the high AT group showed a slower SOT for faces compared with the low AT group, the group difference was not significant ($p = 0.301$), and no other differences in SOTs were apparent between the groups for any of the tasks (p's > 0.651; see **Figure 2A**).

Reaction time data, including saccadic reaction times, is usually positively skewed, and median SOT, rather than mean SOT per participant may be considered appropriate for the current analysis. Although this solution is not recommended for data sets in which conditions have different number of trials (Miller, 1988; as was the case here due to the exclusion of trials not meeting inclusion criteria), a mixed ANOVA was run as suggested by a reviewer. After replacing a further outlier in the high AT group, the 3-way interaction was still significant, $F_{(1,28)} = 4.30$, $p = 0.047$, $\eta_p^2 = 0.133$. Simple main effects demonstrated the same pattern of results as for the analysis based on means (see **Appendix**). Indeed the difference in SOT between the mean and median for each participant was small, ranging on average between 3–5 ms depending on the task condition.

DISCUSSION

The results of our experiment indicate that people with high (though sub-clinical) ATs showed different eye-movement patterns, compared with people with low ATs, when orienting towards faces in natural scenes. In particular, these differences

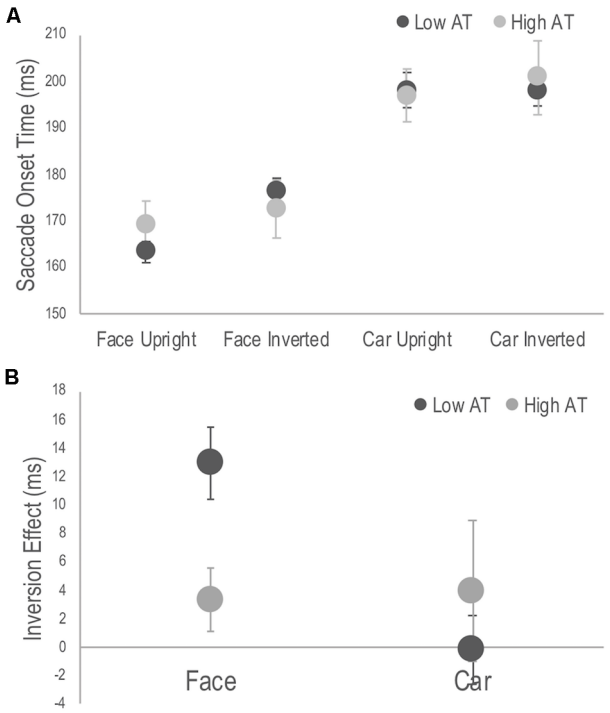

FIGURE 2 | (A) Average saccade onset times (SOTs) to detect the photograph containing a face or a car in the upright and inverted tasks for high and low Autism Trait (AT) Groups. **(B)** Face and car inversion effects, calculated as the difference in mean SOTs between upright and inverted tasks for high and low AT Groups. Error bars indicate standard error of the mean. The low AT group demonstrated a significant face inversion effect ($p < 0.001$), whereas the high AT group did not ($p = 0.170$). The face inversion effect of the low AT group was significantly larger than that of the high AT group ($p = 0.008$). Neither group demonstrate a car inversion effect.

were demonstrated by a reduced latency-based face inversion effect. These effects were found to be specific to the detection of faces with no evidence for differences in inversion effects when detecting inanimate targets, such as cars. Although the current study was not designed to test oculomotor and early-stage visual processing, the lack of a generalized impairment for saccade onset latencies and the specificity of the inversion effects to face targets suggests the oculomotor and visual processing deficits that have sometimes been reported in ASD populations across a range of paradigms are unlikely to account for the face-detection deficit we observed (for reviews, see Simmons et al., 2009; Freedman and Foxe, 2018).

Whereas low AT participants demonstrated a very pronounced face inversion effect, with faster SOTs towards upright than inverted faces, this effect was entirely absent in the participants with high ATs. Previous studies have found reduced or absent face inversion effects in ASD populations (McPartland et al., 2004; Rose et al., 2007) and in a neurotypical population a smaller face inversion effect was found to predict ATs (Wyer et al., 2012), although Weigelt et al. (2012) have cast doubt on the reliability of these findings. One difficulty in making comparisons between studies is that different measures of face processing have been used; for example, participants may be required to match face identity in some studies or expression in others. The reduced saccadic inversion effect reported here suggests that the timing of the activation of face processing mechanisms may be a critical variable, a conclusion that is also supported by the finding in an ASD sample of a reduced inversion effect in the N170 latency when viewing faces (McPartland et al., 2004).

Reports of a lack of face inversion effects in ASD (McPartland et al., 2004; Rose et al., 2007; Vettori et al., 2019) have been used to argue that individuals with ASD use a more feature-based approach to face processing. Typical observers are thought to use a more global or holistic approach to face processing, rather than a feature-by-feature analysis, and it is the disruption to this global analysis from turning the face upside down that produces the face inversion effect (Rossion, 2009). In the current study, a dramatic reduction in a saccade latency-based face inversion effect in participants with higher ATs suggests that this more feature-based approach to face processing extends across the broader autism spectrum. Importantly, it suggests that this feature-based approach operates not only at a slower more deliberate level but also at a faster and more reflexive level as required by the task demands in the current study. Finally, in both ASD and in the broader autism spectrum, previous studies have suggested either a more generalized impairment in global visual processing or a bias in local visual processing (Plaisted et al., 1999; Cribb et al., 2016). This might seem to be inconsistent with the current result given that different inversion effects were established for high and low AT groups when detecting faces, but not when detecting cars. Unlike for faces, however, it is assumed that the processing of non-face objects typically relies more on a feature-based strategy (Farah et al., 1998). As a consequence, reduced face inversion effects may reflect a face-specific anomaly in processing in the high AT participants, though a more general global processing deficit would be expected to be evident only when comparing the upright and inverted face conditions.

Although all participants were able to quickly and accurately select and direct eye-movements towards both face and car target categories, face targets were selected more accurately and with faster response times than for car targets. This replicates the findings in neurotypical adults by Crouzet et al. (2010), highlighting that faces constitute a special category of objects. Across all participants in the current sample, there was a 30-ms advantage in detecting a face as opposed to a car. It may be that humans have an innate specialized face specific module (Kanwisher and Yovel, 2006) or that a general-purpose object processing system develops expertise in face recognition given lifelong repeated exposure to faces (Hoehl and Peykarjou, 2012). A more interactive view suggests that innate tendencies to orient to faces lead to the development of face-sensitive regions in the ventral stream (de Haan et al., 2002). Regardless, it is evident that a clear behavioral advantage for the detection of faces is a strong and robust effect.

Although slower saccade initiation by high AT individuals to faces in a choice reaction time task was not established as expected, a moderate effect size ($\eta_p^2 = 0.038$) in the predicted direction was evident in this sub-clinical population. It remains possible that this effect would be more pronounced in a

clinical sample and could reflect differences in conductance or processing speed within face regions of the ventral stream. Although a trend suggested that the high AT group was slower overall to respond to upright faces than was the low AT group, the saccadic onset in both groups was still faster than what may be expected from ERP studies that have shown an N170 potential evoked by faces in neurotypical adults (e.g., Eimer and Holmes, 2002). The rapid onset of face-directed saccades observed in all participants may be consistent, however, with other reports using ERP or magnetoencephalography (MEG) that have found face-selective activation occurring at 100–120 ms (Eimer and Holmes, 2002; Liu et al., 2002) or even as early as 30–60 ms after stimulus onset in the ventral stream (Braeutigam et al., 2001). It is interesting to note that early visual processing abnormalities have been reported in adults with ASD (compared to healthy control participants), with weaker and less lateralized MEG responses to faces occurring around 145 ms in the ventral stream of the right hemisphere as well as abnormal earlier responses at 30–60 ms over temporal sites (Bailey et al., 2005).

The fast activation of neural processes subserving rapid saccadic responses to faces that we and others have observed may also be explained by processing that passes through subcortical pathways, bypassing the visual cortex, through the superior colliculus, pulvinar, and amygdala (Johnson, 2005). A dynamic causal modeling study based on MEG data suggested that there might be a direct pulvinar-amygdala activation that occurs as early as 70 ms, regardless of emotion or spatial frequency filtering (McFadyen et al., 2017). Human intracranial recording has also established a similar rapid amygdala activation specific to the low spatial frequency components of fearful faces (Méndez-Bértolo et al., 2016). Crucially, ASD has been associated with structural and functional abnormalities in the amygdala (Baron-Cohen et al., 2000), indicating that rapid subcortical activation could explain differences in saccadic anomalies in the high AT group in the current study. Although the amygdala has typically been associated with threat detection, other work suggests that the amygdala mediates goal-directed relevance detection more generally (Sander et al., 2003). Thus, the temporal advantage that we observed in the detection of faces, even though they had a range of different expressions, could reflect the operation of these amygdala-based mechanisms.

Abnormalities in the magnocellular visual system have been reported in both ASD (e.g., Greenaway et al., 2013) and in neurotypical individuals with higher ATs (e.g., Crewther et al., 2015). The magnocellular system is the faster conducting of the two largely separate geniculostriate pathways and preferentially responds to stimuli with lower spatial- and higher temporal-frequencies (Laycock et al., 2007). The magnocellular system is also thought to drive the subcortical route through superior colliculus (Schiller et al., 1979), and, of particular interest here, has been linked to the fast subcortical face detection pathway that subserves automatic face processing (Johnson, 2005). A number of studies in neurotypical adults have demonstrated a link between subcortical activation for faces with low spatial frequencies expected to bias the magnocellular system (Johnson, 2005). There is also evidence for impairments in face and emotion processing in ASD being linked to the low spatial frequency content of face images (e.g., de Jong et al., 2008). Thus, although highly speculative with regard to the current data, it remains possible that anomalies in these face processing mechanisms *via* the superior colliculus, pulvinar amygdala pathway may contribute to the absence of a saccadic advantage for upright compared with inverted faces in the high AT participants.

One potential limitation of the current study is the issue of gender and the relatively lower number of males in the low AT group, despite this imbalance not reaching statistical significance. It should be noted that the direction of this imbalance is consistent with the higher incidence of males diagnosed with ASD (Fombonne, 2005) and the higher number of ATs endorsed by males than females in the general population (Baron-Cohen et al., 2001). Follow-up analyses did not show any effect of gender on task performance, a finding consistent with Wyer et al. (2012), though the current study was not sufficiently powered to include gender in the main analysis. Thus, although it does not appear to have done so, it remains possible that gender may have exerted some influence on the results.

In conclusion, the current study finds evidence for differences in saccadic processing between high and low AT participants, that appears to be specific to face detection, and is most pronounced in the examination of saccadic face inversion effects. This finding reinforces the suggestion that people with high ATs do not treat faces as a special category of object, and instead appear to process them in the same way as they do any object. Alternatively, it could be argued they may process any object as they do a face, though in either case, it appears both types of stimuli may have equal salience in these participants. Taken together then, our findings have revealed an anomaly in the automatic and rapid detection of upright compared with inverted faces in individuals with high ATs.

DATA AVAILABILITY STATEMENT

The datasets generated for this study are available on request to the corresponding author.

ETHICS STATEMENT

The studies involving human participants were reviewed and approved by College of Science, Health & Engineering Human Ethics Sub-Committee, La Trobe University. The participants provided their written informed consent to participate in this study.

AUTHOR CONTRIBUTIONS

RL and MG developed the study concept. All authors contributed to the study design. Testing and data collection were performed by KW and AW. RL performed the data analysis. Data interpretation was made by RL, MG, and SC. KW and AW provided initial drafting of the manuscript, and RL completed the writing. MG and SC provided critical revisions. All authors approved the final version of the manuscript.

REFERENCES

Åsberg Johnels, J., Hovey, D., Zürcher, N., Hippolyte, L., Lemonnier, E., Gillberg, C., et al. (2017). Autism and emotional face-viewing. *Autism Res.* 10, 901–910. doi: 10.1002/aur.1730

Bailey, A. J., Braeutigam, S., Jousmaki, V., and Swithenby, S. J. (2005). Abnormal activation of face processing systems at early and intermediate latency in individuals with autism spectrum disorder: a magnetoencephalographic study. *Eur. J. Neurosci.* 21, 2575–2585. doi: 10.1111/j.1460-9568.2005.04061.x

Bannerman, R. L., Hibbard, P. B., Chalmers, K., and Sahraie, A. (2012). Saccadic latency is modulated by emotional content of spatially filtered face stimuli. *Emotion* 12, 1384–1392. doi: 10.1037/a0028677

Baron-Cohen, S., Ring, H. A., Bullmore, E. T., Wheelwright, S., Ashwin, C., and Williams, S. C. (2000). The amygdala theory of autism. *Neurosci. Biobehav. Rev.* 24, 355–364. doi: 10.1016/s0149-7634(00)00011-7

Baron-Cohen, S., Wheelwright, S., Skinner, R., Martin, J., and Clubley, E. (2001). The autism-spectrum quotient (AQ): evidence from Asperger syndrome/high-functioning autism, males and females, scientists and mathematicians. *J. Autism Dev. Disord.* 31, 5–17. doi: 10.1023/a:1005653411471

Braeutigam, S., Bailey, A. J., and Swithenby, S. J. (2001). Task-dependent early latency (30–60 ms) visual processing of human faces and other objects. *Neuroreport* 12, 1531–1536. doi: 10.1097/00001756-200105250-00046

Chawarska, K., Volkmar, F., and Klin, A. (2010). Limited attentional bias for faces in toddlers with autism spectrum disorders. *Arch. Gen. Psychiatry* 67, 178–185. doi: 10.1001/archgenpsychiatry.2009.194

Christ, S. E., Kanne, S. M., and Reiersen, A. M. (2010). Executive function in individuals with subthreshold autism traits. *Neuropsychology* 24, 590–598. doi: 10.1037/a0019176

Crewther, D. P., Crewther, D., Bevan, S., Goodale, M. A., and Crewther, S. G. (2015). Greater magnocellular saccadic suppression in high versus low autistic tendency suggests a causal path to local perceptual style. *R. Soc. Open Sci.* 2:150226. doi: 10.1098/rsos.150226

Cribb, S. J., Olaithe, M., Di Lorenzo, R., Dunlop, P. D., and Maybery, M. T. (2016). Embedded figures test performance in the broader autism phenotype: a meta-analysis. *J. Autism Dev. Disord.* 46, 2924–2939. doi: 10.1007/s10803-016-2832-3

Crouzet, S. M., Kirchner, H., and Thorpe, S. J. (2010). Fast saccades toward faces: face detection in just 100 ms. *J. Vis.* 10, 16.1–16.17. doi: 10.1167/10.4.16

Davis, C., Castles, A., McAnally, K., and Gray, J. (2001). Lapses of concentration and dyslexic performance on the Ternus task. *Cognition* 81, B21–B31. doi: 10.1016/s0010-0277(01)00129-9

de Haan, M., Humphreys, K., and Johnson, M. H. (2002). Developing a brain specialized for face perception: a converging methods approach. *Dev. Psychobiol.* 40, 200–212. doi: 10.1002/dev.10027

de Jong, M. C., van Engeland, H., and Kemner, C. (2008). Attentional effects of gaze shifts are influenced by emotion and spatial frequency, but not in autism. *J. Am. Acad. Child Adolesc. Psychiatry* 47, 443–454. doi: 10.1097/chi.0b013e31816429a6

Devue, C., and Grimshaw, G. M. (2017). Faces are special, but facial expressions aren't: insights from an oculomotor capture paradigm. *Atten. Percept. Psychophys.* 79, 1438–1452. doi: 10.3758/s13414-017-1313-x

Eimer, M., and Holmes, A. (2002). An ERP study on the time course of emotional face processing. *Neuroreport* 13, 427–431. doi: 10.1097/00001756-200203250-00013

Farah, M. J., Wilson, K. D., Drain, M., and Tanaka, J. N. (1998). What is "special" about face perception? *Psychol. Rev.* 105, 482–498. doi: 10.1037/0033-295x.105.3.482

Faul, F., Erdfelder, E., Buchner, A., and Lang, A.-G. (2009). Statistical power analyses using G* Power 3.1: tests for correlation and regression analyses. *Behav. Res. Methods* 41, 1149–1160. doi: 10.3758/brm.41.4.1149

Fombonne, E. (2005). The changing epidemiology of autism. *J. Appl. Res. Intellect. Disabil.* 18, 281–294. doi: 10.1111/j.1468-3148.2005.00266.x

Freedman, E. G., and Foxe, J. J. (2018). Eye movements, sensorimotor adaptation and cerebellar-dependent learning in autism: toward potential biomarkers and subphenotypes. *Eur. J. Neurosci.* 47, 549–555. doi: 10.1111/ejn.13625

Goldberg, M. C., Lasker, A. G., Zee, D. S., Garth, E., Tien, A., and Landa, R. J. (2002). Deficits in the initiation of eye movements in the absence of a visual target in adolescents with high functioning autism. *Neuropsychologia* 40, 2039–2049. doi: 10.1016/s0028-3932(02)00059-3

Greenaway, R., Davis, G., and Plaisted-Grant, K. (2013). Marked selective impairment in autism on an index of magnocellular function. *Neuropsychologia* 51, 592–600. doi: 10.1016/j.neuropsychologia.2013.01.005

Guillon, Q., Rogé, B., Afzali, M. H., Baduel, S., Kruck, J., and Hadjikhani, N. (2016). Intact perception but abnormal orientation towards face-like objects in young children with ASD. *Sci. Rep.* 6:22119. doi: 10.1038/srep22119

Hoehl, S., and Peykarjou, S. (2012). The early development of face processing—what makes faces special? *Neurosci. Bull.* 28, 765–788. doi: 10.1007/s12264-012-1280-0

Johnson, M. H. (2005). Subcortical face processing. *Nat. Rev. Neurosci.* 6, 766–774. doi: 10.1038/nrn1766

Johnson, M. H., Dziurawiec, S., Ellis, H., and Morton, J. (1991). Newborns' preferential tracking of face-like stimuli and its subsequent decline. *Cognition* 40, 1–19. doi: 10.1016/0010-0277(91)90045-6

Kanne, S. M., Wang, J., and Christ, S. E. (2012). The Subthreshold Autism Trait Questionnaire (SATQ): development of a brief self-report measure of subthreshold autism traits. *J. Autism Dev. Disord.* 42, 769–780. doi: 10.1007/s10803-011-1308-8

Kanwisher, N., and Yovel, G. (2006). The fusiform face area: a cortical region specialized for the perception of faces. *Philos. Trans. R. Soc. Lond. B Biol. Sci.* 361, 2109–2128. doi: 10.1098/rstb.2006.1934

Kelly, D. J., Walker, R., and Norbury, C. F. (2013). Deficits in volitional oculomotor control align with language status in autism spectrum disorders. *Dev. Sci.* 16, 56–66. doi: 10.1111/j.1467-7687.2012.01188.x

Kikuchi, Y., Senju, A., Akechi, H., Tojo, Y., Osanai, H., and Hasegawa, T. (2011). Atypical disengagement from faces and its modulation by the control of eye fixation in children with autism spectrum disorder. *J. Autism Dev. Disord.* 41, 629–645. doi: 10.1007/s10803-010-1082-z

Kovarski, K., Siwiaszczyk, M., Malvy, J., Batty, M., and Latinus, M. (2019). Faster eye movements in children with autism spectrum disorder. *Autism Res.* 12, 212–224. doi: 10.1002/aur.2054

Landry, O., and Chouinard, P. A. (2016). Why we should study the broader autism phenotype in typically developing populations. *J. Cogn. Dev.* 17, 584–595. doi: 10.1080/15248372.2016.1200046

Laycock, R., Crewther, S. G., and Crewther, D. P. (2007). A role for the 'magnocellular advantage' in visual impairments in neurodevelopmental and psychiatric disorders. *Neurosci. Biobehav. Rev.* 31, 363–376. doi: 10.1016/j.neubiorev.2006.10.003

Lerner, M. D., McPartland, J. C., and Morris, J. P. (2013). Multimodal emotion processing in autism spectrum disorders: an event-related potential study. *Dev. Cogn. Neurosci.* 3, 11–21. doi: 10.1016/j.dcn.2012.08.005

Liu, J., Harris, A., and Kanwisher, N. (2002). Stages of processing in face perception: an MEG study. *Nat. Neurosci.* 5, 910–916. doi: 10.1038/nn909

Lozier, L. M., Vanmeter, J. W., and Marsh, A. A. (2014). Impairments in facial affect recognition associated with autism spectrum disorders: a meta-analysis. *Dev. Psychopathol.* 26, 933–945. doi: 10.1017/s0954579414000479

Luna, B., Doll, S. K., Hegedus, S. J., Minshew, N. J., and Sweeney, J. A. (2007). Maturation of executive function in autism. *Biol. Psychiatry* 61, 474–481. doi: 10.1016/j.biopsych.2006.02.030

McFadyen, J., Mermillod, M., Mattingley, J. B., Halász, V., and Garrido, M. I. (2017). A rapid subcortical amygdala route for faces irrespective of spatial frequency and emotion. *J. Neurosci.* 37, 3864–3874. doi: 10.1523/JNEUROSCI.3525-16.2017

McPartland, J., Dawson, G., Webb, S. J., Panagiotides, H., and Carver, L. J. (2004). Event-related brain potentials reveal anomalies in temporal processing of faces in autism spectrum disorder. *J. Child Psychol. Psychiatry* 45, 1235–1245. doi: 10.1111/j.1469-7610.2004.00318.x

Méndez-Bértolo, C., Moratti, S., Toledano, R., Lopez-Sosa, F., Martínez-Alvarez, R., Mah, Y. H., et al. (2016). A fast pathway for fear in human amygdala. *Nat. Neurosci.* 19, 1041–1049. doi: 10.1038/nn.4324

Miller, J. (1988). A warning about median reaction time. *J. Exp. Psychol. Hum. Percept. Perform* 14, 539–543. doi: 10.1037/0096-1523.14.3.539

Miller, M., Chukoskie, L., Zinni, M., Townsend, J., and Trauner, D. (2014). Dyspraxia, motor function and visual-motor integration in autism. *Behav. Brain Res.* 269, 95–102. doi: 10.1016/j.bbr.2014.04.011

Minshew, N. J., Luna, B., and Sweeney, J. A. (1999). Oculomotor evidence for neocortical systems but not cerebellar dysfunction in autism. *Neurology* 52, 917–922. doi: 10.1212/wnl.52.5.917

Nishiyama, T., and Kanne, S. M. (2014). On the misapplication of the BAPQ in a study of autism. *J. Autism Dev. Disord.* 44, 2079–2080. doi: 10.1007/s10803-014-2077-y

Palermo, M. T., Pasqualetti, P., Barbati, G., Intelligente, F., and Rossini, P. M. (2006). Recognition of schematic facial displays of emotion in parents of children with autism. *Autism* 10, 353–364. doi: 10.1177/1362361306064431

Plaisted, K., Swettenham, J., and Rees, L. (1999). Children with autism show local precedence in a divided attention task and global precedence in a selective attention task. *J. Child Psychol. Psychiatry* 40, 733–742. doi: 10.1111/1469-7610.00489

Raven, J. C., Raven, J. C., and Court, J. (1996). *Standard Progressive Matrices: Sets A, B, C, D and E.* Oxford: Oxford Psychologists Press.

Rose, F. E., Lincoln, A. J., Lai, Z., Ene, M., Searcy, Y. M., and Bellugi, U. (2007). Orientation and affective expression effects on face recognition in Williams syndrome and autism. *J. Autism Dev. Disord.* 37, 513–522. doi: 10.1007/s10803-006-0200-4

Rossion, B. (2009). Distinguishing the cause and consequence of face inversion: the perceptual field hypothesis. *Acta Psychol.* 132, 300–312. doi: 10.1016/j.actpsy.2009.08.002

Sander, D., Grafman, J., and Zalla, T. (2003). The human amygdala: an evolved system for relevance detection. *Rev. Neurosci.* 14, 303–316. doi: 10.1515/revneuro.2003.14.4.303

Schiller, P. H., Malpeli, J. G., and Schein, S. J. (1979). Composition of geniculostriate input to superior colliculus of the rhesus monkey. *J. Neurophysiol.* 42, 1124–1133. doi: 10.1152/jn.1979.42.4.1124

Simmons, D. R., Robertson, A. E., Mckay, L. S., Toal, E., Mcaleer, P., and Pollick, F. E. (2009). Vision in autism spectrum disorders. *Vision Res.* 49, 2705–2739. doi: 10.1016/j.visres.2009.08.005

Snow, J., Ingeholm, J. E., Levy, I. F., Caravella, R. A., Case, L. K., Wallace, G. L., et al. (2011). Impaired visual scanning and memory for faces in high-functioning autism spectrum disorders: it's not just the eyes. *J. Int. Neuropsychol. Soc.* 17, 1021–1029. doi: 10.1017/s1355617711000981

Spencer, M. D., Holt, R. J., Chura, L. R., Suckling, J., Calder, A. J., Bullmore, E. T., et al. (2011). A novel functional brain imaging endophenotype of autism: the neural response to facial expression of emotion. *Transl. Psychiatry* 1:e19. doi: 10.1038/tp.2011.18

Takarae, Y., Minshew, N. J., Luna, B., and Sweeney, J. A. (2004). Oculomotor abnormalities parallel cerebellar histopathology in autism. *J. Neurol. Neurosurg. Psychiatry* 75, 1359–1361. doi: 10.1136/jnnp.2003.022491

Vettori, S., Dzhelyova, M., Van der Donck, S., Jacques, C., Steyaert, J., Rossion, B., et al. (2019). Reduced neural sensitivity to rapid individual face discrimination in autism spectrum disorder. *NeuroImage Clin.* 21:101613. doi: 10.1016/j.nicl.2018.101613

Wallace, S., Sebastian, C., Pellicano, E., Parr, J., and Bailey, A. (2010). Face processing abilities in relatives of individuals with ASD. *Autism Res.* 3, 345–349. doi: 10.1002/aur.161

Weigelt, S., Koldewyn, K., and Kanwisher, N. (2012). Face identity recognition in autism spectrum disorders: a review of behavioral studies. *Neurosci. Biobehav. Rev.* 36, 1060–1084. doi: 10.1016/j.neubiorev.2011.12.008

Wilkes, B. J., Carson, T. B., Patel, K. P., Lewis, M. H., and White, K. D. (2015). Oculomotor performance in children with high-functioning autism spectrum disorders. *Res. Dev. Disabil.* 38, 338–344. doi: 10.1016/j.ridd.2014.12.022

Wilson, C. E., Brock, J., and Palermo, R. (2010). Attention to social stimuli and facial identity recognition skills in autism spectrum disorder. *J. Intellect. Disabil. Res.* 54, 1104–1115. doi: 10.1111/j.1365-2788.2010.01340.x

Wyer, N. A., Martin, D., Pickup, T., and Macrae, C. N. (2012). Individual differences in (non-visual) processing style predict the face inversion effect. *Cogn. Sci.* 36, 373–384. doi: 10.1111/j.1551-6709.2011.01224.x

Zalla, T., Seassau, M., Cazalis, F., Gras, D., and Leboyer, M. (2018). Saccadic eye movements in adults with high-functioning autism spectrum disorder. *Autism* 22, 195–204. doi: 10.1177/1362361316667057

Conflict of Interest: The authors declare that the research was conducted in the absence of any commercial or financial relationships that could be construed as a potential conflict of interest.

APPENDIX

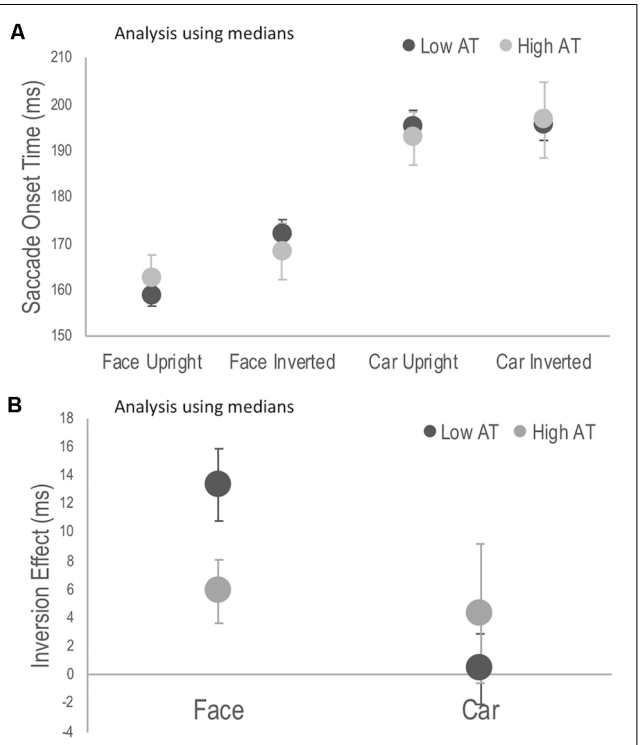

FIGURE A1 | Reanalysis using individual median scores, rather than means as in **Figure 2**. **(A)** Median saccade onset times (SOTs) to detect the photograph containing a face or a car in the upright and inverted tasks for high and low Autism Trait (AT) Groups. **(B)** Face and car inversion effects, calculated as the difference in median SOTs between upright and inverted tasks for high and low Autism Trait (AT) Groups. Error bars indicate standard error of the mean. Error bars indicate SEM.

frontiers in Human Neuroscience

ORIGINAL RESEARCH
published: 30 January 2020
doi: 10.3389/fnhum.2020.00002

Differential Regional Brain Spontaneous Activity in Subgroups of Mild Cognitive Impairment

Qi-Hui Zhou[1†], Kun Wang[2†], Xiao-Ming Zhang[3†], Li Wang[1] and Jiang-Hong Liu[1]*

[1]Department of Neurology, Xuanwu Hospital, Capital Medical University, Beijing, China, [2]Department of Neurology, Beijing Puren Hospital, Beijing, China, [3]Department of Psychiatry, Beijing Huilongguan Hospital, Beijing, China

Background: Amnestic mild cognitive impairment (aMCI) has a high conversion risk to Alzheimer's disease (AD). The aMCI patients may have only a memory deficit (single-domain-aMCI, sd-aMCI) or deficits in multiple cognitive domains (multiple-domain-aMCI, md-aMCI). However, differences in intrinsic brain activity between these two sub-types remain unclear.

Method: Neuropsychological and resting-state functional magnetic resonance imaging (fMRI) data were acquired from 24 patients with sd-aMCI, 23 patients with md-aMCI, and 32 healthy controls (HCs). We used the fractional amplitude of low-frequency fluctuation (fALFF) to characterize the intensity of spontaneous brain activity. The analysis of covariance (ANCOVA) and *post hoc* tests was performed to determine the between-group differences in fALFF.

Results: We found higher fALFF in left-sided superior-to-middle frontal gyri and middle-to-inferior temporal gyri in sd-aMCI compared to both the md-aMCI and HCs. Conversely, a lower fALFF was found in the left inferior parietal lobe in both the md-aMCI and sd-aMCI patients. The fALFF values in the left middle and inferior temporal gyri were correlated with cognitive performances.

Conclusion: The gradual reduction in the left inferior parietal lobe from single to multiple domain aMCI suggest a functional inefficiency underlying cognitive impairment, while increased activity in the frontal and temporal gyri in sd-aMCI rather than md-aMCI might indicate functional compensation. This study indicates differential functional profiles in the sd-aMCI and md-aMCI, which may be helpful for the prediction of the future conversion of aMCI to AD.

Keywords: mild cognitive impairment, resting state, fMRI, the amplitude of low-frequency fluctuation, Alzheimer's disease

OPEN ACCESS

Edited by:
Vasil Kolev,
Institute of Neurobiology (BAS), Bulgaria

Reviewed by:
Zhen Yuan,
University of Macau, China
Bahar Güntekin,
Istanbul Medipol University, Turkey

****Correspondence:***
Jiang-Hong Liu
liujh@xwhosp.org

†These authors have contributed equally to this work

Specialty section:
This article was submitted to Health, a section of the journal Frontiers in Human Neuroscience

Received: *13 July 2019*
Accepted: *07 January 2020*
Published: *30 January 2020*

Citation:
Zhou Q-H, Wang K, Zhang X-M, Wang L and Liu J-H (2020) Differential Regional Brain Spontaneous Activity in Subgroups of Mild Cognitive Impairment. Front. Hum. Neurosci. 14:2. doi: 10.3389/fnhum.2020.00002

INTRODUCTION

Alzheimer's disease (AD) is a leading cause of dementia worldwide. Once the clinical symptoms of dementia emerge, the brain atrophy has been irreversible, rendering the recognition of AD at the early stage an urgent prerequisite for effective intervention. Amnestic mild cognitive impairment (aMCI) has been considered as a highrisk condition of conversion to AD

(Petersen et al., 2001), which is thus a critical stage for early recognition of AD.

The neuropathological basis of aMCI has been investigated extensively. At the stage of aMCI, AD-like patterns of brain change shave been observed, including characteristic patterns of functional and structural atrophies in the temporal and parietal cortices involved in episodic memory (Hu et al., 2014; Farràs-Permanyer et al., 2015). Even though the aMCI diagnosis relies primarily on the presence of memory dysfunction, it is increasingly recognized that aMCI may represent a highly heterogeneous condition and impairments in other cognitive domains were often observed in aMCI patients (Brambati et al., 2009; Lenzi et al., 2011; Li and Zhang, 2015). The aMCI could be classified into single-domain-aMCI (sd-aMCI) and multiple-domain-aMCI (md-aMCI) sub-types (Brambati et al., 2009; Lenzi et al., 2011; Li and Zhang, 2015). The sd-aMCI is characterized by isolated memory impairment, while the md-aMCI is characterized by more widespread cognitive dysfunction involving executive, attention, language, and/or visuospatial abilities (Cid-Fernández et al., 2017). Given that the two sub-types of aMCI have different probabilities of progression to AD (Brambati et al., 2009; Lenzi et al., 2011; Li and Zhang, 2015), it is important to characterize the neural patterns of these subtypes and identify the features that could predict their progression to AD.

However, the relationships between the sd-aMCI and md-aMCI have not been fully clarified. One hypothesis is that the sd-aMCI progresses to md-aMCI, which is an advanced stage toward AD rather than sd-aMCI (Seo et al., 2007; Gu et al., 2019). The sd-aMCI patients were found to have cortical thinning in the left medial temporal lobe relative to healthy controls (HCs), while the md-aMCI patients showed cortical thinning in more widespread regions including the left medial temporal lobe, precuneus, insula, and temporal association cortices (Seo et al., 2007). A combined event-related potential (ERP) and standardized low-resolution brain electromagnetic tomography analysis (sLORETA) study (Gu et al., 2019) found more severe neural deficits during the performance of visuospatial working memory and response inhibition tasks in md-aMCI compared with sd-aMCI patients. In another single-photon emission computed tomography study, reduced metabolism in the fronto-parieto-temporal areas has been observed in both the sd-aMCI and md-aMCI groups, with the md-aMCI group showing additional deficits in the posterior cingulate gyrus (Caffarra et al., 2008). There is also other evidence that the sd-aMCI and md-aMCI reflect two different etiological processes of dementia (Bell-McGinty et al., 2005; Zou et al., 2008; Liu et al., 2017). For instance, the sd-aMCI patients showed more significant volume loss in the left entorhinal cortex and inferior parietal lobe, while the md-aMCI showed larger volume reductions in the right inferior frontal gyrus, right middle temporal gyrus, and bilateral superior temporal gyrus compared to md-aMCI patients (Bell-McGinty et al., 2005). A diffusion tensor imaging (DTI) study reported that the global topological organization of white matter networks was disrupted in patients with md-aMCI but not sd-aMCI (Liu et al., 2017). Our previous study (Zou et al., 2008) of DTI showed decreased FA in the left uncinate fasciculus and left inferior longitudinal fasciculus in sd-aMCI compared to md-aMCI patients. Nonetheless, these studies primarily focused on metabolic and structural differences in patients with sd-aMCI and md-aMCI, how the spontaneous brain activity differs from a regional perspective between both of them remains unknown.

Therefore, we conducted this study to determine the characteristic functional profiles of the subtypes of sd-aMCI and md-aMCI.Neuropsychological and resting-state functional magnetic resonance imaging (fMRI) data were acquired from 24 sd-aMCI patients, 23 md-aMCI patients, and 32HCs. The fractional amplitude of low-frequency fluctuation (fALFF; Zou et al., 2008) was used to measure brain activity intensity. Using this approach, a study has demonstrated that MCI patients had decreased activity in the medial parietal lobe and increased activity in the lateral temporal regions and superior frontal regions (Belleville et al., 2008). Based on these previous functional magnetic resonance imaging (MRI) study in aMCI and the SPECT study comparing the blood flow between sd-aMCI and md-aMCI, we hypothesized that the fALFF changes in both the sd-aMCI and md-aMCI patients would be most pronounced in the posterior temporal regions subserving episodic memory, which has been impaired in MCI and AD patients (Traykov et al., 2007). Givenmore widespread cognitive dysfunction in md-aMCI patients (Albert et al., 2011), the md-aMCI patients may also have functional abnormalities in the prefrontal and parietal cortex. Disrupted brain activity may be associated with cognitive performances.

MATERIALS AND METHODS

Subjects

Twenty-three md-aMCI and 24 sd-aMCI patients were recruited from the Department of Neurology of Xuanwu Hospital, Capital Medical University, between January 2011 and March 2015. Patients were diagnosed according to Petersen's criteria (Petersen et al., 2001) and National Institute on Aging-Alzheimer's Association criteria for MCI due to AD (American Psychiatric Association, 1994) according to the criteria: memory complaint; objective memory impairment; near-normal performances on general cognition and preserved daily life activities measured by Activity of Daily Living Scale (ADL); Clinical Dementia Rating (CDR) score of 0.5; failure to meet the criteria of dementia according to the Diagnostic and Statistical Manual of Mental Disorders, fourth edition (DSM-IV; Wang et al., 2011); hippocampal atrophy measured by the Medial Temporal lobe Atrophy scale (MTA scale).

Thirty-two HCs were recruited in the local community. The HCs were cognitively normal and had a CDR of 0, and no history of psychiatric or neuropsychological diseases. All patients had no use of any psychotropic medications for at least 2 weeks prior to the study. The prevalence of vascular factors such as hypertension, hypercholesterolemia, and heart attack did not differ among the three groups of md-aMCI, sd-aMCI, and HCs.

TABLE 1 | Sample characteristics.

	md-aMCI (*n* = 23)	sd-aMCI (*n* = 24)	HCs (*n* = 32)	*F*	*p*	*Post hoc*
Gender (M/F)	13/10	10/14	14/18			
Age (years)	70.4 ± 8.3	69.8 ± 6.2	67.9 ± 6.4	0.972	0.383	
Education (years)	10.3 ± 3.6	8.3 ± 4.1	11.4 ± 3.6	4.983	0.009	B < A, C
FD	0.23 ± 0.1	0.24 ± 0.1	0.25 ± 0.11	0.397	0.674	
AVLT	4.4 ± 3.6	3.5 ± 2.0	10.9 ± 2.6	99.256	<0.001	A, B < C
MMSE	24.7 ± 3.7	23.9 ± 3.6	28.0 ± 1.9	14.36	<0.001	A, B < C
MoCa	20.4 ± 4.1	19.4 ± 4.6	26.5 ± 2.4	28.995	<0.001	A, B < C
BNT	23.3 ± 2.2	27.9 ± 1.3	29.1 ± 0.7	108.753	<0.001	A < B, C
TMT-A	109.5 ± 19.4	73.1 ± 13.1	54.3 ± 14.2	79.906	<0.001	A > B, C; B > C
TMT-B	222.4 ± 43.3	152.5 ± 38.5	116.1 ± 43.7	40.259	<0.001	A > B, C; B > C

*Data are given as mean ± SD unless otherwise indicated. A, md-aMCI; B, sd-aMCI; C, HC; M, male; F, female; FD, framewise displacement; AVLT, the Auditory Verbal Learning Test; MMSE, Mini-Mental State Examination; MoCA, the Montreal cognitive assessment; BNT, the Boston naming test; TMT, the trail making test. The AVLT, MMSE, MoCA, and BNT were based on numbers correct, and TMT was based on seconds.

All subjects were Han race and right-handed. Exclusion criteria included neurological illnesses, unstable medical condition, substance dependence or abuse within the last year, a history of electroconvulsive therapy, acutely suicidal or homicidal, current pregnancy or breastfeeding, or any contraindications to MRI scan. The protocol was approved by the institutional review board of Xuanwu Hospital of Capital Medical University. All subjects gave written informed consent in accordance with the Declaration of Helsinki. The demographic and clinical data were provided in **Table 1**.

Neuropsychological Tests

All subjects underwent a series of neurological and neuropsychological tests by an experienced neurologist, including mini-mental state examination (MMSE), Montreal cognitive assessment (MoCA), Auditory Verbal Learning Test (AVLT of Chinese version, short delay free recall), Boston naming test (BNT), trail making test (TMT; visual attention and task switching), clock drawing test (CDT; 3-point), and CDR. We used the 3-point CDT to test visuospatial skill, the TMT to test executive function, the BNT to test language skill, and the AVLT (short delay free recall) to test memory ability.

MRI Data Acquisition

The MRI scans were performed on a 3-Tesla scanner (Siemens Medical Solutions, Erlangen, Germany). The resting-state functional images were obtained using an echo-planar imaging sequence: repetition time (TR)/echo time (TE), 2,000 ms/40 ms; 90° flip angle; matrix, 64 × 64; thickness/gap, 4.0 mm/1.0 mm; 28 slices. The resting-state fMRI scanning lasted for nearly 8 min. For a registration propose, T1-weighted structural images were obtained using a magnetization-prepared rapidly acquired gradient-echo (MPRAGE) sequence: repetition time (TR)/echo time (TE), 1,900 ms/2.2 ms; 9° flip angle (FA); matrix, 224 × 256 × 176; voxel size, 1 × 1 × 1 mm^3. Before the resting-state scans, subjects were instructed to keep their eyes closed, remain still without head movement, not think of anything in particular, and not fall asleep during the scan. All subjects reported good adherence to these instructions through confirmation immediately after the MRI scans. No subjects showed obvious structural damage based on their MRI images.

Data Preprocessing

The R-fMRI images were preprocessed with Data Processing Assistant for Resting-State fMRI (DPARSF[1]) based on Statistical Parametric Mapping (SPM12[2]). The first 10 volumes were discarded to allow for magnetization equilibrium. The slice times for the remaining 229 volumes were corrected for different signal acquisition times. The functional volumes were motion-corrected using a six-parameter rigid-body transformation. Subjects with head motion exceeding translation 2 mm or rotation 2° were excluded. The nuisance signals (including Friston 24-parameter model of head-motion parameters, cerebrospinal fluid (CSF) and white matter signals, and linear trend) were regressed out, while the regression of global brain signals was not performed because of a potential induction of negative correlations. Then, derived images were normalized to Montreal Neurological Institute (MNI) space (3 mm^3 isotropic) using Diffeomorphic Anatomical Registration using Exponentiated Lie algebra (DARTEL) tool. The spatial smoothing was performed using Full Wave at Half Maximum 6 mm.

The fALFF Computation

We used the fALFF approach to characterize the intensity of intrinsic neural activity. The fALFF analyses were performed using the DPARSF software. Specifically, after the above preprocessing, the fMRI data were temporally band-pass filtered ($0.01 < f < 0.08$ Hz) to reduce the low-frequency drift and high-frequency respiratory and cardiac noise. The time series of each voxel was transformed into the frequency domain, and the power spectrum was obtained. Because the power of a given frequency is proportional to the square of the amplitude of that frequency component, the square root was calculated at each frequency of the power spectrum, and the averaged square root was obtained across 0.01–0.08 Hz at each voxel. This averaged square root was taken as the ALFF, which was assumed to reflect the absolute intensity of brain activity (Zang et al., 2007).

Previous studies have found that although the ALFF reveals significantly higher ALFF in the posterior cingulate cortex, precuneus, and medial prefrontal cortex, other non-specific areas

[1]http://rfmri.org/DPARSF
[2]http://www.fil.ion.ucl.ac.uk/spm

have also been shown to have higher ALFF, such as the cisterns, the ventricles, and/or the vicinities of large blood vessels (Zou et al., 2008), suggesting that the ALFF approach may be sensitive to signal from physiological noise. To overcome these limits, a ratio of the power of each frequency at a low-frequency range to that of the entire frequency range (i.e., fractional ALFF, fALFF) was computed (Di Paola et al., 2009). Specifically, after the removal of linear trends, the time series for each voxel was transformed into the frequency domain without band-pass filtering. The square root was calculated at each frequency of the power spectrum. The sum of the amplitude across 0.01–0.08 Hz was divided by that of the entire frequency range (0–0.25 Hz). The validity of the fALFF approach in suppressing confounding signals from non-specific areas has been confirmed in a sample of healthy subjects (Di Paola et al., 2009).

Statistical Analysis

Between-Group Comparisons in fALFF

One-way analysis of covariance (ANCOVA) was performed to determine the fALFF differences among the md-aMCI, sd-aMCI, and HC groups, controlling for age, gender, educational level, and mean FD values. The results of ANCOVA were corrected for multiple comparisons with a combination of voxel $p < 0.001$ and cluster $p < 0.05$ according to the Gaussian random field (GRF) theory.

Then, for the clusters showing statistical significance during the ANCOVA, we extracted the mean values of the fALFF, and then, performed *post hoc* analyses to determine their differences between two groups within the md-aMCI, sd-aMCI, and HCs by performing 2-sample *t*-tests with statistical significance determined by a Bonferroni-corrected $p < 0.0083$ (0.05/the number of *t*-tests, which is 6).

Between-Group Comparisons With GM as Covariates

Structural MRI studies have suggested that the aMCI patients have GM loss in many cerebral regions (Kim et al., 2013). The GM loss may produce partial effects on functional images and thus be a confounding factor for the analysis of functional brain images. We, therefore, re-performed the ANCOVA in the fALFF images among the md-aMCI, sd-aMCI, and HC groups by adding the GM images as covariates.

Clinical Correlations

The partial correlation analyses were performed between the fALFF mean values of clusters showing statistical significance during ANCOVA and cognitive measures including MMSE, MoCA, AVLT, BNT, TMT and CDT, with gender, age and educational level served as covariates. The statistical significance was determined by an uncorrected $p < 0.05$.

RESULTS

Demographic Data

As shown in **Table 1**, there were significant group differences in years of education, AVLT, MMSE, MoCa, BNT, TMT-A, and TMT-B ($p < 0.01$), while no differences were found in age and gender. The between-group difference in education was mainly driven by the sd-aMCI group. For the AVLT, MMSE, MoCa, BNT, TMT-A, and TMT-B, both the md-aMCI and sd-aMCI groups showed significant decreases compared to HCs ($p < 0.001$). Poorer performances in TMT-A and TMT-B were found in both md-aMCI and sd-aMCI compared to HCs, and in md-aMCI compared to sd-aMCI ($p < 0.001$).

Between-Group Differences in fALFF

The ANCOVA among the three groups showed significant group effects in the left-sided superior and middle frontal gyri (peak MNI coordinates: −18, 39, −12), middle (peak MNI coordinates: −63, −18, −24) and inferior (peak MNI coordinates: −39, −15, −33) temporal gyri, and inferior parietal lobe (peak MNI coordinates: −51, −51, 24; **Figure 1** and **Table 2**). For these clusters showing statistical significance during the ANCOVA, the *post hoc* analysis showed higher fALFF values in the left-sided superior and middle frontal gyri, the middle and inferior temporal gyri in the sd-aMCI group than both the md-aMCI and HC groups. Conversely, lower fALFF was found in the left inferior parietal lobe in the md-aMCI than the sd-aMCI group, and in the sd-aMCI than the HC group (**Table 2**). As shown in **Supplementary Figure S1**, using the GM volume images as covariates, the fALFF analyses produced results similar to the analyses without GM correction.

Clinical Correlations

As shown in **Table 1** and **Figure 2**, we observed significant positive correlation between the fALFF values of the left inferior temporal gyrus and the MMSE scores within the md-aMCI group. Conversely, a significant negative correlation was observed between the fALFF values of the left middle temporal gyrus and both the MMSE and MoCA scores within the sd-aMCI group.

DISCUSSION

Using the fALFF in dice, the current study examined the differences in resting-state brain activity in patients with the sd-aMCI and md-aMCI subtypes. The results showed that the sd-aMCI differed from md-aMCI in the fALFF values of the left superior-to-middle frontal gyri, the left middle-to-inferior temporal gyri, and the left inferior parietal lobe. The fALFF in the left temporal gyri were associated with cognitive deficits in aMCI patients. The results suggest that the two subtypes of aMCI may have different functional correlates and the fALFF may be a potential measure to differentiate them.

The first important finding is higher fALFF in the left-sided superior-to-middle frontal gyri and middle-to-inferior temporal gyri in the sd-aMCI than both the md-aMCI and HC groups. The superior and middle frontal gyri are involved in a series of cognitive processes, such as executive function and working memory (Kim et al., 2014; Zamora et al., 2016), while the lateral temporal cortex is more involved in episodic memory (Luo et al., 2018). These cognitive functions are typically impaired in AD and MCI patients (Bell-McGinty et al., 2005; Clément and Belleville, 2010; Teipel et al., 2010; Liang et al., 2011; Scheller et al., 2014; Verfaillie et al., 2016; Melrose et al., 2018).

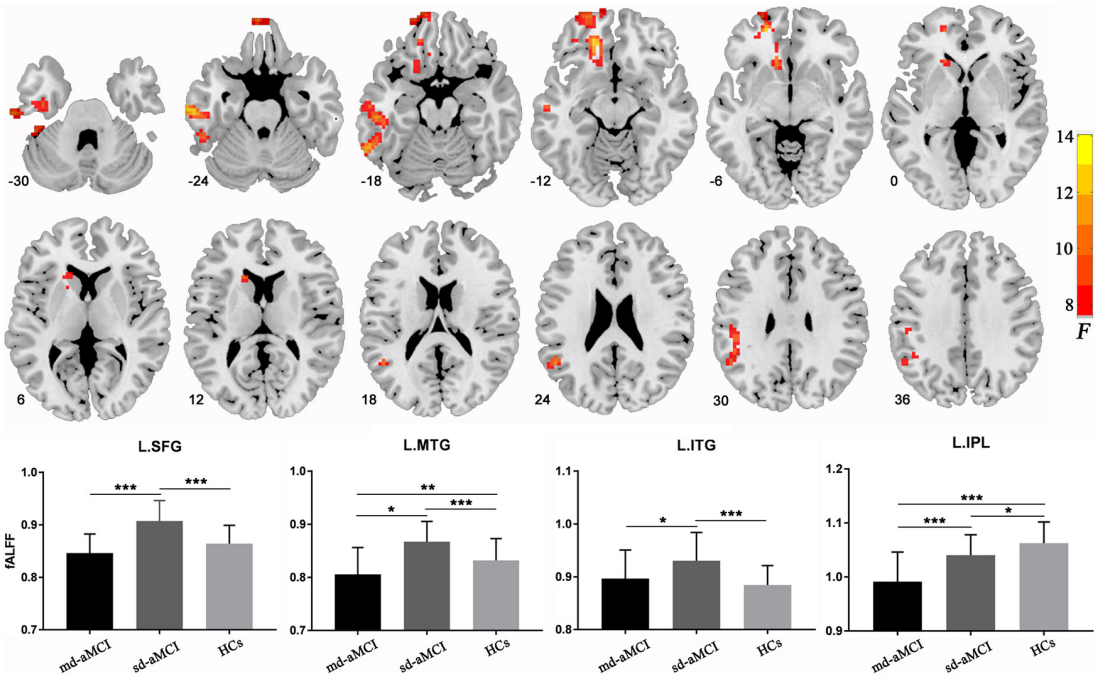

FIGURE 1 | Regions showing between-group differences in fractional amplitude of low-frequency fluctuation (fALFF). The images show a significant group effect on the fALFF in the left frontal gyrus, left middle and inferior temporal gyri, and left inferior parietal lobule. The numbers at the lower-left corner of the image refer to the montreal neurological institute (MNI) coordinates. The bar maps show between-group differences in fALFF in these regions. The data were expressed as mean value ± standard error (SE). $^{*}p < 0.05$; $^{**}p < 0.01$; $^{***}p < 0.001$.

TABLE 2 | Regions showing between-group differences in fALFF.

Region	Voxels	MNI coordinate (x, y, z)	*F*	*Post hoc*
Superior frontal gyrus/Middle frontal gyrus	287	−18, 39, −12	12.35	B > A, C
Middle temporal gyrus	196	−63, −18, −24	12.799	B > A, C
Inferior temporal gyrus	66	−39, −15, −33	9.198	B > A, C
Inferior parietal lobule	93	−51, −51, 24	9.749	A > B; B > C

fALFF, fractional amplitude of low-frequency fluctuation; MNI, Montreal Neurological Institute. A, md-aMCI; B, sd-aMCI; C, HC.

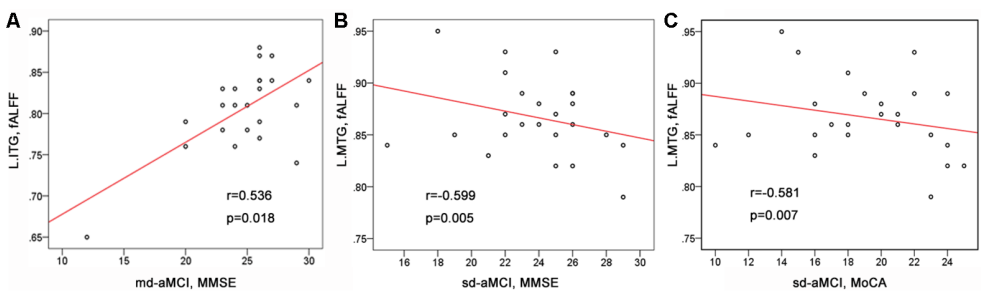

FIGURE 2 | The correlations between the fALFF values and cognitive scores. **(A)** Significant positive correlations between the fALFF of the left inferior temporal gyrus and the mini-mental state examination (MMSE) scores found within the md-Amnestic mild cognitive impairment (aMCI) group. **(B,C)** Significant negative correlations between the fALFF of the left middle temporal gyrus and the MMSE scores, between the fALFF of the left middle temporal gyrus and the MoCA scores found within the single-domain-aMCI (sd-aMCI) group.

Studies have suggested an involvement of the lateral frontal and temporal cortical regions in aMCI (Bell-McGinty et al., 2005; Clément and Belleville, 2010; Teipel et al., 2010; Liang et al., 2011; Scheller et al., 2014; Verfaillie et al., 2016; Melrose et al., 2018). For instance, a study (Verfaillie et al., 2016) combining the R-fMRI and CSF showed that the regional

homogeneity values were associated with the Aβ level of the superior temporal gyrus in patients with sd-aMCI. The thinner temporal cortex has been used to predict the increased risk of future progression to dementia (Teipel et al., 2010). Another study of DTI showed altered fiber integrity in aMCI patients in the callosal genu and anterior midbody connecting the bilateral hemispheres of the prefrontal cortices (Scheller et al., 2014). The GM volume in the superior and middle temporal gyri has been used to differentiate the md-aMCI and sd-aMCI as greater volume loss was observed in patients with md-aMCI compared to sd-aMCI (Bell-McGinty et al., 2005). Despite these structural atrophies, several functional MRI studies (Clément and Belleville, 2010; Liang et al., 2011; Melrose et al., 2018) have shown increased activity in the prefrontal and temporal regions in aMCI patients, which has been considered as a compensatory effect for cognitive impairments. It was proposed that the aMCI patients recruited additional brain regions related to cognitive performances to achieve high demanding cognitive tasks (Clément and Belleville, 2010; Liang et al., 2011; Melrose et al., 2018). Together, higher fALFF in the frontal and temporal gyri in sd-aMCI than both the md-aMCI and HC groups suggest a functional compensation in sd-aMCI patients. It is possible that the sd-aMCI patients may recruit more neural resources from the frontal and temporal regions to compensate for poor cognitive performances and fiber integrity impairment in the bilateral superior and inferior longitudinal fasciculus and left uncinate fasciculus observed in our previous study of DTI (Liu et al., 2017). Further, the behavioral significance of the temporal cortices may be strengthened by significant correlations between the fALFF values of the left temporal cortices and cognitive performances measured by MMSE and MoCA.

In contrast to increased frontal and temporal activities in sd-aMCI patients, we found a gradual reduction in the fALFF values of the left inferior parietal lobe in the md-aMCI and sd-aMCI patients. The inferior parietal lobe is a central node within the posterior DMN, which is highly active at rest but inhibited during goal-directed cognitive tasks (Andrews-Hanna, 2012). The DMN, particularly for the posterior division, plays a key role in highly integrated tasks such as episodic memory (Yi et al., 2015; Sneve et al., 2017). The DMN is among the earliest to show abnormal amyloid deposition and has been the focus of AD and MCI researches (Koch et al., 2015). Most seed-based and independent component analysis of R-fMRI data indicates a loss of connectivity within the DMN in both the aMCI and AD (Dillen et al., 2017; Oishi et al., 2018; Hu et al., 2019). Altered DMN connectivity may be a very early biomarker for AD (Dillen et al., 2017; Oishi et al., 2018; Hu et al., 2019). Reduced GM volume in the inferior parietal lobe has been observed even before the development of aMCI (Oishi et al., 2018). Further, a significant relationship has been found between low GM volume in the right IPL and severity of mental disorientation in aMCI patients (Weise et al., 2018). We, therefore, can speculate that our finding of a gradual reduction in the fALFF of the left inferior parietal lobe from single to multiple-domain cognitive damage may suggest an involvement of the inferior parietal lobe in the neural mechanism of both the single and multiple-domain aMCI.

It is also worthy to note that the fALFF changes in our aMCI patients were predominantlydistributed over the left rather than the right hemisphere. This is consistent with the previous reports of greater amyloid burden on the left hemisphere in aMCI patients (Baron et al., 2001). The VBM studies in AD have demonstrated that the left hemisphere was preferentially affected than the right hemisphere (Karas et al., 2003; Thompson et al., 2003). The right hemisphere may have a "time lag" in developing into structural damage (Oishi et al., 2018). However, the reason underpinning this functional asymmetry needs to be clarified with more targeted research designs.

Despite these important results, several issues need to be further addressed. The small sample may limit the detection of some abnormal brain regions found in previous fMRI studies of aMCI. The structural foundation underlying these brain functional changes remains unclear. Although previous structural MRI studies have suggested the abnormalities of these cortical regions in aMCI (Di Paola et al., 2009; Oishi et al., 2018), a combined analysis of the R-fMRI and structural imaging data (e.g., structural MRI and DTI) will be more helpful for the elucidation of that issue. Our cross-sectional design may limit the assessment of the role of fALFF changes in the subsequent development of dementia. Future prospective studies are warranted to determine how the fALFF of these frontal, temporal and parietal cortices in sd-aMCI and md-aMCI patients change after they convert to AD and how the fALFF differs from the aMCI patients who will be converted and not converted to AD.

In conclusion, we found reduced brain activity in the left inferior parietal lobe but increased activity observed in the left-sided superior-to-middle frontal gyri and the left middle-to-inferior temporal gyri in aMCI patients. These changes may reflect both functional inefficiency and compensation in response to damage at earlier stages of neurodegeneration. These results suggest that the fALFFmaybe sensitive indices for differentiating the sd-aMCI and md-aMCI. Finally, our study demonstrated the neural differences between the sub-types of aMCI from a regional brain perspective and suggests that the md-aMCI might be a more advanced form of the sd-aMCI subtype.

DATA AVAILABILITY STATEMENT

The datasets generated for this study are available on request to the corresponding author.

ETHICS STATEMENT

The studies involving human participants were reviewed and approved by the institutional review board of Xuanwu Hospital of Capital Medical University. The patients/participants provided their written informed consent to participate in this study.

AUTHOR CONTRIBUTIONS

J-HL was responsible for study design. Q-HZ, LW, KW, and X-MZ performed data analysis and article writing.

FUNDING

We thank the funding from the National Natural Science Foundation Youth Project of China (81701779; 81301208), National Key R & D plan (Research on prevention and control of major chronic non infectious diseases) (2018YFC1314500) and the National Natural Science Foundation of China (81801124).

SUPPLEMENTARY MATERIAL

The Supplementary Material for this article can be found online at: https://www.frontiersin.org/articles/10.3389/fnhum.2020.00002/full#supplementary-material.

REFERENCES

Albert, M. S., DeKosky, S. T., Dickson, D., Dubois, B., Feldman, H. H., Fox, N. C., et al. (2011). The diagnosis of mild cognitive impairment due to Alzheimer's disease: recommendations from the National Institute on Aging-Alzheimer's Association workgroups on diagnostic guidelines for Alzheimer's disease. *Alzheimers Dement.* 7, 270–279. doi: 10.1016/j.jalz.2011.03.008

American Psychiatric Association. (1994). *Diagnostic and Statistical Manual of Mental Disorders: DSM-IV*. Washington, DC: American Psychiatric Association.

Andrews-Hanna, J. R. (2012). The brain's default network and its adaptive role in internal mentation. *Neuroscientist* 18, 251–270. doi: 10.1177/1073858411403316

Baron, J. C., Chételat, G., Desgranges, B., Perchey, G., Landeau, B., de la Sayette, V., et al. (2001). *In vivo* mapping of gray matter loss withvoxel-based morphometry in mild Alzheimer's disease. *Neuroimage* 14, 298–309. doi: 10.1006/nimg.2001.0848

Belleville, S., Sylvain-Roy, S., de Boysson, C., and Ménard, M. C. (2008). Characterizing the memory changes in persons with mild cognitive impairment. *Prog. Brain Res.* 169, 365–375. doi: 10.1016/s0079-6123(07)00023-4

Bell-McGinty, S., Lopez, O. L., Meltzer, C. C., Scanlon, J. M., Whyte, E. M., DeKosky, S. T., et al. (2005). Differential cortical atrophy in subgroups of mild cognitive impairment. *Arch. Neurol.* 62, 1393–1397. doi: 10.1001/archneur.62.9.1393

Brambati, S. M., Belleville, S., Kergoat, M. J., Chayer, C., Gauthier, S., and Joubert, S. (2009). Single- and multiple-domain amnestic mild cognitive impairment: two sides of the same coin? *Dement. Geriatr. Cogn. Disord.* 28, 541–549. doi: 10.1159/000255240

Caffarra, P., Ghetti, C., Concari, L., and Venneri, A. (2008). Differential patterns of hypoperfusion in subtypes of mild cognitive impairment. *Open Neuroimag. J.* 2, 20–28. doi: 10.2174/1874440000802010020

Cid-Fernández, S., Lindín, M., and Díaz, F. (2017). Neurocognitive and behavioral indexes for identifying the amnestic subtypes of mild cognitive impairment. *J. Alzheimers Dis.* 60, 633–649. doi: 10.3233/jad-170369

Clément, F., and Belleville, S. (2010). Compensation and disease severity on the memory-related activations in mild cognitive impairment. *Biol. Psychiatry* 68, 894–902. doi: 10.1016/j.biopsych.2010.02.004

Di Paola, M., Luders, E., Di Iulio, F., Cherubini, A., Passafiume, D., Thompson, P. M., et al. (2009). Callosal atrophy in mild cognitive impairment and Alzheimer's disease: different effects in different stages. *Neuroimage* 49, 141–149. doi: 10.1016/j.neuroimage.2009.07.050

Dillen, K. N. H., Jacobs, H. I. L., Kukolja, J., Richter, N., von Reutern, B., Onur, Ö. A., et al. (2017). Functional disintegration of the default mode network in prodromal Alzheimer's disease. *J. Alzheimers Dis.* 59, 169–187. doi: 10.3233/jad-161120

Farràs-Permanyer, L., Guàrdia-Olmos, J., and Peró-Cebollero, M. (2015). Mild cognitive impairment and fMRI studies of brain functional connectivity: the state of the art. *Front. Psychol.* 6:1095. doi: 10.3389/fpsyg.2015.01095

Gu, L., Chen, J., Gao, L., Shu, H., Wang, Z., Liu, D., et al. (2019). Deficits of visuospatial working memory and executive function in single- versus multiple-domain amnestic mild cognitive impairment: a combined ERP and sLORETA study. *Clin. Neurophysiol.* 130, 739–751. doi: 10.1016/j.clinph.2019.01.025

Hu, Y., Du, W., Zhang, Y., Li, N., Han, Y., and Yang, Z. (2019). Loss of parietal memory network integrity in Alzheimer's disease. *Front. Aging Neurosci.* 11:67. doi: 10.3389/fnagi.2019.00067

Hu, Z., Wu, L., Jia, J., and Han, Y. (2014). Advances in longitudinal studies of amnestic mild cognitive impairment and Alzheimer's disease based on multi-modal MRI techniques. *Neurosci. Bull.* 30, 198–206. doi: 10.1007/s12264-013-1407-y

Karas, G. B., Burton, E. J., Rombouts, S. A., van Schijndel, R. A., O'Brien, J. T., Scheltens, P., et al. (2003). A comprehensive study of gray matter loss in patients withAlzheimer's disease using optimized voxel-based morphometry. *Neuroimage* 18, 895–907. doi: 10.1016/s1053-8119(03)00041-7

Kim, C., Chung, C., and Kim, J. (2013). Task-dependent response conflict monitoring and cognitive control in anterior cingulate and dorsolateral prefrontal cortices. *Brain Res.* 1537, 216–223. doi: 10.1016/j.brainres.2013.08.055

Kim, C., Johnson, N. F., and Gold, B. T. (2014). Conflict adaptation in prefrontal cortex: now you see it, now you don't. *Cortex* 50, 76–85. doi: 10.1016/j.cortex.2013.08.011

Koch, K., Myers, N. E., Göttler, J., Pasquini, L., Grimmer, T., Förster, S., et al. (2015). Disrupted intrinsic networks link amyloid-β pathology and impaired cognition in prodromal Alzheimer's disease. *Cereb. Cortex* 25, 4678–4688. doi: 10.1093/cercor/bhu151

Lenzi, D., Serra, L., Perri, R., Pantano, P., Lenzi, G. L., Paulesu, E., et al. (2011). Single domain amnestic MCI: a multiple cognitive domains fMRI investigation. *Neurobiol. Aging* 32, 1542–1557. doi: 10.1016/j.neurobiolaging.2009.09.006

Li, X., and Zhang, Z. J. (2015). Neuropsychological and neuroimaging characteristics of amnestic mild cognitive impairment subtypes: a selective overview. *CNS Neurosci. Ther.* 21, 776–783. doi: 10.1111/cns.12391

Liang, P., Wang, Z., Yang, Y., Jia, X., and Li, K. (2011). Functional disconnection and compensation in mild cognitive impairment: evidence from DLPFC connectivity using resting-state fMRI. *PLoS One* 6:e22153. doi: 10.1371/journal.pone.0022153

Liu, J., Liang, P., Yin, L., Shu, N., Zhao, T., Xing, Y., et al. (2017). White matter abnormalities in two different subtypes of amnestic mild cognitive impairment. *PLoS One* 12:e0170185. doi: 10.1371/journal.pone.0170185

Luo, X., Jiaerken, Y., Huang, P., Xu, X. J., Qiu, T., Jia, Y., et al. (2018). Alterationof regional homogeneityand white matter hyperintensities in amnestic mild cognitive impairment subtypes are related to cognition and CSF biomarkers. *Brain Imaging Behav.* 12, 188–200. doi: 10.1007/s11682-017-9680-4

Melrose, R. J., Jimenez, A. M., Riskin-Jones, H., Weissberger, G., Veliz, J., Hasratian, A. S., et al. (2018). Alterations to task positive and task negative networks during executivefunctioning in mild cognitive impairment. *Neuroimage Clin.* 19, 970–981. doi: 10.1016/j.nicl.2018.06.014

Oishi, A., Yamasaki, T., Tsuru, A., Minohara, M., and Tobimatsu, S. (2018). Decreased gray matter volume of right inferior parietal lobule is associated with severity of mental disorientation in patients with mild cognitive impairment. *Front. Neurol.* 9:1086. doi: 10.3389/fneur.2018.01086

Petersen, R. C., Doody, R., Kurz, A., Mohs, R. C., Morris, J. C., Rabins, P. V., et al. (2001). Currentconcepts in mild cognitive impairment. *Arch. Neurol.* 58, 1985–1992. doi: 10.1001/archneur.58.12.1985

Scheller, E., Minkova, L., Leitner, M., and Klöppel, S. (2014). Attempted and successful compensation in preclinical and early manifest neurodegeneration - a review of task FMRI studies. *Front. Psychiatry* 5:132. doi: 10.3389/fpsyt.2014.00132

Seo, S. W., Im, K., Lee, J. M., Kim, Y. H., Kim, S. T., Kim, S. Y., et al. (2007). Cortical thickness in single- versus multiple-domain amnestic mild cognitive impairment. *Neuroimage* 36, 289–297. doi: 10.1016/j.neuroimage.2007.02.042

Sneve, M. H., Grydeland, H., Amlien, I. K., Langnes, E., Walhovd, K. B., and Fjell, A. M. (2017). Decoupling of large-scale brain networks supports the consolidation of durable episodic memories. *Neuroimage* 153, 336–345. doi: 10.1016/j.neuroimage.2016.05.048

Teipel, S. J., Meindl, T., Wagner, M., Stieltjes, B., Reuter, S., Hauenstein, K. H., et al. (2010). Longitudinal changes in fiber tract integrity in healthy aging and mild cognitive impairment: a DTI follow-up study. *J. Alzheimers Dis.* 22, 507–522. doi: 10.3233/jad-2010-100234

Thompson, P. M., Hayashi, K. M., de Zubicaray, G., Janke, A. L., Rose, S. E., Semple, J., et al. (2003). Dynamics of gray matter loss in Alzheimer's disease. *J. Neurosci.* 23, 994–1005. doi: 10.1523/JNEUROSCI.23-03-00994.2003

Traykov, L., Rigaud, A. S., Cesaro, P., and Boller, F. (2007). Neuropsychological impairment in the early Alzheimer's disease. *Encephale* 33, 310–316. doi: 10.1016/s0013-7006(07)92044-8

Verfaillie, S. C., Tijms, B., Versteeg, A., Benedictus, M. R., Bouwman, F. H., Scheltens, P., et al. (2016). Thinner temporal and parietal cortex is related to incident clinical progression to dementia in patients with subjective cognitive decline. *Alzheimers Dement.* 5, 43–52. doi: 10.1016/j.dadm.2016.10.007

Wang, Z., Yan, C., Zhao, C., Qi, Z., Zhou, W., Lu, J., et al. (2011). Spatial patterns of intrinsic brain activity in mild cognitive impairment and alzheimer's disease: a resting-state functional MRI study. *Hum. Brain Mapp.* 32, 1720–1740. doi: 10.1002/hbm.21140

Weise, C. M., Chen, K., Chen, Y., Kuang, X., Savage, C. R., Reiman, E. M., et al. (2018). Left lateralized cerebral glucose metabolism declines in amyloid-β positive persons with mild cognitive impairment. *Neuroimage Clin.* 20, 286–296. doi: 10.1016/j.nicl.2018.07.016

Yi, D., Choe, Y. M., Byun, M. S., Sohn, B. K., Seo, E. H., Han, J., et al. (2015). Differences in functional brain connectivity alterations associated with cerebral amyloid deposition in amnestic mild cognitive impairment. *Front. Aging Neurosci.* 7:15. doi: 10.3389/fnagi.2015.00015

Zamora, L., Corina, D., and Ojemann, G. (2016). Human temporal cortical single neuron activity during working memory maintenance. *Neuropsychologia* 86, 1–12. doi: 10.1016/j.neuropsychologia.2016.04.004

Zang, Y. F., He, Y., Zhu, C. Z., Cao, Q. J., Sui, M. Q., Liang, M., et al. (2007). Altered baseline brain activity in children with ADHD revealed by resting-state functional MRI. *Brain Dev.* 29, 83–91. doi: 10.1016/j.braindev.2006.07.002

Zou, Q. H., Zhu, C. Z., Yang, Y., Zuo, X. N., Long, X. Y., Cao, Q. J., et al. (2008). An improved approach to detection of amplitude of low-frequency fluctuation (ALFF) for resting-state fMRI: fractional ALFF. *J. Neurosci. Methods* 172, 137–141. doi: 10.1016/j.jneumeth.2008.04.012

Conflict of Interest: The authors declare that the research was conducted in the absence of any commercial or financial relationships that could be construed as a potential conflict of interest.

Advantages of publishing in Frontiers

OPEN ACCESS
Articles are free to read for greatest visibility and readership

FAST PUBLICATION
Around 90 days from submission to decision

HIGH QUALITY PEER-REVIEW
Rigorous, collaborative, and constructive peer-review

TRANSPARENT PEER-REVIEW
Editors and reviewers acknowledged by name on published articles

Frontiers
Avenue du Tribunal-Fédéral 34
1005 Lausanne | Switzerland

Visit us: www.frontiersin.org
Contact us: frontiersin.org/about/contact

REPRODUCIBILITY OF RESEARCH
Support open data and methods to enhance research reproducibility

DIGITAL PUBLISHING
Articles designed for optimal readership across devices

FOLLOW US
@frontiersin

IMPACT METRICS
Advanced article metrics track visibility across digital media

EXTENSIVE PROMOTION
Marketing and promotion of impactful research

LOOP RESEARCH NETWORK
Our network increases your article's readership